

# Operational Approaches to Quantum Correlations and Particle Creation in Field Theory

by

Eric Graham Brown

A thesis  
presented to the University of Waterloo  
in fulfillment of the  
thesis requirement for the degree of  
Doctor of Philosophy  
in  
Physics

Waterloo, Ontario, Canada, 2015

© Eric Graham Brown 2015

I hereby declare that I am the sole author of this thesis. This is a true copy of the thesis, including any required final revisions, as accepted by my examiners.

I understand that my thesis may be made electronically available to the public.

## Abstract

In this thesis we examine a variety of question regarding several quantum information-theoretic concepts as they manifest in the context of relativistic quantum fields. In particular, we study the qualitative and quantitative structure of entanglement (as well as more generalized quantum correlations) in field theory. Primarily we study the nature of vacuum entanglement, but consider spatial correlations in more general field states as well. We also discuss several novel aspects of particle creation phenomena, which generally go hand in hand with the presence of field entanglement. Such investigations are important from two perspectives. First, we gain enlightening new insight into the nature of quantum fields and, therefore, into the fundamental constituents of the matter contained in our universe. Second, we are able to consider the possibility of utilizing the relativistic nature of quantum fields as a resource for quantum technological tasks such as entanglement distribution, information processing, and metrology.

As a general guiding principle, here we approach such questions from an operational perspective. That is, we focus less on the mathematical facts derivable from a given theory and instead attempt to answer in what concretely physical ways such facts manifest themselves. For example, in what ways can vacuum entanglement actually be experimentally detected and measured, at least in principle? Such an approach allows us to circumvent otherwise problematic interpretational issues. It also lends itself more naturally to the proposal of real world experiments regarding, and utilizations of, the physics being investigated. In this thesis we utilize two models of detection as applied to field theory.

The first is one that we will develop from scratch and use to great effect in a number of studies; this is the non-perturbative oscillator detector. In this context, a “detector” is simply some quantum system that is allowed to interact in some way with a quantum field. The response of this system then gives us information about the field properties. Typically such studies are done perturbatively, which presents several severe limitations on what may be investigated. We develop an alternative model, in which the detector is identified as a quantum harmonic oscillator, that allows non-perturbative solutions. We go on to apply this model to a variety of studies. We start by the examining the Unruh effect in a cavity setting. Not only are we able to examine the thermalization behavior of such a detector (which is stronger than what can be achieved perturbatively), we also demonstrate that the Unruh response is largely independent of the cavity boundary conditions, indicating a surprising amount of generality and universality to the phenomenon. We also consider the spacelike extraction of spatial entanglement by a set of such detectors. This includes the harvesting of genuine tripartite entanglement out of the vacuum, as well as the observation that the extractable quantum discord (a generalized measure of quantum correlations) can

be greatly amplified by thermal fluctuations in the field, in opposite behavior to entanglement. This calls into question the nature of quantum discord, but also suggests at the possibility of *using* environmental noise as a quantum computational resource. Next, we use the oscillator detector model to great effect by proposing a method of reliably and sustainably generating and distributing entanglement via a cavity field. This protocol is inherently non-perturbative, and we refer to it as entanglement farming. Lastly, we modify the farming scenario to discover a very sensitive resonance effect that generates a large difference in the protocol output due to a minute change in system parameters, including the length of cavity being used. We put this forth as a potential method of quantum seismic metrology.

The second model that we will consider simply involves performing projective measurements onto a given set of field modes. We will find, however, that such an approach allows us to solve previously intractable problems. In particular, we apply this procedure to the physically sensible choice of localized, positive frequency field modes. Using this model we perform two different studies. In the first, we consider the response of an observer accelerating not through the vacuum state but rather a thermal state. Such a setting has not been (properly) studied previously, due to the computational challenges involved. By applying the localized projective measurement model we are able determine that such an observer sees both an Unruh response from acceleration and a response from the field thermality and that, critically, these responses are distinguishable. We then go on to examine the degradation of quantum correlations between two observers due to the acceleration of one of the observers. This is a prototypical scenario of interest and, by applying realistic measurement assumptions, we obtain results qualitatively different from many previous works on the issue.

In addition to these models, we question the nature of vacuum entanglement and particle creation by considering an operationally straightforward procedure that greatly demystifies these phenomena and puts them on to solid, physically concrete grounds. This operation is that of very quickly introducing a boundary condition onto one's field, for example by creating a mirror. The real particles generated in this process will then be quantum entangled with each other, even if they are created at spatially separate locations, and this entanglement derives exactly from the previously present vacuum entanglement. Not only does this realization provide an operationally satisfying interpretation of vacuum entanglement, it also suggests a straightforward procedure for its experimental verification.

In all of this, the computational framework that we will rely upon is that of Gaussian quantum mechanics. This is a restriction of continuous variable quantum mechanics that, while limited in its applicability, provides extremely powerful computational tools in the cases that it may be used. The scenarios of interest in this thesis fall within this category

and lend themselves naturally to a Gaussian approach. With this we are able to perform, near trivially, many otherwise intractable studies.

The publications that comprise this thesis, in order of presentation, are as follows: [1, 2, 3, 4, 5, 6, 7, 8]. We will also include some material from [9] in the preliminaries, and there is an additional publication, [10], that was performed as part of my doctorate but is not included here.

## Acknowledgements

As I started to make a list of the people that I wanted to thank for their contribution to my studies and to my life over the past three years, I immediately realized that I would almost certainly fail to account for every such person. To those that I have missed, you have the right to a beer at my expense. To everyone who has written one of these, you know how difficult it can be to summarize in a few short words the impact that those of utmost importance have had on your life. It is impossible, and I will not try. I will only write the words that I can, which I know are usually too many. In this I have no choice but to start with my family.

Mom, your unconditional love and pride has been a constant throughout my life. You have always been that person I turn to when I need someone. When I am hurt or unsure, when I need to hear a voice, you are there. You are the epitome of human understanding and empathy, and the compassion that you display with all those around you has always been an example for me. Thank you for showing that to me. Thank you also for the financial support that you provided me during my undergraduate. Lance, this thesis would obviously not be possible without having gotten my smarts from your side of the family. Thank you so much for being a part of my mother's world, and of mine. You have changed my life and my values in ways that I can't even identify, but which I know are there.

Dad, words fail me. Your strength, dedication, warmth, and ease define the scale by which I measure myself as a man. You have always been that beacon, that persona that I strive to emulate. The struggles that you have faced in your life have taught me much about the way I want to lead my own, and your steadfastness through it all has been an inspiration to me. I thank you for the curiosity that you have instilled in me, which let blossom the passion that I now pursue. Life is long and full of stuff. Carolyn, I've known you for the large majority of my life. You loved this strange child unconditionally, and you have always been somebody that I know I can utterly trust and turn to should I need you. Thank you for always convincing dad to take my cats. I can't imagine a life without you in it. Liam and Gaia, you know what you mean to me. I am baffled and overjoyed at the adults you have so quickly become, and feel incredibly lucky to continue watching as you grow in to those you are to be.

Stephanie. The impact that you have had on my life is, by any measure, immeasurable. You are my best friend. You have supported me throughout my personal and academic development with love and understanding. When my mind was not on physics, it was on you. You have helped me to be the better person that I am today, in part by showing me the power of just not taking things so damn seriously. I'm so proud of you for having

found your calling and for pursuing it with such veracity. Although we go different ways in life, I know that we will always be connected by the experiences and love we have shared together. Glen, Gail, and Karl, you are family, in every sense of the word that matters. Thank you for welcoming me into your lives and for being such an important part of mine.

I've had the pleasure of working with an amazing number of amazing people during my doctorate. First and foremost is, of course, my one-of-a-kind supervisor, Robert Mann. Robb, I can never thank you enough for recognizing my need for scientific independence and freedom, and for allowing me to follow my interests unhinged. It is because of this, and the opportunities that arose from it, that I have had such success these three years. You have always been a sure source of advice, expertise, and kindness, both academically and otherwise. Thank you for seeing me through this journey. Eduardo Martín-Martínez, I have no idea what this thesis would look like had you not been my friend, colleague, and mentor throughout so much of it. Your enthusiasm, brilliance, endless energy, and vision are what inspire me to continue bettering myself as a physicist. Your example is and will always be that to which I aspire. I value your friendship dearly, and look forward to many projects and adventures in the future. Nicolas Menicucci, when we first met I found you rather well equipped for getting under my skin. Yet, now I count you as a trusted friend, close colleague, and a constant source of wisdom and perspective in both physics and in life. Gangnam style. Achim Kempf, you have been my teacher, my colleague, and a constant reminder of why I do what I do. Your scientific genius is unparalleled, and your zest for life impeccable. You are an inspiration. Thank you so much for the advice and experience that you have always been so happy to share. Juan León, my first day in Madrid you brought me to your home and got me hammered. I knew from that point on that I would enjoy my time in Spain. Indeed, those six months were arguably the best of my life. Thank you for putting your faith in me and for showing me your world; I look forward to future visits and to many deep conversations. Andrzej Dragan, you have a knack for looking at physics differently, and for discovering those subtleties that make others question what they thought they knew. This has occurred to me multiple times over the course of our interactions, and I'm a more complete scientist today because of it. Thanks for being a friend, and for teaching me how to shred.

Thank you also to all of the other friends and colleagues that I have made during this time, who have supported me and been a source of advice, discussion, and fun. In Waterloo: Aida Ahmadzadegan, Paul McGrath, Sean Stotyn, Wilson Brenna, Robert Jonsson, Miok Park, Danielle Leonard, Alex Smith, Marius Oltean, and many others I am sure to be missing. Abroad: Nicolai Friis, Marcus Huber, Antony Lee, Jason Doukas, and a special thank you to Jorma Louko. A very special thank you also to those who warmly welcomed me during my time in Madrid (in addition to Juan of course): Marco del Rey, Hans

Westman, Emilio Alba, and Luis Garay, among others. Marco, we had some good times man. Thanks for being there. And Zaida Gomez, you came into my life exactly when I needed you, and in a very short time made an impact on me that I have yet to fully understand. You taught me so much about myself, and for that I can never thank you enough. You have become one of my very best friends in the world, and now that world just wouldn't seem right without you in it.

I would also like to take this opportunity to thank those in the physics department at Trent University, for providing me with the knowledge and the passion that has carried me through to this point. Rachel Wortis, Ralph Shiell, Bill Atkinson, Peter Dawson, David Patterson, John Breukelaar, and especially to Alan Slavin. Al, you were the person in my first year at Trent who showed me what I wanted to do with my life, and for this you have the warmest gratitude that I can give. My success is your success.

Lastly, but not to diminish their contributions, I would like to thank NSERC and the taxpayers of Canada for the incredible financial support that they have provided me throughout my academic path, and for their continued support as I enter the next stage of this crazy world I seem to have gotten myself into.



## **Dedication**

This thesis and the work that it represents is dedicated to my brother and sister, Liam and Gaia. As I enter a new stage of my life, you too delve into your own worlds of experience and possibility. Proceed boldly, eyes up, with passion and curiosity. Let your words and actions be clear and sincere. Never, ever stop self-improving. The love that you share with others will be limited only by the love that you lack for yourselves, and your stories limited only by those fears that you fail to face.

# Table of Contents

List of Figures	xvi
<b>1 Introduction</b>	<b>1</b>
1.1 What's this all about? . . . . .	1
1.2 Thesis outline . . . . .	6
<b>I Preliminaries</b>	<b>10</b>
<b>2 Quantum correlations</b>	<b>12</b>
2.1 Entanglement . . . . .	12
2.1.1 Pure state entanglement . . . . .	13
2.1.2 Mixed state entanglement . . . . .	15
2.1.3 Multipartite entanglement . . . . .	18
2.2 Quantum discord . . . . .	19
2.3 Aside: Discord as a bipartite manifestation of tripartite entanglement . . .	22
<b>3 Gaussian quantum mechanics</b>	<b>28</b>
3.1 Basics . . . . .	28
3.2 Important states . . . . .	32
3.3 The symplectic spectrum, purity, and mixedness. . . . .	35

3.4	Quantum correlations in Gaussian states . . . . .	37
3.4.1	The case of two-modes . . . . .	39
3.5	Aside: Why Gaussian states require quantum correlation to have classical correlation . . . . .	41
<b>4</b>	<b>Quantum scalar field theory</b>	<b>44</b>
4.1	Field quantization . . . . .	44
4.2	Choice and change of mode basis . . . . .	47
4.3	Rindler quantization . . . . .	52
4.4	Particle detectors . . . . .	56
4.5	The Unruh effect . . . . .	59
4.6	Vacuum entanglement . . . . .	62
4.7	Field theory in a cavity . . . . .	65
4.8	Symplectic Bogoliubov transformations . . . . .	68
<b>II</b>	<b>The Nonperturbative Oscillator Detector</b>	<b>70</b>
<b>5</b>	<b>The oscillator detector model</b>	<b>74</b>
5.1	The setup . . . . .	74
5.1.1	Hamiltonians generating evolution with respect to different time parameters . . . . .	75
5.1.2	The Unruh-DeWitt Hamiltonian in general scenarios . . . . .	77
5.2	Mechanics of the model . . . . .	83
5.2.1	The symplectic evolution equation . . . . .	83
5.2.2	Free evolution and examples of phase-space Hamiltonians . . . . .	86
5.2.3	The phase space interaction picture . . . . .	89
5.3	Discussion . . . . .	90

<b>6</b>	<b>The Unruh effect in a cavity; thermalization and universality</b>	<b>92</b>
6.1	The setting . . . . .	94
6.2	Thermality . . . . .	96
6.3	Unruh temperature . . . . .	98
6.4	Discussion . . . . .	100
<b>7</b>	<b>Tripartite vacuum entanglement harvesting</b>	<b>102</b>
7.1	Setting and computation . . . . .	104
7.2	Results . . . . .	107
7.3	Discussion . . . . .	109
<b>8</b>	<b>Thermal amplification of discord harvesting</b>	<b>111</b>
8.1	Setting and computation . . . . .	113
8.2	Results . . . . .	115
8.3	Explanations . . . . .	122
8.3.1	Correlation function . . . . .	122
8.3.2	Relation to system-environment entanglement . . . . .	124
8.3.3	Translational invariance . . . . .	125
8.3.4	Entanglement degradation . . . . .	132
8.4	Discussion . . . . .	134
<b>9</b>	<b>Entanglement farming</b>	<b>136</b>
9.1	The model and evolution . . . . .	138
9.2	Results . . . . .	140
9.2.1	Fixed point analysis . . . . .	141
9.2.2	Sustainable entanglement extraction . . . . .	143
9.2.3	Initial thermal field . . . . .	146
9.2.4	Onset of the instability . . . . .	150
9.2.5	Is a fixed point possible for short cycle times? . . . . .	154
9.3	Discussion . . . . .	157

<b>10 Quantum seismology</b>	<b>160</b>
10.1 Setup . . . . .	161
10.2 Sensitivity of the fixed point to time delays . . . . .	163
10.3 Cavities with time dependent length . . . . .	165
10.4 Quantum seismograph . . . . .	166
10.4.1 Two-stage evolution . . . . .	166
10.4.2 Choice of unperturbed cavity parameters . . . . .	167
10.4.3 Detecting vibrations . . . . .	168
10.4.4 Frequency response . . . . .	171
10.4.5 Experimental prospects . . . . .	172
10.5 Discussion . . . . .	174
<b>III Localized Projective Measurements</b>	<b>176</b>
<b>11 Accelerating in a thermal bath</b>	<b>179</b>
11.1 Calculations . . . . .	180
11.2 Discussion . . . . .	187
<b>12 Quantum correlations in accelerated frames: local versus global modes</b>	<b>189</b>
12.1 Setting . . . . .	190
12.2 Global analysis . . . . .	193
12.3 Local analysis . . . . .	196
12.4 Discussion . . . . .	198
<b>IV What does it mean for half of an empty cavity to be full?</b>	<b>200</b>
<b>13 Slamming a mirror</b>	<b>202</b>
13.1 How does one measure the vacuum excitations in a subregion? . . . . .	203

13.2	Formulation and setting . . . . .	205
13.2.1	Local mathematical analysis: local vs. global modes . . . . .	206
13.2.2	Slamming down a mirror . . . . .	210
13.2.3	Three spatial regions . . . . .	212
13.3	Computing the state . . . . .	214
13.3.1	The state of two regions . . . . .	214
13.3.2	The state of three regions . . . . .	217
13.4	With vs. without a mirror . . . . .	219
13.4.1	Time evolution . . . . .	219
13.4.2	Finite-time mirror . . . . .	221
13.5	Entanglement . . . . .	222
13.5.1	Mode-mode entanglement . . . . .	223
13.5.2	The mixedness problem . . . . .	224
13.5.3	Symplectic diagonalization . . . . .	226
13.5.4	Spatial structure of entanglement . . . . .	228
13.5.5	Entangled bursts of particles . . . . .	230
13.5.6	Two mirrors . . . . .	232
13.6	Experimental motivations and prospects . . . . .	234
13.7	Discussion . . . . .	236
<b>14</b>	<b>Conclusions</b>	<b>238</b>
	<b>APPENDICES</b>	<b>242</b>
<b>A</b>	<b>Symplectic diagonalization</b>	<b>243</b>
<b>B</b>	<b>Hilbert space view of the detector symplectic evolution</b>	<b>245</b>
<b>C</b>	<b>Predicting the specifics of thermal amplification</b>	<b>253</b>

D	Relative entropy between Gaussian states	256
E	Adiabaticity for a moving cavity mirror	260
F	Adiabaticity for gravitational waves	263
	References	266

# List of Figures

2.1	The relationship between the entanglement structure of $ \psi\rangle_{ABC}$ and the discord in $\rho_{AB}$ . For given conditions on $ \alpha\rangle$ and $ \beta\rangle$ we display the resulting entanglement structure and the results for the discords $D(A, B)$ and $D(B, A)$ . In the structure diagrams an ellipse represents the presence of bipartite entanglement while a triangle represents the presence of tripartite entanglement. . . . .	26
4.1	The trajectory of a uniformly accelerating observer. Note that this observer is causally disconnected from the left-hand Rindler wedge. . . . .	53
5.1	Harmonic-oscillator detector (red dot) moving through a fixed cavity. This is to illustrate the difference between our setup and those in which the cavity itself is in motion [11]. Note that any number of detectors may be present. . . . .	75
6.1	The detector's (green, dashed) trajectory through the cavity (red, solid) with acceleration $a = 1.6$ . The Gaussian switching function is plotted on the right axis with a jagged magenta line. . . . .	95
6.2	Comparison of different boundary conditions on the detector's temperature as a function of temperature. Not only do we see that it is linear, but that it is nearly numerically identical for all three boundary conditions. . . . .	99
7.1	Entanglements $E_N(ss)$ and $\bar{E}_N(sss)$ as a function of the time $T$ and detector frequency $\Omega$ , where we have set $L = 10$ and $\lambda = 0.01$ . On the right: regions of existence of $E_{ss}$ and $\bar{E}_{sss}$ plotted together. . . . .	108
7.2	Entanglements $E_N(ss)$ and $\bar{E}_N(sss)$ as a function of cavity length $L$ and detector frequency $\Omega$ , where we have set $T = 0.4r$ and $\lambda = 0.01$ . On the right: regions of existence of $E_{ss}$ and $\bar{E}_{sss}$ plotted together. . . . .	108



8.1	The logarithmic negativity between the detectors $E_N$ , as a function of the distance $r$ between them and the time $t$ of evolution in the case that the field is initially in its vacuum state. . . . .	117
8.2	The logarithmic negativity between the detectors as a function of time $t$ , where $r = 3$ . We display the data for the cases that the field is initially in its vacuum state $T = 0$ (solid blue line), and in thermal states of temperatures $T = 0.1$ (red dashed line) and $T = 0.15$ (black dotted line). At a temperature of $T = 0.2$ the entanglement remains nonexistent. We observe that the extracted entanglement rapidly decays with field temperature. . . . .	118
8.3	The mutual information between the detectors $I$ , Eq. (8.6), as a function of the distance $r$ between them and the time $t$ of evolution in the case that the field is initially in its vacuum state. . . . .	119
8.4	The mutual information $I$ (solid blue line) and the Gaussian discord $D$ (dashed red line) between the detectors as a function of time $t$ , where $r = 4$ . The temperature of the field varies in the three plots from (a) $T = 0$ (i.e. the vacuum), (b) $T = 1$ , and (c) $T = 10$ . We observe that as temperature increases both $I$ and $D$ very substantially increase. . . . .	120
8.5	The mutual information $I$ (solid blue line) and the Gaussian discord $D$ (dashed red line) between the detectors as a function of field temperature, where $r = 4$ and $t = 2$ . . . . .	121
8.6	The difference $ \nu_1 - \nu_2 $ of the symplectic eigenvalues of the detector-detector system as a function of time. The field was initially in its vacuum state and the detectors were placed a distance $r = 4$ away from each other. These are the same parameters that were used to plot the mutual information and discord in Fig. (8.4-a), and we note that the qualitative behavior in that figure is exactly the same as we see here. . . . .	126
8.7	The two symplectic eigenvalues $\nu_1$ and $\nu_2$ of the detector-detector system as a function of initial field temperature $T$ . The detectors were placed a distance $r = 4$ away from each other and left to evolve for a time $t = 2$ . We see that the difference $ \nu_1 - \nu_2 $ grows with temperature. . . . .	127
8.8	The mutual information, Eq. (8.24), as a function of $\nu_1$ and $\nu_2$ . We see clearly the increase with $ \nu_1 - \nu_2 $ . . . . .	133

9.1	We plot the logarithmic negativity attained per cycle by detector pairs, as a function of cycle number. On the left this is plotted for a small number of cycles, and on the right for a large number. The three lines correspond to different initial states of the field. The solid (blue) line corresponds to the vacuum state, whereas the dashed (red) line corresponds to a thermal state of temperature $T = 0.5$ and the dotted (black) line to a temperature of $T = 1$ . The time of evolution per cycle was set to $t_f = 20$ . . . . .	144
9.2	The energy input per cycle as a function of cycle number. The solid (blue) line corresponds to the case in which the field is initially in its vacuum state, whereas the dashed (red) line corresponds to a thermal state of temperature $T = 0.5$ and the dotted (black) line to a temperature of $T = 1$ . The time of evolution per cycle was set to $t_f = 20$ . . . . .	146
9.3	The field purity as a function of cycle number. The solid (blue) line corresponds to the case in which the field is initially in its vacuum state, whereas the dashed (red) line corresponds to a thermal state of temperature $T = 0.5$ and the dotted (black) line to a temperature of $T = 1$ . The time of evolution per cycle was set to $t_f = 20$ . . . . .	148
9.4	The thermality estimator $D$ as a function of cycle number. The solid (blue) line corresponds to the case in which the field is initially in its vacuum state, whereas the dashed (red) line corresponds to a thermal state of temperature $T = 0.5$ and the dotted (black) line to a temperature of $T = 1$ . The time of evolution per cycle was set to $t_f = 20$ . . . . .	149
9.5	The logarithmic negativity obtained by the detectors as a function of $\log_{10}(\text{number of cycles})$ . The field was initially in its vacuum state. We see that after a large number of cycles, approximately $10^7$ , the entanglement decays to zero as a result of the increasingly excited off-resonant modes. Note that the sharpness of the drop is due to a lack of resolution, since this plot was generated by evaluating the extracted entanglement at every $2^n$ 'th cycle. . . . .	151
9.6	The order of magnitude of the number of cycles needed for the highly off-resonant modes to start having impact on the detector evolution, leading to entanglement extinction, as a function of coupling constant $\lambda$ . . . . .	152
9.7	The order of magnitude of the number of cycles needed for the off-resonant modes to impact the detectors, as a function of the cycle time $t_f$ . This magnitude is periodic with a period of 16, which is twice the cavity length. . . . .	153

9.8	The logarithmic negativity obtained per cycle in some regimes where there is no fixed point. The field was initially in its vacuum state. The three lines correspond to three different interaction times per cycle, $t_f$ . We represent this in terms of the light-crossing time between the detectors, which since the speed of light is set to unity is just the distance $r = 8/3$ between them. The solid (blue), dashed (red), and dotted (black) lines correspond to $t_f = 1.44r$ , $t_f = 1.48r$ , and $t_f = 1.52r$ , respectively. . . . .	155
10.1	The function $\chi(t)$ with $T = 20$ with $\delta = 0.2T$ . . . . .	163
10.2	The steady-state logarithmic negativity as a function of $f = (T + \Delta t)/L_0$ , where $\Delta t$ is the varied parameter. The other parameters are $\Omega = \pi/L_0$ (resonant with the fundamental mode), $T = 2.5L_0$ , and with the switching parameter $\delta = 0.2T$ . On the left we see that the steady state entanglement is nearly constant as the delay time is changed, except for very well-defined points in which it drops drastically. On the right we zoom in on one of the valleys, and we see that in fact the steady-state entanglement is zero within a small window. . . . .	164
10.3	The logarithmic negativity received per cycle during the period of vibration. Here the vibrational period is set to 1000 times the cycle time (interaction plus rest period totaling a time of $T + \delta t = 2T$ ) and we track three periods of the vibration. Before the vibration the steady-state entanglement was zero, and the entanglement shown in this plot is due solely to the vibration, despite the frequency being such that $\gamma/\omega_1 = 4 \times 10^{-4}$ . The two lines correspond to different vibration magnitudes. The solid (blue) line is such that $A = (1 \times 10^{-3})L_0$ and the dashed (green) line corresponds to $A = (2 \times 10^{-4})L_0$ . . . . .	168
10.4	The steady-state value of $2 \langle \hat{q}_1 \hat{q}_2 \rangle$ as a function of $f = (T + \Delta t)/L_0$ , where $\Delta t$ is the varied parameter. The other parameters are $\Omega = \pi/L_0$ (resonant with the fundamental mode), $T = 2.5L_0$ , and with the switching parameter $\delta = 0.2T$ . . . . .	170
10.5	The steady-state value of $2 \langle \hat{q}_1 \hat{p}_2 \rangle$ as a function of $f = (T + \Delta t)/L_0$ , where $\Delta t$ is the varied parameter. The other parameters are $\Omega = \pi/L_0$ (resonant with the fundamental mode), $T = 2.5L_0$ , and with the switching parameter $\delta = 0.2T$ . . . . .	171

- 10.6 The correlation function  $2\langle\hat{q}_1\hat{p}_2\rangle$  per cycle during the period of vibration. The specific scenario and parameters are the same as in Fig. 10.3. The solid (blue) line corresponds to a vibrational amplitude of  $A = (1 \times 10^{-3})L_0$  and the dashed (green) line to  $A = (2 \times 10^{-4})L_0$ . Note that we achieve an order-of-magnitude increase in this quantity due to the presence of the wave, as compared to the steady state value (approximately  $-0.25 \times 10^{-3}$ , as given by the initial value in this plot). . . . . 172
- 10.7 The maximum value of  $2\langle\hat{q}_1\hat{p}_2\rangle$  achieved over the course of 10 vibrational periods as a function of the log of the vibrational frequency  $\gamma$ . The parameters for the solid line (blue) are the same as for Fig. 10.6:  $L_0 = 8$ ,  $\Omega = \pi/L_0$ ,  $\lambda = 0.01$ , and  $T = 20$  with  $\Delta t = T$ . The dashed line (red) represents the case that all parameters have been scaled by an order of magnitude:  $L_0 = 0.8$ ,  $\Omega = \pi/L_0$ ,  $\lambda = 0.1$ , and  $T = 2$  with  $\Delta t = T$ . In both cases the amplitude of vibration is assumed to scale with the initial length, such that  $A = (1 \times 10^{-3})L_0$  always. We see that by scaling our system in such a way we can achieve sensitivity coverage over a range of vibrational frequencies. 173
- 12.1 A schematic of the type of setup we consider. A two-mode squeezed state is produced from a non-linear crystal in two Gaussian modes  $\phi_A$  (Alice) and  $\phi_B$  (Bob). An observer Rob accelerating with constant proper acceleration  $a$  in the  $x$ -direction carries a detector that makes measurements of the field in a mode  $\psi_R$  at time  $t = 0$  when his velocity,  $v$ , is zero. . . . . 191
- 12.2 A plot of logarithmic negativity  $E_N$  (blue, solid), discord  $D(A, B)$  (green, dashed) and discord  $D(B, A)$  (red, dotted) as functions of  $z = e^{-2\pi\Omega}$ , where the state in consideration is a two-mode squeezed state using Unruh modes with squeezing parameter  $s = 1$ . We see that  $E_N$  and  $D(A, B)$  decay to zero as  $\Omega \rightarrow 0$  whereas  $D(B, A)$  asymptotes to a finite value. . . . . 195
- 12.3 A plot of logarithmic negativity  $E_N$  (blue, solid), discord  $D(A, B)$  (green, dashed) and discord  $D(B, A)$  (red, dotted) as functions of acceleration, where the state being considered is the two-mode squeezed state, with squeezing parameter  $s = 1$ , and with Bob's mode in the localized Gaussian,  $\phi_B(x - 1/a)$  with  $N = 6$  and cut-off value chosen to  $\Lambda L = \frac{1}{3}$ . We see that, unlike when Unruh modes are used, the entanglement experiences sudden death at a finite acceleration. The quantum discord remains even beyond this point of entanglement extinction. Both of the discords, however, decay to zero in the  $aL \rightarrow \infty$  limit. . . . . 198

13.1	Sketch of the one dimensional cavity setting. We start ( $t < 0$ ) considering a cavity in its vacuum state $ 0\rangle_G$ . At some instant ( $t = 0$ ) we slam a mirror separating the cavity into two regions. As explained in the text, the normal modes in these separated subcavities correspond to the localized modes of the cavity without mirror, which we will show suffice to analyze states, correlations and particle production after slamming the mirror. The horizontal line corresponds to $t = 0$ , the diagonal lines represent the light cone starting at the slamming event. . . . .	205
13.2	The cavity for the cases studied in this chapter. The figures on the left correspond to the full cavity without mirrors, the light dotted vertical bars indicating the border of the regions chosen to study localization into two (top) or three (bottom) spatial regions. The right figures show the decomposition in terms of local modes at $t = 0$ for both settings. . . . .	209
13.3	The logarithmic negativity $E_N$ between local modes $u_m$ and $\bar{u}_n$ on the left and right sides of the cavity, respectively. The cavity is divided in two equal regions $r = 0.5R$ . Left: a field mass of $\mu = 0$ . Right: a field mass of $\mu = 15/R$ . . . . .	224
13.4	The logarithmic negativity $E_N$ between local, diagonalizing modes $v_m$ and $\bar{v}_n$ on the left and right sides of the cavity, respectively. The cavity is split into two equal sides, $r = 0.5R$ , and $N = 200$ for both the left and right sides. Left: a field mass of $\mu = 0$ . Right: a field mass of $\mu = 15/R$ . . . . .	228
13.5	The function $ v_1(x) $ in the left-side of the cavity, representing the spatial distribution of entanglement with the opposite side. The parameters are given by $r = 0.5R$ , and $N = 200$ , with different field masses $\mu$ considered: 0 (blue), $10/R$ (light blue) and $50/R$ (green). As can be seen: the larger the mass of the field, the closer the entanglement straddles the boundary between the two sides of the cavity, as expected. . . . .	229
13.6	Evolution of the entanglement spatial distribution for the massive case $\mu = 50/R$ after an elapsed time $t = r/2$ . We can see a peak for the correlations at exactly the position of the particle-burst front as originated from the slamming. The cavity parameters are the same as in Fig. 13.5 . . . . .	231

13.7	Two mirror case: logarithmic negativity $E_N$ between local, diagonalizing modes $v_m^A$ and $v_n^C$ on the left and right-most sides of the cavity, respectively, in the case that the field is massless $\mu = 0$ . The cavity is in this case split into three regions, $\Delta_A = [0, 0.5R - B/2]$ , $\Delta_B = [0.5R - B/2, 0.5R + B/2]$ , $\Delta_C = [0.5R + B/2, R]$ . We have taken $N = 200$ . Left: Size of the middle section $B = 0.1R$ . Right: Size of the middle section $B = 0.2R$ . . . . .	234
13.8	The number expectation value of local modes $u_m$ for the case of a massless field $\mu = 0$ and a cavity split in half $r/R = 0.5$ . . . . .	235
C.1	The mutual information between detectors as a function of $t$ and $r$ , where the field was initiated in a thermal state of temperature $T = 2$ . . . . .	254

# Chapter 1

## Introduction

### 1.1 What's this all about?

This thesis represents a collection of work dedicated to better understanding a range of physical phenomena that lie at the intersection of what have historically been, and still largely are, isolated fields of theoretical physics. The first of these is the broad area of relativistic quantum field theory, primarily used to describe high-energy particle physics. The other is that which encompasses quantum information and quantum computation. Interest in this topic has exploded in the past fifteen years and work is primarily geared towards isolating information-theoretic approaches to (and consequences of) quantum theory, with the hope of developing methods of utilizing the nature of quantum physics for improved, real-world information processing. In recent years there has also been a great deal of work in applying notions from quantum information theory to the context of quantum fields. This research has led to a great number of realizations regarding the structure and consequences of field theory, as well as its connection with gravitation [12, 13]. Here we will be investigating, from an operational perspective, questions regarding the workings and interpretation of several information-theoretic phenomena that arise within field theory. This will largely consist of theoretical studies, but will also include various proposals for real-world implementation and application. Approaching relativistic quantum physics from an informational perspective appears to be a vital endeavor for elucidating the nature of our universe's fundamental constituents, and may furthermore be a crucial element in the future development of quantum technologies.

Quantum field theory (QFT) [14, 15] has, historically, been primarily developed with the goal in mind of constructing a unified framework for describing the elementary particles

that exist in nature and the interaction between them. The result of this endeavor is the famous standard model of particle physics which, while not complete nor entirely unified (the antagonist being the gravitational interaction), has had irrefutable and stunning success in predicting the outcomes of high-energy particle experiments. This is exemplified by the recent confirmation of the existence of the Higgs boson [16, 17]. From this perspective it is difficult to argue that QFT, at least within the energy regimes that we have experimentally explored, does not at least partially describe the fundamental workings of our world.

Nevertheless, even without delving into the problems of combining quantum mechanics and gravity, QFT has some severe (but also deeply intriguing) interpretational issues that are relatively untouched within the context of particle physics. The most obvious of these is that what we actually identify as a particle within field theory is a definite-momentum excitation of the free (non-interacting) vacuum state, and is therefore entirely delocalized in space! This certainly goes against one’s intuitive notion of a “particle” as being a localized entity. One can of course consider coherent superpositions of such particle states in order to construct localized wavepackets, but even this procedure has limits and in fact such a packet can never be strictly localized within a finite region of space [18, 19, 20]. Furthermore, the very question of whether or not a particle *exists* is not as definite as one would assume. As first realized in [21], a uniformly accelerating observer traveling through the vacuum state of a quantum field, that state defined to be void of excitations, *will* in fact observe the presence of particles, in disagreement with his or her inertial counterparts. Specifically, this observer will see themselves immersed in a thermal bath of a temperature proportional to their acceleration. This is the famous Unruh effect which, while physically reasonable (as we will discuss in the main body), is nevertheless conceptually striking and now understood to represent an exemplary case of what is a much more general and universal class of phenomena, which here we will simply refer to as particle creation. The vacuum state of a quantum field (or, really, any many-body system with local interaction) has the puzzling property that the reduced state supported on any finite region of space is *not* in its local vacuum state. Within many-body or condensed matter systems this poses no real interpretational issues. In field theory, however, where excitations are identified with the real, physical particles that compose the matter in our universe, such a realization is rather disturbing. It implies for example that, at least in some mathematical sense, half of an empty box is not empty but rather contains a frothing sea of high-energy quanta. This property of the vacuum state, as is now understood, goes hand in hand with the presence of quantum entanglement between spatially disparate regions, a concept of central importance within quantum information theory. Both of these properties of the vacuum state arise, mathematically unsurprisingly, from the fact that the free Hamiltonian of the field is an



entirely global operator.

Quantum entanglement [22] refers to a type of correlation that can be present between constituent parts of a quantum system. In particular, such correlations are of a purely quantum nature and are strictly stronger than any correlation structure that can be achieved within classical probability theory. Entanglement physically manifests between the statistics of local measurements made on the individual constituents that comprise one's system of interest, and a state displaying this property is called entangled. In addition to being enormously interesting theoretically, as entanglement arguably represents the most quantum of quantum behavior (i.e. furthest from classical intuition), it is also of central importance to quantum information and computation and to information-processing procedures therein [23]. It has been realized that by utilizing the quantum mechanical properties of matter it is possible to perform certain computational tasks more efficiently than by any known classical algorithm. This property is often referred to as the quantum advantage. Indeed the field of quantum cryptography [24], which provides unconditionally secure cryptographic exchanges (at least in theory), has already achieved commercial realization. More generally, the existence of this quantum advantage motivates research aimed towards the realization of scalable quantum computers. While this goal has not yet been achieved by any reasonable definition of achievement, the potential of incredible real-world application has led to the development of a plethora of potential architectures [23].

Indeed a large majority of the primary protocols and algorithms developed within quantum information science critically rely on entanglement. This has led to the perspective of entanglement as being a resource that can be consumed in order to perform useful quantum tasks. The reliable generation and distribution of entanglement is therefore a topic of central importance. In recent years it has also become clear that the simple dichotomy of entangled or not entangled (also called separable) is not nearly sufficient for classifying the degrees of quantum correlation that a state can possess. Within the set of entangled states there is a subset of those that are quantum steerable [25, 26, 27], meaning that one may prepare into certain states a local part of a system to which one does not have access by means of measuring and post-selecting that part to which one does have access. Within this set there is another subset of so called non-local states, which are the states known to break Bell-type inequalities [28]. Even the set of entangled states is now known to be a subset itself of states that display what is called quantum discord (or related measures) [29, 30]; these are states which, while not necessarily entangled, nevertheless display correlations between local measurement statistics that are not reproducible by classical systems or classical probability theory. There is also evidence that, while perhaps limited, discordant but non-entangled state may still be considered as a resource for certain quantum computational protocols, for example [31, 32, 33, 34].

In addition to studying the ways in which quantum information can help us to understand field theory, the past decade has also seen the emergence of interest in studying how field theory can help us in our quantum information and computational goals. For example, what restrictions does relativity place on our ability to quantum compute? From the other perspective, in what ways may relativity aid us in quantum computation beyond what could be achieved otherwise? Such questions fall within the broad category of what many call relativistic quantum information (RQI). This thesis includes aspects of both directions within this cross-collaborative communication. We perform multiple studies ascertaining the structure of vacuum entanglement and particle creation phenomena, as well as developing novel interpretations for such concepts. In the final chapter, for example, we precisely answer in physically concrete terms (in the opinion of the author) exactly what it means for half of an empty box to be full. We also develop several protocols, by the use of relativistic fields, of interest and importance for quantum information processing as well as quantum metrology [35, 36, 37]. This includes a novel and sustainable method for the generation and distribution of entanglement, and a proposal for the development of an extremely sensitive quantum seismograph, with potential (albeit highly tentative) applicability to gravitational wave astronomy. We also introduce the notion of utilizing environmental noise to actually assist in the generation of quantum correlations, rather than viewing it as an obstacle to be overcome. While we will not be discussing much in the way of gravity within this thesis, it is largely believed that gaining a better understanding of the relationship between information theory and relativistic quantum mechanics will play an essential role in uncovering the fundamental nature of quantum gravity.

The majority of this thesis will be focused on studying the vacuum state of a real scalar field. In this sense, what we study here is “nothing”, or at least as close to nothing as one can get. As was discussed above, however, there are some deeply interesting (and perhaps concerning) mathematical properties of this state and field theory in general that, if taken at face value, appear somewhat nonsensical. Primarily, we refer here to the questions of what exactly a particle is, if any exist, and (if so) where they exist. What does it mean for different observers to disagree on the particle content of the universe? Is this even a problem? Perhaps not; Robert Wald wrote [38]:

*“Indeed, I view the lack of an algorithm for defining a preferred notion of ‘particles’ in QFT in curved spacetime to be closely analogous to the lack of an algorithm for defining a preferred system of coordinates in classical general relativity. (Readers familiar only with presentations of special relativity based on the use of global coordinates might well find this fact to be alarming.) In both cases, the lack of an algorithm does not, by itself, pose any difficulty for the formulation of the theory.” - R. Wald*

Here we will opt to circumvent conventional interpretational problems by following an alternative approach to understanding these issues: that of *operationalism*, which is very much the unifying theme behind this entire thesis. In this context, to work operationally means to focus less on the mathematical facts that are derivable from a given theory (e.g. the presence of vacuum entanglement) and make efforts to answer what the actual physical consequences of this fact are (e.g. can we measure and perhaps utilize vacuum entanglement?). Our primary focus will therefore be on developing and using models of measurement and detection, in addition to proposing physical procedures by which the nature of these issues can be physically concreted. More than providing a straightforward and informative manner to do physics, such an approach also lends itself more naturally to discovering ways of experimenting on the given phenomena of interest.

In particular, a large portion of this thesis will be based on introducing a particle detector model and subsequently using it for a variety of studies. In this context, a “particle detector” is the generic name used to describe some quantum system(s) that we let interact in some manner with a field [21, 39, 40]. This represents a basic model of measurement, since in practice any measurement procedure must be performed by interacting one’s measurement device with the system of interest. For example such a model can include the electronic levels of an atom, which interact with the electromagnetic field. The particular response of a detector, resulting from its interaction with the field, then gives us information on the properties of the field. If the detector becomes excited then this would indicate the absorption of a quanta from the field. This therefore tells us that, at least from the perspective of the detector, a particle was present in whatever field state is under consideration. Such an approach therefore allows us to relegate questions of particle content or location to simply asking what a detector model actually sees. As Bill Unruh likes to put it (paraphrasing): “*A particle is that which a particle detector detects*”. Using particle detectors can furthermore give us operational insight into vacuum entanglement. It is known that two detectors locally interacting with a field for a short time, where they are far enough apart that they never come into causal contact, can become entangled through this procedure [41, 42, 43, 44, 4]. This is possible because the detectors are simply swapping some of the pre-existing vacuum entanglement out of the field, and many refer to such a procedure as vacuum *entanglement harvesting*. We will study multiple such protocols in this thesis.

Before continuing to the thesis outline, we should also mention the formalism of Gaussian quantum mechanics (GQM) [45]. This represents a restriction of continuous-variable quantum mechanics to a special class of states (namely, Gaussian states) and interactions (namely, quadratic). While limited in this respect, when applicable, it can be an extremely powerful computational tool that allows one to near-trivially solve otherwise intensive or

intractable problems. Fortunately, most of the questions of interest in this thesis fall within the realm of applicability of GQM, and because of this it is the primary computational formalism with which we perform our work.

## 1.2 Thesis outline

We will start in Part. [I](#) by providing much of the needed background and preliminary material that will be assumed knowledge throughout the rest of the thesis. This is split into the following three chapters:

- To begin, in [Ch. 2](#) we outline the definitions, importance, and methods of computing various measures of quantum correlations. Being the primary construct that will concern us, it will be of vital importance in understanding what quantum correlations are and how to compute how correlated a given quantum state is. In this chapter we will discuss both entanglement, in its various forms, as well as quantum discord: a measure of quantum correlations that goes beyond entanglement.
- In [Ch. 3](#) we will give an overview of the formalism and computational techniques of Gaussian quantum mechanics (GQM). When applicable, GQM can vastly simplify otherwise intensive quantum mechanical calculations. It is the principal computational framework that we will utilize throughout this thesis and, as we will see, allows us to perform tasks that are otherwise intractable.
- To finish the preliminaries, we will discuss in [Ch. 4](#) the basics of scalar quantum field theory with an emphasis on the concepts and phenomena that will be of interest to us. In this chapter and the previous a working knowledge of quantum mechanics and relativity is assumed.

In short: scalar quantum fields constitute the systems of interest with which we will work, quantum entanglement and more general measures of quantum correlations represent the primary aspects of these systems that we wish to investigate, and Gaussian quantum mechanics is the computational tool with which we will perform this investigation.

We will begin the main content of this thesis with Part. [II](#), which represents a large and primary portion of it. In this Part we develop and utilize a model particle-detector that has, within a range of circumstances, considerable advantages over the standard methods that are in wide use. In short, the difference between our model and the canonical one is that

we couple a harmonic oscillator to the field in question, rather than a two-level system. The key to this model is that by using an oscillator we are able to move to the realm of Gaussian quantum mechanics, a framework that allows us to perform computations otherwise impossible. In particular, with this formalism we need not use perturbation theory and may instead solve for the detector-field evolution exactly. This is markedly different from the standard, perturbative approach. With this, we are able to examine explicitly non-perturbative, relativistic quantum phenomena.

- We will start with Ch. 5, in which we introduce the setting within which the oscillator-detector formalism operates, derive the evolution equation that will be the primary tool for the remainder of Part. II, and describe its computational workings.
- In Ch. 6 we will present our first application of the oscillator-detector model, in which we study the Unruh effect within a cavity setting. Indeed we find that the detector experiences a thermal response of temperature proportional to the detector's acceleration. This work is important for several reasons. First, the Unruh effect is typically considered a free space phenomenon, and so observing that it similarly occurs in a cavity setting is a step towards understanding the phenomenon in generality, in addition to providing higher hope of experimental verification in the laboratory. Second, using the oscillator model we are able to not just compute the instantaneous response of the detector but also the non-perturbative thermalization behavior itself! Third, we demonstrate that the results are largely independent of the cavity specifics; namely with regards to its boundary conditions. All three of these points place the Unruh effect on considerably stronger footing, and suggest that it is in fact an extremely general and universal part of nature.
- In Ch. 7 we go on to consider the harvesting of vacuum entanglement by a set of oscillator detectors. In particular, in this study we consider three oscillators simultaneously interacting with the field, and we observe that they are able to become genuinely tripartitely entangled without ever coming into causal contact with one another. This demonstrates that, perhaps initially surprisingly, the vacuum state contains spatial tripartite entanglement that can be extracted. We go on to discuss the implications of our work.
- We then move on to consider the harvesting of more general quantum correlations in Ch. 8. That is, here we examine the extraction of both bipartite entanglement and discord from a field and, importantly, we generalize to the case that the field is in a thermal state rather than solely considering the vacuum. Surprisingly, we discover that the extractable entanglement and discord display very different behaviors as a

function of the field temperature. As would be expected, the entanglement rapidly decays as the temperature is increased. The quantum discord, conversely, can actually be *increased* very significantly by heating up the field. We go on to give various explanations of this phenomenon. This result makes one question the validity of discord as a reasonable measure of quantum correlations. On the other hand, it also suggests that within certain scenarios environmental noise may actually be *helpful* for the generation and utilization of quantum resources.

- In Ch. 9 we study the generation of entanglement via a quantum field from a somewhat different perspective. We consider a protocol in which detector pairs are continuously sent through a cavity field, each time injecting a fresh pair. Each cycle the interaction with the detectors causes a perturbation on the field state and, interestingly, we find that this evolution will eventually reach a fixed point that appears independent of the field's initial state. Furthermore, if in each cycle the detectors are allowed to have causal contact, this steady state is such that each pair exits the cavity having become entangled. Such a protocol therefore represents a means of continuously and sustainably generating entanglement by use of a cavity field, allowing for the aggregation of a computationally significant amount. Rather than entanglement harvesting, we refer to this process as *entanglement farming*.
- Finally, in Ch. 10 we extend the farming scenario to consider the case that there is a time delay in between cycles of detector-field interaction. We discover by doing this that there are regions of parameter space that are highly sensitive to system perturbations, such as a change in the length of the cavity. We propose to use this sensitivity for metrological purposes: by preparing one's system within such a parameter regime, then even a minute system disturbance results in a significant alteration of the protocol output. We demonstrate that this can be used as a type of ultra-sensitive quantum seismograph. We go on to discuss potential applications.

We will then move on in Part. III with another, previously introduced model of measurement in field theory. This model consists of assuming that an observer may perform a projective measurement onto some positive-frequency field mode (presumably a localized mode); a change of reference frame is then given as a change of coordinates with respect to which one represents this mode. With this we will discuss two studies into the nature of quantum correlations and particle creation.

- In Ch. 11 we utilize the projective measurement formalism to study the case of a single uniformly accelerating observer and compute their Unruh response due to

acceleration. However, unlike the canonical scenario in which the field is prepared in the inertial vacuum state, here we consider the case that the field is in a thermal state of some temperature. The observer will then experience a response from the field thermality in addition to a thermal Unruh response. One of the primary questions we wish to answer in this work is: can the observer distinguish between these two contributions? Previous work, based on faulty methodology, claimed that he or she could not do so. Our work demonstrates this to be false, and that such an observer can in fact distinguish between what are, in a sense, thermal and quantum fluctuations. Given our results, we question the use of acceleration as a metrological tool for the measurement of ultra-cold temperatures.

- In Ch. 12 we will study the degradation of quantum correlations (both entanglement and discord) that occurs between two observers when one of those observers is uniformly accelerating. This is a prototypical and fairly seminal scenario within RQI. Unfortunately, most of the initial works on the topic made (among other erroneous assumptions) the mistake of considering entanglement between field modes that are globally spread throughout space. Clearly this is not physically realistic in any real-world measurement scenario, but it was hoped that the obtained results would qualitatively hold when considering local modes instead. As we demonstrate in Ch. 12, this is not the case. In fact, when using local modes the degradation of correlations is qualitatively worse than when using global modes.

Continuing, we finish in Part. IV with a single chapter. This chapter is, in the opinion of the author, the most important and conceptually satisfying of this thesis.

- In Ch. 13, we will return to the interpretationally challenging fact that, in some mathematical sense, half of an empty box is full. In this chapter we will use a local quantization scheme to explicitly compute the reduces states of two sides of a cavity vacuum field, and the correlations between them. We will then consider the scenario in which a mirror is very rapidly placed between these two regions. By doing so, we reveal that the “particles” present in the vacuum state are mathematically equivalent to the real particles dynamically generated by the act of introducing the mirror. In this way we physically concrete what it means for half of an empty box to be full: this is just a mathematical statement that introducing a mirror creates particles, a phenomenon which is physically unsurprising and not at all mysterious. We furthermore promote such a procedure as a way of, for the first time, experimentally demonstrating the existence of vacuum entanglement in the laboratory.

We end in Ch. 14 with a summary of our work and some concluding remarks.

**Part I**

**Preliminaries**



If put into one sentence, this thesis uses the tools of Gaussian quantum mechanics (GQM) to study the nature of quantum correlations within the framework of scalar quantum field theory. As such, before continuing to the main body, we will devote this Part to outlining the necessary concepts from each of these three topics.

First, in Ch. 2 we discuss the notion of quantum correlations; their importance to physics, how they are defined, and how they are quantified. This will principally include quantum entanglement. We will introduce entanglement in both bipartite and tripartite quantum systems, and in both pure and mixed states. We will additionally present what is called the quantum discord, which is a purported type of quantum correlation that may be present even in the absence of entanglement. As an aside we will discuss in what way entanglement and discord are related to each other, by using material from [9].

Second, in Ch. 3 we introduce the formalism of GQM and study in detail its aspects most important to our exposition, including the evaluation of quantum correlation measures for Gaussian states. When applicable, the computational ease of GQM can vastly simplify otherwise challenging calculations. Fortunately, throughout this thesis we work in regimes in which GQM applies, and it will therefore represent our instrument of choice.

Third, in Ch. 4 we give a comprehensive overview of scalar field theory as it applies to this thesis. This includes a discussions of Bogoliubov transformation (and their formulation within a Gaussian framework), as well as detailed overviews of particle-detectors, the Unruh effect, and vacuum entanglement (not the topics you find in a standard QFT textbook).

# Chapter 2

## Quantum correlations

In this chapter we give an introductory description of quantum correlations, including the well known quantum entanglement as well as the relatively newer quantum discord, purported to be a more general form of quantum correlation.

### 2.1 Entanglement

We first discuss quantum entanglement [22], a concept that is central to nearly all of this thesis. Put simply, entanglement is a property of composite quantum systems and refers to a specific type of correlation between their constituents. By correlation, I am referring to correlation displayed in the statistics of local measurement outcomes. The presence of entanglement, however, implies the presence of purely quantum mechanical correlations that, critically, are quantitatively stronger than any correlation possible within classical probability theory. In particular, entangled states include those for which measurement statistics violate Bell's inequality [46, 47]. This result leads to Bell's theorem [48], which takes seriously the original EPR argument [49] and demonstrates that if quantum mechanics functions via classical hidden variables then these variables must necessarily be nonlocal. Entanglement is, therefore, of extreme fundamental importance. Its existence demonstrates that we must discard one of two basic beliefs about nature: we must either give up the notion that there exists an objective, ontological reality or we must accept that there are physical processes that act in an unboundedly nonlocal manner.

In addition to our fundamental understanding of nature, entanglement has furthermore become of central importance to quantum information and computation science. In the past

two decades it has become understood as a resource, one that must be produced and which can then be used to perform tasks. Critically, in order to create entanglement between two systems it is required that those systems interact either directly with each other or indirectly via transmission of a quantum carrier. Put another way, entanglement cannot be created or increased through local operations and classical communication (LOCC). This means that it is generally difficult to distribute between parties, and novel approaches to entanglement distribution will be a common theme throughout this thesis. If two parties share an entangled state, however, it can be utilized for a plethora of quantum computation and communication tasks, and indeed is the primary quantum ingredient in many of the better-than-classical computational algorithms that have made quantum information and computation the booming field that it is today. Examples of well-known protocols that utilize entanglement include quantum key distribution [50, 51, 52], dense coding [53], and quantum teleportation [54].

### 2.1.1 Pure state entanglement

We will first describe bipartite entanglement in the case that the global quantum state is pure. That is, we are given some pure state on a joint Hilbert space  $|\psi\rangle \in \mathcal{H}_A \otimes \mathcal{H}_B$ , representing the state of quantum system consisting of two distinct subsystems or sets of degrees of freedom. A typical scenario to consider is one in which two agents, Alice and Bob, possess each one of these subsystems (e.g. each may possess a qubit, in which case  $|\psi\rangle$  would be some two-qubit state). The joint state  $|\psi\rangle$  may display correlations between the two subsystems, in the sense that the outcomes of single-shot measurements performed by Alice and Bob on their individual systems will be correlated. If a joint state contains *no* correlations, this means that it can be represented as a tensor product state of the two reduced states on Hilbert spaces  $\mathcal{H}_A$  and  $\mathcal{H}_B$ . In the case of global pure states this condition is equivalent to the state being separable, defined to mean without entanglement. That is, a pure, separable state  $|\psi\rangle$  can be written in the form

$$|\psi\rangle = |\psi\rangle_A \otimes |\psi\rangle_B, \quad \text{separable.} \quad (2.1)$$

This is the case in which Alice simply possesses state  $|\psi\rangle_A$  and Bob the statistically independent state  $|\psi\rangle_B$ . If a pure state cannot be written in this form, then it is entangled. A simple example of an entangled state is the two-qubit Bell state  $|\Phi^+\rangle = (|00\rangle + |11\rangle)/\sqrt{2}$ , where we make use of the notation  $|00\rangle \equiv |0\rangle_A \otimes |0\rangle_B$  and  $|11\rangle \equiv |1\rangle_A \otimes |1\rangle_B$ . There is no local change of basis that will bring  $|\Phi^+\rangle$  to a product state of the form Eq. (2.1), and it is therefore an entangled state.

At times, however, especially when dealing with higher dimensional systems, it is not always obvious from observation whether or not a bipartite state is entangled. Given local bases  $\{|i\rangle_B\}$  and  $\{|j\rangle_B\}$  of local Hilbert spaces  $\mathcal{H}_A$  and  $\mathcal{H}_B$  respectively, each of some given dimension, a general pure state on the joint system  $\mathcal{H}_A \otimes \mathcal{H}_B$  takes the form

$$|\psi\rangle = \sum_{ij} c_{ij} |ij\rangle. \quad (2.2)$$

This state is therefore separable iff the coefficient matrix is decomposable into an outer product  $c_{ij} = c_i c_j$ . To find a simple, consistent method for checking this condition let us take advantage of the fact that for any such state there exists a pair of bases  $\{|\tilde{i}\rangle_A\}$  and  $\{|\tilde{j}\rangle_B\}$  such that the state takes the form

$$|\psi\rangle = \sum_i \sqrt{p_i} |\tilde{i}\tilde{i}\rangle. \quad (2.3)$$

This is known as the Schmidt decomposition of the state  $|\psi\rangle$ , and the number of non-zero probabilities  $p_i$  is referred to as its Schmidt rank. We see therefore that  $|\psi\rangle$  is separable iff its Schmidt rank is 1. Critically, this criterion also implies that it is separable iff the reduced states on  $\mathcal{H}_A$  and  $\mathcal{H}_B$  are pure, meaning that their density matrices are of rank-1. To see this, recall that the reduced state on  $\mathcal{H}_A$  is given by the partial trace  $\hat{\rho}_A = \text{Tr}_B(|\psi\rangle\langle\psi|) = \sum_j \langle j_B|\psi\rangle\langle\psi|j_B\rangle$ , where the trace is taken over any chosen basis of  $\mathcal{H}_B$ . The reduced state  $\hat{\rho}_B$  is computed similarly. Taking the partial trace of Eq. (2.3) we see immediately that

$$\hat{\rho}_A = \sum_i p_i |\tilde{i}\rangle\langle\tilde{i}|. \quad (2.4)$$

Thus, as claimed, the state  $|\psi\rangle$  is separable iff  $\hat{\rho}_A$  is rank-1. A density matrix of rank greater than one represents what is referred to as a mixed state, meaning that there is classical uncertainty regarding in what quantum state one's system actually resides. A state that is not mixed is called pure. Thus, the pure state  $|\psi\rangle$  is entangled iff the reduced state  $\hat{\rho}_A$  is mixed. Note that the spectrum  $\{p_i\}$  of  $\hat{\rho}_B$  will be equivalent to that of  $\hat{\rho}_A$ , and thus it does not matter which reduced state is considered. This therefore provides a simple criterion for checking whether or not a pure, bipartite state is entangled or not, because mixedness is easily checked independent of basis, and one does not need to perform a Schmidt decomposition. For example both the criteria  $\hat{\rho}_A^2 \neq \hat{\rho}_A$  and  $\text{Tr}(\hat{\rho}_A^2) < 1$  are necessary and sufficient for mixedness, and thus for  $|\psi\rangle$  to be entangled.

We now have a criterion for determining the existence of bipartite entanglement in a pure state. We would like, however, to also have quantitative measure with which we can

answer the question of “how much” entanglement we have. For pure states this is equivalent to how mixed the reduced states are, for which we use the von Neumann entropy

$$S(A) = S(B) = -\text{Tr}(\hat{\rho}_A \log \hat{\rho}_A) = -\sum_i p_i \log p_i, \quad (2.5)$$

where, unless otherwise specified, we use  $\log \equiv \log_2$ . Here and throughout this thesis we will be making use of the notation  $S(A) \equiv S(\hat{\rho}_A)$  and  $S(B) \equiv S(\hat{\rho}_B)$ . The reduced entropy is a natural measure of entanglement for pure states. Note that it is zero iff  $|\psi\rangle$  is separable. On the other hand, we note that  $S(A)$  is maximized when the spectrum of  $\hat{\rho}_A$  is uniform  $p_i = 1/d_A$ , where  $d_A$  is the dimension of  $\mathcal{H}_A$ . Equivalently, the reduced state takes the form  $\hat{\rho}_A = I/d_A$ , and in this case  $\hat{\rho}_A$  is called maximally mixed. Its entropy in this case is  $S(A) = \log d_A$ . A bipartite state  $|\psi\rangle$  contains the most entanglement possible, and is referred to as maximally entangled, if its reduced states are maximally mixed. The Bell state  $|\Phi^+\rangle = (|00\rangle + |11\rangle)/\sqrt{2}$ , for example, is a maximally entangled two-qubit state with  $S(A) = 1$ .

### 2.1.2 Mixed state entanglement

Let us now generalize to the case of global mixed states, i.e. where the bipartite state shared by Alice and Bob is generally represented by some density operator  $\hat{\rho}_{AB}$ . In this case, how does one define separability? As discussed previously, a critical aspect of entanglement is that it cannot be created or increased via LOCC. A natural definition of separability is thus provided by stating that a separable state is one that can be created purely through LOCC. It is straightforward to see that this is equivalent to the set of states in which, with probability  $p_k$ , Alice and Bob locally prepare some states  $\hat{\rho}_k^A$  and  $\hat{\rho}_k^B$ , respectively. That is, a general separable state is one that can be represented as a convex combination of product states

$$\hat{\rho}_{AB} = \sum_k p_k \hat{\rho}_k^A \otimes \hat{\rho}_k^B, \quad \text{separable.} \quad (2.6)$$

We see that in case of pure states this definition reduces to that of Eq. (2.1). Before continuing to discuss more general measures of entanglement, it is important to note that for globally mixed states the reduced entropies are *not* measures of entanglement, and will generally be non-zero even for separable states. This is unsurprising, since for example the mixed product state  $\hat{\rho}_{AB} = \hat{\rho}_A \otimes \hat{\rho}_B$  clearly has mixed reduced states and yet displays no correlations. This leads to another important point, however, in that globally mixed

states can be separable yet still contain correlations. To this end we introduce the mutual information:

$$I(A, B) = S(A) + S(B) - S(A, B), \quad (2.7)$$

where  $S(A, B) \equiv S(\hat{\rho}_{AB})$ . This represents an entropic measure of the total correlation between the two systems. For globally pure states this clearly reduces to  $I(A, B) = I(|\psi\rangle\langle\psi|) = 2S(A)$ , and thus vanishes iff the state is separable. That is, a pure state is correlated iff it is entangled. For globally mixed states, however, this is not the case. The mutual information vanishes,  $I(A, B) = 0$ , iff we have a product state  $\hat{\rho}_{AB} = \hat{\rho}_A \otimes \hat{\rho}_B$ . A convex combination of product states, i.e. separable states in general, will have non-zero mutual information and will display correlations between measurement outcomes.

Returning now to mixed state entanglement itself, we must discuss how one can determine if a general state is entangled (it is not always easy from observation alone to determine if a state can be put into the form of Eq. (2.6)) and, as much as possible, how to quantify this entanglement. We will begin with the simplest criterion for determining the existence of entanglement. This is known as the Peres-Horodecki or the positive partial transpose (PPT) criterion [55, 56]. To introduce it, let us first recall the definition of the partial transpose. If we have a general bipartite states of the form

$$\hat{\rho}_{AB} = \sum_{ijkl} c_{ijkl} |i\rangle\langle j| \otimes |k\rangle\langle\ell|, \quad (2.8)$$

then the partial transpose acting on this state (where here we will choose to apply the transpose to the second system) is defined as

$$\hat{\rho}_{AB}^{\Gamma_B} = \sum_{ijkl} c_{ijkl} |i\rangle\langle j| \otimes (|k\rangle\langle\ell|)^T = \sum_{ijkl} c_{ijkl} |i\rangle\langle j| \otimes |\ell\rangle\langle k|. \quad (2.9)$$

Given this, the PPT criterion states that if  $\hat{\rho}_{AB}$  is separable then  $\hat{\rho}_{AB}^{\Gamma_B}$  is positive semi-definite. That is, if  $\hat{\rho}_{AB}^{\Gamma_B}$  has at least one negative eigenvalue, then  $\hat{\rho}_{AB}$  is entangled. Importantly, in the case that the dimension of  $\mathcal{H}_A \otimes \mathcal{H}_B$  is less than or equal to 6 (e.g. two qubits) then the reverse implication also holds. Namely, for  $2 \times 2$  and  $2 \times 3$  dimensional systems  $\hat{\rho}_{AB}$  is separable iff  $\hat{\rho}_{AB}^{\Gamma_B}$  is positive semi-definite. For higher dimensional systems, unfortunately, a positive semi-definite partially transposed state is not necessarily separable. In this case, any entanglement not witnessed by this criterion is referred to as bound entanglement [57].

This criterion also leads to a measure of mixed-state entanglement which, while of questionable quantitative meaning, is useful in that it is very easily computable (unlike

more rigorously defined measures that we discuss below). This measure is referred to as the negativity of the state in question,  $\mathcal{N}(A, B)$ , and is defined as the absolute value of the sum of the negative eigenvalues of  $\hat{\rho}_{AB}^{\Gamma_B}$  [58]:

$$\mathcal{N}(A, B) = \sum_{\lambda_i^{\Gamma_B} < 0} |\lambda_i^{\Gamma_B}|, \quad \lambda_i^{\Gamma_B} \in \text{spec}(\hat{\rho}_{AB}^{\Gamma_B}). \quad (2.10)$$

Importantly, this measure has the property that it is non-increasing under LOCC, an essential characteristic of any reasonable measure of entanglement. In general, a quantity that satisfies this can be referred to as an entanglement monotone. A secondary monotone that derives from the PPT criterion is referred to as the logarithmic negativity  $E_N(A, B)$ , and can be defined in terms of the negativity as [58, 59]

$$E_N(A, B) = \log(2\mathcal{N}(A, B) + 1). \quad (2.11)$$

The advantage of the logarithmic negativity is that it satisfies the condition of being additive under tensor products. That is, if we consider four subsystems  $A$ ,  $B$ ,  $C$ , and  $D$ , where the joint state of these systems is a product state of the form  $\hat{\rho}_{AB} \otimes \hat{\rho}_{CD}$  (i.e. there are no correlations between  $AB$  and  $CD$ ) then the total logarithmic negativity in the system is just the addition of that in  $AB$  and in  $CD$ :  $E_N(\hat{\rho}_{AB} \otimes \hat{\rho}_{CD}) = E_N(A, B) + E_N(C, D)$ .

Although the negativity and logarithmic negativity are entanglement monotones, they unfortunately do not represent in any operational manner “how much” entanglement there is in a system. Given their ease of computation they will constitute the primary measure by which we quantify entanglement in this thesis, but it is important to keep in mind this limitation. Although we will not be directly using them, it is worth pointing out two other more operationally defined measures of entanglement. Unfortunately, for anything beyond two qubits they are generally extremely difficult to actually compute. These two measures are the entanglement of formation  $E_F(A, B)$  [60, 61] and the distillable entanglement  $E_D(A, B)$  [62]. The entanglement of formation quantifies how many maximally entangled, pure state Bell pairs must be utilized in order to convert them into  $\hat{\rho}_{AB}$  through LOCC. On the other hand, the distillable entanglement quantifies how many such Bell pairs can be obtained through LOCC starting with the state  $\hat{\rho}_{AB}$ . Both of these measures reduce to the reduced entropy  $S(A)$  in the case of pure states. Importantly, the two measures are not generally equivalent, rather they satisfy  $E_D \leq E_F$ . That is, in general less Bell pairs can be distilled from a state than the number of pairs that went into making it. The entanglement that cannot be distilled is, as mentioned above, referred to as bound entanglement and is not registered by the PPT criterion.

### 2.1.3 Multipartite entanglement

To finish our introduction to entanglement we will briefly discuss the notion of multipartite entanglement, the structure of which is generally much more complex than that of bipartite entanglement. Let us consider an  $n$ -partite system, meaning that we have split the Hilbert space of our system in question into a product of  $n$  constituent parts,  $\mathcal{H} = \mathcal{H}_1 \otimes \dots \otimes \mathcal{H}_n$ . We begin with the definition of a fully separable state across this ensemble, meaning a state in which no bipartition between any two subsets of the  $n$  constituents contains entanglement. Extending the definition of separability in Eq. (2.6), such a state can always be locally put into the form of a convex combination of product states

$$\hat{\rho} = \sum_k p_k \hat{\rho}_k^{(1)} \otimes \dots \otimes \hat{\rho}_k^{(n)}. \quad (2.12)$$

This represents the set of states that can be constructed via LOCC among  $n$  parties.

On the opposite end of the spectrum is a state which exhibits full,  $n$ -partite entanglement. By definition, such a state is entanglement across all bipartite partitions of the whole system. In the case of global pure states this corresponds to obtaining a mixed state upon taking any possible partial trace. In this thesis we will consider tripartitely entangled states, but no higher. Importantly, there are known to be two inequivalent classifications of genuinely, tripartitely entangled states. Restricting ourselves to three qubits, these two states are known as the GHZ state [63]

$$|GHZ\rangle = \frac{1}{\sqrt{2}}(|000\rangle + |111\rangle), \quad (2.13)$$

and the W state

$$|W\rangle = \frac{1}{\sqrt{3}}(|001\rangle + |010\rangle + |100\rangle). \quad (2.14)$$

These states are representatives to two inequivalent classes of tripartite entanglement, in the sense that it is impossible to transform one such state to the other by LOCC [64]. The key difference that can be observed between these two states is that in the GHZ state no two pairs of qubits are entangled upon tracing out the third (i.e. the entanglement present is fully a property of the three qubits combined), whereas in the W state every pair of qubits among the three do display bipartite entanglement with each other (i.e. the entanglement is concentrated in the bipartite links).

There are in addition states which are partially separable, and partially entangled, in the sense that there is entanglement present in the system but is not of a multipartite



nature. A trivial three-qubit example of such a state is  $|0\rangle|\Phi^+\rangle$ , where  $|\Phi^+\rangle$  is a two-qubit bell state. Clearly there is no entanglement across the bipartition isolating the first qubit, and thus this state is not tripartitely entangled. Although concrete measures of multipartite entanglement have been developed, we will not require such measures in this thesis and will therefore not discuss them; the interested reader is referred to [65, 22].

## 2.2 Quantum discord

In this section we discuss the quantum discord, which is a measure proposed to quantify quantum correlations that in general extend beyond entanglement [29, 30]. While in the case of a pure state the entanglement does provides a complete enumeration of quantum correlations (indeed for pure states the discord reduces to the entanglement entropy), it is now understood that in a mixed quantum state there can exist quantum correlations, in the sense that its joint-measurement statistics cannot be described by classical probability theory, even if the state in question is separable. The quantum discord [29], along with several other proposed measures [30], purport to quantify these generalized quantum correlations. In addition to being of theoretical interest [66, 67, 9, 68], discord has also received considerable attention regarding its potential as a quantum computational resource in the absence of entanglement [31, 32, 69, 70, 71, 72]. While the full utility of discord is still far from certain, and many of the protocols discovered have been criticised as being either highly construed and not very useful or in reality utilizing entanglement in an unobvious way, there are inarguably several examples of discord being a genuinely useful quantum resource. A prime example of this is the realization in [33, 34], and the recent experimental demonstration in [73], that quantum discord quantifies the amount of distillable entanglement generated between a system and a measurement apparatus upon performing a local measurement.

The discord  $D(A, B)$  is an entropic measure of the quantumness of correlations between  $A$  and  $B$ , given state  $\hat{\rho}_{AB}$ , where such quantumness is characterized by the impossibility to both locally access information about  $A$  by measurement on  $B$  and to obtain it without modifying the state of the system. We start by recalling the definition of the mutual information Eq. (2.7).  $I(A, B)$  is a measure of the total correlations between the bipartition  $A$  and  $B$ , both quantum and classical. We can also give an alternative definition of the mutual information that takes the form

$$J(A, B) \equiv S(A) - S(A|B), \tag{2.15}$$

where  $S(A|B)$  is the conditional entropy of system  $A$  given a determination (i.e. a measurement) on system  $B$ . In classical probability theory the conditional (Shannon) entropy  $H(X|Y)$  of two random variables  $X$  and  $Y$  is defined as the average entropy of  $X$  given a determination of  $Y$ :  $H(X|Y) = \sum_y p_y H(X|Y = y)$  where  $p_y$  is the probability of  $Y$  taking the value  $y$ . Classically, Bayes' rule implies that the two definitions of mutual information are equivalent.

The quantum discord is defined to be the difference between these classically equivalent quantities,  $D(A, B) \equiv I(A, B) - J(A, B)$ . The fact that this can be nonzero in the quantum regime comes from the way that we define the quantum conditional entropy, which involves a measurement over  $B$ . As is well known, measurement in quantum mechanics is operationally very different from the classical notion of measurement as merely an update of knowledge. The definition of quantum mutual information should follow similarly to its classical counterpart, and to this end we define a quantity

$$S(A|B)_{\{\Pi_j\}} \equiv \sum_j p_j S(\hat{\rho}_{A|\Pi_j}), \quad (2.16)$$

where  $\{\hat{\Pi}_j\}$  is a positive operator valued measure (POVM) performed on system  $B$  and  $p_j \equiv \text{Tr}(\hat{\Pi}_j \hat{\rho}_B)$  is the probability of outcome  $j$ .  $S(\hat{\rho}_{A|\Pi_j})$  is the entropy of the post-measured state  $\hat{\rho}_{A|\Pi_j}$  on  $A$  given that outcome  $j$  was achieved. This state is given by the reduction  $\hat{\rho}_{A|\Pi_j} = \text{Tr}_B(\hat{\rho}_{AB|\Pi_j})$  to  $A$  of the global post-measured, post-selected state  $\hat{\rho}_{AB|\Pi_j} = p_j^{-1}(\hat{I}_A \otimes \hat{M}_j)\hat{\rho}_{AB}(\hat{I}_A \otimes \hat{M}_j^\dagger)$ , where the set  $\{\hat{M}_j\}$  consists of the measurement operators that define the POVM  $\hat{\Pi}_j = \hat{M}_j^\dagger \hat{M}_j$ .

It is this definition of  $S(A|B)_{\{\Pi_j\}}$  that we will use in Eq. (2.15). The quantity  $J(A, B)$  is thus to be thought of as a measure of classical correlation, telling us how much we are able to learn about system  $A$  from a measurement on system  $B$ . The discord  $D(A, B) = I(A, B) - J(A, B)$  therefore is what one is left with upon subtracting the classical correlation away from the total correlations. The remainder is interpreted as being of a purely quantum nature.

Critically, however, the conditional entropy as given by Eq. (2.16) depends on our choice of measurement. To ensure that the discord only picks up correlations that are quantum we should choose the measurement that minimizes this quantity; thereby giving us the definition of quantum discord

$$\begin{aligned} D(A, B) &\equiv I(A, B) - J(A, B) \\ &= S(B) - S(A, B) + \inf_{\{\Pi_j\}} S(A|B)_{\{\Pi_j\}}. \end{aligned} \quad (2.17)$$

The measurement on  $B$  that achieves this minimization is the one for which we learn the most we possibly can about  $A$ . Whatever uncertainty is left in  $A$  must therefore be due to the quantumness of the correlations, as opposed to simply a bad choice of measurement. Without this minimization we risk including classical correlations in our measure.

For pure states the entanglement entropy  $S(A) = S(B)$  provides a complete measure of quantum correlations, and fortunately the discord is straightforwardly shown to reduce to  $D(A, B) = S(B)$  for pure states. Another property worth noting is that in general the discord is not symmetric,  $D(A, B) \neq D(B, A)$ . One consequence of this is that a state with zero discord in the one case may not be zero in the other. A state has zero discord in the sense that  $D(A, B) = 0$  iff the state takes the form

$$\hat{\rho}_{AB} = \sum_k p_k \hat{\rho}_k^A \otimes |k\rangle_B \langle k|_B, \quad (2.18)$$

where  $\{|k\rangle_B\}$  form an orthonormal basis on  $B$ ,  $\{\rho_k^A\}$  are a set of density operators (not necessarily rank-one or orthogonal) on  $A$  and  $\sum_k p_k = 1$ . Such a state is referred to as being quantum-classical, and has zero quantum correlations from the perspective of measurement on  $B$ . Notice that the condition necessary for  $D(A, B) = 0$  is more restrictive than the condition for  $\hat{\rho}_{AB}$  to be separable, Eq. (2.6). We can therefore have mixed states that are void of entanglement but nevertheless contain quantum correlations as witnessed by nonzero discord. A state that is completely devoid of quantum correlations,  $D(A, B) = D(B, A) = 0$  can be locally put into the form  $\hat{\rho}_{AB} = \sum_k p_k |k\rangle_A \langle k|_A \otimes |k\rangle_B \langle k|_B$ , where on each system the set  $\{|k\rangle\}$  are orthogonal. This gives us a good intuitive idea of how it is possible for a state to have quantum correlations despite being separable; a completely classical state is one for which the correlations can be described by classical probability. In general, non-orthogonality within a mixture still allows correlation structures not captured by classical probabilities, even if they do not imply entanglement.

Unfortunately the minimization over measurements necessary to compute the discord can be very difficult or impossible to actually perform the minimization for even moderately sized systems [74]. Often authors have limited themselves to minimizing over projective valued measurements (PVMs) rather than over all possible POVMs, but even so it can often not be done. Of particular interest to us is the notion of Gaussian quantum discord [75], which we will discuss in the next chapter.

## 2.3 Aside: Discord as a bipartite manifestation of tripartite entanglement

Note: this section derives from the work [9], in collaboration with Eric J. Webster, Eduardo Martín-Martínez, and Achim Kempf.

Here we will take the opportunity to discuss some connections between the presence of discord in a separable state  $\hat{\rho}_{AB}$  and the structure of both bipartite and tripartite entanglement within this state's purification  $|\psi\rangle_{ABC}$ <sup>1</sup>. We propose to regard bipartite discord not as, in some sense, a competitor to entanglement. Instead, we propose to view discord as being a manifestation of entanglement, namely multipartite entanglement in the purified system. We also conjecture, although we do not pursue it here, that there similarly may exist natural and potentially useful notions of  $n$ -partite discord for  $n > 2$ , which in turn can be expressed in terms of  $n$  and  $n + 1$  partite entanglement of a larger system. This may even help elucidate the structure of multipartite entanglement in general.

Our primary results are as follows: we show that the presence of discord in any separable bipartite state of any system  $AB$  requires the presence of *both* bipartite and tripartite entanglement in the purification  $ABC$ . Indeed, we show that tripartite entanglement is required for *any* correlations in  $AB$ , quantum or classical. Then for the correlations in  $AB$  to be quantum we show that, in addition to the tripartite entanglement, bipartite entanglement in  $AC$  and/or  $BC$  is required. More precisely,  $AC$  entanglement creates  $D(A, B)$  discord and  $BC$  entanglement creates  $D(B, A)$  discord.

We first give a simple and general proof of our primary result. We will start by showing the requirement of bipartite entanglement in  $AC$  or  $BC$ , and in particular we will see that the presence of a quantum-classical or classical-quantum state is directly related to where such bipartite entanglement is located. That is, if the subsystem  $AC$  is separable, then  $D(A, B) = 0$  and if  $BC$  is separable, then  $D(B, A) = 0$ . To show this, we make use of a powerful formula for  $D(A, B)$  given by [76]:

$$D(A, B) = E_F(A, C) - E_F(AB, C) + E_F(AC, B), \quad (2.19)$$

---

<sup>1</sup>We refer here to the fact that any mixed state may be represented as the reduction of a pure state on a larger Hilbert space. That is, for some  $\hat{\rho}$  acting on Hilbert space  $\mathcal{H}_A$  there always exists another Hilbert space  $\mathcal{H}_B$  and a pure state  $|\psi\rangle \in \mathcal{H}_A \otimes \mathcal{H}_B$  such that  $\hat{\rho} = \text{Tr}_B(|\psi\rangle\langle\psi|)$ . This is easily seen since any pure state can be represented as a Schmidt decomposition, and thus any  $\hat{\rho} = \sum_i \lambda_i |i\rangle\langle i|$  will have a purification  $|\psi\rangle = \sum_i \sqrt{\lambda_i} |i\rangle \otimes |i\rangle$ . Notice that the dimension of the ancilla system  $\mathcal{H}_B$  must be at least as large as the rank of  $\hat{\rho}$ . Also note that the purification of a given state is not unique, since applying any local unitary on the ancilla system will produce another purification. In this section, we take the two-qubit space  $\mathcal{H}_{AB}$  to be the system acted on by our density operator, and  $\mathcal{H}_C$  we take to be the purifying ancilla system

where  $E_F$  is the entanglement of formation and, for example,  $E_F(AB, C)$  is the entanglement between system  $C$  and the combined system  $AB$ . Similarly, we have

$$D(A, C) = E_F(A, B) - E_F(AC, B) + E_F(AB, C).$$

Together these yield

$$D(A, B) + D(A, C) = E_F(A, C) + E_F(A, B),$$

however in our case we are considering systems  $AB$  that are separable, and so  $E_F(A, B) = 0$ . Thus, if  $AC$  is also separable this implies  $D(A, B) + D(A, C) = 0 \implies D(A, B) = 0$ , since discord is always non-negative. An analogous argument can be made for the  $BC$  separable case.

Secondly, we can show that lack of genuine tripartite entanglement in the pure state  $|\psi\rangle_{ABC}$  implies that there are no correlations between  $A$  and  $B$ <sup>2</sup>. In order for  $|\psi\rangle_{ABC}$  to be genuinely tripartitely entangled it is necessary and sufficient that all three bipartitions  $(AB)C$ ,  $(AC)B$ , and  $A(BC)$  be entangled. Since the state on  $AB$  is assumed mixed we have that there *is* entanglement in the bipartition  $(AB)C$ . Thus in order for tripartite entanglement to *not* be present it must be that at least one of the other bipartitions is separable. With out loss of generality let us assume that  $A(BC)$  is separable, meaning that the purified state can always be put in the form

$$|\psi\rangle_{ABC} = |\psi\rangle_A \otimes \sum_i \sqrt{p_i} |i\rangle_B \otimes |i\rangle_C. \quad (2.20)$$

The reduced state on  $AB$  is thus trivially

$$\hat{\rho}_{AB} = |\psi\rangle_A \langle\psi|_A \otimes \sum_i p_i |i\rangle_B \langle i|_B, \quad (2.21)$$

which is clearly uncorrelated, neither quantumly nor classically.

We thus have a simple proof of a quite general result: the presence of any correlation in the separable, mixed system  $\hat{\rho}_{AB}$  requires its purification  $|\psi\rangle_{ABC}$  to be tripartitely entangled, and if one wishes those correlations to have any quantum nature this further requires that the purification also contains bipartite entanglement.

It should be noted that this implication does not in general occur in the opposite direction. Namely, if a state on  $AB$  is uncorrelated this does *not* imply that the state's

---

<sup>2</sup>This proof was pointed out to us by Nicolai Friis and Marcus Huber

purification will be without either tripartite or bipartite entanglement. A simple example of this is any product state in which both  $A$  and  $B$  are mixed:  $\hat{\rho}_{AB} = \hat{\rho}_A \otimes \hat{\rho}_B$ . Clearly this state has neither classical nor quantum correlations. Purifying this state is trivially achieved by purifying  $\hat{\rho}_A$  and  $\hat{\rho}_B$  individually such that the purifying addition  $C$  has the same dimension as  $AB$ . This pure state is trivially seen to contain both bipartite and tripartite entanglement.

We will also discuss our findings in simple systems and examine the relationships between discord and purified entanglement in more detail. To this end, we will examine states of three qubits and states of three-mode Gaussian states. In these simple scenarios all calculations can be done explicitly and this allows us to show, among other interesting insights, that the property just proven above is not only sufficient but also necessary. That is, not only does the lack of bipartite or tripartite entanglement imply vanishing discord in the reduced state, but vanishing discord in the reduced state also implies that there is either no bipartite or no tripartite entanglement in the purification. The case of three-mode Gaussian states will be discussed in the next chapter.

Here, however, we will specialize to the case of two qubits that are in a rank-2 state  $\hat{\rho}_{AB}$ , such that its purification  $|\psi\rangle_{ABC}$  will consist of only one extra qubit  $C$ . As above, we further require the state  $\hat{\rho}_{AB}$  to be separable because we want to understand how the presence of discord between  $A$  and  $B$  is to be understood in terms of the entanglement structure of the purified system. If we were to allow entanglement between  $A$  and  $B$  then this would trivially imply nonzero discord. There would therefore be no necessary conditions on the purified system to ensure the presence of discord. In this scenario we will see that the requirement of both tripartite and bipartite entanglement in  $|\psi\rangle_{ABC}$  is both necessary and sufficient for the presence of discord in  $\hat{\rho}_{AB}$ .

To this end we can write the most general (up to relative phases) two-qubit, rank-2, separable state as

$$\hat{\rho}_{AB} = q |0\rangle\langle 0| \otimes |0\rangle\langle 0| + (1 - q) |\alpha\rangle\langle \alpha| \otimes |\beta\rangle\langle \beta|, \quad (2.22)$$

where  $0 < q < 1$  and

$$|\alpha\rangle \equiv \cos(\pi\alpha/2) |0\rangle + \sin(\pi\alpha/2) |1\rangle, \quad (2.23)$$

$$|\beta\rangle \equiv \cos(\pi\beta/2) |0\rangle + \sin(\pi\beta/2) |1\rangle \quad (2.24)$$

are real combinations of the basis states  $|0\rangle$  and  $|1\rangle$ . We don't consider the cases when  $q = \{0, 1\}$  because then  $\hat{\rho}_{AB}$  will be a (pure) product state and thus will trivially have zero discord. Note that we don't lose any generality by choosing the first projector to be

$|0\rangle\langle 0| \otimes |0\rangle\langle 0|$ . Also note however that we *have* lost generality by not including a relative phase between the two terms and by assuming that  $|\alpha\rangle$  and  $|\beta\rangle$  are *real* combinations of the basis vectors. This exclusion will not affect the primary result presented here, as will be explained below.

We now ask under what circumstances  $\hat{\rho}_{AB}$  contains discord. Recall that the discord  $D(A, B)$  when  $B$  performs the required measurement is not generally equivalent to the discord  $D(B, A)$  when  $A$  performs the measurement. Indeed one can be zero while the other is nonzero. Clearly in our state of interest both of the discords will be trivially zero if  $|\alpha\rangle = \pm|0\rangle$  or  $|\beta\rangle = \pm|0\rangle$  because in this case  $\hat{\rho}_{AB}$  is a product state. Aside from this we know that  $D(A, B) = 0$  identically if  $\langle\beta|0\rangle = 0$ , i.e. if  $|\beta\rangle = \pm|1\rangle$  (as can be seen directly from the definition of a zero-discord state Eq. (2.18)). A similar condition holds for  $D(B, A) = 0$ . Concisely we can state

$$D(A, B) = 0 \quad \text{iff } \{|\beta\rangle = \pm|1\rangle \text{ or } |\alpha\rangle = \pm|0\rangle \text{ or } |\beta\rangle = \pm|0\rangle\}, \quad (2.25)$$

and

$$D(B, A) = 0 \quad \text{iff } \{|\alpha\rangle = \pm|1\rangle \text{ or } |\alpha\rangle = \pm|0\rangle \text{ or } |\beta\rangle = \pm|0\rangle\}. \quad (2.26)$$

The goal is now to compare these possibilities with those of the entanglement structure of the purification  $|\psi\rangle_{ABC}$ . Without loss of generality the purification is

$$|\psi\rangle_{ABC} = \sqrt{q}|0\rangle|0\rangle|0\rangle + \sqrt{1-q}|\alpha\rangle|\beta\rangle|1\rangle \quad (2.27)$$

Let us now consider from this the reduced state  $\hat{\rho}_{AC}$ . Tracing over  $B$  and labeling  $c_\alpha \equiv \cos(\pi\alpha/2)$  etc, we have

$$\hat{\rho}_{AC} = \begin{pmatrix} q & \sqrt{q(1-q)}c_\beta c_\alpha & 0 & \sqrt{q(1-q)}c_\beta s_\alpha \\ \sqrt{q(1-q)}c_\beta c_\alpha & (1-q)c_\alpha^2 & 0 & (1-q)c_\alpha s_\alpha \\ 0 & 0 & 0 & 0 \\ \sqrt{q(1-q)}c_\beta s_\alpha & (1-q)c_\alpha s_\alpha & 0 & (1-q)s_\alpha^2 \end{pmatrix}. \quad (2.28)$$

The partially transposed eigenvalues of  $\hat{\rho}_{AC}$  can then be readily computed and it is found that only one of the four, which we will call  $\lambda$ , can ever be negative. Recall that since  $\hat{\rho}_{AC}$  has dimension  $2 \times 2$  the PPT criterion is both a necessary and sufficient condition for separability. Thus  $\hat{\rho}_{AC}$  is entangled iff  $\lambda$  is negative. From this it is easy to show that

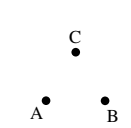
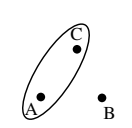
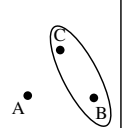
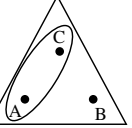
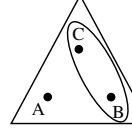
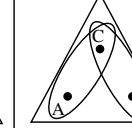
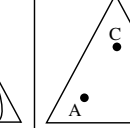
$ \alpha\rangle$	$\pm 0\rangle$	$\neq \pm 0\rangle$	$\pm 0\rangle$	$\pm 1\rangle$	$\neq \pm\{ 0\rangle,  1\rangle\}$	$\neq \pm\{ 0\rangle,  1\rangle\}$	$\pm 1\rangle$
$ \beta\rangle$	$\pm 0\rangle$	$\pm 0\rangle$	$\neq \pm 0\rangle$	$\neq \pm\{ 0\rangle,  1\rangle\}$	$\pm 1\rangle$	$\neq \pm\{ 0\rangle,  1\rangle\}$	$\pm 1\rangle$
Entanglement structure							
$D(A, B)$	0	0	0	$> 0$	0	$> 0$	0
$D(B, A)$	0	0	0	0	$> 0$	$> 0$	0

Figure 2.1: The relationship between the entanglement structure of  $|\psi\rangle_{ABC}$  and the discord in  $\rho_{AB}$ . For given conditions on  $|\alpha\rangle$  and  $|\beta\rangle$  we display the resulting entanglement structure and the results for the discords  $D(A, B)$  and  $D(B, A)$ . In the structure diagrams an ellipse represents the presence of bipartite entanglement while a triangle represents the presence of tripartite entanglement.

$\hat{\rho}_{AC}$  is almost always entangled, being separable iff  $\alpha = \{0, 2\}$  or  $\beta = \{1, -1\}$ , i.e. iff  $|\alpha\rangle = \pm|0\rangle$  or  $|\beta\rangle = \pm|1\rangle$ . Additionally it becomes trivially separable if  $q$  is equal to 0 or 1, but we will not consider this case. The separability of  $\hat{\rho}_{BC}$  follows similar conditions. Concisely:

$$\hat{\rho}_{AC} \text{ is separable iff } \{|\alpha\rangle = \pm|0\rangle \text{ or } |\beta\rangle = \pm|1\rangle\}, \quad (2.29)$$

$$\hat{\rho}_{BC} \text{ is separable iff } \{|\beta\rangle = \pm|0\rangle \text{ or } |\alpha\rangle = \pm|1\rangle\}. \quad (2.30)$$

Let us further consider the separability of  $\hat{\rho}_{AC}$ , because the two different conditions for separability mean two very different things. We see that the first condition,  $|\alpha\rangle = \pm|0\rangle$ , coincides with the  $A$  system being a product onto the  $BC$  system; under this condition the 3-qubit state takes the product form  $|\psi\rangle_{ABC} = |0\rangle \otimes |\psi\rangle_{BC}$ . Of course in this case  $\hat{\rho}_{AB}$  is separable, as we've seen, but it also clearly has zero discord and we see that this is compatible with Eqs. (2.25, 2.26). The second condition,  $|\beta\rangle = \pm|1\rangle$ , is much more interesting. In this case the reduced state of  $A$  is mixed rather than pure, meaning that despite  $A$  not being entangled with  $B$  nor with  $C$  it *is* entangled with the  $BC$  system as a whole. In fact, in this case we have genuine tripartite entanglement occurring in the state  $|\psi\rangle_{ABC}$  that is of the GHZ type discussed in Subsect. 2.1.3.

We can take the conditions for zero discord and separability in Eqs. (2.25, 2.26) and (2.29, 2.30) respectively and find that they match up very nicely; we display the resulting pattern in Fig. 2.1. There are two interesting things to notice from this pattern. Firstly, at



least in the simple setting we are considering here, it appears that the presence of discord in  $\hat{\rho}_{AB}$  is *equivalent*, in the sense of necessity and sufficiency, to there being both bipartite and tripartite entanglement in the purified system (notice that when there is no bipartite entanglement, i.e. a GHZ type state  $|000\rangle + |111\rangle$ , there is no discord). Secondly we very clearly see the asymmetry of discord  $D(A, B) \neq D(B, A)$  represented in the entanglement structure.

As an important note, recall that we neglected to include relative phases in our state (2.22). In the analysis we've done here this is not a problem and the structure in Fig. 2.1 will continue to hold if phases are included. The reasons for this are that 1) the nullity of discord depends only on the orthogonality the projectors in Eq. (2.22), which for us will not be affected by phases and 2) the partially transposed eigenvalues do not depend on any relative phases and thus the entanglement structure of  $|\psi\rangle_{ABC}$  will be independent of them as well. Thus we are justified in using the simplifying assumption of no phases, reducing our phase space from six dimensions ( $q$ ,  $\alpha$  and  $\beta$  plus three phases) down to three dimensions.

# Chapter 3

## Gaussian quantum mechanics

The formalism of Gaussian quantum mechanics (GQM) is of central importance to this entire thesis, as it constitutes the computational framework that is utilized throughout. GQM deals with a special class of continuous-variable states referred to as Gaussian states. These in fact account for a wide range of states that are of interest in quantum information, quantum optics, and relativistic field theory; they include vacuum, thermal, squeezed, and coherent states [77, 78]. Indeed the formalism turns out to be perfect for answering all of the problems presented in this thesis.

In this chapter we will give a brief and functionality-based overview of GQM, including what Gaussian states are, their properties, and how they evolve. A more complete introduction can be found in [45], among many other resources available in the literature. Unless otherwise stated or cited, full derivations of the content presented in this chapter can be found in [45].

### 3.1 Basics

Consider a set of continuous-variable bosonic modes. These can describe, for example, a set of  $N$  quantum harmonic oscillators or the modes of a field (or both, as we will in this thesis). We label the quadrature operators for each mode  $(\hat{q}_i, \hat{p}_i)$  for each  $i = 1 \dots N$ , where these operators satisfy the canonical commutation relations  $[\hat{q}_i, \hat{p}_j] = i\delta_{ij}$ . We can package these degrees of freedom into a phase-space vector of the form:

$$\hat{\mathbf{x}} = (\hat{q}_1, \hat{p}_1, \hat{q}_2, \hat{p}_2, \dots, \hat{q}_N, \hat{p}_N)^T. \quad (3.1)$$

These quadrature operators are related to the creation and annihilation operators of each mode by

$$\hat{q}_i = \frac{1}{\sqrt{2}}(\hat{a}_i + \hat{a}_i^\dagger), \quad \hat{p}_i = \frac{i}{\sqrt{2}}(\hat{a}_i^\dagger - \hat{a}_i). \quad (3.2)$$

In this notation the canonical commutation relations  $[\hat{q}_i, \hat{p}_j] = i\delta_{ij}$  take the form

$$[\hat{x}_i, \hat{x}_j] = i\Omega_{ij}, \quad (3.3)$$

where  $\Omega_{ij}$  are the entries of a matrix called the symplectic form, which is given by

$$\Omega = \bigoplus_{i=1}^N \begin{pmatrix} 0 & 1 \\ -1 & 0 \end{pmatrix}. \quad (3.4)$$

A Gaussian state  $\hat{\rho}$  of such a system is by definition one that can be completely described by its first and second moments,  $\langle \hat{x}_i \rangle = \text{Tr}(\hat{\rho}\hat{x}_i)$  and  $\langle \hat{x}_i\hat{x}_j \rangle = \text{Tr}(\hat{\rho}\hat{x}_i\hat{x}_j)$ . Equivalently, its Wigner function (see [78] for an example) takes the form of a Gaussian. We will here use Gaussian states that have zero mean  $\langle \hat{x}_i \rangle = 0$ . The utility of a Gaussian state is that it can be fully described by its  $2N \times 2N$  covariance matrix  $\sigma$ , the entries of which are<sup>1</sup>

$$\sigma_{ij} = \langle \hat{x}_i\hat{x}_j + \hat{x}_j\hat{x}_i \rangle. \quad (3.5)$$

This matrix contains all of the information about a Gaussian state. It is this fact, that we can describe such a state by a finite dimensional matrix  $\sigma$  rather than by an infinite dimensional operator  $\hat{\rho}$ , that accounts for the great utility and power of GQM. It is important to note that this formalism can also extend to Gaussian states of non-zero mean (indeed this is what coherent states are), but we will not need that generalization for the purposes of this thesis.

The covariance matrix of our system can be decomposed into  $2 \times 2$  blocks:

$$\sigma = \begin{pmatrix} \sigma_1 & \gamma_{12} & \gamma_{13} & \cdots \\ \gamma_{21}^T & \sigma_2 & \gamma_{23} & \cdots \\ \gamma_{31}^T & \gamma_{32}^T & \sigma_3 & \cdots \\ \vdots & \vdots & \vdots & \ddots \end{pmatrix}. \quad (3.6)$$

---

<sup>1</sup>Note that this definition differs by a factor of two from what is usually called the covariance matrix. Our definition offers the advantage that the vacuum state is represented by the identity matrix, as will be explained.

Given this, specifying the reduced state of a subset of modes is entirely trivial when working with Gaussian states. One must simply use the rows and columns of the total covariance matrix that corresponds to the modes one wishes to isolate. For example the reduced state of the first two modes of our ensemble, which we will represent by the covariance matrix  $\sigma_{12}$ , is simply given by the first  $4 \times 4$  block of  $\sigma$ :

$$\sigma_{12} = \begin{pmatrix} \sigma_1 & \gamma_{12} \\ \gamma_{12}^T & \sigma_2 \end{pmatrix}, \quad (3.7)$$

where the  $2 \times 2$  covariance matrices  $\sigma_1$  and  $\sigma_2$  represent the reduced states of the first and second modes on their own, respectively. The  $2 \times 2$  matrix  $\gamma_{12}$  encodes the correlations between the two modes; they are in a product state with respect to each other iff  $\gamma_{12} = 0$ .

Let our ensemble of oscillators/modes have fundamental frequencies  $\omega_i$ ,  $i = 1 \cdots N$ . The free Hamiltonian associated with our system is then given by

$$\hat{H}_{\text{free}} = \sum_{i=1}^N \omega_i \hat{a}_i^\dagger \hat{a}_i = \sum_{i=1}^N \frac{\omega_i}{2} (\hat{p}_i^2 + \hat{q}_i^2), \quad (3.8)$$

where we have ignored any constant addition to  $\hat{H}_{\text{free}}$  since this will have no impact on the states or evolution considered. Note, for example, that the expected energy of any free Gaussian state can be computed via

$$E = \langle \hat{H}_{\text{free}} \rangle = \sum_{i=1}^N \frac{\omega_i}{2} (\text{Tr} \sigma_i - 2), \quad (3.9)$$

where  $\sigma_i$  are the covariance matrices of the individual modes, and we have subtracted off the ground state contribution such that the energy of a ground/vacuum state is by definition zero. The value of  $(\text{Tr} \sigma_i - 2)/2$  is easily seen to be the expected excitation number  $\langle \hat{a}_i^\dagger \hat{a}_i \rangle$  of mode- $i$  (i.e. the particle number if interpreted as a field mode); this will be discussed further in Ch. 4. The total expected excitation of the system is therefore given by  $(\text{Tr} \sigma - 2N)/2$ .

Of critical importance is the fact that any unitary evolution generated by a quadratic Hamiltonian will preserve the Gaussianity of a state [77]. Any such unitary operation  $\hat{U}$  on the Hilbert space of states corresponds to a symplectic transformation on the phase space that, in the Heisenberg picture, transforms the quadrature operators into new quadrature operators that are linear combinations of the old:  $\hat{\mathbf{x}} \rightarrow \hat{U}^\dagger \hat{\mathbf{x}} \hat{U} = \mathbf{S} \hat{\mathbf{x}}$ . Here  $\mathbf{S}$  is required to be a symplectic matrix, meaning that it satisfies

$$\mathbf{S} \Omega \mathbf{S}^T = \mathbf{S}^T \Omega \mathbf{S} = \Omega. \quad (3.10)$$

The condition (3.10) is equivalent to the requirement that the canonical commutation relations  $[\hat{q}_i, \hat{p}_j] = i\delta_{ij}$  are preserved throughout the change of basis. On the level of the covariance matrix it is easy to see that this transformation acts as

$$\boldsymbol{\sigma} \rightarrow \boldsymbol{\sigma}' = \mathbf{S}\boldsymbol{\sigma}\mathbf{S}^T. \quad (3.11)$$

The method of computing the symplectic matrix corresponding to a quadratically generated  $\hat{U}$  is straightforward, and involves using the Baker-Campbell-Hausdorff (BCH) formula  $\exp(\hat{X})\hat{Y}\exp(-\hat{X}) = \hat{Y} + [\hat{X}, \hat{Y}] + [\hat{X}, [\hat{X}, \hat{Y}]]/2! \cdots$  to determine how the unitary acts on quadrature operators. If  $\hat{X}$  is quadratic in the quadratures then the result will be a symplectic linear combination of quadratures, which can then be used to read off the symplectic transformation  $\mathbf{S}$ .

Local operations are especially easy to handle when working in GQM. Imagine that we split our  $N$  mode Gaussian system into two sets  $A$  and  $B$ , with  $m < N$  modes and  $N - m$  modes respectively. We can then structure our phase space basis such that the state of the total system is decomposed as

$$\boldsymbol{\sigma} = \begin{pmatrix} \boldsymbol{\sigma}_A & \boldsymbol{\gamma}_{AB} \\ \boldsymbol{\gamma}_{AB}^T & \boldsymbol{\sigma}_B \end{pmatrix}, \quad (3.12)$$

where  $\boldsymbol{\sigma}_A$  is the  $2m \times 2m$  dimensional covariance matrix describing the reduced state of ensemble  $A$ , etc. If we then apply a local Gaussian operation  $\hat{U}_A \otimes \hat{U}_B$  to this state, the symplectic representation of this transformation is given not by a tensor product but rather a direct sum:  $\mathbf{S}_A \oplus \mathbf{S}_B$ , where  $\mathbf{S}_A$  and  $\mathbf{S}_B$  are the local symplectic transformations corresponding to  $\hat{U}_A$  and  $\hat{U}_B$ , respectively. Acting on  $\boldsymbol{\sigma}$  this gives the transformation

$$\boldsymbol{\sigma} \rightarrow \begin{pmatrix} \mathbf{S}_A \boldsymbol{\sigma}_A \mathbf{S}_A^T & \mathbf{S}_A \boldsymbol{\gamma}_{AB} \mathbf{S}_B^T \\ \mathbf{S}_B \boldsymbol{\gamma}_{AB}^T \mathbf{S}_A^T & \mathbf{S}_B \boldsymbol{\sigma}_B \mathbf{S}_B^T \end{pmatrix}. \quad (3.13)$$

Symplectic transformations come in two important categories, characterized by whether or not they change the total excitation number  $(\text{Tr}\boldsymbol{\sigma} - 2N)/2$  of the system. These are referred to as passive transformations, which leave this number unchanged, and active transformations, which modify it. Mathematically, a passive symplectic matrix  $\mathbf{S}$  is one that is orthogonal in addition to being symplectic (thus preserving the trace of  $\boldsymbol{\sigma}$ ). An active transformation is one that is not orthogonal. We will see important examples of both of these categories in the next section.

## 3.2 Important states

Extremely important to this thesis is the easily shown fact that the ground/vacuum state  $|0\rangle_1 |0\rangle_2 \cdots |0\rangle_N$  of the Hamiltonian Eq. (3.8) is a Gaussian state, and in fact its covariance matrix simply takes the form of the  $2N \times 2N$  identity matrix:

$$\boldsymbol{\sigma}_{\text{vac}} = \mathbf{I}_{2N}. \quad (3.14)$$

This indeed can be seen as a simple version of Wick's theorem. We note for example that this state has vanishing excitation number  $(\text{Tr}\boldsymbol{\sigma}_{\text{vac}} - 2N)/2 = 0$ , as should be the case. Notice also that because the free Hamiltonian is devoid of coupling between modes this state is equivalent to a product of single modes, each of which are in their ground state. In the language of GQM this is trivially seen from the fact that  $\boldsymbol{\sigma}_{\text{vac}}$  has no off-diagonal terms, implying that there are no correlations between modes. From this ground state any other pure state which can be reached from it by a quadratically generated unitary is also Gaussian. What's more, any pure Gaussian state (of the same number of modes) can be reached by this method. It is also important to note that the ground state is a state of minimal uncertainty, and thus any pure Gaussian state is as well. We will discuss further the connections between uncertainty and purity in the next section. As for mixed states, any state obtained from partial tracing a Gaussian state will also be Gaussian, and all mixed Gaussian states can be obtained by first obtaining a pure Gaussian state on an extended system and then partial tracing.

An important example of a set of pure, Gaussian states is the class of squeezed states. We will first focus on single-mode states. A single-mode squeezed state is one obtained from a single-mode ground state by the unitary transformation  $\hat{U}_{\text{sq}}(r) = \exp(\frac{r}{2}(\hat{a}^\dagger{}^2 - \hat{a}^2))$ , where  $r$  is called the squeezing parameter. In the phase space picture this transformation takes the symplectic form  $\mathbf{S}_{\text{sq}} = \text{diag}(e^{r/2}, e^{-r/2})$ . Acting this matrix on the ground state (i.e. the  $2 \times 2$  identity), we obtain the single-mode squeezed state

$$\boldsymbol{\sigma}_{\text{sq}} = \begin{pmatrix} e^r & 0 \\ 0 & e^{-r} \end{pmatrix}. \quad (3.15)$$

This state is called squeezed because its Gaussian distribution in phase space has been squeezed in one dimension (in this case the  $p$  dimension) and elongated in the other as compared to the ground state. Put another way, we have obtained more certainty in  $p$  at the cost of less certainty in  $q$ . It is still, however, a minimal uncertainty state, as is easily confirmed. Note also that the squeezing operation is an example of an active transformation.

Another important symplectic transformation is a phase space rotation. Again just considering a single-mode system for the moment, a rotation is produced by a unitary of the form  $\hat{U}_{\text{rot}} = \exp(it\hat{a}^\dagger\hat{a})$ . The symplectic matrix corresponding to this transformation is simply a rotation matrix:

$$\mathbf{S}_{\text{rot}} = \begin{pmatrix} \cos t & \sin t \\ -\sin t & \cos t \end{pmatrix}. \quad (3.16)$$

This is an example of a passive transformation. Note, importantly, that this is exactly the way that free evolution is represented on the phase space level. Such a transformation leaves the ground/vacuum state invariant, as does any passive transformation since  $\mathbf{S}\mathbf{S}^T = \mathbf{I}$  if  $\mathbf{S}$  is orthogonal. This makes sense, of course, since a passive transformation leaves unchanged the energy of a state. Since the ground state is that of minimal energy, no passive transformation can possibly bring it to any other as this would imply an increase of energy.

There also exist generalizations of the above two transformations to higher-mode systems. An example worth looking at here is the two-mode squeezed state, which is produced from the two-mode ground state  $|0\rangle_1|0\rangle_2$  by the unitary operator  $\hat{U}_{\text{sq}}(r) = \exp(\frac{r}{2}(\hat{a}_1\hat{a}_2 - \hat{a}_1^\dagger\hat{a}_2^\dagger))$ . The symplectic transformation corresponding to this unitary is given by

$$\mathbf{S}_{\text{sq}} = \begin{pmatrix} \cosh r & 0 & \sinh r & 0 \\ 0 & \cosh r & 0 & -\sinh r \\ \sinh r & 0 & \cosh r & 0 \\ 0 & -\sinh r & 0 & \cosh r \end{pmatrix}. \quad (3.17)$$

Applying this to the ground state,  $\hat{U}_{\text{sq}}|0\rangle_1|0\rangle_2$ , we obtain the two-mode squeezed state

$$\boldsymbol{\sigma}_{\text{sq}} = \begin{pmatrix} \cosh 2r & 0 & \sinh 2r & 0 \\ 0 & \cosh 2r & 0 & -\sinh 2r \\ \sinh 2r & 0 & \cosh 2r & 0 \\ 0 & -\sinh 2r & 0 & \cosh 2r \end{pmatrix}. \quad (3.18)$$

We present this exemplary state as it displays several characteristics that are of importance. First, note that the two modes are correlated with each other, as the off-diagonal blocks are nonzero. Given that the state is pure, this therefore implies that the two modes are entangled. Let us compare Eq. (3.18) with the form of the state vector in the Hilbert space. Applying  $\hat{U}_{\text{sq}}(r)$  to the two-mode ground state it is straightforward to show that this two-mode squeezed state is

$$|\psi\rangle = \frac{1}{\cosh r} \sum_{n=1}^{\infty} \tanh^n r |n\rangle |n\rangle. \quad (3.19)$$

Indeed this state is clearly entangled, and the reduced state of one of the two modes will be mixed. Importantly, a two-mode squeezed state is of exactly the correct form such that the reduced state of a single mode is in a thermal state (i.e. the density matrix is diagonal in the energy basis with probability entries that follow a Boltzmann distribution):

$$\hat{\rho}_A = \text{Tr}_B |\psi\rangle \langle\psi| = \frac{1}{\cosh^2 r} \sum_{n=1}^{\infty} \tanh^{2n} r |n\rangle \langle n| = \frac{1}{\mathcal{Z}} \sum_{n=1}^{\infty} e^{-n\omega/T} |n\rangle \langle n|, \quad (3.20)$$

where  $\omega$  is the frequency (energy spacing) of the mode in question,  $T$  is its temperature, and  $\mathcal{Z} = \sum_n \exp(-n\omega/T)$  is the partition function. Here we have made the identification  $\exp(-\omega/T) = \tanh^2 r$ , but of course in general a thermal state need not be considered as having been derived from a two-mode squeezed state. Given that the partial trace of any Gaussian state is also Gaussian, we have realized the very important result that thermal states are also Gaussian. We also immediately see the form of the covariance matrix of a thermal state, which we obtain by performing the partial trace (i.e. taking the first block) of Eq. (3.18):  $\sigma_A = \text{diag}(\cosh 2r, \cosh 2r) \equiv \text{diag}(\nu, \nu)$ . That is, the covariance matrix of a single-mode thermal state is proportional to the identity. The proportionality constant we label as  $\nu$  and, as is easily shown from the above example (i.e. taking  $\nu = \cosh 2r$  and  $\exp(-\omega/T) = \tanh^2 r$ ), is related to the thermal statistics via

$$\frac{\nu - 1}{2} = \langle n \rangle = \frac{1}{\exp(\omega/T) - 1}, \quad (3.21)$$

where  $\langle n \rangle$  is the expectation value of which energy level the state is in (in field theory language, this is the expected particle content of the mode in question).

In a general ensemble of  $N$  modes with Hamiltonian Eq. (3.8) a thermal state of temperature  $T$  will be a product state of single-mode thermal states, each of temperature  $T$ . This follows from the fact that the Hamiltonian contains no coupling term between modes. Given what we have just learned about single-mode thermal states, this implies that an  $N$ -mode thermal state takes the covariance matrix

$$\sigma_{\text{therm}} = \bigoplus_{i=1}^N \begin{pmatrix} \nu_i & 0 \\ 0 & \nu_i \end{pmatrix}, \quad (3.22)$$

where

$$\nu_i = \frac{\exp \omega_i \beta + 1}{\exp \omega_i \beta - 1}, \quad \beta \equiv 1/T. \quad (3.23)$$



### 3.3 The symplectic spectrum, purity, and mixedness.

The values  $\nu_i$  defined above are referred to as the symplectic eigenvalues of the state. We gave their values above in the case of a thermal state, but in general the symplectic spectrum of any Gaussian state  $\sigma$  is a very important characterization of the state. Every  $N$ -mode Gaussian state has  $N$  symplectic eigenvalues  $\nu_i$ , which are so called because they are invariant under symplectic transformations. They are *not* generally the same as the regular eigenvalues. Any covariance matrix  $\sigma$  is symplectically diagonalizable, meaning that there exists a symplectic matrix  $\mathbf{S}$  which brings the state to a diagonal form given by  $\mathbf{S}\sigma\mathbf{S}^T = \mathbf{D} = \text{diag}(\nu_1, \nu_1, \nu_2, \nu_2, \dots, \nu_N, \nu_N)$ . This diagonalized form is also known as the Williamson normal form of the state. We note, for example, that both the vacuum and thermal states are already in their Williamson normal forms. The vacuum state has all symplectic eigenvalues equal to unity,  $\nu_i = 1$ . As we have discussed, any pure Gaussian state can be obtained by symplectically transforming the vacuum. Seeing as  $\nu_i$  are invariant under symplectic transformations, we can immediately conclude that all pure Gaussian states have symplectic eigenvalues all equal to unity. The symplectic spectrum therefore gives us information on the purity or mixedness of a state. Indeed, the result can be strengthened to the statement that a Gaussian state is pure iff all symplectic eigenvalues are equal to unity. A thermal state, for example, is mixed and accordingly has symplectic eigenvalues greater than unity, as we have seen.

The symplectic eigenvalues of a state must always be larger than or equal to unity:  $\nu_m \geq 1 \forall m$ . This is in fact simply a statement of the uncertainty principle, which is saturated iff all symplectic eigenvalues are equal to unity. That is, a pure Gaussian state saturates the uncertainty principle, as we have already pointed out. Any uncertainty in the state beyond this must be caused by classical uncertainty, i.e. mixedness. An informationally rigorous measure of mixedness is the von Neumann entropy  $S(\sigma) \equiv S(\hat{\rho})$  of the state, the Hilbert space form of which is given in Eq. (2.5). In GQM this can be shown to take a form that depends solely on the symplectic eigenvalues:

$$S(\sigma) = \sum_{i=1}^N f(\nu_i), \quad (3.24)$$

where

$$f(x) = \frac{x+1}{2} \log\left(\frac{x+1}{2}\right) - \frac{x-1}{2} \log\left(\frac{x-1}{2}\right). \quad (3.25)$$

The entropy is zero for a pure state, when  $\nu_i = 1$  for all  $i$ .

Furthermore, one can easily obtain information about the purity of mixedness of a state without even needing to compute the symplectic eigenvalues. This is based on the fact that  $\det \boldsymbol{\sigma}$  is a symplectic invariant (which follows from the fact that  $\det \mathbf{S} = 1$  for any symplectic matrix, as is easily deduced from Eq. (3.10)). This means that  $\det \boldsymbol{\sigma} = \prod_i \nu_i^2$ , independent of in what quadrature basis  $\boldsymbol{\sigma}$  is represented. We can actually use this to define a quantitative measure of state purity  $P$  that will be used in this thesis:

$$P = \frac{1}{\sqrt{\det \boldsymbol{\sigma}}} = \prod_i \nu_i^{-1}. \quad (3.26)$$

For pure and mixed states we obtain  $P = 1$  and  $P < 1$ , respectively.

The easiest way to compute the symplectic eigenvalues of a state (if one does not care about the diagonalizing transformation) is to compute the regular eigenvalues of the matrix  $i\boldsymbol{\Omega}\boldsymbol{\sigma}$ , which come in pairs of  $\{\pm\nu_i\}$ . There are situations, however, in which one would also like to compute the diagonalizing symplectic transformation itself. The method for doing this is provided in Appendix. A. An operation that will be important in Ch. 13, for example, is the local diagonalization of a bipartite, pure state. Imagine that we split our set of modes into two groups,  $A$  and  $B$ . The joint state  $\boldsymbol{\sigma}$  can then be decomposed as in Eq. (3.12). Let us assume that this state is pure. That is, we assume that the symplectic eigenvalues  $\nu_i$  of  $\boldsymbol{\sigma}$  are all equal to unity. This does not mean, however, that the symplectic eigenvalues of the reduced covariance matrices  $\boldsymbol{\sigma}_A$  and  $\boldsymbol{\sigma}_B$  are all equal to unity; indeed they will not be if the bipartitions are entangled (i.e. if  $\boldsymbol{\gamma}_{AB}$  is nonzero). Let us label the ‘‘local’’ symplectic eigenvalues of these reduced states as  $\nu_i^{(A)}$  and  $\nu_i^{(B)}$ . Because  $\boldsymbol{\sigma}$  is pure these two spectra will in fact be equivalent (with the larger of the two systems having extra symplectic eigenvalues equal to unity); this is equivalent to the fact that the standard local spectra of the reduced density operators in a pure bipartition are equal to each other. Let  $\mathbf{S}_A$  be the local symplectic transformation that diagonalizes  $\boldsymbol{\sigma}_A$ , and similarly we have  $\mathbf{S}_B$ . Let us then apply these local transformations to our state by acting on  $\boldsymbol{\sigma}$  with the joint transformation  $\mathbf{S}_A \oplus \mathbf{S}_B$ :

$$(\mathbf{S}_A \oplus \mathbf{S}_B)\boldsymbol{\sigma}(\mathbf{S}_A \oplus \mathbf{S}_B)^T = \begin{pmatrix} \mathbf{D}_A & \boldsymbol{\gamma}_D \\ \boldsymbol{\gamma}_D^T & \mathbf{D}_B \end{pmatrix}. \quad (3.27)$$

The reduced states have now been put into their Williamson normal forms. Because this is a purely local operation the entanglement between the two sides has not been modified. Importantly, *if* the global state is pure then this transformation produces a correlation matrix  $\boldsymbol{\gamma}_D$  that is diagonal as well [45]. This is analogous to the Hilbert space Schmidt decomposition of a pure, bipartite state. In the literature on Gaussian quantum mechanics such a covariance matrix is said to be in *standard form*. The fact that  $\boldsymbol{\gamma}_D$  is diagonal means

that in this locally transformed basis we obtain a product of pure, two-mode states. That is, each pair is uncorrelated with any others. Generally each such pair of modes will be entangled (in particular, they will be in a two-mode squeezed state). Performing this local symplectic diagonalization is therefore a method of isolating the entanglement between  $A$  and  $B$  into simple pairs of modes (rather than the entanglement between a given mode in  $A$  and the rest of the system being spread across multiple modes in both  $A$  and  $B$ ).

In the case that  $\sigma$  is mixed we unfortunately cannot perform the same feat. We can, of course, still locally diagonalize the reduced systems. This removes any mode-mode correlation within  $A$  and  $B$  themselves. However in this case the resulting correlation matrix  $\gamma_D$  will not generally be diagonal, meaning that we can still have a given mode in  $A$  being correlated with multiple modes in  $B$ , and vice versa.

### 3.4 Quantum correlations in Gaussian states

Here we will discuss how to extend the concepts of Ch. 2 to the case of Gaussian states. In the case of pure Gaussian states, for example, the entanglement across a bipartition of modes is quantified by the entropy of one of the reduced states. Let us take a two-mode squeezed state as an example, Eq. (3.18). This state is pure (the two symplectic eigenvalues of the covariance matrix are both equal to unity). The symplectic eigenvalue of its single-mode reduced state, however, is  $\nu = \cosh 2r > 1$  for  $r > 0$  and thus has reduced entropy  $S = f(\cosh 2r)$ , as given by Eq. (3.24).

In the case of mixed states, on the other hand, we would like to obtain a Gaussian version of the PPT criterion presented in Sect. 2.1. As was discussed, a separable state will be such that its partially transposed version is still a valid density matrix (i.e. it is positive definite). In the case of Gaussian states the story follows very similarly. The act of transposing a density matrix corresponds in phase space to a reflection across the  $q$  axis [79], i.e. applying the operation  $p \rightarrow -p$ . Applying a partial trace over the subset of modes in system  $B$  is therefore given by reflecting all those momentum operators of the modes in  $B$ . Let there be  $m$  modes in system  $A$  and  $N - m$  modes in system  $B$ . On the level of the covariance matrix the partial transpose acts to transform a state partitioned as in Eq. (3.12) into a new matrix  $\sigma^{\Gamma_B}$  that is given by

$$\sigma \rightarrow \sigma^{\Gamma_B} = (\mathbf{I}_A \oplus \mathbf{\Lambda}_B)\sigma(\mathbf{I}_A \oplus \mathbf{\Lambda}_B), \quad (3.28)$$

where  $\mathbf{I}_A$  is the  $m \times m$  identity matrix and  $\mathbf{\Lambda}_B$  is an  $(N - m) \times (N - m)$  matrix of the form  $\mathbf{\Lambda}_B = \text{diag}(1, -1, 1, -1, \dots, 1, -1)$ . Similar to the way in which the eigenvalues of a density

matrix give information about its mixedness whereas the eigenvalues of its partial transpose give information about its entanglement, the same is true of covariance matrices and their symplectic eigenvalues. By computing the symplectic eigenvalues  $\tilde{\nu}_i$  of the partially transposed covariance matrix  $\sigma^{\Gamma_B}$  we obtain information about the entanglement between  $A$  and  $B$  given state  $\sigma$ . Similar to a density matrix, which if separable will continue to be a valid density matrix after partial transposition, a separable Gaussian state will be such that  $\sigma^{\Gamma_B}$  is still a valid covariance matrix, meaning that the partially transposed symplectic eigenvalues satisfy

$$\sigma \text{ separable} \implies \tilde{\nu}_i \geq 1 \quad \forall i. \quad (3.29)$$

That is, if any of the  $\tilde{\nu}_i$  are less than unity then the state is entangled.

As discussed in Ch. 2, the PPT criterion will in general be both a necessary and sufficient criterion for separability only when  $\dim(A \otimes B) \leq 6$ . In the case of Gaussian states it can be demonstrated that the PPT criterion as just described is necessary and sufficient for  $1+N$  mode systems [80, 81]. That is, if one side of a bipartition contains only a single mode then any Gaussian state will be separable across this bipartition iff it satisfies the PPT criterion. More generally there can exist bound entanglement, which will not be witnessed by this procedure. Similar to our previous discussion on the PPT criterion, we can define an easily computed measure of entanglement. In particular, we will present the form of the logarithmic negativity Eq. (2.11) in the case of Gaussian states, which can be shown to take the form [58]

$$E_N(A, B) = - \sum_{\tilde{\nu}_i < 1} \log \tilde{\nu}_i. \quad (3.30)$$

That is, we take those partially transposed symplectic eigenvalues that are less than unity (which there will only be if the state is entangled), and sum over the logarithms of those values.

The quantum discord can also be defined for Gaussian states. Unfortunately the optimization procedure makes the discord very difficult to evaluate in general, and closed formulas are not known for general Gaussian states. Only in the case of two-mode states can a closed formula be obtained, and even in this case optimization is performed over a limited set of measurements. We will therefore save the discussion of discord for the following subsection, which focuses on two-mode Gaussian states.

### 3.4.1 The case of two-modes

Of particular importance to us in this thesis will be the case of two modes, one on either side of the partition. In this case  $E_N > 0$  iff the state is entangled. We will take a two-mode state of the form Eq. (3.7). In this case it is straightforward to demonstrate that the two symplectic eigenvalues, which we will label  $\nu_{\pm}$ , satisfy

$$2\nu_{\pm}^2 = \Delta \pm \sqrt{\Delta^2 - 4 \det \boldsymbol{\sigma}_{12}}, \quad (3.31)$$

where  $\Delta = \det \boldsymbol{\sigma}_1 + \det \boldsymbol{\sigma}_2 + 2 \det \boldsymbol{\gamma}_{12}$ . Similarly, it is immediate to see that the symplectic eigenvalues  $\tilde{\nu}_{\pm}$  obtained from the partially transposed covariance matrix must satisfy the same relation except that partial transposition acts to change the sign of  $\det \boldsymbol{\gamma}_{12}$ . We thus have that

$$2\tilde{\nu}_{\pm}^2 = \tilde{\Delta} \pm \sqrt{\tilde{\Delta}^2 - 4 \det \boldsymbol{\sigma}_{12}}, \quad (3.32)$$

where  $\tilde{\Delta} = \det \boldsymbol{\sigma}_1 + \det \boldsymbol{\sigma}_2 - 2 \det \boldsymbol{\gamma}_{12}$ . We thus see that the PPT criterion takes the form of the following inequality:

$$\tilde{\Delta} \leq 1 + \det \boldsymbol{\sigma}_{12}. \quad (3.33)$$

The larger of the two partially transposed symplectic eigenvalues,  $\tilde{\nu}_+$ , will always be greater than or equal to unity. The logarithmic negativity for two-mode state is therefore given by

$$E_N = \max(0, -\log \tilde{\nu}_i). \quad (3.34)$$

In addition, it will be useful to note that by combining Eq. (3.33) with the uncertainty relation  $\nu_{\pm} \geq 1$  it is possible to derive the following simple criterion for two-mode separability [79]:

$$\det \boldsymbol{\gamma}_{12} \geq 0 \implies \boldsymbol{\sigma} \text{ separable.} \quad (3.35)$$

Let us now move on to introduce quantum discord in Gaussian states. As discussed above, the discord is generally very difficult to compute due to the required optimization over measurements. When working with Gaussian states, the best that has been achieved in this regard is to optimize over the restricted set of Gaussian measurements (namely, measurements that preserve Gaussianity) [75]. This gives the quantity known as Gaussian discord. For notational convenience let us momentarily define  $\alpha = \det \boldsymbol{\sigma}_1$ ,  $\beta = \det \boldsymbol{\sigma}_2$ ,

$\gamma = \det \boldsymbol{\gamma}_{12}$ , and  $\delta = \det \boldsymbol{\sigma}_{12}$ . The Gaussian quantum discord for a two-mode state then permits the analytic solution

$$D(1, 2) = f(\sqrt{\beta}) - f(\nu_+) - f(\nu_-) + f(\sqrt{E}), \quad (3.36)$$

where  $\nu_{\pm}$  are the symplectic eigenvalues as given by Eq. (3.31), the function  $f$  is given by Eq. (3.25), and

$$E = \begin{cases} \frac{2\gamma^2 + (-1+\beta)(-\alpha+\delta) + 2|\gamma|\sqrt{\gamma^2 + (-1+\beta)(-\alpha+\delta)}}{(-1+\beta)^2} & \text{for } (\delta - \alpha\beta)^2 \leq (1 + \beta)\gamma^2(\alpha + \delta), \\ \frac{\alpha\beta - \gamma^2 + \delta - \sqrt{\gamma^4 + (-\alpha\beta + \delta)^2 - 2\gamma^2(\alpha\beta + \delta)}}{2\beta} & \text{otherwise.} \end{cases}$$

Note that this is the case in which the optimized measurement has been performed on system-2. Recall that in general the discord will depend on which system is being measured:  $D(1, 2) \neq D(2, 1)$ .

It should be noted that although there is circumstantial evidence that Gaussian measurements are actually optimal for Gaussian states [82], there is as of yet no proof of this, and so it is possible that the Gaussian discord may slightly overestimate the true value of discord in general.

There is a rather curious property of discord in Gaussian states that is worth discussing. As was first suggested in [75] and later proven in [83], a Gaussian state has zero quantum discord if and only if it is in a product state, i.e. iff it has no correlations whatsoever. This property is not just true of the Gaussian discord, in which solely Gaussian measurements are considered, but rather the full quantum discord in which all measurements are considered within the optimization.

The presence or absence of quantum discord in two-mode Gaussian states is rather curious in that there is zero discord if and only if the two modes are in a product state. This property was first suggested in [75] and later proven in [83]. It is somewhat surprising that this is the case because Gaussian states are often considered to be the ‘‘most classical’’ of quantum states, and yet it is impossible for a two-mode Gaussian state to possess classical correlations without also possessing quantum correlations. As part of our exposition we will now discuss one concrete way of understanding why this is the case, an argument that is based on the work presented in Sect. 2.3.

### 3.5 Aside: Why Gaussian states require quantum correlation to have classical correlation

Note: this section derives from the work [9], in collaboration with Eric J. Webster, Eduardo Martín-Martínez, and Achim Kempf.

Here we will be considering two-mode Gaussian states that can be purified with a single extra mode. Our goal is twofold. First, we find that by coupling the result presented in Sect. 2.3 with several known properties of pure, three-mode Gaussian states we obtain a very simple explanation as to why a Gaussian state requires quantum correlations in order to also have classical correlations. This gives a clean example of how the result proven in Sect. 2.3 can be used to understand otherwise puzzling properties. Second, we are able to easily prove that for this set of Gaussian states, similar to the qubits presented previously, the identification of non-zero discord  $D(A, B)$  with the presence of both bipartite and tripartite entanglement in the purification is a two-way implication, in the sense of necessity and sufficiency.

As in Sect. 2.3, in order for  $AB$  to be mixed we assume that the bipartition  $(AB)C$  is entangled. Thus the genuine tripartite entanglement in the system  $ABC$  vanishes iff either  $A(BC)$  is separable or  $(AC)B$  is separable (or both). Since the total system is pure, separability between a bipartition is equivalent to it taking a product form. We will now state the results of this section and then discuss before going on to prove them. In a pure Gaussian state over the three-mode system  $ABC$ , if we assume that the subsystem  $AB$  is separable then the three following equivalencies hold:

$$AC \text{ separable} \iff A(BC) \text{ separable} \tag{3.37}$$

$$BC \text{ separable} \iff (AC)B \text{ separable} \tag{3.38}$$

$$AB \text{ product} \iff A(BC) \text{ or } (AC)B \text{ separable.} \tag{3.39}$$

From these result we can make take two immediate observations. First, since now  $D(A, B) = 0 \iff D(B, A) = 0 \iff \rho_{AB} = \rho_A \otimes \rho_B$  it follows trivially that the general result presented in Sect. 2.3 is here a two-way implication. Namely,  $D(A, B) = 0$  iff there is no bipartite or tripartite entanglement in the purification.

Secondly, we now observe a very clear picture as to why zero discord in a Gaussian state implies that it is a product state. Recall from Sect. 2.3 that tripartite entanglement in the purification is required for *any* correlations to be present in  $AB$ , classical or quantum, and the further addition of bipartite entanglement in the purification is what allows these

correlations to have a quantum nature. In the case at hand however we see that it is impossible to allow classical correlations without automatically allowing quantum correlations as well. Namely, if  $AB$  is separable then it is impossible to have tripartite entanglement in the purification  $ABC$  without also having bipartite entanglement in both the  $AC$  and  $BC$  subsystems. This is very much unlike the set of qubits or more general quantum systems; here there is no GHZ type state in the sense of all two-party subsystems being separable while the system as a whole is tripartitely entangled. This severe restriction on the set of Gaussian states is what constrains the set of zero discord Gaussian states to product states. There can be no classical correlation without quantum correlation.

To prove that when  $AB$  is separable the three equivalencies hold, consider the covariance matrix of a (not generally pure) three-mode Gaussian state:

$$\sigma_{ABC} = \begin{pmatrix} \sigma_A & \gamma_{AB} & \gamma_{AC} \\ \gamma_{AB}^T & \sigma_B & \gamma_{BC} \\ \gamma_{AC}^T & \gamma_{BC}^T & \sigma_C \end{pmatrix}, \quad (3.40)$$

A  $4 \times 4$ , two-mode reduced state  $\sigma_{ij}$  is a product state iff  $\gamma_{ij} = 0$ , where  $i, j = \{A, B, C\}$ . A general two-mode Gaussian state  $\sigma_{ij}$  can be shown to satisfy the inequality  $\Delta_{ij} \leq \det \sigma_{ij} + 1$ , where  $\Delta_{ij} = \det \sigma_i + \det \sigma_j + 2 \det \gamma_{ij}$ , [45]. This is in fact a representation of the partial uncertainty relation applied to the given reduced state.

However, we will be considering the case in which this three-mode state is pure (i.e. assuming that  $\sigma_{AB}$  can be purified with a single extra mode). This is easily seen to be equivalent to the condition that every two-mode reduced state has at least one symplectic eigenvalue equal to unity (this is also the assumption that we must initially make about  $\sigma_{AB}$ ). In this case it is also easily shown that the above inequality saturates [45]. That is, we will have

$$\Delta_{ij} = \det \sigma_{ij} + 1. \quad (3.41)$$

Furthermore, since the mixedness of the two sides of any pure-state bipartition are equal, we have trivially

$$\det \sigma_{ij} = \det \sigma_k. \quad (3.42)$$

The fact that the uncertainty relation saturates in our case, Eq. (3.41), acts to boost the condition Eq. (3.35) to a necessary and sufficient one:

$$\det \gamma_{ij} \geq 0 \iff \sigma_{ij} \text{ separable.} \quad (3.43)$$



Lastly, we will find it useful to consider what is known as the standard form [45] of our general, pure, three-mode Gaussian state. Standard form can always be reached by local symplectic transformations, and therefore putting it into this form has no bearing on the correlation structure between modes. Amazingly, the correlation structure is fully determined by just three numbers, namely the local symplectic eigenvalues of each mode  $\nu_i = \sqrt{\det \sigma_i}$ . The standard form covariance matrix takes the form of Eq. (3.40) with  $\sigma_i = \text{diag}(\nu_i, \nu_i)$  and  $\gamma_{ij} = \text{diag}(e_{ij}^+, e_{ij}^-)$ , where

$$e_{ij}^{\pm} = \frac{1}{2\sqrt{\nu_i \nu_j}} [([(\nu_i - \nu_j)^2 - (\nu_k - 1)^2][(\nu_i - \nu_j)^2 - (\nu_k + 1)^2])^{\frac{1}{2}} \pm ([(\nu_i + \nu_j)^2 - (\nu_k - 1)^2][(\nu_i + \nu_j)^2 - (\nu_k + 1)^2])^{\frac{1}{2}}]. \quad (3.44)$$

With Eqs. (3.41-3.44) we can now easily prove Eqs. (3.37-3.39), assuming that  $\sigma_{AB}$  is separable. By Eq. (3.43) this assumption is equivalent to  $\det \gamma_{AB} \geq 0$ .

Trivially, we have  $A(BC)$  separable  $\implies A(BC)$  product  $\implies AC$  product  $\implies AC$  separable, where the first implication is due to the total state being pure. To show the other direction, we can combine Eqs. (3.41,3.42) to obtain

$$1 - \det \sigma_A = \det \gamma_{AB} + \det \gamma_{AC}. \quad (3.45)$$

The left side of this equation must be less than or equal to zero, since  $\det \sigma_A \geq 1$  with equality only when  $\sigma_A$  is pure. Since  $\sigma_{AB}$  is assumed separable we have  $\det \gamma_{AB} \geq 0$ . Similarly, if  $\sigma_{AC}$  is separable it will be that  $\det \gamma_{AC} \geq 0$ . If this is the case then the right hand side of the above equation must be greater than or equal to zero, implying that the only solution is for both sides to be zero. This implies that  $\det \sigma_A = 1$ , meaning that  $\sigma_A$  is pure and thus that the bipartition  $A(BC)$  is separable. Thus we find that  $AC$  separable  $\implies A(BC)$  separable. Combining with the trivial other direction we have therefore proven Eq. (3.37). Similarly, Eq. (3.38) is proven by the same method.

Lastly, to prove Eq. (3.39) we note that one direction is trivial:  $A(BC)$  or  $(AC)B$  separable  $\implies AB$  product. To prove the other direction we use the fact that  $AB$  is a product state iff  $\gamma_{AB} = 0$ . In standard form this is equivalent to  $e_{AB}^+ = e_{AB}^- = 0$ . From Eq. (3.44) we find that these conditions are both satisfied only if  $\nu_A = 1$  or  $\nu_B = 1$ , equivalently  $\det \sigma_A = 1$  or  $\det \sigma_B = 1$ . This is exactly the statement that  $AB$  product  $\implies A(BC)$  or  $(AC)B$  separable. This completes the proof of Eq. (3.39).

# Chapter 4

## Quantum scalar field theory

We now wish to discuss the primary quantum construct that will be considered in this thesis: that of a scalar quantum field. Quantum field theory (QFT) is of course immensely important in theoretical physics, and is the mathematical basis behind our current understanding of particle physics. It is an immense topic, as can be discerned from any of the texts on the subjects (e.g. [14, 15]). Here we will not be concerned with particle interactions (although we will be considering similar physics) nor with problems of renormalization. In fact we will only be considering the simplest case of quantum field theory, that of a scalar field  $\hat{\phi}$ . This does, however, provide a good model for describing the quantum nature of the electromagnetic field (the primary difference being that a scalar field lacks polarization).

The physics discussed in this thesis is rather more similar to that typically associated with quantum fields in curved spacetimes [39]. We will not, however, at any point be considering anything other than Minkowski spacetime, and so we will not need the full machinery of QFT in curved spacetime. Indeed we will be further simplifying matters by only considering scalar fields in 1 + 1-dimensional Minkowski space, often in the context of cavities (i.e. fields bounded to some finite, flat region of space). We will first discuss the required concepts within free space (i.e. without a cavity), including quantization in Rindler coordinates, the Unruh effect, and vacuum entanglement. We will conclude this chapter with a summary of how things change when considering a cavity field.

### 4.1 Field quantization

In this section we will describe the basics of field quantization, outlining the critical characteristics of a scalar field. We will work in 1 + 1-dimensional Minkowski space, with

coordinates  $(t, x)$  and metric signature  $\eta_{\alpha\beta} = \text{diag}(1, -1)$ . A scalar quantum field  $\hat{\phi}(x, t)$  is then a quantized, single-component field, the evolution of which is determined by the Poincaré invariant action

$$S = \frac{1}{2} \int dx dt \left( (\partial_t \hat{\phi})^2 - (\partial_x \hat{\phi})^2 - \mu^2 \hat{\phi}^2 \right), \quad (4.1)$$

where  $\mu$  is the mass that we associate with the field in question. Identifying the canonical momentum operator  $\hat{\pi} = \partial_t \hat{\phi}$  and performing a Legendre transform we obtain the corresponding field Hamiltonian

$$\hat{H} = \frac{1}{2} \int dx \left( (\partial_t \hat{\phi})^2 + (\partial_x \hat{\phi})^2 + \mu^2 \hat{\phi}^2 \right). \quad (4.2)$$

We will often refer to this as the free Hamiltonian of the field. More generally there may be interaction terms between the field and other quantum systems, or between the field and itself.

The field evolution generated by this Hamiltonian is such that  $\hat{\phi}$  satisfies the Klein-Gordon equation

$$(\square + \mu^2)\hat{\phi}(x, t) = 0, \quad (4.3)$$

where  $\square = \partial_t^2 - \partial_x^2$ . Being an observable, we demand that  $\hat{\phi}$  be Hermitian. We may then expand the field into a linear combination of Hermitian solutions to this equation of motion. Being in the continuum, there is a continuous set of such solutions (this will change when considering a cavity field) and thus we may represent  $\hat{\phi}$  in the general form

$$\hat{\phi}(x, t) = \int dk \left( u_k(x, t)\hat{a}_k + u_k^*(x, t)\hat{a}_k^\dagger \right), \quad (4.4)$$

where  $(\square + \mu^2)u_k = 0$  and as of yet the  $\{\hat{a}_k\}$  are some unspecified set of operators. Note that we are implicitly working in the Heisenberg picture, as it is the operator  $\hat{\phi}(x)$  that is evolving with time. As such, any state of our quantum field will be time independent. Importantly, we will demand that the solutions  $\{u_k\}$  form a complete orthonormal mode basis with respect to the Klein-Gordon inner product, evaluated at some fixed time

$$(f, g) = i \int dx (f^* \dot{g} - \dot{f}^* g), \quad (4.5)$$

where the over-dot represents differentiation with respect to time  $t$ . This is the unique inner product to be preserved under Klein-Gordon evolution. With respect to this inner product we demand

$$(u_k, u_{k'}) = \delta(k - k'), \quad (u_k^*, u_{k'}^*) = -\delta(k - k'), \quad (u_k, u_{k'}^*) = 0. \quad (4.6)$$

Consolidating the Klein-Gordon inner product with Eq. (4.4), we find that  $\hat{a}_k = (u_k, \hat{\phi})$  and  $\hat{a}_k^\dagger = -(u_k^*, \hat{\phi})$ . Plugging these back into the field decomposition and expanding out the inner products we find the completeness relations associated with the solution space to be

$$\begin{aligned} 0 &= \int dk (u_k^*(x', t)u_k(x, t) - u_k(x', t)u_k^*(x, t)), \\ \delta(x - x') &= i \int dk (\dot{u}_k(x', t)u_k^*(x, t) - \dot{u}_k^*(x', t)u_k(x, t)). \end{aligned} \quad (4.7)$$

Note that we are not, at this point, choosing any particular mode basis. As will be very important, making such a choice also corresponds to a particular choice of operators  $\{\hat{a}_k, \hat{a}_k^\dagger\}$ .

The canonical momentum field associated with  $\hat{\phi}$  is given by the time derivative  $\hat{\pi} = \partial_t \hat{\phi}$ . We then demand that these pairs satisfy the canonical commutation relations at a given time  $t$

$$\begin{aligned} [\hat{\phi}(x, t), \hat{\phi}(x', t)] &= 0, \\ [\hat{\pi}(x, t), \hat{\pi}(x', t)] &= 0, \\ [\hat{\phi}(x, t), \hat{\pi}(x', t)] &= i\delta(x - x'). \end{aligned} \quad (4.8)$$

Using Eqs. (4.4) and (4.7) it is straightforward to see that these commutation relations are equivalent to the following set:

$$\begin{aligned} [\hat{a}_k, \hat{a}_{k'}] &= 0 \\ [\hat{a}_k^\dagger, \hat{a}_{k'}^\dagger] &= 0 \\ [\hat{a}_k, \hat{a}_{k'}^\dagger] &= \delta(k - k'). \end{aligned} \quad (4.9)$$

We immediately recognize that the set  $\{\hat{a}_k, \hat{a}_k^\dagger\}$  satisfy the standard canonical commutation relations associated with the annihilation and creation operators of a Fock basis. As such, we may define a vacuum state (which, critically, depends on the mode basis that we have chosen) that satisfies

$$\hat{a}_k |0\rangle = 0 \quad \forall k. \quad (4.10)$$

A state containing excitations (i.e. particles) with respect to this chosen basis is then obtained by applying creation operators to the vacuum state. A one-particle state in

mode- $k$ , for example, is  $|1_k\rangle = \hat{a}_k^\dagger |0\rangle$ . In general, a particle state containing  $n^{(1)}$  in mode- $k_1$ ,  $n^{(2)}$  particles in mode- $k_2$ , etc, is given by

$$|n_{k_1}^{(1)}, n_{k_2}^{(2)}, \dots\rangle = (n^{(1)}! n^{(2)}! \dots)^{-1/2} (\hat{a}_{k_1}^\dagger)^{n^{(1)}} (\hat{a}_{k_2}^\dagger)^{n^{(2)}} \dots |0\rangle. \quad (4.11)$$

The particle-number of a given mode- $k$  is associated with the observable  $\hat{N}_k = \hat{a}_k^\dagger \hat{a}_k$ , the number operator, with respect to which a particle state  $|n_k\rangle$  is an eigenvector with eigenvalue  $n_k$ :  $\hat{N}_k |n_{k'}\rangle = n_k |n_k\rangle \delta(k - k')$ , where the delta-function is a necessary artifact of working in a continuous basis. If we we apply an infrared cutoff to the field (as we will when working in a cavity) then this is regularized  $\delta(k - k) \rightarrow \delta_{kk'}$ . The total particle number, across all modes, is then given by the total number operator  $\hat{N} = \int dk \hat{N}_k$ . Even for general states  $|\psi\rangle$  of non-definite particle content, the expected particle number will be computed as  $\langle \psi | \hat{N} | \psi \rangle$ .

## 4.2 Choice and change of mode basis

In the previous section we maintained that the solutions  $\{u_k, u_k^*\}$  can be composed of any orthonormally complete basis of solutions to the Klein-Gordon equation, and that the choice of a particular basis corresponds to a choice set of ladder operators  $\{\hat{a}_k, \hat{a}_k^\dagger\}$ . Critically, this also implies that different choices of mode basis are associated with different choices of Fock bases, and in particular the vacuum state of one choice may not coincide with that of another. There should, however, be a particular choice of mode basis such that the corresponding vacuum state minimizes the energy of the system, with respect to the Hamiltonian Eq. (4.2). As it turns out, in the case of curved spacetime backgrounds this is not always the case [39]. Here, however, we will only be considering Minkowski spacetime, in which case there is indeed a well defined, stationary state of minimum energy. It should also be pointed out that, given we are dealing with an infinite number of degrees of freedom, there may exist two choices of basis that are technically unitarily inequivalent [38]. This is the case when the particle content is finite or zero in one basis but infinite in the other. Indeed we will see an example of this in Part. IV. This fact brings up a fundamental problem, however, regarding which basis we should choose. In this thesis we will not be overly concerned with these issues, and the approaches taken here are sufficiently operational that these considerations will never impact the results we obtain.

To continue, let us consider again the solution set  $\{u_k, u_k^*\}$  to the Klein-Gordon Eq. (4.3). The most obvious choice of solutions consist of the entirely delocalized plane waves

$$u_k(x, t) = \frac{1}{\sqrt{4\pi\omega_k}} \exp i(kx - \omega_k t), \quad (4.12)$$

where the dispersion relation following from Eq. (4.3) is  $\omega_k^2 = k^2 + \mu^2$ . The normalization factor follows from Eqs. (4.5) and (4.6). This mode basis takes a special place among the others, as it happens to be the one that diagonalizes the free field Hamiltonian, in the following sense. It is straightforward to see that when using the mode functions Eq. (4.12) in the expansion Eq. (4.4) of  $\hat{\phi}$ , that the Hamiltonian Eq. (4.2) takes the form (up to a constant value that does not impact the physics)

$$\hat{H} = \int dk \omega_k \hat{a}_k^\dagger \hat{a}_k = \int dk \omega_k \hat{N}_k, \quad (4.13)$$

where we recognize  $\hat{N}_k = \hat{a}_k^\dagger \hat{a}_k$  to be the number operator of mode- $k$ . This shows us very clearly that particle states with respect to this mode basis are states of definite energy, and thus are stationary states:

$$\hat{H} |n_{k_1}^{(1)}, n_{k_2}^{(2)}, \dots\rangle = (\omega_{k_1} n_{k_1}^{(1)} + \omega_{k_2} n_{k_2}^{(2)} + \dots) |n_{k_1}^{(1)}, n_{k_2}^{(2)}, \dots\rangle. \quad (4.14)$$

We see that each level of excitation of a given mode- $k$  adds energy  $\omega_k$  to the system. That is, each mode is mathematically equivalent to a quantum harmonic oscillator with energy spacing  $\omega_k$ . It can similarly be demonstrated that each excitation of mode- $k$  carries a momentum  $k$  such that particle states are also states of definite momentum (as seen by computing the field momentum operator from the standard stress-energy tensor [39]). Because of this, it is this Fock basis that is often ascribed as being the one of physical relevance, and what is commonly referred to as a “particle” is exactly an excitation with respect to this basis. That is, a “particle” is an excitation of definite energy  $\omega_k$  and momentum  $k$ , associated with a stationary mode basis. From this point onwards we will reserve the notation  $u_k, \hat{a}_k$  to be used exclusively for the stationary-mode basis (with respect to the free Hamiltonian) of whatever system is being considered (be it in free space or in a cavity). The vacuum state of this basis,  $|0\rangle$  such that  $\hat{a}_k |0\rangle = 0 \forall k$ , is therefore the unique state that we take as being devoid of particles. It is the state of lowest possible energy,  $\hat{H} |0\rangle = 0$  (note that in Eq. (4.13) we have already subtracted off the diverging vacuum energy contribution).

A defining characteristic of such a stationary-mode basis is that the free Heisenberg evolution of the ladder operators satisfy  $\hat{U}^\dagger(t) \hat{a}_k \hat{U}(t) = e^{-i\omega_k t} \hat{a}_k$  and  $\hat{U}^\dagger(t) \hat{a}_k^\dagger \hat{U}(t) = e^{i\omega_k t} \hat{a}_k^\dagger$ , where  $\hat{U}(t) = \exp(i\hat{H}t)$  is the free evolution operator. The evolution of the ladder operators then translates into the Heisenberg evolution of the field, and is commonly represented as a time evolution of the mode functions themselves, Eq. (4.12). This is exactly how the time dependence of the modes  $u_k(x, t) = u_k(x) e^{-i\omega_k t}$  is to be understood, as representing the quantum Heisenberg evolution of the field. As an aside, note that in the phase-space representation this corresponds exactly to a rotation of the form Eq. (3.16).

While the choice of mode functions  $u_k$  as given by Eq. (4.12) certainly enjoys a special post of physical significance, ultimately there is no reason why we cannot quantize our field with respect to any other orthonormally complete mode basis. Indeed the description of certain phenomena of interest require us to do exactly this and, critically, to be able to transform from one basis to another. The most common example of where such an operation is useful is in the description of particle-creation phenomena. There may be a disturbance to the system for example (as described by some additional, time-dependent Hamiltonian terms) which evolves the mode basis such that what was previously a stationary basis before the disturbance is no longer so afterwards. In such a case the vacuum state of the original basis may not correspond with the final vacuum state. Since we are working in the Heisenberg picture (although this is not required), meaning that the state vector does not evolve, the state afterwards may not be the physical vacuum even if it was so originally. Another scenario is that of transforming one's spacetime coordinates to match those of some other observer. Such a transformation translates into a transformation of mode basis. We will see an important example of this in the next section.

Being a linear vector space, we can transform any basis  $u_k$  of solutions to the Klein-Gordon to any other basis  $v_\ell$  by means of a linear transformation of the form

$$v_\ell(x, t) = \int dk (\alpha_{\ell k} u_k(x, t) + \beta_{\ell k} u_k^*(x, t)), \quad (4.15)$$

where the transformation coefficients are given by

$$\alpha_{\ell k} = (v_\ell, u_k), \quad \beta_{\ell k} = -(v_\ell, u_k^*). \quad (4.16)$$

This is generically referred to as a Bogoliubov transformation, the coefficients  $\alpha_{\ell k}$  and  $\beta_{\ell k}$  of which are time independent (resulting from the time independence of the Klein-Gordon inner product with respect to Klein-Gordon evolution). The inverse transformation is easily shown to be

$$u_k(x, t) = \int d\ell (\alpha_{\ell k}^* v_\ell(x, t) - \beta_{\ell k} v_\ell^*(x, t)). \quad (4.17)$$

Such a transformation does not modify physical observables, rather it is simply a way of expanding the field operator  $\hat{\phi}$  in a different basis of mode functions. The field itself, however, is entirely equivalent in either case:

$$\hat{\phi} = \int dk (u_k \hat{a}_k + u_k^* \hat{a}_k^\dagger) = \int d\ell (v_\ell \hat{b}_\ell + v_\ell^* \hat{b}_\ell^\dagger), \quad (4.18)$$

where  $\hat{b}_\ell$  and  $\hat{b}_\ell^\dagger$  are the ladder operators corresponding to the new mode basis. From this equality we can find that the transformations Eqs. (4.15, 4.17) take the following form on the ladder operators:

$$\hat{b}_\ell = \int dk(\alpha_{\ell k}^* \hat{a}_k - \beta_{\ell k}^* \hat{a}_k^\dagger), \quad (4.19)$$

$$\hat{a}_k = \int d\ell(\alpha_{\ell k} \hat{b}_\ell + \beta_{\ell k}^* \hat{b}_\ell^\dagger). \quad (4.20)$$

Importantly, in order for this transformation to be unitary it is straightforward to show that the coefficients of any Bogoliubov transformation must satisfy the conditions

$$\int dk(\alpha_{mk} \alpha_{nk}^* - \beta_{mk} \beta_{nk}^*) = \delta(m - n), \quad (4.21)$$

$$\int dk(\alpha_{mk} \beta_{nk} - \beta_{mk} \alpha_{nk}) = 0.$$

Of particular relevance to this thesis is the fact that the transformation in Eq. (4.19) is a linear transformation between sets of ladder operators, meaning that it is also a linear transformation between sets of quadrature operators defined as in Eq. (3.2). Thus, as explained in Ch. 3, it is a transformation that preserves the Gaussianity of a state. The conditions in Eqs. (4.21), in fact, ensure that such a Gaussian transformation is symplectic. We will not pursue this connection further now, as it is more applicable to this thesis (and is simpler) in the case of a countable set of modes (e.g. as in a cavity). We will therefore return to this in Sect. 4.7.

Consider a general Bogoliubov transformation as it acts on the ladder operators, Eq. (4.19). One immediate observation is that, as was alluded to earlier, the vacuum state of one mode basis does not in general coincide with that of another. Only in the case that all of the  $\beta$ -coefficients vanish will the two bases share a common vacuum state, as in that case the annihilation operators  $\hat{b}_\ell$  are linear combinations of just annihilation operators  $\hat{a}_k$ . More generally, if we label  $|0\rangle$  as being the vacuum state corresponding to  $\{\hat{a}_k, \hat{a}_k^\dagger\}$ , then we will have

$$\hat{b}_\ell |0\rangle = \int dk(\alpha_{\ell k}^* \hat{a}_k - \beta_{\ell k}^* \hat{a}_k^\dagger) |0\rangle = - \int dk \beta_{\ell k}^* |1_k\rangle \neq 0, \quad (4.22)$$

where  $|1_k\rangle$  are single-particle states of the  $\{\hat{a}_k, \hat{a}_k^\dagger\}$  basis. There will, rather, be a different state  $|\tilde{0}\rangle$  that acts as the vacuum state of the  $\{\hat{b}_\ell, \hat{b}_\ell^\dagger\}$  basis, that state defined to satisfy  $\hat{b}_\ell |\tilde{0}\rangle = 0 \forall \ell$ . The  $\beta$ -coefficients can be used to garner information on the particle content



of the vacuum state within a different basis. For example if we work with the vacuum state  $|0\rangle$  and ask what the particle content of this state is in mode- $\ell$  of the  $\{\hat{b}_\ell, \hat{b}_\ell^\dagger\}$  basis, as given by the number operator  $\hat{N}_\ell^{(b)} = \int d\ell \hat{b}_\ell^\dagger \hat{b}_\ell$ , the answer is easily seen to be

$$\langle 0 | \hat{N}_\ell^{(b)} | 0 \rangle = \int dk |\beta_{\ell k}|^2. \quad (4.23)$$

Before continuing we will give a simple example of a Bogoliubov transformation following a change of spacetime coordinates. In particular, let us consider a simple Lorentz transformation. We imagine an inertial observer  $O_1$  who attaches coordinates  $(t, x)$  to the  $1 + 1$  Minkowski space in which he lives. Namely, his worldline is described by  $x = 0$  for all times  $t$ . From the perspective of  $O_1$ , the plane wave modes of the field (i.e. those that diagonalize the Hamiltonian) are given by Eq. (4.12). Now consider a second inertial observer  $O_2$  that is traveling relative to  $O_1$  with velocity  $v$  (to be clear, here as everywhere we set the speed of light to unity,  $c = 1$ ). Observer  $O_2$  labels spacetime points using another set of coordinates  $(t', x')$  that are given by the Lorentz transformation  $t' = \gamma(t - vx)$  and  $x' = \gamma(x - vt)$ , where  $\gamma = (1 - v^2)^{-1/2}$ . This means that  $O_2$  decomposes the field using a *different* set of plane wave modes  $\bar{u}_{k'}$  given by

$$\bar{u}_{k'}(x, t) = \frac{1}{\sqrt{4\pi\omega_{k'}}} \exp i(k'x' - \omega_{k'}t'). \quad (4.24)$$

We can now compute the Bogoliubov transformation  $\bar{u}_{k'} = \int dk (\alpha_{k'k} u_k + \beta_{k'k} u_k^*)$  between these two sets of modes, evaluating the coefficients via Eq. (4.16). This is straightforward to carry out, and the result is seen to be

$$\alpha_{k'k} = \sqrt{\frac{\omega_k}{\omega_{k'}}} \delta(k' - \gamma(k - v\omega_k)), \quad (4.25)$$

$$\beta_{k'k} = 0. \quad (4.26)$$

Importantly (and unsurprisingly), we see that  $\beta_{k'k} = 0$  and therefore that no particle production occurs when changing between inertial frames. If  $O_1$  observes the vacuum state, for example, then  $O_2$  will as well. We will see an example in the next section of a coordinate transformation which is *not* passive in this sense. Furthermore, we see from the  $\alpha_{k'k}$  coefficients that plane wave modes of momentum  $k$  as seen by  $O_1$  are observed by  $O_2$  as plane wave modes of momentum  $k' = \gamma(k - v\omega_k)$ , from which it is easily also seen that  $\omega_{k'} = \gamma(\omega_k - vk)$ . That is, the two observers experience red/blue shifts with respect to each other. Indeed the form of the result is exactly as should have been expected, as it simply represents the Lorentz transformation applied to the four-momentum  $k^\alpha = (\omega_k, k)$ .

### 4.3 Rindler quantization

At the end of the last section we saw a simple example of a passive Bogoliubov transformation, in which the vacuum state is not changed under the transformation. Here, we will explore another Bogoliubov transformation for which this is not the case, i.e. it is an active transformation in which the  $\beta$ -coefficients are non-zero. Aside from being a good example, this transformation is the starting point for many of the phenomena that we will explore throughout this thesis, most notably in Part. III. Even beyond this, the material in this section is an excellent starting ground to understanding both the Unruh effect as well as vacuum entanglement, phenomena that most of Part. II is devoted to exploring. We will provide proper introductions to these effects in Sects. 4.5 and 4.6.

In the last section we saw the Bogoliubov transformation corresponding to a Lorentz transformation between one inertial set of coordinates and another. Here, we will instead consider a change of coordinates from those of an inertial observer to those of a non-inertial observer. We will observe that in this case the transformation is no longer passive. Specifically, we will consider a non-inertial coordinate system corresponding to an ensemble of uniformly accelerating observers. Let  $\tau$  be the proper time of such an observer. By definition, the worldline  $x^\mu(\tau) = (t(\tau), x(\tau))$  of a uniformly accelerated observer has constant proper acceleration  $a = \sqrt{|\eta_{\mu\nu} a^\mu a^\nu|}$ , where  $\eta_{\mu\nu}$  is the Minkowski metric (only because we are working in Minkowski space) and  $a^\mu = \partial_\tau^2 x^\mu$  is the observer's 4-acceleration. It is trivial to confirm that such a worldline is given by

$$t = a^{-1} \sinh a\tau, \quad x = a^{-1} \cosh a\tau. \quad (4.27)$$

In other words, in the inertial  $(t, x)$  coordinates this trajectory is the hyperbola  $x = \sqrt{t^2 + a^{-2}}$ . This is displayed in Fig. 4.1, where the distance to the origin at closest approach is  $1/a$ . Note that this observer, assuming that they uniformly accelerate for all time, is causally disconnected from the left-hand wedge. We will refer to these two wedges as Rindler wedges. That is, the observer sees a horizon (here called a Rindler horizon), which is always a proper distance  $1/a$  away. The trajectory of a more highly accelerated observer would be represented by a tighter hyperbola, hugging more closely to the horizon.

The world line in Eq. 4.27 suggests introducing a new set of spacetime coordinates  $(\tau, \xi)$  suited for uniformly accelerating observers. These are known as Rindler coordinates [84, 39], and are given implicitly by

$$t = a^{-1} e^{a\xi} \sinh a\tau, \quad x = a^{-1} e^{a\xi} \cosh a\tau. \quad (4.28)$$

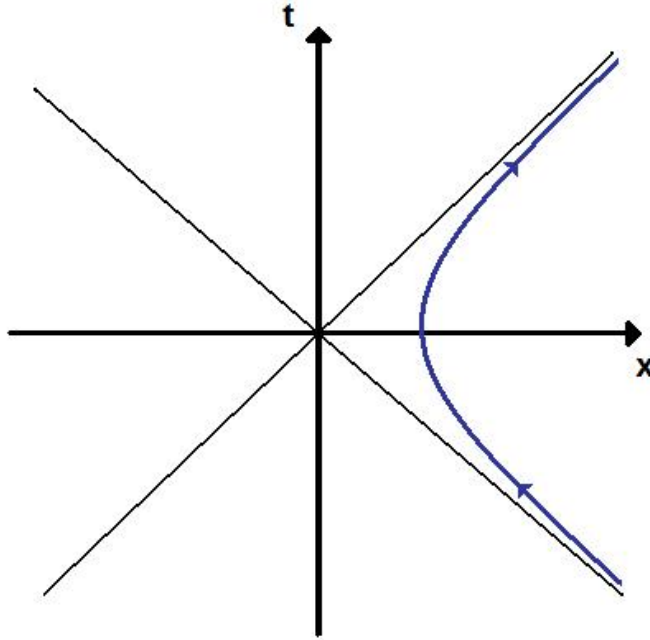


Figure 4.1: The trajectory of a uniformly accelerating observer. Note that this observer is causally disconnected from the left-hand Rindler wedge.

These coordinates define an ensemble of uniformly accelerating observers, of different accelerations, which together cover the right Rindler wedge. Each such observer lays at a constant value of  $\xi$ , the one at  $\xi = 0$  being that of proper acceleration  $a$ . More generally, an observer laying at constant  $\xi$  has proper acceleration  $ae^{-a\xi}$ . The proper time of such an observer is given by  $e^{a\xi}\tau$ . These coordinates only cover the right Rindler wedge seen in Fig. 4.1, the area of  $x > |t|$ . A second coordinate patch can similarly be used to define the left wedge by changing  $x \rightarrow -x$  in Eq. 4.28.

Importantly, the metric in these coordinates is easily seen to be conformally equivalent to the Minkowski metric:  $ds^2 = e^{2a\xi}(d\tau^2 - d\xi^2)$ . This implies that, assuming we are working with a massless field in  $1 + 1$  dimensions (which we will for the purposes of this section),

the Klein-Gordon equation is invariant under this coordinate transformation <sup>1</sup>

$$(\partial_t^2 - \partial_x^2)\hat{\phi} = 0 \implies (\partial_\tau^2 - \partial_\xi^2)\phi = 0. \quad (4.29)$$

This fact will greatly simplify the analysis in this section. More generally, in higher dimension and with massive fields this will not be the case, and more work is required. Qualitatively, however, the results will be unchanged in more general scenarios [85], at least in regards to the phenomena that will be discussed in Sects. 4.5 and 4.6.

Given Eq. (4.29), we know that plane-waves with respect to the Rindler coordinates are solutions to the Klein-Gordon equation. These solutions are exactly the plane-wave solutions that the set of Rindler observers see as being stationary modes, excitations of which they interpret as being particles. These are referred to as Rindler modes:

$$w_\ell^R(\xi, \tau) = \frac{1}{\sqrt{4\pi\omega_\ell}} \exp i(\ell\xi - \omega_\ell\tau), \quad (4.30)$$

where here  $\omega_\ell = |\ell|$  since we are working with a massless field, and the  $R$  represents that these are the Rindler modes corresponding to the right Rindler wedge. There will be a similarly defined set of left Rindler modes  $w_\ell^L$ . Combined, these two sets of modes represent a complete mode basis with respect to which the field operator can be expanded:

$$\hat{\phi} = \int d\ell (w_\ell^R \hat{b}_\ell^R + w_\ell^{R*} \hat{b}_\ell^{R\dagger} + w_\ell^L \hat{b}_\ell^L + w_\ell^{L*} \hat{b}_\ell^{L\dagger}), \quad (4.31)$$

where here  $\hat{b}_\ell^R$  and  $\hat{b}_\ell^L$  are the annihilation operators corresponding to the right and left Rindler modes, respectively. We can, for example, define the state  $|0_R\rangle$  to be that which is annihilated by these operators:

$$\hat{b}_\ell^R |0_R\rangle = \hat{b}_\ell^L |0_R\rangle = 0 \quad \forall \ell. \quad (4.32)$$

---

<sup>1</sup>We will not be explicitly dealing with quantum fields in curved spacetimes in this thesis, and thus have not devoted time discussing the theory. For this point, however, it is worth mentioning some brief details. As a generalization to what was just stated in the main text, the wave equation  $\square\phi = 0$  is invariant under conformal transformations, i.e. those that transform the metric as  $g_{\mu\nu} \rightarrow \Omega g_{\mu\nu}$ , where  $\Omega$  is an arbitrary scalar function over the spacetime. This is seen from the fact that, in general spacetimes with some given coordinate system, the d'Alembertian operator is given by  $\square = g^{\mu\nu} \nabla_\mu \nabla_\nu$ , where  $\nabla_\mu$  is the covariant derivative. In flat spacetime this reduces to the usual wave operator  $\square = \eta^{\mu\nu} \partial_\mu \partial_\nu$ . The general form evaluates to the expression  $\square = (\sqrt{-g})^{-1} \partial_\mu (\sqrt{-g} g^{\mu\nu} \partial_\nu)$ , where  $g$  is the determinant of the metric tensor  $g_{\mu\nu}$ , and  $g^{\mu\nu}$  is its metric inverse. Under a conformal transformation we have  $g \rightarrow \Omega^2 g$  and  $g^{\mu\nu} \rightarrow \Omega^{-1} g^{\mu\nu}$ , and thus the d'Alembertian transforms as  $\square \rightarrow \Omega^{-1} \square$ , leaving the wave equation invariant. See [39] for a full treatment of quantum fields in curved spacetimes.

This state is referred to as the Rindler vacuum, and is the vacuum as would be observed by Rindler observer (either on the right or left wedge). Unlike the example in the previous section, however, this state is *not* equivalent to the Minkowski vacuum (the vacuum state as seen by inertial observers). That is, the coefficients  $\beta_{\ell k}^R = -(w_\ell^R, u_k)$  and  $\beta_{\ell k}^L = -(w_\ell^L, u_k)$  are nonzero. This implies that if the field is in the Minkowski vacuum, then uniformly accelerating observers will nevertheless see particles!

To see this we can explicitly compute the Bogoliubov coefficients between the Minkowski and Rindler plane-wave modes. This is rather labor-intensive, however. There is instead a more elegant and enlightening approach that we will sketch here [21, 39], though without going into detail. The trick is to consider a third set of modes, corresponding to annihilation operators  $\hat{d}_\ell^{(1)}$  and  $\hat{d}_\ell^{(2)}$  that we call the Unruh modes. These modes are defined such that we obtain the Rindler modes from the Unruh modes via a set of two-mode squeezing operations (see Sect. 3.2) for each frequency  $\ell$ :

$$\begin{aligned}\hat{b}_\ell^R &= \cosh(r_\ell)\hat{d}_\ell^{(1)} + \sinh(r_\ell)\hat{d}_\ell^{(2)\dagger}, \\ \hat{b}_\ell^L &= \cosh(r_\ell)\hat{d}_\ell^{(2)} + \sinh(r_\ell)\hat{d}_\ell^{(1)\dagger},\end{aligned}\tag{4.33}$$

where the squeezing parameters are given by  $r_\ell = \tanh^{-1}(e^{-\pi\omega_\ell/a})$ . The mode functions corresponding to these Unruh modes, which for the sake of this section we will just label  $v_\ell^{(1)}$  and  $v_\ell^{(2)}$ , are then seen to be

$$\begin{aligned}v_\ell^{(1)} &= \cosh(r_\ell)w_\ell^L + \sinh(r_\ell)w_\ell^R, \\ v_\ell^{(2)} &= \cosh(r_\ell)w_\ell^R + \sinh(r_\ell)w_\ell^L.\end{aligned}\tag{4.34}$$

We will not go into details here, but it can be demonstrated (see [21, 39]) that these Unruh modes are purely positive frequency in the Minkowski mode basis, meaning that the overlaps  $(v_\ell^{(1)}, u_k^*)$  and  $(v_\ell^{(2)}, u_k^*)$  are vanishing. This means that the transformation from the Minkowski plane-wave mode basis to the Unruh mode basis is passive. That is, the Unruh vacuum defined by  $\hat{d}_\ell^{(1)}|0_U\rangle = \hat{d}_\ell^{(2)}|0_U\rangle = 0$  is *equivalent* to the standard Minkowski vacuum,  $|0_U\rangle = |0\rangle$ . From this, the form of the Minkowski vacuum in the Rindler basis follows trivially, as it is simply a collection of two-mode squeezed states between Rindler modes. Recalling the form of a two-mode squeezed state, Eq. (3.19), we immediately obtain

$$|0\rangle = \bigotimes_\ell \frac{1}{\cosh r_\ell} \sum_n \tanh^n r_\ell |n^L\rangle |n^R\rangle,\tag{4.35}$$

where  $|n^L\rangle$  and  $|n^R\rangle$  are the particle-number states with respect to the Rindler basis. We will use the form of this state as a starting point for our discussions in Sects. 4.5 and 4.6.

## 4.4 Particle detectors

Here we will discuss a concept of central importance to this thesis, as well as lay out some bread and butter methods that Ch. 5 is devoted to superseding. In the material presented above we have broadly and very formally discussed the notion of a particle as being an excitation with respect to the stationary mode basis as seen by some observer. While the use of this definition of a particle makes sense within the context of particle physics, where in practice the excitations of a non-interacting theory need only be discussed at infinity, there are nevertheless several severe issues with this interpretation. The most obvious is that under this definition a particle is a completely delocalized entity. There is furthermore the strange fact that, as we have discussed and will soon see in more detail, the particle content of a given quantum state is observer-dependent.

The point of this section is to introduce a theoretical tool that lets one play with the same physics, but from a far more operational and physically concrete perspective, a central theme in this thesis. The idea is to ask what properties of the state of a quantum field may actually be physically measured. To this end we utilize a model of measurement in which we have some other quantum system, which we call the detector, and which we let interact in some way with the quantum field. The response of the detector due to this interaction then provides us with information on the properties of the field. An obvious real world example of such a setup would, for example, be an atom in an electromagnetic field. An electronic excitation of the atom would be caused by the absorption of a photon, and this would tell us that a photon was previously present in the field; a detection. Obviously there are an infinite number of ways in which this general setup can be mathematically constructed, but the idea is the same: more energy in a field (i.e. more particles) will generically lead to a more energetic response from the detector. This allows us to avoid the difficult interpretational issues inherent in a formal construction by simply asking what one actually sees when looking at a field. As Bill Unruh likes to put it, *a particle is that which a particle detector detects*.

Here we will introduce one concrete model, the so called Unruh-DeWitt detector [21, 39]. The reader is referred to [40] for an overview of this model within the context of relativistic quantum information, as well as related models and literature. The model that we will present in Ch. 5, and which will be used throughout Part II, will represent a minor (but significant) modification of this. In the Unruh-DeWitt model, we consider a two-level quantum system (i.e. a qubit), of energy gap  $\Omega$ , that is locally coupled to a field  $\hat{\phi}$  via an interaction Hamiltonian of the form  $\hat{H}_I = \lambda \hat{\mu} \hat{\phi}(x_d)$ . Here,  $\lambda$  is a number that represents the strength of the interaction,  $\hat{\mu} = \hat{\sigma}_+ + \hat{\sigma}_-$  is referred to as the monopole operator of the qubit, where  $\sigma_+$  and  $\sigma_-$  are its raising and lowering operators (i.e.  $\hat{\mu}$  is the just the

Pauli- $X$  operator), and  $\hat{\phi}(x_d)$  is the quantum field evaluated at the (classical) position  $x_d$  of the detector. It will be most advantageous to work in the interaction picture, in which case the interaction Hamiltonian is

$$\hat{H}_I(\tau) = \lambda(\tau)\hat{\mu}(\tau)\hat{\phi}(x_d(\tau), t(\tau)), \quad (4.36)$$

where  $\hat{\phi}(x, t)$  takes the generic form of Eq. (4.4), and where typically the mode basis used will be the plane wave modes, Eq. (4.12). Here we are parameterizing the evolution with respect to the proper time  $\tau$  of the detector, which if in motion will not generally be equivalent to  $t$ . In the interaction picture monopole operator (i.e. its freely evolved form) is given by  $\hat{\mu}(\tau) = e^{i\Omega\tau}\hat{\sigma}_+ + e^{-i\Omega\tau}\hat{\sigma}_-$ . Lastly, by generally including time dependence in  $\lambda(\tau)$  we are able to tune the interaction strength as a function of time. In particular, this is used for turning on and off one's detector. For this reason,  $\lambda(\tau)$  is also to be called the window function or the switching function.

Here we will not worry about the specific world line  $(x(\tau), t(\tau))$  taken by the qubit detector. In general we are interested in its response due to its interaction with the field. To derive the evolution of the detector we will work perturbatively in powers of the coupling strength  $\lambda$ , meaning that we require  $\lambda \ll 1$ . Working perturbatively also means, however, that we are restricted to short-time and small-energy phenomena. As we will see, the great advantage of the model to be introduced in Ch. 5 is that it may be solved without the use of perturbation theory. Let us consider the case where  $\lambda(\tau)$  is nonzero over a time interval  $\tau \in [0, T]$ . The unitary evolution generated by Eq. (4.36) can be formally represented as the time-ordered exponential  $\hat{U}(T) = \mathcal{T} \exp[-i \int_0^T d\tau \hat{H}_I(\tau)]$ . Expanding this to second order in  $\lambda$  gives  $\hat{U}(T) = \hat{I} + \hat{U}_1(T) + \hat{U}_2(T) + \mathcal{O}(\lambda^3)$ , where

$$\hat{U}_1(T) = -i \int_0^T d\tau \hat{H}_I(\tau), \quad \hat{U}_2(T) = - \int_0^T d\tau \int_0^\tau d\tau' \hat{H}_I(\tau) \hat{H}_I(\tau'). \quad (4.37)$$

Suppose that our initial state is the ground state for the detector and the vacuum state for the field, namely:  $\hat{\rho}_0 = |0\rangle\langle 0| \otimes |0\rangle\langle 0|$ , where we will take the operator to the left of the tensor product to be that of the detector. It is easily seen that the evolution of this state by the above unitary is, up to second order in  $\lambda$ , given by  $\hat{\rho}(T) = \hat{\rho}_0 + \hat{\rho}_1(T) + \hat{\rho}_2(T)$  where

$$\hat{\rho}_1 = \hat{U}_1 \hat{\rho}_0 + \hat{\rho}_0 \hat{U}_1^\dagger, \quad (4.38)$$

$$\hat{\rho}_2 = \hat{U}_1 \hat{\rho}_0 \hat{U}_1^\dagger + \hat{U}_2 \hat{\rho}_0 + \hat{\rho}_0 \hat{U}_2^\dagger. \quad (4.39)$$

Here we are interested in the reduced state of the detector, obtained by tracing out the field from  $\hat{\rho}(T)$ . We therefore consider taking the partial trace of each of the pieces.

Of course, we have that  $\text{Tr}_F \hat{\rho}_0 = |0\rangle \langle 0|$  is the zeroth order term for the detector state. Considering now the partial trace of  $\hat{\rho}_1$ , note that we have

$$\hat{U}_1 \hat{\rho}_0 = -i \int_0^T d\tau \lambda(\tau) e^{i\Omega\tau} |1\rangle \langle 0| \otimes \hat{\phi}(\tau) |0\rangle \langle 0|. \quad (4.40)$$

Here,  $\hat{\phi} |0\rangle$  is going to be a linear combination of one-particle states, and thus taking the partial trace over  $\hat{U}_1 \hat{\rho}_0$  will give zero. This similarly occurs for  $\hat{\rho}_0 \hat{U}_1^\dagger$ . Thus,  $\hat{\rho}_1$  does not contribute to the reduced state of the detector, meaning that there is no first-order contribution.

For the second order contribution, let's first consider the term  $\hat{U}_1 \hat{\rho}_0 \hat{U}_1^\dagger$  and its partial trace. It is straightforward to see that

$$\hat{U}_1 \hat{\rho}_0 \hat{U}_1^\dagger = \int_0^T \int_0^T d\tau d\tau' \lambda(\tau) \lambda(\tau') e^{-i\Omega(\tau-\tau')} |1\rangle \langle 1| \otimes \hat{\phi}(\tau') |0\rangle \langle 0| \hat{\phi}(\tau), \quad (4.41)$$

where here we are using the notation  $\hat{\phi}(\tau) = \hat{\phi}(x_d(\tau), t(\tau))$ . As will be explained in a moment, the rest of the  $\hat{\rho}_2$  terms do not contribute to the excitation probability of the detector, and thus we can read off the second-order excitation probability, which we will label  $p_+$ , to be

$$p_+ = \int_0^T \int_0^T d\tau d\tau' \lambda(\tau) \lambda(\tau') e^{-i\Omega(\tau-\tau')} \langle 0| \hat{\phi}(\tau) \hat{\phi}(\tau') |0\rangle, \quad (4.42)$$

where the two-point (Wightman) function  $\langle 0| \hat{\phi}(\tau) \hat{\phi}(\tau') |0\rangle$  must be computed given whatever trajectory has been chosen for the detector. The form and properties of the Wightman function in scalar field theory are well known [14, 39]. We will see an explicit example of how to use this result in the following section.

Let us now mention the  $\hat{U}_2 \hat{\rho}_0$  and  $\hat{\rho}_0 \hat{U}_2$  terms. Without going into detail, it is easy to see that upon partial tracing they each give to the detector density matrix a contribution proportional to  $|0\rangle \langle 0|$  (from the  $\hat{\sigma}_- \hat{\sigma}_+$  terms) and that all other contribution vanish. The  $|0\rangle \langle 0|$  term is actually equal to the negative of Eq. (4.42), and so acts to normalize the state.

To finish this section it is worth noting that in much of the literature utilizing this model (particularly those works detailing the Unruh effect and similar phenomena) it is not the probability of excitation that is computed, but rather the the probability of excitation per unit time  $R_+ = dp_+/dT$ . This is usually referred to as the transition rate. It is used in the case where we have constant interaction strength,  $\lambda = \text{const}$ , which has been switched on



for all time. Introducing the variable  $\Delta = \tau - \tau'$ , it is easy to see that in such a case the transition rate reduces to

$$\begin{aligned} R_+ &= \lambda^2 \int_{-\infty}^{\infty} d\Delta e^{-i\Omega\Delta} \langle 0 | \hat{\phi}(\Delta) \hat{\phi}(0) | 0 \rangle, \\ &= \lambda^2 \int_{-\infty}^{\infty} d\Delta e^{-i\Omega\Delta} W(\Delta) \end{aligned} \tag{4.43}$$

where we have used the fact that the vacuum Wightman function, which we also denote  $W$ , depends only on the difference  $\Delta$ . The reason that the transition rate is used is because, this being in the large-time regime, perturbation theory breaks down. That is, the second order probability  $p_+$  diverges as  $T$  goes to infinity. The rate, however, remains well behaved. As we will see an example of in the next section, one is still able to make great use of the transition rate alone.

## 4.5 The Unruh effect

In this section we will introduce the so called Unruh effect [21], a standard example of particle creation phenomena. Simply put, the Unruh effect is a phenomenon by which an observer accelerating through the vacuum state of a quantum field will *not* observe the field to be in the vacuum state (devoid of particles), but rather will observe themselves to be immersed in a thermal bath of a temperature proportional to their proper acceleration,  $a$ . In the canonical example this temperature takes the value  $T = a/2\pi$  (in natural units).

An extensive description and overview of the Unruh effect and related literature can be found in [85]. This effect represents an important prototype of particle creation in general, and indeed is mathematically equivalent to the near-horizon Hawking effect of an eternal, Schwarzschild black hole [39, 86]. Unfortunately, the extreme accelerations required to obtain a measurable thermal response make direct experimental validation of the Unruh effect unachievable with current technology. Indirect experimental proposals, however, and highly related phenomena that *have* been observed in the laboratory are discussed in detail in [85]. Given the large body of literature pointing to the same qualitative phenomenon from many varied approaches and perspectives, there is little doubt that the Unruh effect is a true property of nature. Indeed, as can be seen using particle detector models, the effect in all of its generalities can simply be understood as the result of having a time-dependent interaction Hamiltonian; the resulting excitations of one's system thus being entirely expected. Here we will only briefly discuss the mathematical means by which the Unruh effect can be understood. We will be exploring its novel aspects in Ch. 11 and 6.

To begin, the Unruh effect can (at least in an idealized approach) be immediately garnered from the discussion in Sect. 4.3 and by Eq. (4.35). As we saw, the Minkowski vacuum state can be represented in the Rindler modes basis (i.e. the plane-wave mode basis as described by uniformly accelerated observers) as a collection of two-mode squeezed states between the right-wedge and left-wedge Rindler modes. As can be seen in Fig. 4.1, however, a uniformly accelerating observer is causally disconnected from one of the two wedges (i.e. the observer sees a horizon). In order to describe the state that such a person would measure we therefore need to trace over the region to which they don't have access. Say that our observer is isolated to the right-wedge, as in Fig. 4.1, such that we must trace over the left-wedge Rindler modes from the Eq. (4.35). As was seen in Sect. 3.2, the reduced state of a two-mode squeezed is exactly a thermal state. From the specific collection that we have in Eq. (4.35), with squeezing parameters  $r_\ell = \tanh^{-1}(e^{-\pi\omega_\ell/a})$ , we find that a uniformly accelerating observer of acceleration  $a$  will see the vacuum field to instead be in the state

$$\begin{aligned}\hat{\rho}_R = \text{Tr}_L |0\rangle\langle 0| &= \bigotimes_\ell \frac{1}{\cosh^2 r_\ell} \sum_n \tanh^{2n} r_\ell |n^R\rangle\langle n^R| \\ &= \bigotimes_\ell \frac{1}{\mathcal{Z}_\ell} \sum_n e^{-2\pi n\omega_\ell/a} |n^R\rangle\langle n^R|,\end{aligned}\tag{4.44}$$

where  $\mathcal{Z}_\ell = \sum_n e^{-2\pi n\omega_\ell/a}$ . This is exactly a thermal state of temperature  $T = a/2\pi$ . Each Rindler mode of energy gap  $\omega_\ell$  (which are the stationary modes of our observer) is in its own thermal state of temperature  $T$ , and the ensemble is given by a product state of each such thermal state, resulting in a many-mode thermal state.

This derivation is that which was first demonstrated by Unruh [21] and shows that, at least within the highly idealized scenario we are considering, a uniformly accelerated observer of acceleration  $a$  sees themselves in a thermal bath of temperature  $a/2\pi$ , despite the fact that the state under consideration is the Minkowski vacuum state. There is, however, one very strong criticism (among others) that motivates us to investigate further. This is that, in the current construction, we require previous knowledge that our observer is to be uniformly accelerating for all of time, in order that the partial trace procedure makes operational sense. If sometime in the future the observer stops accelerating then they *will* immediately have informational access to the opposing Rindler wedge. Of course, the response of the observer should not depend on what he or she will be doing in the future, and this motivates us to take a somewhat different approach.

Indeed the idea of using a particle detector, Sect. 4.4, provides such an alternative. The response of a detector model, and its transition rate, are quantities that can be evaluated

locally in time and thus do not suffer from the same criticism. We can imagine sending an Unruh-DeWitt detector on an accelerating trajectory, that given by Eq. (4.27). The transition rate, as given by Eq. (4.43), is given for a general trajectory  $(x(\tau), t(\tau))$ . The specific world line one wishes to use simply goes into the Wightman function  $W(\tau) \equiv \langle \hat{\phi}(\tau)\hat{\phi}(0) \rangle$ , where we use the notation  $\hat{\phi}(\tau) = \hat{\phi}(x(\tau), t(\tau))$ . The Unruh effect in this context is validated by realizing that the vacuum state Wightman function evaluated along the accelerated trajectory Eq. (4.27) is equivalent to the  $T = a/2\pi$  thermal state Wightman function evaluated along an inertial trajectory. This means that the accelerating detector will respond exactly as would an inertial detector traveling in a thermal state.

It is actually very straightforward to see this. All we need to know is that the vacuum Wightman function for a massless scalar field decays like the inverse square of the proper distance between the two points being evaluated [39, 14]. Thus, in our case we have

$$W(\tau) \propto \frac{1}{|(x(\tau), t(\tau)) - (x(0), t(0))|^2} = \frac{a^2}{2} \frac{1}{\cosh(a\tau) - 1}, \quad (4.45)$$

where in the second equality we have input the trajectory of Eq. (4.27). From here, it can be immediately seen that this Wightman function satisfies the famous KMS condition [87, 88, 89]

$$W(\tau) = W(-\tau + i\beta), \quad (4.46)$$

where  $\beta = 2\pi/a$  is the inverse Unruh temperature. This is exactly the condition needed in order to be a thermal state of said temperature <sup>2</sup>.

This condition can be directly understood in terms of the transition rate of an Unruh-DeWitt detector, Eq. (4.43). From this equation, notice that the transition rate is proportional to the Fourier transform  $\tilde{W}$  of the Wightman function, evaluated at the detector energy gap  $\Omega$ :  $R_+ = \sqrt{2\pi}\lambda^2\tilde{W}(\Omega)$ , where the prefactor is unimportant for the current argument. Following the derivation of Sect. 4.4 is it straightforward to show that the probability per unit time for the detector to *decay* from its excited state to its ground state, which we will label  $R_-$ , is given by the same formula but with  $\Omega \rightarrow -\Omega$ . This result is easily deduced from symmetry arguments as well. Thus, the decay rate is similarly given by  $R_- = \sqrt{2\pi}\lambda^2\tilde{W}(-\Omega)$ . Now, in Fourier space it is easy to see that the KMS condition,

---

<sup>2</sup>In general a thermal state  $\hat{\rho} = \exp(\beta\hat{H})/\mathcal{Z}$  will have this property. Consider two observables  $\hat{A}$  and  $\hat{B}$ , which evolve according to  $\hat{A}(t) = e^{i\hat{H}t}A(0)e^{-i\hat{H}t}$ . It is then a straightforward calculation to see that  $\langle A(t)B(0) \rangle_\rho = \langle B(0)A(t+i\beta) \rangle_\rho$ , where  $\langle \cdot \rangle_\rho = \text{Tr}(\hat{\rho}\cdot)$  takes the expectation value with respect to the thermal state  $\hat{\rho}$ .

Eq. (4.46), is given by  $\tilde{W}(\Omega) = e^{-\beta\Omega}\tilde{W}(-\Omega)$ . We therefore find that the transition rates of our detector undergoing acceleration satisfy the condition

$$\frac{R_+}{R_-} = e^{-\beta\Omega}. \quad (4.47)$$

This is an example of a detailed balance equation, generally used to characterize systems in equilibrium. In our case this is exactly the condition expected of a system of energy gap  $\Omega$  in thermal equilibrium at inverse temperature  $\beta$ <sup>3</sup>.

This demonstrates that an accelerating particle detector measures a thermal response, at exactly the temperature  $T = a/2\pi$  that is suggested by Unruh’s original argument.

## 4.6 Vacuum entanglement

In this section we will introduce a notion that is of central importance to this thesis: that of vacuum entanglement. The vacuum state  $|0\rangle$  has the peculiar property that, despite in some sense it describing the state of there being “nothing”, it nevertheless displays quantum correlations between spatially separated regions. The existence of vacuum entanglement is immediately discernible from the material in Sects. 4.3 and 4.5. Namely, Eq. (4.35) says that the Minkowski vacuum is a collection of two-mode squeezed state between Rindler modes having support only in the right wedge and those with support in the left. That is, the two Rindler wedges (i.e. the right and left halves of the space) are entangled with each other. As we saw in the previous section, when we trace over one side of space we obtain a mixed state, Eq. (4.44). Since globally the vacuum state is pure, this implies entanglement.

Mathematically, vacuum entanglement is not at all surprising; it follows directly as a result of the fact that the vacuum is defined with respect to global operators. An interesting property of the entanglement between complementary regions in space (as measured by the entanglement entropy) is that it is generally proportional to the area of the boundary between said regions [90, 91]. This is referred to as the area law, and it has led to considerable interest in relating this entanglement entropy to the Bekenstein-Hawking entropy of black holes [92]. More generally much work has been performed, using a variety

---

<sup>3</sup>Let us label the population (i.e. probability of occupation) of the ground and excited states as  $P_0$  and  $P_1$ , respectively. The rates of change of these populations are then given by  $\dot{P}_0 = R_-P_1 - R_+P_0$  and  $\dot{P}_1 = R_+P_0 - R_-P_1$ . In equilibrium we will have  $\dot{P}_0 = \dot{P}_1 = 0$ , giving  $R_-P_1 - R_+P_0 = 0$  and therefore  $R_+/R_- = P_1/P_0 = e^{-\beta\Omega}$ , where in the last equality we have taken the specific case of a thermal state in which the populations are thermally distributed.

of mathematical approaches and models, to understand and characterize the properties of this entanglement [93]. The existence of spatial entanglement is similarly present in condensed matter and lattice systems [94, 95], being a generic property of extended systems with local interactions, of which a quantum field is simply a continuum limit. Indeed long range entanglement and the area law within this context have become an integral part of the study of many-body systems [96]. While in such systems experimental proposals have been put forth for the verification of vacuum entanglement (e.g. a pair of trapped ions [97]), to the author’s knowledge no feasible, concrete proposal has previously been suggested for its verification in a true, relativistic, quantum field (e.g. the photon field). In Ch. 13 we will propose such an experiment.

In addition, it has been demonstrated that this entanglement may be “harvested” (i.e. swapped) to auxiliary quantum systems (e.g. particle detectors) without the need for those systems to causally interact [41, 42, 43, 44, 4]. Such entanglement may then (in principle) be used for quantum informational procedures. This notion of vacuum entanglement harvesting provides a satisfying operational demonstration of this phenomenon. Each detector individually experiences vacuum fluctuations resulting from the act of interacting them with the field. The fluctuations that each experience, however, are quantum correlated. This correlation may then be transferred to the states of the detectors such that they may become dicordant or even entangled.

Harvesting will in fact be a paradigm that we return to more than once in this thesis, and constitutes a large portion of Part. II. Given this, it is worth outlining the basic working of the protocol within the context of Unruh-DeWitt detectors, as first computed in [41]. Let us consider two such detectors,  $a$  and  $b$ , both of energy gap  $\Omega$  and that have worldlines  $(x_a(\tau), \tau)$  and  $(x_b(\tau), \tau)$ , where for simplicity we will assume that both their proper times  $\tau$  coincide. We will also assume that they have the same switching functions  $\lambda(\tau)$ . Neither of these assumptions are necessary, but they will simplify this brief discussion. Important to assume, however, is that we have small coupling  $\lambda \ll 1$ . In this way we are able to utilize perturbation theory. We imagine that both detectors are switched on for localized or semi-localized time period (e.g. taking  $\lambda(\tau)$  to be a Gaussian) such that this time period is shorter than the distance  $|x_a - x_b|$  between them. In this way we rule out the possibility of communication between the two detectors (put concretely, the reduced state of each detector will be equivalent to what it would have been had the other detector not been present). We then simply follow the same perturbative procedure that was outlined in Sect. 4.4, where now when we trace out the field we will be left with a two-qubit density matrix for our two detectors. It is a straightforward calculation to show that to leading order (i.e. second order in  $\lambda$ ) this state after allowing the detectors to run

through their evolution (over all time) is given by

$$\hat{\rho}_{\text{det}} = \begin{pmatrix} 1 - p_+^{(a)} - p_+^{(b)} & 0 & 0 & X \\ 0 & p_+^{(a)} & Y_{ab} & 0 \\ 0 & Y_{ba} & p_+^{(b)} & 0 \\ X & 0 & 0 & 0 \end{pmatrix}. \quad (4.48)$$

Here we are taking the basis ordering  $\{|00\rangle, |01\rangle, |10\rangle, |11\rangle\}$ , where detector- $a$  takes the first position. The quantities  $p_+^{(a)}$  and  $p_+^{(b)}$  are the individual transition probabilities of the two detectors, as computed in Sect. 4.4. For example we have

$$p_+^{(a)} = \int_{-\infty}^{\infty} \int_{-\infty}^{\infty} d\tau d\tau' \lambda(\tau) \lambda(\tau') e^{-i\Omega(\tau-\tau')} W(\tau_a, \tau_a'), \quad (4.49)$$

where we are using the notation  $W(\tau_a, \tau_a') \equiv \langle 0 | \hat{\phi}(x_a(\tau), \tau) \hat{\phi}(x_a(\tau'), \tau') | 0 \rangle$ . The other entries of the density matrix are computed to be

$$Y_{ab} = \int_{-\infty}^{\infty} \int_{-\infty}^{\infty} d\tau d\tau' \lambda(\tau) \lambda(\tau') e^{-i\Omega(\tau-\tau')} W(\tau_a, \tau_b'), \quad (4.50)$$

and similarly for  $Y_{ba}$ , and

$$X = - \int_{-\infty}^{\infty} d\tau \int_{-\infty}^{\tau} d\tau' \lambda(\tau) \lambda(\tau') e^{i\Omega(\tau+\tau')} (W(\tau_a, \tau_b') + W(\tau_b, \tau_a')). \quad (4.51)$$

Given this, one can then determine if the two qubits are entangled or not by, for example, computing the negativity  $\mathcal{N}$  between them. As explained in Ch. 2, this is done by taking the partial transpose of Eq. (4.48) and computing the eigenvalues of the resulting matrix. If one or more of these eigenvalues is negative then the two detectors are entangled. The negativity, Eq. (2.10), is the sum of all such eigenvalues. For simplicity let us take  $p_+^{(a)} = p_+^{(b)} = p_+$  (i.e. both detectors are undergoing the same local evolution). Then it is easy to see that the negativity is given by

$$\mathcal{N} = \max(0, |X| - p_+). \quad (4.52)$$

Namely, the detectors become entangled if  $|X| > p_+$ . This makes sense once one recognizes that  $X$  corresponds to the amplitude of virtual particle exchange between the detectors, and this contribution must fight against the local noise  $p_+$  that each detector experiences. While it will clearly be easier to entangle the detectors if they are allowed within each

other's lightcones, since the Wightman function  $W(\tau_a, \tau_b')$  is larger inside the lightcone than out, there are nevertheless parameter regions in which the two can become entangled even being entirely causally disconnected from each other [41, 42, 43, 44, 4], and this exactly corresponds to swapping some of the preexisting vacuum entanglement out of the field. Unfortunately we also see that the negativity obtained is of order  $\lambda^2$ , which will be extremely small. In terms of any practical use, therefore, such a procedure is highly questionable. We will discuss in Ch. 9 one possibly protocol for overcoming this weakness.

Before finishing this section it is worth mentioning some potentially confusing points regarding the two-detector density matrix, Eq. (4.48). First is the fact that there appears to be zero probability for *both* detectors to become excited. This is simply because here we work to order  $\lambda^2$  only, which is the leading order. Such an event has probability of order  $\lambda^4$ , and is therefore not included at leading order. Similarly, it is confusing that the reduced states of the individual detectors are unchanged by the presence of the other, despite the fact that in Eq. (4.48) we have made no assumptions about whether or not the two detectors have causal overlap. This is again because we are only working to second order. Mutual influence between the detectors would involve the emission of a quanta by one detector and subsequent re-absorption by the other, which is again a  $\lambda^4$  process. Note, however, that this is not necessarily the case were we to initialize the detectors in non-energy-eigenstates [98, 99].

## 4.7 Field theory in a cavity

Throughout the majority of this thesis we will be considering cavity scenarios, in which the field is bound to a finite region of space and subject to some chosen boundary condition. The primary difference in such a case, as compared to the physics described above, is that now the mode solutions are discretely parameterized, rather than continuously. We will very quickly outline the form of these differences.

The form of the mode functions must satisfy whatever boundary conditions one applies to the boundary edges of one's cavity. We will give the form of the stationary mode functions for three cases: those of periodic, Dirichlet, and Neumann boundary conditions. In all cases we will take the cavity to be of length  $L$ , and we will take the coordinate values  $x = 0$  and  $x = L$  to be the left and right boundaries, respectively. In the case of a periodic cavity of length  $L$  (which would correspond to physical settings such as closed optical fibres or microwave guides or any other setting with a torus topology), the modes

are the set of right and left-moving waves similar to what we had in the continuum case:

$$u_n(x, t) = \frac{1}{\sqrt{2\omega_n L}} \exp i(k_n x - \omega_n t), \quad \text{periodic}, \quad (4.53)$$

where  $n$  is an integer,  $k_n = 2n\pi/L$  (negative (positive)  $n$  corresponds to left-moving (right-moving) modes) and  $\omega_n^2 = k_n^2 + \mu^2$ .

If instead we impose the Dirichlet boundary conditions  $\hat{\phi}(L, t) = \hat{\phi}(0, t) = 0$  (the two walls of the cavity are ideal mirrors) we find that the mode functions are the stationary waves

$$u_n(x, t) = \frac{1}{\sqrt{\omega_n L}} e^{-i\omega_n t} \sin(k_n x), \quad \text{Dirichlet}, \quad (4.54)$$

where now we have  $k_n = n\pi/L$  and the index  $n$  only runs over the natural numbers,  $n \in \mathbb{Z}^+$ . This is because now the two solutions  $\pm n$  are no longer linearly independent (they are in fact the same solution).

In the case of a Neumann cavity (this is to say,  $\partial_x \hat{\phi}(L, t) = \partial_x \hat{\phi}(0, t) = 0$ ), the modes become

$$u_n(x, t) = \frac{1}{\sqrt{\omega_n L}} e^{-i\omega_n t} \cos(k_n x), \quad \text{Neumann}, \quad (4.55)$$

where as in the Dirichlet case we have  $k_n = n\pi/L$  and the index is positive:  $n \in \mathbb{Z}^+$ .

In all of these cases, the normalization factors are such that the modes form an orthonormal basis with respect to the Klein-Gordon inner product

$$(u_k, u_{k'}) = \delta_{kk'}, \quad (u_k^*, u_{k'}^*) = -\delta_{kk'}, \quad (u_k, u_{k'}^*) = 0, \quad (4.56)$$

where the inner product is still of the form Eq. (4.5) except that now the integration is performed only over the region of the cavity.

Given one of these boundary conditions, the field operator can then be expanded as a sum of solutions

$$\hat{\phi}(x, t) = \sum_n (u_n(x, t) \hat{a}_n + u_n^*(x, t) \hat{a}_n^\dagger). \quad (4.57)$$

Given this, we are able to show (by the same means as that described for Eq. (4.7)) that the mode functions will satisfy the completeness relations

$$\begin{aligned} 0 &= \sum_n (u_n^*(x', t) u_n(x, t) - u_n(x', t) u_n^*(x, t)), \\ \delta(x - x') &= i \sum_n (\dot{u}_n(x', t) u_n^*(x, t) - \dot{u}_n^*(x', t) u_n(x, t)). \end{aligned} \quad (4.58)$$



As before, we can take the canonical commutation relations of the field and its conjugate momentum to deduce that the raising and lowering operators of the modes must satisfy the commutation relations

$$\begin{aligned} [\hat{a}_n, \hat{a}_{n'}] &= 0 \\ [\hat{a}_n^\dagger, \hat{a}_{n'}^\dagger] &= 0 \\ [\hat{a}_n, \hat{a}_{n'}^\dagger] &= \delta_{nn'}. \end{aligned} \quad (4.59)$$

Similar to the continuum case, the free Hamiltonian of the field take the form  $\hat{H} = \sum_n \omega_n \hat{N}_n$ , where  $\hat{N}_n = \hat{a}_n^\dagger \hat{a}_n$  is the number operator for mode- $n$ . We define the cavity vacuum state  $|0\rangle$  to be the state that satisfies  $\hat{a}_n |0\rangle = 0$  for all  $n$ , and particle states can similarly be defined following the prescription of Sect. 4.1.

We can also perform a Bogoliubov transformation to a non-stationary mode basis described by mode functions  $v_m$ :

$$v_m(x, t) = \sum_n (\alpha_{mn} u_n(x, t) + \beta_{mn} u_n^*(x, t)), \quad (4.60)$$

$$u_n(x, t) = \sum_m (\alpha_{mn}^* v_m(x, t) - \beta_{mn} v_m^*(x, t)), \quad (4.61)$$

where the coefficients are given by the mode function overlaps with respect to the Klein-Gordon inner product, of the same form as in Eq. (4.16). Acting on the raising and lowering operators, where we define  $\{\hat{b}_m, \hat{b}_m^\dagger\}$  to be the operators corresponding to the  $v_m$  basis, this transformation takes the form

$$\hat{b}_m = \sum_n (\alpha_{mn}^* \hat{a}_n - \beta_{mn}^* \hat{a}_n^\dagger), \quad (4.62)$$

$$\hat{a}_n = \sum_m (\alpha_{mn} \hat{b}_m + \beta_{mn}^* \hat{b}_m^\dagger). \quad (4.63)$$

Lastly, the unitary conditions for this transformation (equivalently, those that make it symplectic) are

$$\begin{aligned} \sum_j (\alpha_{mj} \alpha_{nj}^* - \beta_{mj} \beta_{nj}^*) &= \delta_{mn}, \\ \sum_j (\alpha_{mj} \beta_{nj} - \beta_{mj} \alpha_{nj}) &= 0. \end{aligned} \quad (4.64)$$

## 4.8 Symplectic Bogoliubov transformations

A Bogoliubov transformation, as defined in the sections above, is simply a linear transformation on the quadrature operators of field modes, and is therefore a Gaussian operation. Furthermore, the unitarity conditions Eqs. (4.21,4.64) equivalently guarantee that such a transformation is symplectic (i.e. that the canonical commutation relations are preserved). In this short section we will very quickly discuss Bogoliubov transformations within this context. For convenience we will work in a cavity setting such that we have a countable spectrum of modes.

Given a set of ladder operators  $\{\hat{a}_n, a_n^\dagger\}$  corresponding to some field mode basis, we can associate with this set of harmonic oscillators the collection of conjugate position and momentum operators  $\{\hat{q}_n, \hat{p}_n\}$  defined as in Eq. (3.2), which can be collected into the phase space vector of operators  $\hat{\mathbf{x}} = (\hat{q}_1, \hat{p}_1, \hat{q}_2, \hat{p}_2, \dots)^T$ , as was done in Ch. 3. The Bogoliubov transformation to a new set of modes, as given by the first of Eq. (4.62), then takes the linear form  $\hat{\mathbf{x}} \rightarrow \mathbf{S}\hat{\mathbf{x}}$ , where the matrix  $\mathbf{S}$  is easily seen to take the block form

$$\mathbf{S} = \begin{pmatrix} \mathbf{S}_{11} & \mathbf{S}_{12} & \cdots \\ \mathbf{S}_{21} & \mathbf{S}_{22} & \cdots \\ \vdots & \vdots & \ddots \end{pmatrix}, \quad (4.65)$$

with

$$\mathbf{S}_{mn} = \begin{pmatrix} \text{Re}(\alpha_{mn} - \beta_{mn}) & \text{Im}(\alpha_{mn} + \beta_{mn}) \\ -\text{Im}(\alpha_{mn} - \beta_{mn}) & \text{Re}(\alpha_{mn} + \beta_{mn}) \end{pmatrix}. \quad (4.66)$$

It is straightforward to work out, given the form of this matrix, that the conditions in Eq. (4.64) guarantee it to be symplectic,  $\mathbf{S}\mathbf{\Omega}\mathbf{S}^T = \mathbf{S}^T\mathbf{\Omega}\mathbf{S} = \mathbf{\Omega}$ , where  $\mathbf{\Omega}$  is the symplectic form as given by Eq. (3.4).

Recall from Ch. 3 that a passive transformation is one in which the average particle content does not change, and is represented by a symplectic matrix that is also orthogonal. In terms of a Bogoliubov transformation, we have learned that this property is exactly represented by the condition that all  $\beta$ -coefficients are zero. It is easy to show that these two conditions are equivalent, and we will do so explicitly here. The proof relies first on  $\mathbf{S}$  being symplectic, meaning that Eq. (4.64) is satisfied. Assuming this, and taking all  $\beta$  coefficients to be zero, we have  $\sum_j \alpha_{mj} \alpha_{nj}^* = \delta_{mn}$ . Let us denote  $\alpha_{mj} = g_{mj} + ih_{mj}$ . This condition then reads  $\sum_j (g_{mj}g_{nj} + h_{mj}h_{nj}) = \delta_{mn}$  and  $\sum_j (g_{nj}h_{mj} - g_{mj}h_{nj}) = 0$ . Now, given that  $\beta = 0$  we see that the blocks in Eq. (13.30) take the form  $\mathbf{S}_{mn} = g_{mn}\mathbf{I}_2 + h_{mn}\mathbf{\Omega}_2$ ,

where  $\mathbf{I}_2$  is the  $2 \times 2$  identity and  $\mathbf{\Omega}_2$  is the single mode ( $2 \times 2$ ) symplectic form. We must check that  $\mathbf{S}\mathbf{S}^T = \mathbf{I}$ . To this end, we note that the  $mn$ 'th block of  $\mathbf{S}\mathbf{S}^T$  is given by  $[\mathbf{S}\mathbf{S}^T]_{mn} = \sum_j \mathbf{S}_{mj} \mathbf{S}_{nj}^T = \sum_j [(g_{mj}g_{nj} + h_{mj}h_{nj})\mathbf{I} - (g_{nj}h_{mj} - g_{mj}h_{nj})\mathbf{\Omega}_2] = \delta_{mn}\mathbf{I}_2$ , where we have used  $\mathbf{\Omega}_2^2 = -\mathbf{I}_2$ . This demonstrates that the transformation is symplectic if  $\beta = 0$ , and the opposite direction is trivially seen to hold as well.

## Part II

# The Nonperturbative Oscillator Detector

For many years, the well-known Unruh-Dewitt model [100], as discussed in Sect. 4.4, has been used to explore phenomenological aspects of quantum field theory. The great success of this model, which couples a qubit to a quantum field using a simple monopole interaction, has been its use in analyzing the observer dependence of relativistic quantum phenomena; most notably the Unruh effect [21]. This result does not require the use of Bogoliubov transformations between inequivalent field expansions and the subsequent tracing over degrees of freedom beyond a horizon. It is instead a consequence of a direct calculation of the response of the detector when traversing a timelike hyperbolic trajectory in spacetime. Additionally, the Unruh-Dewitt model is actually a very good basic description of the light-matter interaction and reproduces quite well the interaction between atoms and light when no exchange of angular momentum is involved [101]. The main shortcoming of this model, however, is that its evaluation is limited to perturbation theory. One is therefore barred from using it to study problems in which a perturbative expansion is not a good approximation. These include strong coupling, long times and high-average-energy exchange processes.

In this part of the thesis we will introduce and utilize another particle-detector model consisting of a quantum harmonic oscillator rather than a qubit, an idea that has been proposed before in other contexts [102, 103, 104, 105, 106, 107, 108]. In other words, we simply replace two energy levels with infinitely many evenly-spaced levels. Nevertheless, qubits are, in many cases, just approximations to systems with many more levels, so in some ways our description for a particle detector is more natural. Given that most symmetric potentials in nature can be approximated by a harmonic potential for low energies, a harmonic-oscillator detector can model a wide range of detectors, from atomic electromagnetic levels to molecular vibrational spectra. In particular, we will consider such detectors in the context of cavity fields (i.e. the fields they interact with will present an IR cutoff), meaning that the field modes are discrete.

Using an oscillator detector has significant advantages over the standard Unruh-DeWitt (qubit-based) detector. First, the quantum evolution can be solved *nonperturbatively*. As we will see, this results from being able to utilize Gaussian quantum mechanics, as described in Ch. 3. Many of the scenarios of interest in relativistic quantum theory involve quadratic Hamiltonians, thus making this formalism widely applicable.

Second, the evolution can be evaluated by simply solving (in general numerically) a set of coupled, ordinary, first-order, linear differential equations. Furthermore, the form of this ODE is universal, meaning that one can solve a large range of problems with minimal effort. In particular, this approach can be used to solve (a) arbitrary time-dependent trajectories, (b) arbitrary quadratic, time-dependent interaction Hamiltonians and boundary conditions, (c) arbitrary Gaussian initial states of the field and detectors, (d) any number

of cavity modes, and (e) any number of detectors. As we will see, a wide range of different scenarios can therefore be solved non-perturbatively by the same simple differential equation, which implies considerable explanatory power and computational gain. For example, as we will see, there is no need to repeat the numeric calculation whenever we want to change a given initial state if the time-dependent Hamiltonian mediating the interaction is the same. This is rather unlike the perturbative Unruh-DeWitt model in which considerably more effort is required. This universality, plus the ability to sidestep perturbation theory, is the true power of this approach to detector models.

One obvious limitation of this approach is that to solve the equations in practice one is forced to apply an infrared cutoff to the field. However, an infrared cutoff naturally appears when studying quantum field theories in finite volumes (e.g., optical cavities, periodic waveguides, etc.), and so this formalism enables us to non-perturbatively solve problems of quantum field theories in curved spacetimes inside cavities, a matter of great interest that has not been thoroughly explored to date. If a tabletop experiment in which relativistic quantum phenomena is to appear, discrete systems [109] or superconducting circuits [110, 111, 112, 113] have an edge in terms of experimental feasibility.

Although in practice one is also forced to use a UV cutoff (namely, computing with only a finite number of modes), in all results presented here we have been careful to find a convergent solution with respect to the number of field modes. Specifically, we run the simulation with more and more modes until the results do not change anymore. As such, this is not a practical limitation.

The idea of using harmonic oscillators in relativistic quantum field theory as particle detectors to obtain non-perturbative results was explored by other authors who reported interesting analytical results in [105, 106]. The practical scope of their approach, however, remains to be seen—thus far it has been limited to very concrete problems due to complexities and the number of assumptions and approximations required to obtain quantitative results. In performing our analysis we shall employ an arguably more powerful Gaussian formalism, which provides a more efficient way to address problems of time evolution when considering quadratic Hamiltonian and Gaussian states. In this sense our approach is similar to that of Dragan and Fuentes [107], who made use of the Gaussian formalism to study a time-independent, quadratic Hamiltonian of two coupled harmonic oscillators. This approach had some advantages insofar as it did not require any perturbative approximations. However, their analysis was limited to 1) a single field mode and 2) time-independent Hamiltonian. Under that proviso, only stationary scenarios and very simple trajectories of detectors can be considered. To study a particular non-inertial scenario (namely eternal uniform acceleration) they relied on the existence of Bogoliubov transformations between inertial modes and Rindler modes, rendering thermality an a-priori assumption instead of

a consequence. Furthermore, by applying free Bogoliubov transformations to a single field mode, they were unable to see border effects when analyzing the Unruh effect in cavities. Indeed, the applicability/validity of continuum Bogoliubov transformations for eternally accelerating observers in cavity settings in any regime is a rather obscure topic that has not been thoroughly understood to date.

In this Part of the thesis we will begin in Ch. 5 by introducing the general setting behind this model and describing the mechanics of its use. Once we know how to use the model we move on to apply it to a variety of scenarios of interest. First, we consider in Ch. 6 the case of an oscillator-detector undergoing uniform acceleration through a cavity in order to elucidate the nature (if any) of the Unruh effect in a cavity. We find that indeed the Unruh effect still occurs inside a cavity, and that there is a surprising universality to the obtained results, being largely independent of the boundary conditions applied to the cavity. Next, in Ch. 7 we use the model to examine the phenomenon of entanglement harvesting, demonstrating both bipartite and tripartite harvesting. In Ch. 8 we continue to consider the harvesting of correlations but rather than entanglement focus on quantum discord. What we find is that, surprisingly, the harvested discord *increases* as we increase the temperature of the cavity field, in exact opposition to the behavior of entanglement. In Ch. 9 we move to another paradigm in which many pairs of detectors are allowed to sequentially interact with a cavity field. What we discover is that such a procedure can actually be used as a preparation technique for the field state that allows for the sustainable production and distribution of entanglement. We refer to this protocol as entanglement farming. Lastly, in Ch. 10 we take the farming setup and discuss how such a system may be useful for metrological purposes. In particular we show that such a system can be engineered to be extremely sensitive to external influence and we demonstrate this via the detection of periodic motion of the cavity walls. That is, the setup can act as a quantum mechanical seismograph.

# Chapter 5

## The oscillator detector model

Note: this chapter derives from the work [1], in collaboration with Eduardo Martín-Martínez, Nicolas C. Menicucci, and Robert B. Mann.

In this chapter we will introduce the model that will be used for the rest of this Part of the thesis. We will begin by reviewing the general scenario under consideration and discuss some important subtleties regarding evolution with respect to different time parameters, before moving on to outline the workings of the model itself.

As an important note, it must be stressed that this method carries far more general applicability than simply to field-detector models. The evolution equation that we will derive can be applied to any arbitrary collection of coupled oscillators or modes, for example within condensed matter systems. While in this thesis we do not stray from its use as a field-detector model, what we have is in fact a far more general tool.

### 5.1 The setup

One might suspect that replacing a qubit (two energy levels) with an oscillator (infinite energy levels) in our detector model would complicate the problem, but it in fact becomes significantly *simplified*. The essential feature that makes this possible is that all states in the problem are Gaussian with no displacement, and all evolutions are generated by quadratic Hamiltonians. As discussed in Ch. 3, such evolution preserves the Gaussian nature of the states. This means that we can fully describe the evolving state by a covariance matrix rather than a density operator.



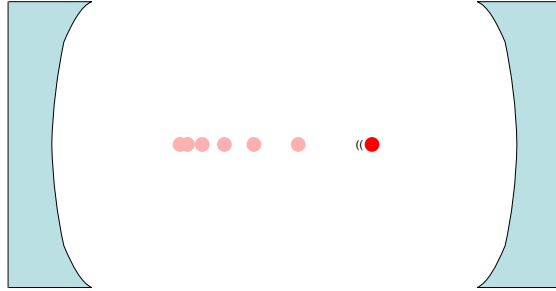


Figure 5.1: Harmonic-oscillator detector (red dot) moving through a fixed cavity. This is to illustrate the difference between our setup and those in which the cavity itself is in motion [11]. Note that any number of detectors may be present.

For calculational purposes, we assume that an IR cutoff of some length  $L$  has been imposed on the field.<sup>1</sup> As such, our physical model is that of a detector or detectors generally moving around in a cavity. There is an important distinction to be made here with other models that consider the cavity itself as being in motion [11]. In our work, by contrast, the cavity is large and fixed, and the detector moves within it (if it moves at all). See Fig. 5.1.

### 5.1.1 Hamiltonians generating evolution with respect to different time parameters

In relativistic scenarios it is important to keep in mind that Hamiltonians generate evolution with respect to a given time parameter that does not necessarily coincide with the proper time of some (or any) of the proper times of the physical subsystems that are in interaction. When we consider the global Hamiltonian of multipartite systems we would need to express it in terms of a common time parametrization. Due to this, we also wish to provide a discussion of how to generate evolution with respect to an arbitrary time parameter. While in this thesis we will take the evolution time parameter to be that of the proper time  $\tau$  of our detector, in more general settings it may be useful to evolve in a global time coordinate  $t$ , particularly in the case where there are multiple detectors in which each detector  $j$  has a different proper time coordinate  $\tau_j$  associated with it. The

---

<sup>1</sup>This is necessary because we want to use matrix algebra to (generally numerically) solve the resulting differential equations, although a formal generalization of our method to the continuum limit may be possible in the form of integro-differential equations. This is the focus of current work.

calculation is most straightforward in the Heisenberg picture, although applies equally well in the Schrödinger or interaction pictures. In this way we provide a “dictionary” by which we can transform to any other time coordinate. In Sec. 5.1.2 we continue by introducing the general form of the Hamiltonian that we will utilize with our model.

Let us proceed, then, by considering a general time-dependent Hamiltonian  $\hat{H}(t)$ , which generates evolution of the entire system in the global time coordinate  $t$ . This Hamiltonian includes the free Hamiltonian for each system, as well as interactions. With respect to  $t$ , the Heisenberg equation of motion for a general operator  $\hat{A}(t)$ , possibly having explicit dependence on  $t$ , is

$$\frac{d}{dt}\hat{A}(t) = \frac{i}{\hbar}[\hat{H}(t), \hat{A}(t)] + \frac{\partial\hat{A}(t)}{\partial t}. \quad (5.1)$$

A different choice of time coordinate can be taken into account by applying the chain rule. For the moment, let us choose the new time variable to be the local proper time  $\tau_j$  that parametrizes the worldline  $(x(\tau_j), t(\tau_j))$  traversed by detector  $j$ . Applying the chain rule gives

$$\begin{aligned} \frac{d}{d\tau_j}\hat{A}[t(\tau_j)] &= \left. \frac{dt}{d\tau_j} \frac{d}{dt}\hat{A}(t) \right|_{t=t(\tau_j)} \\ &= \left. \frac{dt}{d\tau_j} \frac{i}{\hbar}[\hat{H}(t), \hat{A}(t)] + \frac{dt}{d\tau_j} \frac{\partial\hat{A}(t)}{\partial t} \right|_{t=t(\tau_j)} \\ &= \frac{i}{\hbar} \left[ \left( \frac{dt}{d\tau_j} \hat{H}[t(\tau_j)] \right), \hat{A}[t(\tau_j)] \right] + \frac{\partial\hat{A}[t(\tau_j)]}{\partial\tau_j}. \end{aligned} \quad (5.2)$$

Thus, we can start with the Hamiltonian  $\hat{H}(t)$ , which generates translations in the global time coordinate  $t$ , and then define

$$\hat{H}_j(\tau_j) := \frac{dt}{d\tau_j} \hat{H}[t(\tau_j)] \quad (5.3)$$

as the Hamiltonian (for the entire system) as seen by detector  $j$ , which generates evolution for the entire system with respect to the proper time coordinate  $\tau_j$ . The derivative  $dt/d\tau_j$  is the redshift factor for an observer in the detector’s reference frame, which provides an overall scaling of all energies in the combined system (because this is what such an observer would experience). Notice that although the notion of proper time is local, we need to be able to evolve the entire system with respect to this coordinate because we are working in the Heisenberg picture. This is not a problem as long as  $t(\tau_j)$  is an invertible function

over the range of times of interest. The equivalence of the two pictures is made explicit by defining Heisenberg operators that are more natural to the detector's frame:

$$\hat{A}_j(\tau_j) := \hat{A}[t(\tau_j)]. \quad (5.4)$$

We can now use Eqs. (5.3) and (5.4) to rewrite Eq. (5.2) as

$$\frac{d}{d\tau_j} \hat{A}_j(\tau_j) = \frac{i}{\hbar} [\hat{H}_j(\tau_j), \hat{A}_j(\tau_j)] + \frac{\partial \hat{A}_j(\tau_j)}{\partial \tau_j}. \quad (5.5)$$

For example, if  $\hat{A}(t)$  were to represent the position of the second hand on a wristwatch worn by an observer traveling with detector  $j$ , then it would make more sense to consider  $\hat{A}_j(\tau_j)$  because this operator would have a simpler evolution with respect to  $\tau_j$  than  $\hat{A}(t)$  would with respect to  $t$  (since the wristwatch evolves more simply with respect to  $\tau_j$  than with respect to  $t$ ). Similarly, it will be easier to start with the simple version of the wristwatch's Hamiltonian  $\hat{H}_j(\tau_j)$  and then invert Eq. (5.3) to obtain

$$\hat{H}(t) = \frac{d\tau_j}{dt} \hat{H}_j[\tau_j(t)] \quad (5.6)$$

(which will be more complicated) for use in the global Hamiltonian.

The upshot of all of this is that we can define a single Hamiltonian  $\hat{H}(t)$  for the whole system with respect to some global time coordinate  $t$  and then use Eq. (5.3) to transform it to any other time coordinate we wish to use for the evolution. Furthermore, when building up this Hamiltonian, it will sometimes be easier to start by defining a piece of it with respect to local proper time and then use Eq. (5.6) to figure out what this piece looks like in the global time coordinate.

### 5.1.2 The Unruh-DeWitt Hamiltonian in general scenarios

We have to be careful when we want to deal with Hamiltonians generating translations with respect to different time parameters, above all when we want to describe the interaction of systems that have different proper times.

Indeed, in general scenarios it is not trivial to define either the interaction nor the free Hamiltonian in different pictures. In this section, we will help guide the reader by introducing the following notation: We will call  $\hat{H}^S$ ,  $\hat{H}^I$ ,  $\hat{H}^H$  respectively the complete Hamiltonian in the Schrödinger, interaction, and Heisenberg pictures. In later sections we will remove this as it will be clear from context which picture we are working in. Also for

the purposes of this section we will include a superindex  $t$  or  $\tau$  denoting with respect to which time the Hamiltonian is a generator of translations. Lastly, we will denote with the subscript  $F$  the free part of the Hamiltonian and  $I$  the interaction part (this will continue to be used through the following chapters).

We will consider the interaction of a number of particle detectors with a quantum field. To model this interaction we will consider an X-X coupling of the form of the Unruh-DeWitt Hamiltonian, Eq. (4.36). Note, however, that the formalism we present is much more general than this, and we can in fact use any quadratic Hamiltonian that we like. For our immediate purposes we choose to use the X-X coupling in order to compare with previous works. For the sake of clarity, let us start our reasoning with a very simple scenario: let us consider a single detector of level spacing  $\Omega$  undergoing general motion in flat spacetime with an associated proper time  $\tau$  and a scalar quantum field that we will choose to expand in terms of plane-wave solutions in terms of a global Minkowskian time  $t$ .

The coupling given in Eq. (4.36) was presented already in the interaction picture. For our purposes, however, we will find it more convenient to work in either the Schrödinger or Heisenberg pictures. In the Schrödinger picture, the Unruh-DeWitt interaction is described by the following Hamiltonian

$$\hat{H}_{\text{int}}^{\text{S}} = \lambda(\tau)\hat{\mu}^{\text{S}}\hat{\phi}^{\text{S}}[x(\tau)], \quad (5.7)$$

where  $\lambda(\tau)$  is the switching (or window) function,  $\hat{\mu}^{\text{S}}$  is the monopole moment of the detector and  $\hat{\phi}^{\text{S}}[x(\tau)]$  is the field operator evaluated along the worldline of the detector parametrized in terms of the proper time  $\tau$ :

$$\hat{\phi}^{\text{S}}[x(\tau)] = \sum_n \left( u_n[x(\tau)]\hat{a}_n + u_n^*[x(\tau)]\hat{a}_n^\dagger \right), \quad (5.8)$$

$$\hat{\mu}^{\text{S}} = (\hat{a}_d + \hat{a}_d^\dagger), \quad (5.9)$$

where  $u_n(x)$  are the ( $t = 0$ ) stationary mode functions determined by whichever boundary conditions are applied to the cavity; one of Eqs. (4.53,4.54,4.55). Notice that the time dependence of the switching function  $\lambda(\tau)$  allows us to control the interaction by, for example, turning on and off the detector at desired times.

Let us start from a very well known result from first principles: we can write the free Hamiltonian for the field, and the free Hamiltonian of the detector in their respective times

in the Schrödinger picture:

$$\hat{H}_{\text{free,field}}^{\text{S},t} = \sum_n \omega_n \hat{a}_n^\dagger \hat{a}_n, \quad (5.10)$$

$$\hat{H}_{\text{free,det}}^{\text{S},\tau} = \Omega \hat{a}_d^\dagger \hat{a}_d. \quad (5.11)$$

Now, to write the complete free Hamiltonian we cannot just naively sum these two terms together because they generate translations with respect to different time parameters. We would need first to transform them to a common time parameterization. We will see that in order to recover the correct form of the well-known Unruh-DeWitt Hamiltonian in the interaction picture, we must transform the field Hamiltonian to generate translations in the proper time of the detectors. In this way, using (5.6) we have that

$$\hat{H}_{\text{free,field}}^{\text{S},\tau} = \frac{d}{d\tau} t(\tau) \sum_n \omega_n \hat{a}_n^\dagger \hat{a}_n, \quad (5.12)$$

where  $t(\tau)$  is determined by the worldline taken by the detector. We can thus write the complete Hamiltonian in the Schrödinger picture generating translations in  $\tau$  as

$$\hat{H}^{\text{S},\tau} = \hat{H}_{\text{free}}^{\text{S},\tau} + H_{\text{int}}^{\text{S},\tau},$$

where

$$\hat{H}_{\text{free}}^{\text{S},\tau} = \frac{d}{d\tau} t(\tau) \sum_n \omega_n \hat{a}_n^\dagger \hat{a}_n + \Omega \hat{a}_d^\dagger \hat{a}_d \quad (5.13)$$

$$\hat{H}_{\text{int}}^{\text{S},\tau} = \lambda(\tau) (\hat{a}_d + \hat{a}_d^\dagger) \sum_n \left( u_n[x(\tau)] \hat{a}_n + u_n^*[x(\tau)] \hat{a}_n^\dagger \right). \quad (5.14)$$

Note that the free Hamiltonian is not time independent as it was in the case where the detector is inertial.

In most textbooks [39], calculations involving non-inertial detectors coupled to the field are dealt with in the interaction picture. We will see that we recover the well-known form of the interaction Unruh-DeWitt Hamiltonian by changing from the Schrödinger to the interaction picture. Recall the transformation between the Schrödinger and the interaction pictures:

$$\hat{H}^{I,\tau} = \hat{U}_{\text{free}}^\dagger(\tau) \hat{H}^{\text{S},\tau} \hat{U}_{\text{free}}(\tau), \quad (5.15)$$

where  $\hat{U}_{\text{free}}(\tau)$  is the free evolution operator, i.e. the solution to the Schrödinger equation in  $\tau$  using just the free Hamiltonian  $\hat{H}_F^{S,\tau}$ :

$$i \frac{d}{d\tau} \hat{U}_{\text{free}}(\tau) = \hat{H}_{\text{free}}^{S,\tau} \hat{U}_{\text{free}}(\tau), \quad (5.16)$$

Notice that in this case the transformation is non-trivial due to the non-trivial dependence on  $\tau$  of the global time parameter  $t(\tau)$ . This yields an explicit time dependence of the field's free Hamiltonian. Since  $\hat{H}_F^{S,\tau}$  commutes with itself at different times, we can solve Eq. (5.16) explicitly without needing to worry about time ordering:

$$\begin{aligned} \hat{U}_{\text{free}}(\tau) &= \exp \left[ -i \int_0^\tau d\tau \hat{H}_{\text{free}}^S \right] \\ &= \exp \left[ -i \int_0^\tau d\tau \left( \frac{d[t(\tau)]}{d\tau} \sum_n \omega_n \hat{a}_n^\dagger \hat{a}_n + \Omega \hat{a}_d^\dagger \hat{a}_d \right) \right] \\ &= \exp \left[ -i \left( \sum_n \omega_n \hat{a}_n^\dagger \hat{a}_n \right) t(\tau) - i \Omega \hat{a}_d^\dagger \hat{a}_d \tau \right], \end{aligned} \quad (5.17)$$

This operator leaves invariant the free parts of the Hamiltonian, and its action on the  $\hat{a}_n$  and  $\hat{a}_d$  operators is

$$\hat{U}_{\text{free}}^\dagger(\tau) \hat{a}_n \hat{U}_{\text{free}}(\tau) = e^{-i\omega_n t(\tau)} \hat{a}_n, \quad (5.18)$$

$$\hat{U}_{\text{free}}^\dagger(\tau) \hat{a}_d \hat{U}_{\text{free}}(\tau) = e^{-i\Omega \tau} \hat{a}_d, \quad (5.19)$$

allowing us to write the Unruh-Dewitt Hamiltonian in the interaction picture with respect to the parameter  $\tau$  as

$$\begin{aligned} \hat{H}^{I,\tau} &= \frac{dt(\tau)}{d\tau} \sum_n \omega_n \hat{a}_n^\dagger \hat{a}_n + \Omega \hat{a}_d^\dagger \hat{a}_d + (\hat{a}_d e^{-i\Omega \tau} + \hat{a}_d^\dagger e^{i\Omega \tau}) \\ &\times \lambda(\tau) \sum_n \left( \hat{a}_n u_n[x(\tau), t(\tau)] + \hat{a}_n^\dagger u_n^*[x(\tau), t(\tau)] \right), \end{aligned} \quad (5.20)$$

where

$$u_n[x(\tau), t(\tau)] = e^{-i\omega_n t(\tau)} u_n[x(\tau)]. \quad (5.21)$$

Thus we recover the standard form of the Unruh-Dewitt Hamiltonian [39] in the interaction picture that generates translations with respect to time  $\tau$  starting from the well known free Hamiltonians (in the Schrödinger pictures, with respect to their respective natural time parameters) after transforming to a common time  $\tau$  and changing to the interaction picture.

We will find it convenient for use in the next section to work in the Heisenberg picture. We will use the fact that the form of the complete Hamiltonian in the Heisenberg picture coincides with the form of the complete Hamiltonian in the Schrödinger picture, assuming we take any given operator to be in the corresponding picture. To see this, note that the transformation between the two pictures is by the full time-evolution operator  $\hat{U}(\tau)$ , which satisfies the full Schrödinger equation

$$i\frac{d}{d\tau}\hat{U}(\tau) = \hat{H}^{\text{S},\tau}\hat{U}(\tau). \quad (5.22)$$

The Hamiltonian in the Heisenberg picture is obtained from its Schrödinger-picture counterpart by the usual transformation between the two pictures for any operator:

$$\hat{H}^{\text{H},\tau} = \hat{U}^\dagger(\tau)\hat{H}^{\text{S},\tau}\hat{U}(\tau). \quad (5.23)$$

This means that we do not have to do any work to modify the Schrödinger-picture Hamiltonian in order to use it in the Heisenberg picture. All we have to do is reinterpret all operators within it as being Heisenberg-picture operators instead of Schrödinger-picture ones.

While we will not be needing this in the current thesis, it is straightforward and useful to write the most general X-X type Hamiltonian for an arbitrary number of detectors undergoing general trajectories with different proper times  $\tau_j$  and with time dependent couplings. However, if multiple detectors have different proper times then we again need to be careful. One must always make a choice of time, and in this more general case it makes sense to use the global Minkowski time  $t$ . Transforming the Hamiltonian to time  $t$  and reinterpreting all operators in the Heisenberg picture yields

$$\begin{aligned} \hat{H}^{\text{H},t} = & \sum_{n=1}^N \omega_n \hat{a}_n^\dagger \hat{a}_n + \sum_{j=1}^M \frac{d\tau_j(t)}{dt} \left[ \Omega_j \hat{a}_{d_j}^\dagger \hat{a}_{d_j} \right. \\ & \left. + \sum_{n=1}^N \lambda_{nj}(t) (\hat{a}_{d_j} + \hat{a}_{d_j}^\dagger) (u_n[x_j(t)] \hat{a}_n + u_n^*[x_j(t)] \hat{a}_n^\dagger) \right] \end{aligned} \quad (5.24)$$

where  $x_j(t)$  is the trajectory of the  $j$ -th detector parametrized in terms of the global Minkowskian time  $t$ , and all operators are now understood to be in their Heisenberg representation. We will see in the next section how working in this representation allows us to derive a simple, number-valued equation of motion that describes the full evolution of the detectors+field state.

To recapitulate, the Hamiltonian above represents a set of  $N + M$  time-dependent coupled harmonic oscillators.  $M$  of them are oscillator-based Unruh-DeWitt detector modes (labeled with the index  $d_j$ ), and the other  $N$  are modes of the quantum field inside a cavity (labeled with an integer index  $n$ ). Notice that there is no direct detector-detector coupling, and the field is a free field, meaning there is no coupling directly between field modes either.

We emphasize that Eq. (5.24) is not the most general form of the Hamiltonian that could be imagined in this scenario. It is simply the same as the original Unruh-DeWitt detector model. The connection is made by choosing no relative phase between  $\hat{a}_{d_j}$  and  $\hat{a}_{d_j}^\dagger$  in the interaction term, which makes their sum proportional to the position (monopole moment) of the oscillator. In general, our formalism, to be presented now, is capable of solving far more general interaction models, provided they are quadratic.

Our general problem is now this: given detector worldlines  $[t(\tau_j), x(\tau_j)]$  and an initial (Gaussian) state for the detectors and field, evolve the detectors and the field using the Hamiltonian in Eq. (5.24), and consider the reduced state of the detectors after the evolution. In order to make use of the simplification afforded by the use of Gaussian states and quadratic Hamiltonians, in the next section we will derive a differential equation using the symplectic formalism of Gaussian quantum mechanics. This will let us compute the covariance matrix for the field and detectors throughout the evolution, and since the state remains Gaussian the whole time, this is equivalent to tracking the evolution of the full state itself.

It is also important to note that while Eq. (5.24) will in general be very useful when considering some ensemble of detectors, in the work presented in this thesis we will find it more convenient to parameterize the evolution via the proper time rather than the global time  $t$ . This is because in the applications discussed here we either have only a single non-stationary detector (in which case we use proper time  $\tau$ ) or we have multiple detectors that are stationary, the proper times of which are therefore equivalent to the global time  $t$ . The Hamiltonian that we will actually use here is thus of the form given by the addition of Eqs. (5.13,5.14), equally well interpreted in the Heisenberg picture, as just explained.

While the derivation of our method requires the use of the Schrödinger or Heisenberg picture (they work out exactly the same since the covariance matrix is just a collection of expectation values), it does not work directly from the interaction picture. Once the method is presented, however, and we let ourselves work entirely within the phase space formulation, then an interaction-like picture can be defined that works in the same manner as the interaction picture does in the Hilbert space. We will describe this at the end of the next section.



## 5.2 Mechanics of the model

In the case of an oscillator detector the great advantage is that one is able to utilize the Gaussian formalism. The reader should review the material in Ch. 3, especially with regards to symplectic evolution. As a reminder, the symplectic evolution of a given Gaussian state (under which Gaussianity is preserved) will generically be generated by a quadratic Hamiltonian (thus acting linearly on the collection of quadrature operators). The whole idea behind the oscillator-detector model is that the dynamics of this process can be fully described within a phase-space formulation, without needing to refer directly to any operators in a given Hilbert space.

We describe here the way in which this is carried out. For completeness we also include in Appendix B an alternative, but more complicated and less elegant method of solving for the system evolution. While we will not utilize the alternative in this thesis, we did use it to verify several of the preliminary calculations obtained using the primary solution method, to be now presented.

### 5.2.1 The symplectic evolution equation

The derivation of the key equation is actually incredibly simple. Indeed it can also be derived purely within classical Liouville theory [38]. This brings up an important point regarding why this approach is significantly easier and more powerful than the standard Unruh-DeWitt two-level model. By working within a Gaussian regime we ensure that all transformations are linear, and thus can be completely represented classically. Of course the interpretation of the results is different, as it is understood that underneath it all we are working with a quantum Wigner function as opposed to a classical Liouville distribution. It is therefore meaningful to talk about things like entanglement, for example. But the mechanics of the system, in particular time evolution (as is our interest here), can be described fully classically.

Let us now derive the primary equation of motion that will be used throughout this part of the thesis. We take a general system of  $M$  detectors and  $N$  fields modes, described by some (generally time-dependent) quadratic Hamiltonian  $\hat{H}(t)$ . Let us consider the set of Heisenberg-picture quadrature operators  $\{\hat{q}_{d_j}(t), \hat{p}_{d_j}(t)\}$  for each detector and  $\{\hat{q}_n(t), \hat{p}_n(t)\}$  for each field mode, where for the moment let us take  $t$  to be the global time parameter with respect to which the field evolves, although this need not be the case. These quadrature operators are related to the creation and annihilation operators of each mode by Eq. (3.2).

We can combine these operators into the following vector:

$$\hat{\mathbf{x}}(t) = (\hat{q}_{d_1}(t), \hat{p}_{d_1}(t), \dots, \hat{q}_{d_M}(t), \hat{p}_{d_M}(t), \hat{q}_1(t), \hat{p}_1(t), \dots, \hat{q}_N(t), \hat{p}_N(t))^T. \quad (5.25)$$

Note that the transpose operation merely transposes the shape of an operator-valued vector; it does nothing to the operators themselves.

To compute the evolution of  $\hat{\mathbf{x}}(t)$  we recall from Ch. 3 that as long as  $\hat{H}(t)$  is quadratic in the quadrature operators (equivalently, quadratic in the ladder operators) then the unitary evolution  $\hat{U}(t)$  that it generated will act linearly on the quadratures

$$\hat{\mathbf{x}}(t) = \hat{U}^\dagger(t)\hat{\mathbf{x}}_0\hat{U}(t) = \mathbf{S}(t)\hat{\mathbf{x}}_0, \quad (5.26)$$

where  $\hat{\mathbf{x}}_0 = \hat{\mathbf{x}}(0)$  is the initial vector and the time-dependent transformation  $\mathbf{S}(t)$  is symplectic, Eq. (3.10). Correspondingly, the evolution of the state as given by the evolution of the covariance matrix (either in the Schrödinger or the Heisenberg picture), takes the form

$$\boldsymbol{\sigma}(t) = \mathbf{S}(t)\boldsymbol{\sigma}_0\mathbf{S}(t)^T, \quad (5.27)$$

where  $\boldsymbol{\sigma}_0$  is the initial state. Our goal is to find a differential equation for  $\mathbf{S}(t)$  that represents the evolution generated by a quadratic Hamiltonian. Note that in general there would also be a phase-space displacement term,  $\hat{\mathbf{x}} \rightarrow \mathbf{S}\hat{\mathbf{x}} + \mathbf{y}$ , generated by linear terms in  $\hat{H}(t)$ . While making such a generalization would be simple, in our work we have only utilized purely quadratic Hamiltonians and thus will not need to consider this extension.

A general time-dependent, quadratic Hamiltonian  $\hat{H}(t)$  can be written as

$$\hat{H} = \hat{\mathbf{x}}^T \mathbf{F}(t) \hat{\mathbf{x}}, \quad (5.28)$$

where  $\mathbf{F}(t)$  is a Hermitian matrix of c-numbers containing any explicit time-dependence of the Hamiltonian. This matrix is very important, as it represents the phase-space construction of whatever Hamiltonian we choose to use. We can now write the Heisenberg equation for the time evolution of the quadratures:

$$\frac{d}{dt}\hat{\mathbf{x}} = i[\hat{H}, \hat{\mathbf{x}}] \quad (5.29)$$

Writing this out in components and using Eq. (3.3) we obtain

$$\begin{aligned} \frac{d}{dt}\hat{x}_j &= i[\hat{H}, \hat{x}_j] = i \sum_{mn} F_{mn}(t) [\hat{x}_m \hat{x}_n, \hat{x}_j] \\ &= \sum_{mn} F_{mn}(t) (\hat{x}_m \Omega_{jn} + \Omega_{jm} \hat{x}_n), \end{aligned} \quad (5.30)$$

where  $\Omega_{jn}$  is the  $j, n$ 'th component of the symplectic form, Eq. (3.4). This expression can be collected back into a vector as

$$\frac{d}{dt}\hat{\mathbf{x}} = \boldsymbol{\Omega}\mathbf{F}^{\text{sym}}(t)\hat{\mathbf{x}}, \quad (5.31)$$

where  $\mathbf{F}^{\text{sym}} = \mathbf{F} + \mathbf{F}^{\text{T}}$ . We now plug in Eq. (5.26), giving

$$\frac{d}{dt}[\mathbf{S}(t)]\hat{\mathbf{x}}_0 = \boldsymbol{\Omega}\mathbf{F}^{\text{sym}}(t)\mathbf{S}(t)\hat{\mathbf{x}}_0, \quad (5.32)$$

where we used the fact that  $\hat{\mathbf{x}}_0$  is time independent. Let us now take the commutator with  $\hat{\mathbf{x}}_0^{\text{T}}$  on both sides:

$$\begin{aligned} \left[ \left( \frac{d}{dt}\mathbf{S}(t) \right) \hat{\mathbf{x}}_0, \hat{\mathbf{x}}_0^{\text{T}} \right] &= \left[ \boldsymbol{\Omega}\mathbf{F}^{\text{sym}}(t)\mathbf{S}(t)\hat{\mathbf{x}}_0, \hat{\mathbf{x}}_0^{\text{T}} \right] \\ \frac{d}{dt}\mathbf{S}(t)[\hat{\mathbf{x}}_0, \hat{\mathbf{x}}_0^{\text{T}}] &= \boldsymbol{\Omega}\mathbf{F}^{\text{sym}}(t)\mathbf{S}(t)[\hat{\mathbf{x}}_0, \hat{\mathbf{x}}_0^{\text{T}}]. \end{aligned} \quad (5.33)$$

Since  $[\hat{\mathbf{x}}_0, \hat{\mathbf{x}}_0^{\text{T}}] = i\boldsymbol{\Omega}$ , which is an invertible matrix of c-numbers, we can cancel it, yielding the following first-order, linear, ordinary differential equation for the symplectic matrix:

$$\frac{d}{dt}\mathbf{S}(t) = \boldsymbol{\Omega}\mathbf{F}^{\text{sym}}(t)\mathbf{S}(t). \quad (5.34)$$

While simple, this equation is the primary result of this chapter, and is the equation to be used in the following five chapters. Solving this equation with the initial condition  $\mathbf{S}(0) = \mathbf{I}$  (such that  $\hat{\mathbf{x}}_0 = \mathbf{S}(0)\hat{\mathbf{x}}_0$ ) is completely equivalent to solving the standard Hilbert space evolution with the Hamiltonian-unitary formalism. It represents a Schrödinger-type equation in phase space, the difference now being that it is a matrix differential equation rather than an operator differential equation. Indeed, Eq. (5.34) can actually be utilized with any arbitrary collection of coupled oscillators or modes, for example within condensed matter systems. While in this thesis we do not stray from its use as a field-detector model, what we have above is a far more general tool.

Note, importantly, that in order to actually solve this equation (e.g. numerically) we need to work with finite dimensional matrices. This means only considering a finite number of field modes within the evolution. That is, what we must do is to take a UV cutoff, ignoring modes of sufficiently high energy. This is actually not a concern with regards to the results we will present, because in every case we have ensured that our results are not affected by this cutoff. We do this by increasing the number of modes included in the

simulation until our result in question no longer notably changes with respect to further increasing the cutoff. That is, we ensure that our results converge and we make sure to include enough modes so as not to have the cutoff introduce artifacts into the results.

Of critical importance is the observation that, because we are not working in the interaction picture, any time-dependence in the Hamiltonian (and thus in the matrix  $\mathbf{F}(t)$ ) is due to explicit time-dependence imposed on the system. Examples of this include smoothly switching on one's detector through modulation of the window function  $\lambda(t)$  [1] and the time-dependence induced by acceleration (a scenario that we will consider in the next chapter). Throughout the majority of the applications presented in this thesis, however, we will not actually have any such time-dependence. This is because, aside from Ch. 6, we will be considering stationary detectors with sharp switching profiles (i.e.  $\lambda(t)$  will be piecewise constant). In such cases solving Eq. (5.34) becomes significantly easier. If  $\mathbf{F}$  is time-independent then it will (obviously) commute with itself at different times, meaning that we need not worry about time-ordering and the solution is given by the simple matrix exponential:

$$\mathbf{S}(t) = \exp(\boldsymbol{\Omega}\mathbf{F}^{\text{sym}}t). \quad (5.35)$$

This solution method can also be applied in the case that one's system is piecewise time-independent. In such a scenario the evolution over each piece may be separately solved via Eq. (5.35). The full evolution may then be garnered by multiplying together each evolution matrix.

## 5.2.2 Free evolution and examples of phase-space Hamiltonians

Above we have fully described the mechanical workings of our solution method. One need simply identify the phase-space matrix  $\mathbf{F}(t)$  corresponding to one's multimode Hamiltonian (be this in regards to a detector-field interaction or otherwise) via Eq. (5.28), take  $\mathbf{F}^{\text{sym}}(t) = \mathbf{F}(t) + \mathbf{F}(t)^T$ , and then solve the matrix differential equation Eq. (5.34).

If  $\mathbf{F}$  is time-independent then we may simply identify the solution via Eq. (5.35). One such trivial instance is when there is no interaction, and the Hamiltonian consists solely of the free part  $\hat{H} = \hat{H}_{\text{free}}$ . This translates into  $\mathbf{F} = \mathbf{F}_{\text{free}}$  having only a free evolution contribution as well. For a generic collection of bosonic modes the free Hamiltonian will be of the form given by Eq. (3.8), in which case it is clear that  $\mathbf{F}_{\text{free}}^{\text{sym}} = \text{diag}(\omega_1, \omega_1, \omega_2, \omega_2, \dots)$ . Multiplying by the symplectic form, Eq. (3.4), we see immediately that  $\boldsymbol{\Omega}\mathbf{F}_{\text{free}}^{\text{sym}}$  is exactly the generator of single mode rotations. Thus, following Eq. (5.35), the symplectic free

evolution is simply

$$\mathbf{S}_{\text{free}}(t) = \bigoplus_n \begin{pmatrix} \cos \omega_n t & \sin \omega_n t \\ -\sin \omega_n t & \cos \omega_n t \end{pmatrix}. \quad (5.36)$$

That is, free evolution consists of single-mode rotations. It follows from this, for example, that the vacuum and thermal states are stationary. In Hilbert space we know this to be true because the density matrices of these states are diagonal in the energy eigenbasis with respect to  $\hat{H}_{\text{free}}$ . In phase space we know this because vacuum and thermal states, the covariance matrices of which are given by Eqs. (3.14) and (8.2) respectively, are zero-mean and single-mode rotationally symmetric.

As an important example, we may consider the case of a single detector undergoing motion in a field. As discussed in Sect. 5.1.2, in such a case we must take account of the fact that the proper time  $\tau$  of the detector will be different from the global time  $t$  with respect to which the field evolves. In such a case we can evolve with respect to  $\tau$ , and the free Hamiltonian generating translations in this time parameter will be

$$\hat{H}_{\text{free}} = \Omega \hat{a}_d^\dagger a_d + \frac{dt(\tau)}{d\tau} \sum_n \omega_n \hat{a}_n^\dagger \hat{a}_n, \quad (5.37)$$

where  $\Omega$  is the energy gap of the detector. This corresponds to a phase space Hamiltonian matrix

$$\mathbf{F}_{\text{free}}^{\text{sym}} = \begin{pmatrix} \Omega & 0 \\ 0 & \Omega \end{pmatrix} \oplus \frac{dt}{d\tau} \left[ \bigoplus_n \begin{pmatrix} \omega_n & 0 \\ 0 & \omega_n \end{pmatrix} \right]. \quad (5.38)$$

This matrix is not actually time-independent, because of the  $dt/d\tau$  term. However, the solution to Eq. (5.34) can be represented as the (generally time ordered) exponential of the time integral of  $\Omega \mathbf{F}_{\text{free}}^{\text{sym}}$ . Here,  $\Omega \mathbf{F}_{\text{free}}^{\text{sym}}$  commutes with itself at different times and the total derivative  $dt/d\tau$  is eliminated upon integrating over  $\tau$  such that the solution is immediately seen to be

$$\mathbf{S}_{\text{free}}(\tau) = \begin{pmatrix} \cos \Omega \tau & \sin \Omega \tau \\ -\sin \Omega \tau & \cos \Omega \tau \end{pmatrix} \oplus \left[ \bigoplus_n \begin{pmatrix} \cos \omega_n t & \sin \omega_n t \\ -\sin \omega_n t & \cos \omega_n t \end{pmatrix} \right]. \quad (5.39)$$

That is, the detector freely evolves with respect to its time  $\tau$  and the field freely evolves with respect to its time  $t$ . Note that this exactly fits with how we know that free evolution acts on the annihilation and creation operators of a given system, Eq. (5.18).

Of course here we will be more concerned with scenarios in which there is an interaction Hamiltonian that couples a detector (or a number of detectors) to some cavity field in question. That is, we would have  $\hat{H}(\tau) = \hat{H}_{\text{free}} + \hat{H}_{\text{int}}(\tau)$ . In phase space this corresponds to  $\mathbf{F}(\tau) = \mathbf{F}_{\text{free}} + \mathbf{F}_{\text{int}}(\tau)$ . Let us continue with our example of a single, generally non-stationary detector following the worldline  $x(\tau)$ . Working in the Schrödinger picture and taking the Unruh-DeWitt coupling, we have

$$\hat{H}_{\text{int}} = \lambda(\tau)(\hat{a}_d + \hat{a}_d^\dagger) \sum_n \left( u_n[x(\tau)]\hat{a}_n + u_n^*[x(\tau)]\hat{a}_n^\dagger \right), \quad (5.40)$$

where the mode functions  $u_n(x)$  are given by the  $t = 0$  case of one of Eqs. (4.53,4.54,4.55) depending on what boundary conditions are imposed on the cavity, or something more complicated if you want to be fancy, which we won't be. For example let us consider our moving detector inside a periodic cavity of length  $L$ . This means that we have a collection of field modes with both positive and negative wavenumbers  $k_n = 2\pi n/L$ , corresponding to right-moving and left-moving modes respectively. As explained just after Eq. (5.34), in any calculation using this method we must, in practice, take only a finite number of field modes into consideration. The reader should note, however, that we have ensured that all results are independent of this exclusion (meaning that we always include enough modes). Thus, let us take  $N$  right-moving modes and  $N$  left-moving modes, meaning that  $n = \{-N, -N + 1, \dots, N\}$ . Given this, it is straightforward to see that the Hamiltonian of Eq. (5.40) corresponds to the phase space matrix

$$\mathbf{F}_{\text{int}}^{\text{sym}}(\tau) = 2\lambda(\tau) \begin{pmatrix} \mathbf{0}_2 & \mathbf{X}_P(\tau) \\ \mathbf{X}_P^T(\tau) & \mathbf{0}_{4N} \end{pmatrix}, \quad (5.41)$$

where  $\mathbf{0}_n$  is the  $n \times n$  matrix of zeros and

$$\mathbf{X}_P(\tau) = \begin{pmatrix} \frac{\cos(k_{-N}x(\tau))}{\sqrt{4\pi N}} & \frac{-\sin(k_{-N}x(\tau))}{\sqrt{4\pi N}} & \frac{\cos(k_{-N+1}x(\tau))}{\sqrt{4\pi(N-1)}} & \frac{-\sin(k_{-N+1}x(\tau))}{\sqrt{4\pi(N-1)}} & \dots & \frac{\cos(k_N x(\tau))}{\sqrt{4\pi N}} & \frac{-\sin(k_N x(\tau))}{\sqrt{4\pi N}} \\ 0 & 0 & 0 & 0 & \dots & 0 & 0 \end{pmatrix} \quad (5.42)$$

We use the subscript  $P$  to denote that this the case for a periodic cavity. The block form of this matrix makes sense, as the interaction term contains no self-interactions (i.e. detector-detector or field-field), rather only between the detector and field. Also note that in the case of a periodic cavity we will, throughout this thesis, simply neglect the zero mode,  $n = 0$ , as is common practice. The legitimacy of this omission is discussed in [114].

If instead we are using a Dirichlet or Neumann cavity then the form of  $\mathbf{X}$  will be modified. In both of these cases, for example, the field modes are labeled only by positive  $n$ . This because the  $n$ 'th mode function in Eq. (4.54) or (4.55) is not linearly independent

from the same mode function with  $-n$ . In other words, we do not need negative values of  $n$  in order to have a complete mode basis, unlike in the periodic case. Thus in these cases we will take the first  $N$  modes, such that  $n = \{1, \dots, N\}$ . For both Dirichlet and Neumann boundary conditions, the mode wavenumbers take the values  $k_n = \pi n/L$ , and it is straightforward to see that we have

$$\mathbf{F}_{\text{int}}^{\text{sym}}(\tau) = 2\lambda(\tau) \begin{pmatrix} \mathbf{0}_2 & \mathbf{X}_{D/N}(\tau) \\ \mathbf{X}_{D/N}^T(\tau) & \mathbf{0}_{2N} \end{pmatrix}, \quad (5.43)$$

where the  $\mathbf{X}$  matrix for the Dirichlet and Neumann cases is, respectively,

$$\mathbf{X}_D(\tau) = \begin{pmatrix} \frac{\sin(k_1 x(\tau))}{\sqrt{\pi}} & 0 & \frac{\sin(k_2 x(\tau))}{\sqrt{2\pi}} & 0 & \dots & \frac{\sin(k_N x(\tau))}{\sqrt{\pi N}} & 0 \\ 0 & 0 & 0 & 0 & \dots & 0 & 0 \end{pmatrix}, \quad (5.44)$$

and

$$\mathbf{X}_N(\tau) = \begin{pmatrix} \frac{\cos(k_1 x(\tau))}{\sqrt{\pi}} & 0 & \frac{\cos(k_2 x(\tau))}{\sqrt{2\pi}} & 0 & \dots & \frac{\cos(k_N x(\tau))}{\sqrt{\pi N}} & 0 \\ 0 & 0 & 0 & 0 & \dots & 0 & 0 \end{pmatrix}. \quad (5.45)$$

Throughout much of this thesis we will be considering scenarios in which we have more than one detector interacting with the field. In such a case, one simply needs to add corresponding rows to the matrix  $\mathbf{X}$ . We will see this explicitly in later chapters.

### 5.2.3 The phase space interaction picture

In standard (Hilbert space) quantum mechanics, the interaction picture is a useful way of taking account of the free evolution of a system when studying the physics of some given interaction, at least in the case that the interaction Hamiltonian  $\hat{H}_I(t)$  is explicitly time-dependent. If this is not so then it can in some cases be more useful to *not* move to the interaction picture, as it may be easier to deal with a full (free plus interaction), time-independent Hamiltonian than it is to deal with solely an interaction, but time-dependent, Hamiltonian. A precise example of this is presented above, where in the case of a (piecewise) time-independent system we can solve the evolution simply by evaluating Eq. (5.35). In the case that we begin with an explicitly time-dependent interaction Hamiltonian, however, adding “more” time dependence by moving to the interaction picture is more than compensated for by not having to worry about the free Hamiltonian in one’s evaluation of the evolution equation.

While in the derivation above we have explicitly *not* worked in the interaction picture, we are now able to take the result and consider what is, in a sense, a “phase space interaction picture”. We will use this practice in Ch. 6 when we consider an accelerating oscillator detector. In this section we will therefore continue to consider the evolution with respect to proper time  $\tau$ , rather than  $t$ . We use the fact that the *free* symplectic evolution of our system is trivially solvable, for example as given by Eq. (5.39) in the case of a single detector. Let us introduce the notation  $\mathbf{K}(\tau) = \Omega \mathbf{F}^{\text{sym}}(\tau)$ . From Eq. (5.34), the evolution matrix solves the equation of motion  $\dot{\mathbf{S}}(\tau) = \mathbf{K}(\tau)\mathbf{S}(\tau)$ , where here the overdot represents differentiation with respect to  $\tau$ . This matrix can be split into the free and interaction parts:  $\mathbf{K}(\tau) = \mathbf{K}_{\text{free}} + \mathbf{K}_{\text{int}}$ , where  $\mathbf{K}_{\text{free}} = \Omega \mathbf{F}_{\text{free}}^{\text{sym}}$  and  $\mathbf{K}_{\text{int}}(\tau) = \Omega \mathbf{F}_{\text{int}}^{\text{sym}}(\tau)$ .

As just discussed, the free evolution is trivially solved from the equation  $\dot{\mathbf{S}}_{\text{free}} = \mathbf{K}_{\text{free}}\mathbf{S}_{\text{free}}$ . Let us then apply the same procedure as is usually done when moving to an interaction picture. We will define an interaction picture symplectic evolution matrix  $\mathbf{S}^I(\tau)$  and an interaction picture interaction generator  $\mathbf{K}_{\text{int}}^I(\tau)$ , defined as

$$\begin{aligned}\mathbf{S}^I(\tau) &\equiv \mathbf{S}_{\text{free}}^{-1}(\tau)\mathbf{S}(\tau), \\ \mathbf{K}_{\text{int}}^I(\tau) &\equiv \mathbf{S}_{\text{free}}^{-1}(\tau)\mathbf{K}_{\text{int}}(\tau)\mathbf{S}_{\text{free}}(\tau).\end{aligned}\tag{5.46}$$

It is then easily seen that the evolution equation  $\dot{\mathbf{S}}(\tau) = \mathbf{K}(\tau)\mathbf{S}(\tau)$  is equivalent to

$$\frac{d\mathbf{S}^I(\tau)}{d\tau} = \mathbf{K}_{\text{int}}^I(\tau)\mathbf{S}^I(\tau).\tag{5.47}$$

The evaluation of  $\mathbf{S}^I(\tau)$  can then be accomplished by standard numerical techniques. The full Heisenberg evolution matrix is then simply  $\mathbf{S}(\tau) = \mathbf{S}_0(\tau)\mathbf{S}^I(\tau)$ , and the evolved state of the detector-field system is given by  $\boldsymbol{\sigma}(\tau) = \mathbf{S}(\tau)\boldsymbol{\sigma}_0\mathbf{S}(\tau)^T$ .

### 5.3 Discussion

By applying the Gaussian formalism, we have addressed the problem of time evolution of a particle detector undergoing relativistic movement inside of a cavity. With this, we are able to tackle arbitrary multimode time-dependent problems and solve them nonperturbatively. This is markedly different from the standard Unruh-DeWitt model, as discusses in Sect. 4.4, that can generally only be solved perturbatively. Remarkably, the only fundamental change between the standard approach and our work is that we use a harmonic oscillator to describe a detector, rather than a qubit.



In addition to being nonperturbative, the methods we have presented lead to a computationally efficient way of solving a great range of problems involving an arbitrary number of particle detectors coupled to quantum fields inside a cavity. The flexibility of the model extends to the following: (1) the detectors can undergo arbitrary relativistic motion; (2) they can have arbitrary quadratic interaction with the field; (3) the field and detectors can begin in any Gaussian initial state; and (4) our description of the field can include any number of modes. The vast range of scenarios that this can encompass are all solved by the same number-valued, linear, first-order ordinary differential equation. We have the additional advantage that for a given evolution, we do not need to solve the equation again if we decide to change the initial state. As a demonstration of this applicability, we will in the following chapters apply this approach to study a wide variety of relativistic quantum phenomena.

The advantage of working nonperturbatively, in general, is that it allows us to access phenomena that are inherently nonperturbative. This means phenomena involving (one or several of) high coupling, high energy, and large evolution time scales. Several of the studies to be presented in the following chapters are of exactly this nature, particularly as regards long-time phenomena. The question of thermalization, for example, is one that cannot be addressed properly using perturbation theory. This will come into play in our next chapter, in which we demonstrate that the state of a uniformly accelerating oscillator detector in fact becomes thermal, which is a *stronger* statement than saying it has a thermal response, as is derived using the perturbative methods of Sect. 4.4.

We conclude this chapter by noting that there are many other problems of interest not studied in this thesis, but which can now be easily addressed using our formalism. Applications to cavity settings in curved spacetimes are an obvious example. Another would be the non-perturbative study of the dynamical Casimir effect and similar phenomena [115]. Indeed, there are in fact many potential applications of this model to further the study that will be presented in Part. IV of this thesis, as will be discussed there.

# Chapter 6

## The Unruh effect in a cavity; thermalization and universality

Note: this chapter derives from the work [2], in collaboration with Wilson G. Brenna, Robert B. Mann, and Eduardo Martín-Martínez.

One of the chief predictions of quantum field theory in curved spacetimes is the well-known Unruh effect [21, 85]. It dictates that a detector with constant acceleration  $a$  in free space, in which the field is in the Minkowski vacuum, will experience a response equivalent to its submersion into a heat bath with a temperature proportional to its acceleration. This phenomenon is intrinsically related to the Hawking effect [116], and understanding it is essential in order to investigate more complex phenomena such as black hole dynamics and possible quantum corrections to relativistic gravity.

As was discussed in Sect. 4.5, the first derivations of the Unruh effect was based on the characterization of the Minkowski vacuum in a unitarily inequivalent Rindler quantization. This approach, however, is not above criticism. A number of very strong assumptions have to be made in order to justify the observation of a thermal bath by an accelerated observer in the Minkowski vacuum. For example, the infinite amount of energy required to sustain the eternal Rindler trajectory. It has also been argued that difficulties arise in defining a Minkowski vacuum when boundary conditions are specified on the scalar field on a manifold [117]. Despite these criticisms, we also saw in Sect. 4.5 that the same predictions can be obtained by using an accelerated particle detector model. It is this same method of studying the Unruh effect that we will utilize in this chapter, the difference being now we will make use of the non-perturbative approach discussed in the previous chapter and, furthermore, consider the Unruh effect within a cavity.

We saw that it is relatively easy to perturbatively show that the response of an accelerated detector to the vacuum state is Planckian. However, perturbation theory is not the most appropriate approach to study the thermalization properties of the detector. In practice this is mainly because higher orders of perturbation theory would be required, increasing the calculational complexity even beyond those of non-perturbative methods. More fundamentally, thermalization is an equilibrium result that is often only achieved over the course of long time scales. In general, such time scales will not be accessible to perturbation theory since the perturbative parameter  $|\lambda\langle H\rangle\Delta T|$  becomes larger as time increases. Reasonable criticism may therefore be raised about a perturbative claim of thermalization. While in this chapter we will not consider energy or time scales that would break perturbation theory, we are able to use the non-perturbative oscillator approach to check whether or not an accelerating detector evolves to thermal state, a significantly stronger statement than the thermal statistics obtainable within a perturbative treatment. That is, one should not only check that the probability of excitation of the detector has a Planckian response, one should also check to what extent the state of the detector becomes thermal if the detector is carefully switched on and if the interaction lasts for long enough times. This requires a complete calculation of the detector's density matrix; it is a common misconception that a detector's Planckian response implies that the detector thermalizes, because of the possibility of off-diagonal coherence terms in the density matrix. By the use of non-perturbative methods of Ch. 5 we can make sure that thermalization is achieved and that it is not an artifact of the use of perturbation theory applied in regimes beyond its applicability.

We consider in this current chapter the thermality of accelerated detectors in cavities with different boundary conditions. We will indeed demonstrate non-perturbatively that an accelerated oscillator detector coupled to the vacuum state of a cavity scalar field thermalizes to a temperature proportional to its acceleration. Furthermore, we demonstrate that this occurs independent of the boundary conditions imposed on the cavity. Surprisingly, in fact, the numerical results vary very little with respect to different boundary conditions.

We do note that there has previously been an effort to understand how imposing different boundary conditions modifies the response of detectors in non-inertial scenarios in free space. For example work has been done in a very different context to examine the continuum Rindler case [118], and a number of boundary conditions in Hartle-Hawking vacua have been studied [119]. However, these studies do not tell us if the boundary effects of a cavity will prevent a uniformly accelerating particle detector from thermalizing due to the Unruh effect.

Our findings indicate that in all of the scenarios under consideration, the Unruh effect occurs. We observe that the detector achieves thermalization with temperature propor-

tional to acceleration. Thus, not only does the Unruh effect occur inside a cavity (which imposes an IR-cutoff on the field and, furthermore, isolates the field in the cavity from the rest of the spacetime), it appears to occur independently of the details of this IR cutoff and of the spatial distribution of the cavity modes. This demonstrates that the Unruh effect, which many have argued relies on idealized details and thus cannot lead to thermalization [120, 121, 122], is in fact a very general and universal phenomenon and that thermalization of particle detectors can be computed non-perturbatively. Not only is this a remarkable result from a fundamental point of view, it also gives hope to the possibility of an experimental realization of the Unruh effect in quantum optical settings, where it has been shown that general relativistic scenarios can already be simulated [123].

## 6.1 The setting

We will consider a uniformly accelerated oscillator detector, prepared in its ground state, going through a cavity prepared in the vacuum state. The acceleration will be labeled  $a$  and the length of the cavity will be  $L$ . The trajectory will be such that the detector starts moving inside the cavity with a given initial speed, with a constant acceleration in a direction opposite to its initial motion. Hence the detector will be decelerated while crossing the cavity. It reaches the center of the cavity exactly when it reaches zero speed, and then travels back to the initial point with increasing speed until it reaches the position in which it started, having the same speed as when it entered the cavity but in the opposite direction. Parameterized by the proper time  $\tau$  of the detector, this uniformly accelerated worldline takes the form

$$t(\tau) = \frac{1}{a} \sinh(a\tau), \quad x(\tau) = \frac{L}{2} + \frac{1}{a} [\cosh(a\tau) - 1] \quad (6.1)$$

This trajectory within the cavity, as a function of the detector's proper time, is shown in Fig. 6.1. For larger values of the acceleration the detector will exit the cavity. In principle this is an issue as computationally we must mirror the field modes outside of the cavity. However, over the range of accelerations that we will consider the coupling decays so quickly past the edges that these tails will have negligible contribution to the observed final state.

To have a clean signature one must be careful with the way in which the detector is switched on [124, 1] since a sudden switching stimulates strong quantum fluctuations that may overcome the Unruh effect. In order to reduce switching noise we ensure that the interaction is sufficiently smoothly switched on, following a Gaussian time profile, such

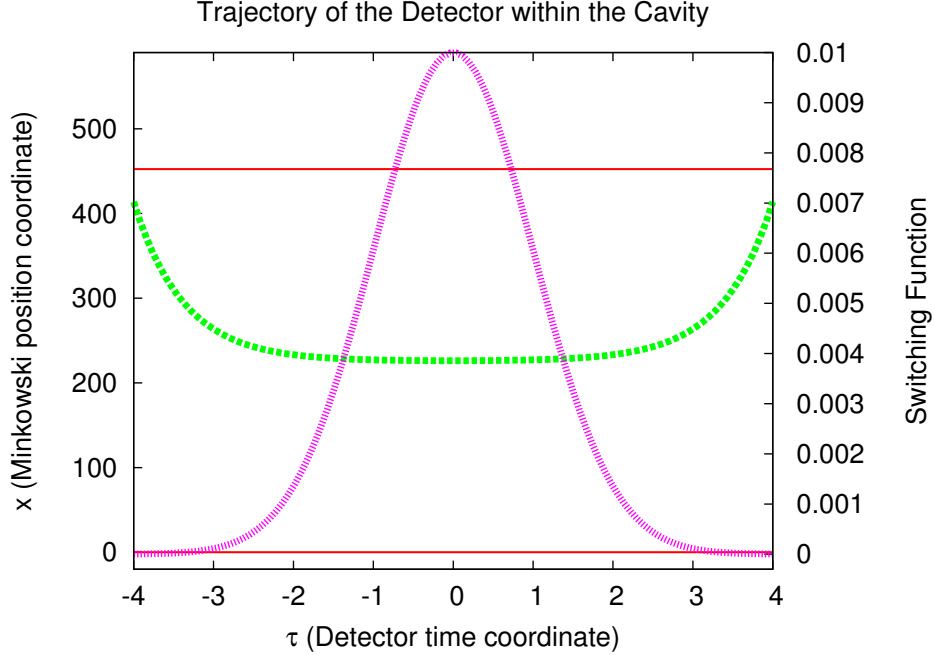


Figure 6.1: The detector’s (green, dashed) trajectory through the cavity (red, solid) with acceleration  $a = 1.6$ . The Gaussian switching function is plotted on the right axis with a jagged magenta line.

that switching noise effects are negligible. In particular, the switching function that we use has the form

$$\lambda(\tau) = \lambda_0 \exp(-\tau^2/2\delta^2). \quad (6.2)$$

We prepare the ground state of the detector and the vacuum of the field at a time  $\tau = -T$  where the interaction is switched on following the Gaussian profile above, the atom has some initial speed and starts decelerating until it reaches the centre of the cavity at time  $\tau = 0$ . The detector continues accelerating until the time  $\tau = T$  when it reaches the initial point again. In the settings that we shall analyze, we will consider as parameters  $T = 4$ ,  $\delta = 8/7$  and  $\lambda_0 = 0.01$ . With these parameters we find that the switching is more than smooth enough for our purpose; namely the detector’s response from the switching noise is negligible compared with the response from acceleration. Furthermore, we will take the length of the cavity to be  $L = 144\pi$ . We take this rather large value in order to ensure that the detector stays within the cavity throughout its evolution. We could have simply taken a more compact window function  $\lambda(\tau)$  in order to avoid this, but then we would introduce

non-negligible switching noise. Lastly, we will take the energy gap of the detector to be  $\Omega = 3$ . This means that, inertially, the detector would be resonant with quite a high field mode (specifically, mode  $n = 432$  for the Dirichlet and Neumann cavities, and  $n = 216$  for the periodic cavity). From the perspective of the detector, the field modes will undergo a large degree of redshift and blueshift over the course of its accelerating trajectory. The large choice of  $\Omega$  was made in order to ensure that the detector does not see the frequency of the fundamental cavity mode blueshifted above  $\Omega$ , at which point the detector would not be near resonance with *any* mode, and would thus effectively stop interacting with the field.

Computationally, we will utilize the phase space interaction picture as described in Sect. 5.2.3, where the matrix  $\mathbf{F}_{\text{int}}^{\text{sym}}$  is as given in Eq. (5.41) or (5.43) with the matrix  $\mathbf{X}$  given by one of Eqs. (5.42,5.44,5.45), depending on which boundary conditions are imposed on the cavity. As discussed above, in this chapter we will consider all three conditions. For each case we transform to the phase space interaction picture, such that we are left with Eq. 5.47, which we numerically integrate from  $-T = -4$  to  $T = 4$  and with the parameters as quoted above. Upon solving for the symplectic evolution matrix, we apply it to the detector+field initial covariance matrix (in this case, the identity matrix) to obtain the evolved covariance matrix, as in Eq. (5.27). We then isolate the  $2 \times 2$  covariance matrix of the detector  $\sigma_d$ , which fully characterizes the reduced state of the detector after it has undergone its evolution through cavity.

## 6.2 Thermality

In order to conclude that the detector has experienced a thermal Unruh bath during its acceleration, we look for two things: first, that the detector has evolved to a thermal state and, second, that the corresponding temperature grows linearly with the acceleration experienced by the detector. We will now explain the means by which we check the first condition: whether or not the detector has evolved to a state that is actually thermal. The non-perturbative approach introduced in the previous chapter is in fact very well suited for this purpose. Not only is thermality easily tested, but because we have the exact (non-perturbative) state of the detector we are able to make a definitive statement about thermalization. In order to make conclusions about thermalization using perturbation theory, one would at the least need to expand to higher orders, and at the worst it would be impossible due to the long time scales typically required for thermalization to occur, where perturbation theory may break down.

Gaussian states that are zero mean in phase space, as we are dealing with here, can be

fully characterized by their mixedness, squeezing, and rotation. Thus, once the detector has completed its evolution it will be, up to single-mode rotation (i.e. free evolution), in a squeezed thermal state of the form

$$\boldsymbol{\sigma}_d = \begin{pmatrix} \nu e^r & 0 \\ 0 & \nu e^{-r} \end{pmatrix}, \quad (6.3)$$

where  $\nu$  is the covariance matrix's symplectic eigenvalue and  $r$  is its squeezing parameter. These diagonal entries are just the eigenvalues of  $\boldsymbol{\sigma}_d$ ,  $\lambda_{\pm} = \nu e^{\pm r}$ , from which the symplectic eigenvalue and squeezing parameter follow as  $\nu = \sqrt{\lambda_+ \lambda_-}$  and  $e^{2r} = \lambda_+ / \lambda_-$ . We must now determine whether the amount of thermality introduced by  $\nu$  is a much greater contributor to the energy of the detector's state compared to the amount of squeezing. If so, then the state can be said to be nearly thermal. If they are comparable, or if squeezing has the greater contribution, then we can not claim that the detector thermalizes.

To compare these two effects we study how they contribute to the free energy of the detector, as given by Eq. (3.9) for our single detector mode. Applying this equation to our detector of energy gap  $\Omega$  and with covariance matrix Eq. (6.3) we see that the energy is  $E = \Omega(\nu \cosh r - 1)$ . For small squeezing (which is satisfied in our scenario) we can expand this to leading order in  $r$ , yielding

$$E = \Omega \left[ (\nu - 1) + \frac{1}{2} \nu r^2 \right]. \quad (6.4)$$

Since  $\nu$  is of order unity (and is in fact remains very close to unity for our situation) a good test for thermality is thus

$$\nu - 1 \gg r^2 \quad (6.5)$$

If this inequality is satisfied then the detector can be said to be very nearly thermal. Equivalently, if

$$\delta \equiv \frac{r^2}{\nu - 1}$$

is very small, the detector is said to be thermal.

We find that the detector thermalizes very well in all of the three boundary conditions considered: periodic, Dirichlet, and Neumann. We find numerically that for the parameters given in Sect. 6.1,  $\delta$  is on the order of  $10^{-6}$  in all three cases. That is, the squeezing experienced by the oscillator is extremely minute compared to its thermality, and thus the detector can be said to be very nearly thermal.

The first of our two conditions to verifying the Unruh effect (thermality and temperature proportional to acceleration) is satisfied for all three boundary conditions.

### 6.3 Unruh temperature

We are now in a position to compute the temperature of the evolved detector  $\sigma_d$ . For a single oscillator of frequency  $\Omega$  the form of an exactly thermal state is  $\sigma_d^{\text{therm}} = \text{diag}(\nu, \nu)$ , for which the temperature is (see Sect. 3.2)

$$T = \Omega \left[ \ln \left( \frac{\nu + 1}{\nu - 1} \right) \right]^{-1}. \quad (6.6)$$

Since in our scenario we have already confirmed that our detector thermalizes to an excellent approximation we are able to use this equation to compute the temperature of our detector with negligible error, where  $\nu = \sqrt{\lambda_+ \lambda_-}$  as above.

Given all of this, we will additionally find it convenient to make partial use of a perturbative treatment, as presented in Sect. 4.4. This is because, as discussed above, over the course of its evolution the detector will observe massive red and blue shifts in the field modes. This means that we are required to include a very large number of field modes in our integration of Eq. (5.47), because even very high energy modes will, for a short time in the detector's evolution, be redshifted enough that they become non-negligibly resonant with the detector. Indeed, for the higher accelerations that were considered we found that we needed 9000 modes in order to achieve convergence. This goes beyond a reasonable numerical integration in the non-perturbative approach. However, for lower accelerations, in which we were able to properly apply the oscillator detector formalism, we found good agreement between the temperature obtained from Eq. (6.6) and the temperature computed using the standard perturbative approach, as indeed it should since any difference will be of order  $\mathcal{O}(\lambda^4)$ . That is, we may perturbatively compute the probability of transition to the first energy level, assume that it takes the form of a Boltzmann distribution (which we only know it does because we have non-perturbatively confirmed that the state is thermal), and compute the temperature from this. For the low-acceleration regime, in which we used 240 field modes, we have confirmed that both approaches agree. Extending to higher accelerations, and thus requiring more modes (specifically, we included 9000), we solely used the perturbative approach in order to compute the temperature of the detector as a function of acceleration. The result of this is plotted in Fig. 6.2 for all three boundary conditions. We emphasize, however, that the non-perturbative approach was essential to this exercise in order to confirm thermality, without which deriving a temperature from the perturbative excitation probability would be nonsensical.

Remarkably we find that for all three boundary conditions the temperature of the detector upon exiting the cavity grows linearly with acceleration, demonstrating that the



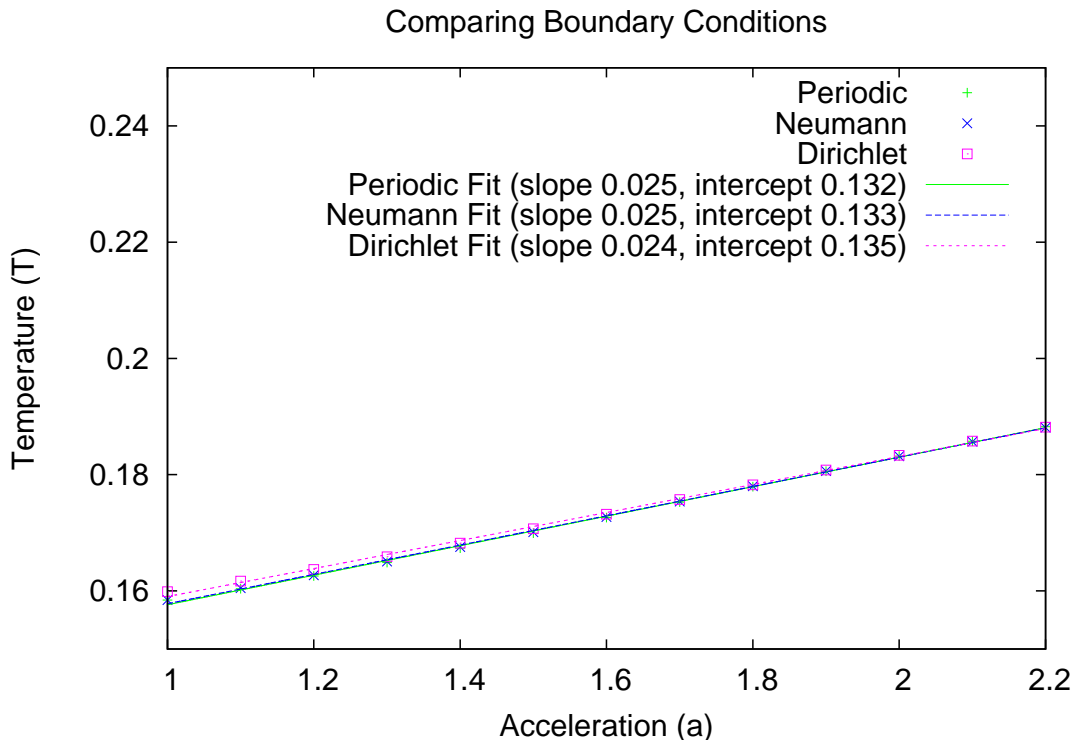


Figure 6.2: Comparison of different boundary conditions on the detector’s temperature as a function of temperature. Not only do we see that it is linear, but that it is nearly numerically identical for all three boundary conditions.

qualitative features expected of the Unruh effect are very much independent of the details of the cavity. This settles any doubt regarding whether or not there exists at least some form of the Unruh effect when an IR-cutoff for the field is introduced (i.e. when inside a cavity). There has been some skepticism [120, 121, 122] stemming from the large number of technical assumptions that go into the canonical derivation of the Unruh effect [21] and how the presence of a cavity might alter or even eliminate its existence. We have demonstrated not only thermality and the existence of the effect in a cavity, but furthermore that the boundary conditions ascribed to this cavity are all but irrelevant. Indeed the numerical similarity between the different cases is striking.

We note that the slope of the detector temperature with respect to acceleration is not equal to the value of  $1/2\pi$  predicted by the canonical free-space derivation. This is not overly surprising since we are working in a cavity setting rather than free space; sig-

nificant border effects should be expected when studying such phenomena. Our results demonstrate, however, that the inclusion of an IR cutoff does not destroy the Unruh effect understood as the thermal response of a particle detector with a temperature proportional to the acceleration, and what is more, that the detector actually thermalizes to that particular temperature. If we were to take our cavity to the continuum limit we would expect the slope to converge to the usual value of  $1/2\pi$ . We leave such a study for future work.

Lastly, while we have not included it in this chapter, we note that in [2] we additionally considered the case in which the coupling between the detector and field was of an  $XP$  nature, rather than  $XX$ . That is, we took the detector to couple instead to the conjugate momentum field  $\hat{\pi}$ . Interestingly, in such a case we found that the results were all but identical to those presented above. This lends further credence to the notion that the Unruh effect is in fact a very general and universal phenomenon.

## 6.4 Discussion

In this chapter we have used the non-perturbative methods introduced in Ch. 5 to solve for the evolution of an oscillator detector undergoing uniform acceleration through a cavity field. We demonstrated that the Unruh effect does indeed occur inside a cavity, and additionally that this result is independent of the boundary conditions applied to the field, implying that the Unruh effect is in fact a very universal phenomenon. Specifically, we have considered vacuum cavity fields with periodic, Dirichlet, and Neumann boundary conditions. In all three cases we have observed that an accelerating oscillator detector evolves to a thermal state and that the temperature obtained by the detector increases linearly with its acceleration. Furthermore the results between the three cases are numerically very similar. This indicates that not only is the phenomenon qualitatively universal but, with respect to the case of boundary conditions, also quantitatively universal.

Moreover, our use of the non-perturbative oscillator model has allowed us to make significantly stronger claims regarding the thermality experienced by the detector than can be made using the standard perturbative framework typically employed in the literature. That is, we have concluded that in our scenario an accelerating detector in fact evolves to a thermal state, rather than merely exhibiting a thermal response function. Questions of thermalization cannot be made in perturbation theory without resorting to higher order expansions, and in some scenarios may actually be impossible due to the large time scales often required for thermalization, where perturbation theory breaks down.

More generally, the results of this chapter suggest that the Unruh effect and similar phenomena such as Hawking radiation may be largely independent of the details of the

system [85]. In addition to theoretical interest, such universality bodes well for an eventual experiment where the Unruh effect could be measured.

# Chapter 7

## Tripartite vacuum entanglement harvesting

Note: this chapter derives from the work [3], in collaboration with Krzysztof Lorek, Daniel Pecak, and Andrzej Dragan.

One of the central concepts of interest in this thesis is that of vacuum entanglement. As discussed in Sect. 4.6, the vacuum state of a quantum field displays quantum correlations between spatially separated points. That is, the quantum vacuum fluctuations at point  $x_A$  and point  $x_B$  are correlated. As a result, disjoint regions of space will generically be entangled with each other. This is especially interesting because it is the vacuum state that we are dealing with, the state that we perceive as being empty. This does bring up, however, the challenge of answering in what sense this entanglement physically manifests itself. The primary paradigm we use in this thesis to understand physical phenomena is operationalism. We are attempting to answer in what real, observable ways something presents itself. With regards to vacuum entanglement there are several ways of going about this. We present a new operational interpretation in Ch. 13, for example. Here, however, we will return to a topic that has been studied by several other authors, that of entanglement harvesting [41, 42, 43, 44]. We will examine this phenomenon using the non-perturbative approach introduced in Ch. 5, and furthermore extend the study by looking at the harvesting of tripartite entanglement.

The standard scenario of vacuum entanglement harvesting is that of two particle detectors locally interacting with a field at different points. By doing this, the detectors may become entangled with each other, even if they remain spacelike separated over the course of their evolution! Of course, it is well known that no local operations can increase

entanglement between two quantum systems [23]. In the case at hand however there is already entanglement present in the vacuum state of the field between spatially separated degrees of freedom, and so by interacting with the field locally, multiple detectors can swap this entanglement out of the field to become entangled themselves. This is true even if the detectors remain spacelike separated throughout their evolution, meaning that they can become entangled without any direct causal mutual influence. They both experience vacuum noise (i.e. excitations due to switching), but the noise that they experience is correlated, and so their excitation statistics become correlated as well. While in practice the amount of entanglement extracted is typically minute, and therefore unlikely to be useful in any way for quantum informational tasks, it is interesting that we are in principle harvesting a usable computational resource out of “nothing”.

So far the studies have largely been limited to the case of bipartite entanglement harvesting. Perturbative calculations involving more than two detectors can be quite intensive and, in general, computing tripartite entanglement measures for mixed states can be exceedingly difficult. In this chapter we demonstrate the existence of tripartite entanglement in a vacuum field and characterize its extraction by a trio of oscillator detectors. One may find this surprising given the fact that all three-point correlation functions vanish in the vacuum. However while it is true that GHZ-type tripartite entanglement is witnessed by the three-point function, tripartitely entangled states also include those of W-type entanglement, which may be non-zero even when the three-point function is vanishing (see Sect. 2.1.3 to recall how we define GHZ and W-type tripartite entanglement). Indeed we demonstrate that the tripartite entanglement is in fact more easily accessible than bipartite. We observe a rich and interesting structure of the vacuum entanglement that has yet to be fully understood.

We employ the non-perturbative oscillator-detector method for the case when three point-like detectors, initially all uncorrelated and in their ground states, interact with the vacuum state of a massless scalar field. We only consider the case when the time of interaction is shorter than the light crossing time between the detectors. This rules out the possibility of creation of entanglement via signaling (exchange of quanta). All of the entanglement generated between the detectors must therefore have been harvested from the pre-existing entanglement present in the vacuum. In particular we consider the case of a periodic cavity field in which the three detectors are placed equidistantly. Although the final state of the detectors alone is mixed, this symmetry allows for the easy verification of genuine tripartite entanglement between them that has been swapped from the field. We compare the regime of parameters for which the tripartite entanglement is harvested with the parameters for which bipartite entanglement is achieved between two detectors alone, and we find that in fact tripartite entanglement is more easily harvested.

It should be noted that a previous paper, [125], has also demonstrated the extraction of W-type tripartite entanglement from a quantum field. The differences between this work and our own are significant however, in that here our computations are entirely non-perturbative and we provide detailed data on the regions in parameter space in which the detectors obtain tripartite entanglement. Furthermore in our study we consider a cavity field rather than one in free space. This is important because any verification and utilization of such harvested entanglement is very likely to come about through a cavity-type scenario similar to the case of [112].

## 7.1 Setting and computation

Here we describe the the scenario in which we are going to be working, as well as describe some of the specifics regarding computation. To begin, it should be noted that standard, bipartite entanglement harvesting can be achieved using the non-perturbative oscillator approach, unsurprisingly. For example in the next chapter we will see an explicit example of this, in Fig. 8.1. Bipartite harvesting is not our focus in this chapter, as the phenomenon has been previously well-studied using the standard perturbative framework. Rather, in this chapter we will focus on the harvesting of tripartite entanglement, and will directly compare this with the bipartite case.

We consider three stationary detectors in a one-dimensional, periodically identified cavity of length  $L$  with a massless scalar field. Both the field and the detectors are initially in their ground states and are thus not entangled with each other. At time  $t = 0$  the detectors are sharply switched on to start interacting with the field and the system is allowed to evolve until time  $t = T$ . After this interaction the entanglement between the detectors is examined. Sharply switching on the detectors means that at  $t = 0$  we discontinuously change the coupling from zero to a constant, non-zero value  $\lambda$ . This, along with the fact that the detectors are unmoving, means that our Hamiltonian is time-independent over the period of evolution in which we are interested,  $t \in (0, T)$ . We are thus able to easily solve for the system evolution by utilizing the exact solution Eq. (5.35). What is more, the fact that the detectors are stationary means that their proper time is equivalent to the global time parameter  $t$ , and we need not worry about dealing with different time parameters. In fact this type of setting (stationary detectors with sharp switching) will also be used in the following two chapters, in which we similarly will use Eq. (5.35). One may be concerned that sharply switching on the detectors will cause divergences of some sort, and indeed in more than one spatial dimension sharp switching is problematic [124]. In  $1 + 1$  dimensions, however, the response of the field and detectors

to this operation is perfectly finite (of course they *will* respond to some degree, as they must in order to become entangled).

We will take our three detectors to be stationary at locations  $x_1$ ,  $x_2$ , and  $x_3$ , each of frequency  $\Omega$ . Following the prescription of Sect. 5.2, the system (detector+field) evolution is given on the level of the covariance matrix by performing the operation  $\boldsymbol{\sigma}(t) = \mathbf{S}(t)\boldsymbol{\sigma}_0\mathbf{S}(t)^\top = \mathbf{S}(t)\mathbf{S}(t)^\top$ , where the second equality follows from the fact that our initial state is the ground state for the detectors plus the vacuum state for the field, meaning that  $\boldsymbol{\sigma}_0 = \mathbf{I}$ . Following Eq. (5.35), the symplectic evolution matrix is given by  $\mathbf{S}(t) = \exp(\boldsymbol{\Omega}\mathbf{F}^{\text{sym}}t)$ , where  $\boldsymbol{\Omega}$  is the symplectic form and the matrix  $\mathbf{F}^{\text{sym}} = \mathbf{F}_{\text{free}}^{\text{sym}} + \mathbf{F}_{\text{int}}^{\text{sym}}$  is as specified in Sect. 5.2.2. Namely, since we are working with a periodic cavity the free part we will be  $\mathbf{F}_{\text{free}}^{\text{sym}} = (\Omega, \Omega, \Omega, \omega_N, \omega_{N-1}, \dots, \omega_{N-1}, \omega_N)$ , where  $\omega_n = |k_n| = 2\pi|n|/L$ . The interaction part will then be given by Eq. (5.41), where now the coupling constant  $\lambda$  is time-independent and the  $\mathbf{X}$  matrices will be given by

$$\mathbf{X}_P = \begin{pmatrix} \frac{\cos(k_{-N}x_1)}{\sqrt{4\pi N}} & \frac{-\sin(k_{-N}x_1)}{\sqrt{4\pi N}} & \frac{\cos(k_{-N+1}x_1)}{\sqrt{4\pi(N-1)}} & \frac{-\sin(k_{-N+1}x_1)}{\sqrt{4\pi(N-1)}} & \dots & \frac{\cos(k_Nx_1)}{\sqrt{4\pi N}} & \frac{-\sin(k_Nx_1)}{\sqrt{4\pi N}} \\ 0 & 0 & 0 & 0 & \dots & 0 & 0 \\ \frac{\cos(k_{-N}x_2)}{\sqrt{4\pi N}} & \frac{-\sin(k_{-N}x_2)}{\sqrt{4\pi N}} & \frac{\cos(k_{-N+1}x_2)}{\sqrt{4\pi(N-1)}} & \frac{-\sin(k_{-N+1}x_2)}{\sqrt{4\pi(N-1)}} & \dots & \frac{\cos(k_Nx_2)}{\sqrt{4\pi N}} & \frac{-\sin(k_Nx_2)}{\sqrt{4\pi N}} \\ 0 & 0 & 0 & 0 & \dots & 0 & 0 \\ \frac{\cos(k_{-N}x_3)}{\sqrt{4\pi N}} & \frac{-\sin(k_{-N}x_3)}{\sqrt{4\pi N}} & \frac{\cos(k_{-N+1}x_3)}{\sqrt{4\pi(N-1)}} & \frac{-\sin(k_{-N+1}x_3)}{\sqrt{4\pi(N-1)}} & \dots & \frac{\cos(k_Nx_3)}{\sqrt{4\pi N}} & \frac{-\sin(k_Nx_3)}{\sqrt{4\pi N}} \\ 0 & 0 & 0 & 0 & \dots & 0 & 0 \end{pmatrix} \quad (7.1)$$

Note that in this study we take  $N = 50$ , which we found to be more than sufficient to obtain convergence of our results.

After performing this evolution up to time  $t = T$  we will have the covariance matrix  $\boldsymbol{\sigma}(T)$ . From this we then isolate the  $6 \times 6$  reduced covariance matrix of the three detectors, which we will label  $\boldsymbol{\sigma}_{123}$ . This matrix can generically be decomposed into  $2 \times 2$  blocks as follows:

$$\boldsymbol{\sigma}_{123} = \begin{pmatrix} \boldsymbol{\sigma}_1 & \gamma_{12} & \gamma_{13} \\ \gamma_{12} & \boldsymbol{\sigma}_2 & \gamma_{23} \\ \gamma_{13} & \gamma_{23} & \boldsymbol{\sigma}_3 \end{pmatrix}. \quad (7.2)$$

The diagonal blocks are the covariance matrices of corresponding detectors alone, and the off-diagonal blocks contain information about the correlations between the different detectors. It is this matrix from which we will extract information regarding the entanglement among the detectors.

The detectors have been chosen to be aligned as  $(x_1, x_2, x_3) = (\frac{1}{6}L, \frac{1}{2}L, \frac{5}{6}L)$ , where 0 and  $L$  are the coordinates of the walls of the cavity. For periodic boundary conditions this

alignment is symmetric in the sense that each detector is placed at the distance  $\frac{L}{3}$  away from either of the remaining two, and hence the state of the system is invariant under the exchange of any two detectors. This will in fact make it easier to determine whether or not the trio are tripartitely entangled.

To compute the bipartite logarithmic negativity between a given pair  $ij$  of detectors we must first obtain their reduced state by isolating the appropriate blocks of  $\sigma_{123}$  to obtain the  $4 \times 4$  covariance matrix

$$\sigma_{ij} = \begin{pmatrix} \sigma_i & \gamma_{ij} \\ \gamma_{ij}^T & \sigma_j \end{pmatrix}. \quad (7.3)$$

The logarithmic negativity between these two modes is then computed via Eq. (3.34).

Now, how do we determine if there is tripartite entanglement present among our three detectors? By definition, a tripartite system contains genuine tripartite entanglement if and only if the state is inseparable across all three of the possible bipartitions  $ij|k$  [45]. Here what we truly care about is the existence or absence of tripartite entanglement, and less so its actual value. Thus we estimate the amount of tripartite entanglement using the geometrical average of the logarithmic negativities across all the bipartitions:

$$\bar{E}_N(ijk) = \sqrt[3]{E_N(i|jk)E_N(j|ik)E_N(k|ij)}. \quad (7.4)$$

This quantity does not constitute a proper entanglement measure, but certainly it provides a yes-or-no answer to whether or not there is tripartite entanglement in the system. Since we are using a the periodic cavity, the fact that the three detector state is symmetric under detector permutation means that to determine the presence of tripartite entanglement we need only consider a single bipartition, since the other two will be equivalent. This symmetry furthermore allows for a convenient trick that facilitates the easy calculation of the logarithmic negativity across a given bipartition. The fully symmetric state in this case will be of the form

$$\sigma_{\text{periodic}} = \begin{pmatrix} \sigma_1 & \gamma & \gamma \\ \gamma & \sigma_1 & \gamma \\ \gamma & \gamma & \sigma_1 \end{pmatrix}. \quad (7.5)$$

The entanglement across, say, the bipartition 12|3 can be easily computed by using an example of what has been called unitary localization [126, 127]. To this end, we consider applying a beam-splitter operation to the 12 mode subsystem, which over the three detectors is given by

$$\mathbf{S}_{\text{BS}} = \begin{pmatrix} \mathbf{I}/\sqrt{2} & -\mathbf{I}/\sqrt{2} & \mathbf{0} \\ \mathbf{I}/\sqrt{2} & \mathbf{I}/\sqrt{2} & \mathbf{0} \\ \mathbf{0} & \mathbf{0} & \mathbf{I} \end{pmatrix}. \quad (7.6)$$



Being a unitary operation solely acting on the 12 subsystem, this does not affect the entanglement across the 12|3 bipartition. Furthermore, with mode symmetry this operation is seen to isolate all correlations solely between modes 2 and 3:

$$\mathbf{S}_{\text{BS}}\boldsymbol{\sigma}_{\text{periodic}}\mathbf{S}_{\text{BS}}^T = \begin{pmatrix} \sigma_1 - \gamma & \mathbf{0} & \mathbf{0} \\ \mathbf{0} & \sigma_1 + \gamma & \sqrt{2}\gamma \\ \mathbf{0} & \sqrt{2}\gamma & \sigma_1 \end{pmatrix}. \quad (7.7)$$

From here, we can apply Eq. (3.34) to compute the logarithmic negativity between modes 2 and 3 of this transformed state. This will be equivalent to the bipartite entanglement across the 12|3 partition which, as stated above for this symmetric case, is a necessary and sufficient indicator of genuine multipartite entanglement among all three detectors.

## 7.2 Results

In this section we present the results that have been obtained for the detector alignment described above. We compute the entanglement among the three detectors for a range of parameter values. We demonstrate that indeed tripartite entanglement can be spacelike harvested (i.e. without causal contact between detectors) from the vacuum field, and we observe a rich structure in this regard. We furthermore show that the tripartite entanglement is in fact *easier* to harvest than is bipartite. All the results have been evaluated at a fixed value of the coupling constant  $\lambda = 0.01$ . The time of interaction  $T$  will be presented here in the units of  $r$ , where  $r = \frac{L}{3}$  is the light-crossing time between neighbouring detectors. Hence for times  $T > r$  neighbouring detectors are within a timelike regime, and for  $T < r$  within a spacelike one, meaning that in the latter case they could not have been in causal contact and all the entanglement generated in the system must be due to extraction from the field.

Due to the symmetry that we have imposed among the detectors, we will now denote all the detectors by  $s$ , so  $E_N(ss)$  is the bipartite entanglement between a pair, which is identical for each pair, and  $\bar{E}_N(sss)$  is the measure we use for tripartite entanglement, which via Eq. (7.4) and symmetry is equal to  $E_N(s|ss)$ . For simplicity the former will be referred to simply as “bipartite entanglement” and the latter - as “tripartite entanglement”.

We have produced plots of the amount of entanglement as a function of  $T$  and  $\Omega$  (the frequency of the detectors), at a fixed value of  $L = 10$ . This is given in Fig. 7.1, where we plot both  $E_N(ss)$  and  $\bar{E}_N(sss)$ . In agreement with intuition, most entanglement is being produced after the light-crossing time of the neighbouring detectors, which is  $r$ . There

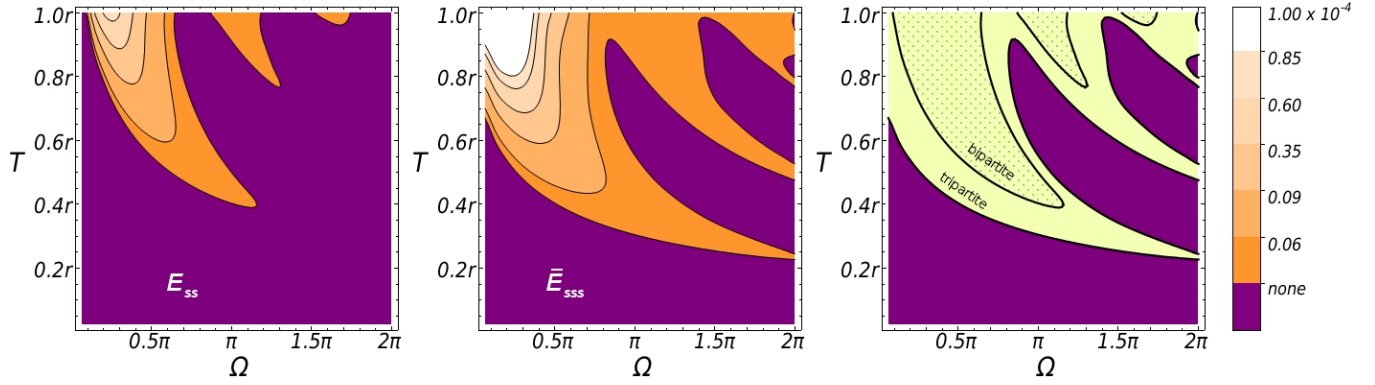


Figure 7.1: Entanglements  $E_N(ss)$  and  $\bar{E}_N(sss)$  as a function of the time  $T$  and detector frequency  $\Omega$ , where we have set  $L = 10$  and  $\lambda = 0.01$ . On the right: regions of existence of  $E_{ss}$  and  $\bar{E}_{sss}$  plotted together.

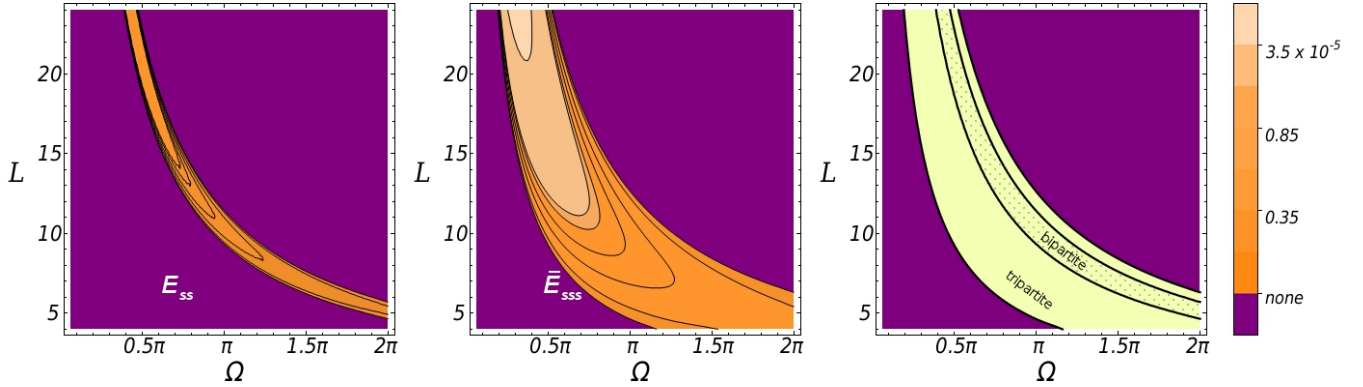


Figure 7.2: Entanglements  $E_N(ss)$  and  $\bar{E}_N(sss)$  as a function of cavity length  $L$  and detector frequency  $\Omega$ , where we have set  $T = 0.4r$  and  $\lambda = 0.01$ . On the right: regions of existence of  $E_{ss}$  and  $\bar{E}_{sss}$  plotted together.

are however regions in the  $T, \Omega$  plane along which both types of entanglement persist deeply into the spacelike regime. This entanglement does not diminish under increasing the number of field modes  $N$  and hence it is not an artifact of the imposed UV cutoff, but is rather a true physical effect. Moreover the regions where tripartite entanglement is produced are certainly broader than for those of bipartite, meaning that the tripartite entanglement emerges earlier and is therefore easier to be harvested. This however is not surprising if we recall that  $\bar{E}_N(sss) = E_N(s|ss)$  and we obtain  $E_N(ss)$  from  $E_N(s|ss)$  by tracing out one of the detectors. This is a local operation and so can only decrease the amount of entanglement, which implies that  $E_N(ss)$  always has to be less than or equal to  $\bar{E}_N(sss)$ , as can be seen from our results.

To examine the dependence of the results on  $L$  we have produced in Fig. 7.2 a plot of entanglement versus  $L$  and  $\Omega$ , having been produced at fixed  $T = 0.4r$ . In the  $L, \Omega$  plane we find a hyperbolic curve along which both bipartite and tripartite entanglement have been extracted by this time. Again, as must generally be the case, the region of non-zero tripartite entanglement is larger than that of bipartite. We also note that, within this scenario, the longer the cavity is and the smaller the detector frequency is the more entanglement can be spacelike extracted.

### 7.3 Discussion

We have used the non-perturbative oscillator-detector approach to examine the harvesting of both bipartite and of genuine tripartite entanglement from the vacuum field of a cavity. That is, a set of detectors interacting with a common quantum field can become entangled without causal contact by means of swapping the spatial entanglement present in the field. We have demonstrated that from the vacuum state of a periodically-identified cavity field genuine tripartite entanglement can be harvested. This tripartite entanglement is expected to be of the W-type, due to the fact that the three-point functions of the vacuum field are vanishing. In fact, it is considerably easier to obtain tripartite entanglement than bipartite between any two of the three detectors. Indeed, we have been able to obtain tripartite entanglement after a time of interaction considerably smaller than the light-crossing time between pairs of detector. Specifically we see that a time as small as  $t = 0.21r$ , where  $r$  is the distance between detectors, can be sufficient. We have provided detailed maps of the regions in parameter space in which bipartite and tripartite entanglement can be harvested.

Although we have not included it here, it is further demonstrated in [3] that entanglement harvesting out of a periodic cavity field is considerably easier than from a Dirichlet

cavity field. This result along with those presented here have considerable applicability towards the eventual experimental confirmation, as well as possible utilization, of entanglement harvesting scenarios. They furthermore may be applicable to more general system-bath setups than what we have considered here, helping to point the way towards optimal strategies for generating quantum correlation utilizing such systems.

# Chapter 8

## Thermal amplification of discord harvesting

Note: this chapter derives from the single-author work [4].

Entanglement, a form of quantum correlation without classical analogue, has long been understood to be a key resource in many of the procedures developed in quantum computation and information [22]. While the mutual information generically quantifies the total amount of correlation between subsystems that can potentially be useful for computational tasks, entanglement has proven to have the purely quantum nature that gives an advantage over classical computation. As discussed in Sect. 2.2, in the past decade there has been an explosion of interest in the so called quantum discord [29, 128], as well as similar measures [30], that purport to quantify quantum correlations that entanglement generally overlooks. That is, a separable (non-entangled) state may still possess quantum correlations in the sense that its joint-measurement statistics cannot be described by classical probability theory. In addition to being of theoretical interest [30, 66, 67, 9, 68], discord has also received considerable attention regarding its potential as a quantum computational resource [32, 69, 70, 71, 72, 33, 34, 73].

We have also discussed in Sect. 4.6 and the previous chapter the notion of vacuum entanglement harvesting, in which the spatial entanglement present in the vacuum state of a quantum field may be swapped to a pair detectors, even if these detectors have no causal contact. In this chapter we will again use the Gaussian formalism to consider the harvesting of entanglement into a pair of oscillator detectors, but here will furthermore study the harvesting of mutual entanglement and of quantum discord. Excepting [129], such studies have not previously been undertaken in the literature. For the discord, we

will specifically use the measure known as the Gaussian discord, [75], introduced in Sect. 3.4.1. The primary contribution of this chapter is that we will study the extraction of such correlations while simultaneously generalizing the initial state of the cavity field to consider not only the vacuum but also thermal states of varying temperature. As we will see, the results obtained by doing this are very surprising and, arguable, exciting both from a theoretical point of view as well as from a practical one.

Before continuing, we wish to point out that the ability to locally extract discord does *not* follow from the same physics that allows the well-known creation of discord through local channels [130]. Such creation generally comes at the cost of reduced mutual information, and discord *cannot* be locally created from a product state. In the correlation harvesting scenario we consider two detectors that are initially uncorrelated, and both their discord and mutual information are increased from zero due to their local interactions with the field.

Studying the effects of thermal fluctuations on our ability to harvest correlations is clearly an important part of understanding how to actually perform such a procedure in a laboratory setting, since at least some level of noise will always be present in realistic setups. Generally, it is understood that noise experienced by one’s system has a detrimental effect on the correlations present in that system due to the decoherence that such noise typically induces. One should similarly expect that thermality in a field will reduce the ability of detectors to harvest correlations from the field; the increased thermal fluctuations will cause the detectors to become more mixed and furthermore it is known that the spatial entanglement present in a field reduces with temperature [131, 132]. However, there have also been several studies demonstrating that discord is typically more robust than entanglement against the detrimental effects of noise [133, 134, 135, 10, 7], and we might therefore hope that in a harvesting scenario discord will hold out better.

Our findings are in fact much better than this hope would warrant. While we find that, as expected, the harvested entanglement decays rapidly to zero as the field temperature is increased, we simultaneously find that both the mutual information *and* the Gaussian quantum discord between the detectors actually *increase* with field temperature. This increase is in fact quite drastic, with an improvement of multiple orders of magnitude being achievable. This increased extraction of both classical and quantum correlations is what we will refer to as “thermal amplification”.

After presenting our results, we go on to discuss multiple ways in which this surprising result can be explained and understood. Of particular importance is a detailed analysis that takes advantage of the translational invariance of the periodic cavity field that we will be using in this study. We illustrate that our system can be decomposed into two dynamically

decoupled systems, each with only a single detector, and for which the evolution behavior is easily understood. By this we are able to explain both the thermal amplification of mutual information and discord, as well as the decay of entanglement, in terms of the correlating properties of passive Gaussian transformations. Using this, we find that we can also make accurate predictions for the strength of thermal amplification as a function of the system parameters. The new perspective on correlation-harvesting that we introduce in this explanation is something that we feel is interesting and worthy of study in its own right.

The thermal amplification of discord is especially surprising, as discord is purported to measure purely quantum correlations. This finding introduces the exciting possibility of using a cavity field to locally generate what is an appreciable amount of discord, which can then be used in discord-based quantum computing. This is especially so since, apparently, experimentalists need not be concerned with keeping their cavity very cold. For example, it is known that the discord and related measures quantify the amount of distillable entanglement that can be activated by local interaction with an ancilla system [33, 34, 73]. Thus it seems that while thermal fluctuations are indeed detrimental to entanglement directly, they may indirectly be of great benefit to its generation. We let ourselves ponder the possibility that this type of thermal amplification will lead to the development of what may be called “noise-assisted quantum computation”.

After the initial preprint of the manuscript that led to this chapter we became aware that similar results to ours had been observed in [136]. This paper, however, considers a very different scenario (in their case the oscillator detectors are *directly* coupled), uses very different techniques, and contains very different interpretations from what we present here. Furthermore, in addition to presenting some interesting and counterintuitive results, it is our goal here to explain the phenomenon of thermal amplification from several independent points of view. In this way, we hope to aid in the possibility of utilizing this effect in experiment and in practical application.

## 8.1 Setting and computation

The setting that we will consider is essentially the same as that used in Ch. 7, except that we will just consider two detector rather than three, and we will generalize the initial state of the field to include thermal states. We will continue to work with a periodic cavity field, in which our two detectors are stationary at positions  $x_1$  and  $x_2$ , and are sharply switching on at time  $t = 0$ . We consider a sufficiently large number  $N$  of field modes of positive

wavenumber  $k$ , and  $N$  modes of negative wavenumber, such that further increasing this number no longer modifies the results of the computation.

The method of computing the symplectic evolution matrix  $\mathbf{S}(t)$  of the system is exactly as explained in Sect. 7.1, except now with only two detectors (e.g. the matrix  $\mathbf{X}_P$  will be given by the first four rows of Eq. 7.1). Upon obtaining  $\mathbf{S}(t)$ , the state of the system (detectors+field) as a function of time from initial state  $\boldsymbol{\sigma}_0$  is described by  $\boldsymbol{\sigma}(t) = \mathbf{S}(t)\boldsymbol{\sigma}_0\mathbf{S}(t)^T$ . It is important to stress that the computation of  $\mathbf{S}(t)$  in no way depends on the initial state. This is therefore very convenient when applied to studies of different initial states, such as in this chapter, because the dependence on the initial state can be studied without recomputing the evolution.

Here, as previously, we will consider the detectors and the field to be initially uncorrelated, although this is not necessary for the formalism. Further, we will initialize the detectors in their ground states and initialize the field in a thermal Gibbs state of temperature  $T$ . This includes the  $T = 0$  limit, which is the vacuum state. The covariance matrix of the ground/vacuum state of system of oscillators/modes is simply given by the identity matrix. Specifically, for the pair of detectors and the field:

$$\boldsymbol{\sigma}_{\text{ground}}^{(d)} = \mathbf{I}_4, \quad \boldsymbol{\sigma}_{\text{vac}}^{(f)} = \mathbf{I}_{4N}. \quad (8.1)$$

More generally, a thermal state of the field is given by the covariance matrix

$$\boldsymbol{\sigma}_{\text{therm}}^{(f)} = \bigoplus_{n=-N}^N \begin{pmatrix} \nu_n & 0 \\ 0 & \nu_n \end{pmatrix}, \quad (8.2)$$

where

$$\nu_n = \frac{\exp \omega_n \beta + 1}{\exp \omega_n \beta - 1}, \quad \beta \equiv 1/T, \quad (8.3)$$

are the symplectic eigenvalues of a thermal state (see Sect. 3.3). This means that the initial state we use is of the form

$$\boldsymbol{\sigma}_0 = \boldsymbol{\sigma}_{\text{ground}}^{(d)} \oplus \boldsymbol{\sigma}_{\text{therm}}^{(f)}. \quad (8.4)$$

After evolution by some time  $t$ , the state of our system will take the generic form

$$\boldsymbol{\sigma} = \begin{pmatrix} \boldsymbol{\sigma}^{(d)} & \boldsymbol{\gamma} \\ \boldsymbol{\gamma}^T & \boldsymbol{\sigma}^{(f)} \end{pmatrix}, \quad (8.5)$$



where  $\boldsymbol{\sigma}^{(d)}$  is the covariance matrix representing the reduced state of the detectors. From  $\boldsymbol{\sigma}^{(d)}$ , we may compute the logarithmic negativity  $E_N$  between the detector by Eq. 3.34, the Gaussian quantum discord  $D(1,2)$  by Eq. 3.36, and the mutual information by

$$I = S(\boldsymbol{\sigma}_1) + S(\boldsymbol{\sigma}_2) - S(\boldsymbol{\sigma}^{(d)}), \quad (8.6)$$

where  $\boldsymbol{\sigma}_1$  and  $\boldsymbol{\sigma}_2$  are the reduced,  $2 \times 2$  covariance matrices of the individual oscillators, and the von Neumann entropy  $S$  of a Gaussian state is given by Eq. (3.24). Recall from Sect. 2.2 that, in general, the discord is not symmetric with respect to which oscillator the measurement is performed on:  $D(1,2) \neq D(2,1)$ . However, in our our scenario we will find that the two detectors are symmetric under exchange, and thus here we will have  $D \equiv D(1,2) = D(2,1)$ . It should also be noted that although there is circumstantial evidence that Gaussian measurements are optimal for Gaussian states [82], there is as of yet no proof of this, and so it is possible that the Gaussian discord may slightly overestimate the true value of discord in general.

In the following section, all data presented will be using the following parameter values: the length of the cavity is  $L = 100$ , the coupling strength for both detectors is  $\lambda = 0.05$ , the detector frequencies are both  $\Omega = 40\pi/L \approx 1.26$  (meaning that they are resonant with the 20<sup>th</sup> field modes, both right and left-moving), and the number of right and left-moving field modes is  $N = 80$  (this number was chosen such that further increasing  $N$  does not perceivably alter the results).

## 8.2 Results

We can now present the primary results of this chapter, which were obtained using the formalism above. We consider what occurs when two detectors, initially in their ground states, are injected into a cavity field that is either in its vacuum state or in a thermal state. We then track the evolution of correlation measures between the detectors, including logarithmic negativity  $E_N$ , mutual information  $I$ , and Gaussian quantum discord  $D$ . The results obtained for logarithmic negativity follow exactly as would be intuitively expected, and thus it will not be our primary focus here. Rather it is the mutual information and discord that display unexpected behavior and will take up the majority of this chapter. In this section we will merely present our results, and in the following section we will go on to give several explanations for them and discuss.

In short, our primary result is as follows: thermality of the field can be used to *increase* the amount of non-entanglement correlation that is extracted from the field by the

detectors. That is, both the mutual information *and* the quantum discord that are extracted increase as a function of field temperature  $T$ . On the other hand, the harvested entanglement rapidly vanishes as  $T$  is increased, agreeing with intuition.

In the following, we use  $r = |x_1 - x_2|$  to indicate the distance between the detectors. The results of our calculations are independent of the absolute positions  $x_1$  and  $x_2$ , rather only on their difference  $r$ , because a periodically identified vacuum or thermal field is translationally invariant.

Although entanglement will not be our primary focus here, since its behavior follows as expected, for completeness we will include some data regarding its extraction in our scenario. This will also be used as a comparison with the other measures discussed below. We begin by presenting some data for the case that the field starts in the vacuum. In Fig. 8.1 we plot the logarithmic negativity between the detectors as a function of the distance  $r$  between them and the time  $t$  of evolution in the case that the field is initially in its vacuum state. If we compute the same information when the field is instead started in a thermal state, we find that the magnitude of this plot rapidly decays with temperature. This behavior is as expected, and follows one's intuition regarding thermal fluctuations as being a source of decohering noise. As an example, we plot in Fig. 8.2 the logarithmic negativity as a function of time for several different field temperatures. At a distance of  $r = 3$ , we find that any extractable entanglement is completely extinguished by the time the temperature reaches the small value of  $T = 0.2$ .

Moving on, we plot in Fig. 8.2 the mutual information between the detectors, Eq. (8.6), in the same scenario (i.e. with the field initially in its vacuum state). This clearly displays very different behavior as compared to the logarithmic negativity. We don't bother displaying the Gaussian discord here, Eq. (3.36), because in this case the discord is only very slightly less than the mutual information (see Fig. 8.4) and thus follows the same behavior. This on its own is an interesting finding: the harvested mutual information consists almost entirely of quantum correlations (at least as quantified by the Gaussian discord). We will see that when considering a thermal field of high temperature this is no longer the case.

Another obvious point to make is that, unlike entanglement, the detectors begin to gain some mutual information (as well as discord) immediately after the interaction is turned on (see Fig. 8.4), and this statement is independent of the distance  $r$  between them. Indeed the amount of correlation becomes appreciable far before the light crossing time  $t = r$  between the detectors, the time at which they come into causal contact. Such immediate generation of correlations was also seen in [129] using a perturbative framework and in the context of the Fermi problem (i.e. when one of the detectors starts in an excited state).

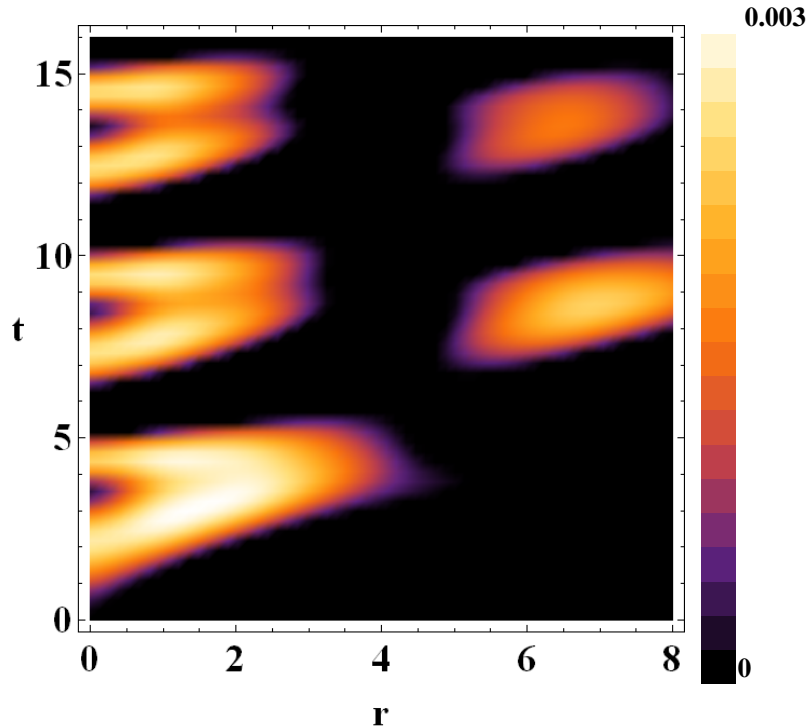


Figure 8.1: The logarithmic negativity between the detectors  $E_N$ , as a function of the distance  $r$  between them and the time  $t$  of evolution in the case that the field is initially in its vacuum state.

It is not overly surprising to find these results. Physically, the field at spatially separated positions is known to be correlated, and so the response of detectors at these positions should be expected to be correlated as well. While entanglement is clearly a different story, there is no reason to suspect that more general correlations should not begin accumulating immediately after initializing the interaction. Mathematically, it is straightforward to show for small  $t$ , by expanding the symplectic evolution Eq. (5.35) in powers of  $t$ , that the off-diagonal block  $\gamma_{12}$  of the detector-detector covariance matrix generically grows as order  $t^2$ . This implies that the detectors must necessarily have non-zero correlation for any finite time.

We remind the reader that the local harvesting of discord that we observe is *not* the same as the known ability to create discord through local operations [130]. Local operations *cannot* increase the mutual information, and often an increase in discord through local operations comes at the cost of an overall reduction in mutual information. Local

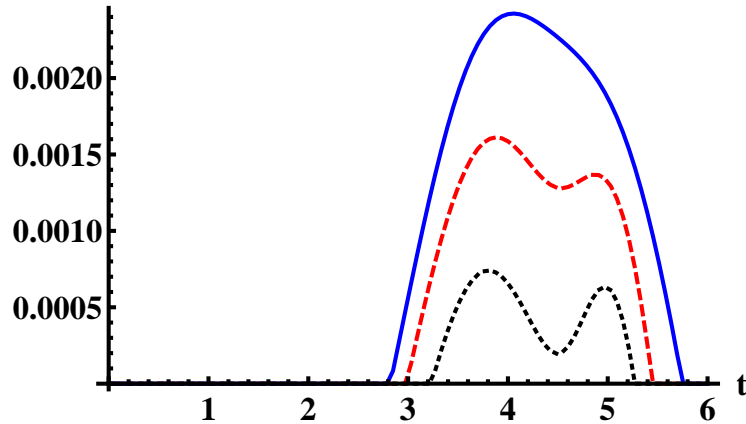


Figure 8.2: The logarithmic negativity between the detectors as a function of time  $t$ , where  $r = 3$ . We display the data for the cases that the field is initially in its vacuum state  $T = 0$  (solid blue line), and in thermal states of temperatures  $T = 0.1$  (red dashed line) and  $T = 0.15$  (black dotted line). At a temperature of  $T = 0.2$  the entanglement remains nonexistent. We observe that the extracted entanglement rapidly decays with field temperature.

operations cannot introduce discord into a product state. Here we are clearly seeing a different phenomenon, since both the discord and the mutual information are increasing from zero.

We now go on to present our primary results. Plotted in Fig. 8.4 is the mutual information and Gaussian discord between the detectors as a function of time, where the detectors have been placed at a distance  $r = 4$  away from each other. We display three plots: the first for the case that the field is initialized in its vacuum state (i.e. at temperature  $T = 0$ ), the second for the case that the field is initialized in a thermal state at temperature  $T = 1$ , and the third for a temperature of  $T = 10$ . What we observe is that as the field temperature is increased both the obtained mutual information *and* discord are *increased* as well, and by orders of magnitude at that. Note that all plots in Fig. 8.4 were made using the same symplectic evolution matrix  $\mathbf{S}(t)$  (i.e. it only needed to be solved for once); for each of the three different plots the same  $\mathbf{S}(t)$  was simply applied to a different initial covariance matrix.

To examine the limits of this behavior, we plot in Fig. 8.5 the mutual information and discord as a function of field temperature  $T$  up to very high temperatures, where the detectors were placed at a distance  $r = 4$  away from each other and left to evolve for a time  $t = 2$ . We can see that, although slowing down, the mutual information continues

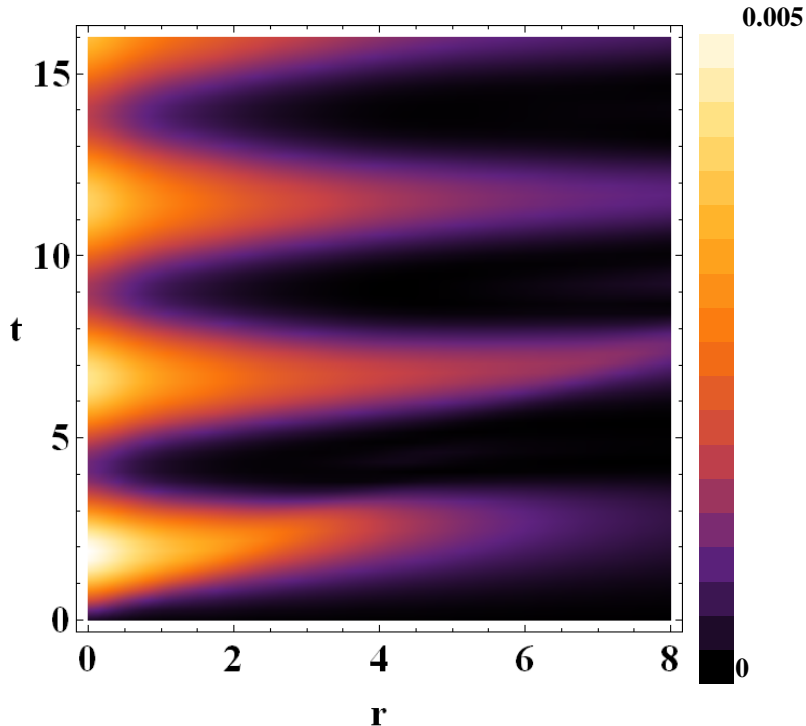


Figure 8.3: The mutual information between the detectors  $I$ , Eq. (8.6), as a function of the distance  $r$  between them and the time  $t$  of evolution in the case that the field is initially in its vacuum state.

to increase even at a temperature of  $T = 60$ . The discord, on the other hand, reaches its maximum at approximately  $T = 6$  before slowly decaying. Even though the amplification of discord (a measure of *quantum* correlations) does eventually cease, this field temperature is relatively very high and well into what one would call a purely classical regime. Nevertheless, it is reassuring to see that thermal decoherence *does* eventually start to hinder the harvested discord. Indeed it must, as for high temperatures the two-point correlation function is known to have a purely classical limit.

How do our results change with other parameters of the system, such as the coupling strength and distance? Also, what is the behavior in the long-time limit? In terms of the coupling strength  $\lambda$  the harvesting changes as expected: increasing  $\lambda$  generically increases the amount of harvested correlations as given by each of our measures. Unfortunately we cannot consider indefinitely large  $\lambda$  in our model because the UV modes will become significant in the evolution and one would need to work without a UV cutoff. In the long

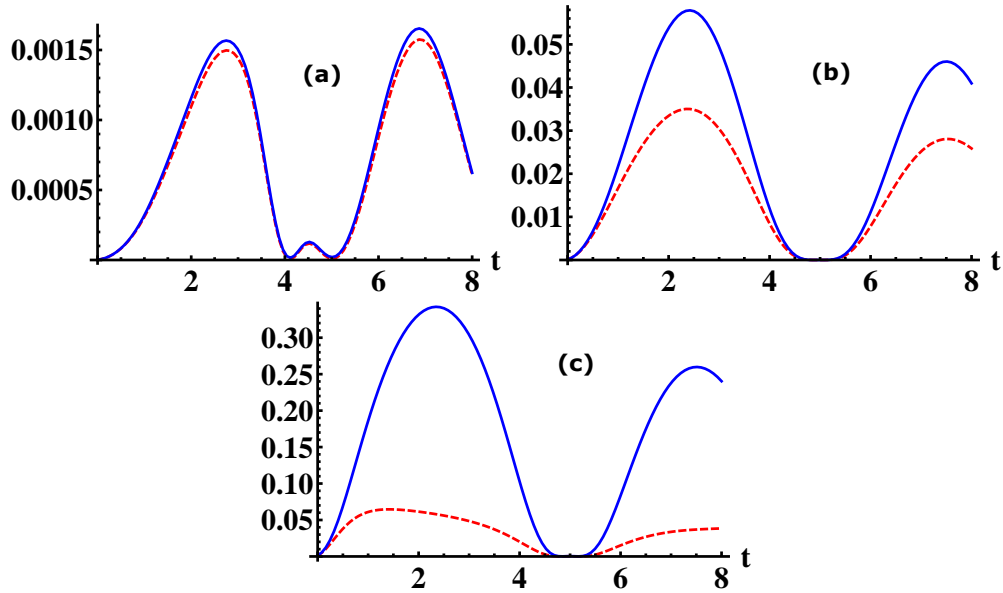


Figure 8.4: The mutual information  $I$  (solid blue line) and the Gaussian discord  $D$  (dashed red line) between the detectors as a function of time  $t$ , where  $r = 4$ . The temperature of the field varies in the three plots from (a)  $T = 0$  (i.e. the vacuum), (b)  $T = 1$ , and (c)  $T = 10$ . We observe that as temperature increases both  $I$  and  $D$  very substantially increase.

time limit the mutual information and discord of the detectors do not approach zero, as may have been expected. Rather they continue to oscillate with a characteristic period of  $2\pi/\Omega = 5$ , and with their mean values generically maintained near the values seen in Figs. 8.4 and 8.5 for a given temperature. Regarding the dependence on distance  $r$ , we defer the discussion of this to Sect. 8.3.1 and the Appendix. C, but the short story is that the mutual information and discord follow the same qualitative behavior with time as well as with temperature (i.e. thermal amplification still occurs) for different distances.

There are several further points to make on these results. We see that as temperature increases the difference between the mutual information and the discord grows greater. In the vacuum case, as we noted above,  $I$  and  $D$  are nearly equivalent. This implies that the correlations obtained by the detectors are mostly of a quantum nature, with little contribution coming from classical correlations. As the field temperature increases, however, we find that classical correlations begin to take on the dominant role. Nevertheless, for temperatures up to about  $T = 6$  the harvested discord *does* increase by almost two orders of magnitude from the vacuum case. This is very surprising considering how quickly any

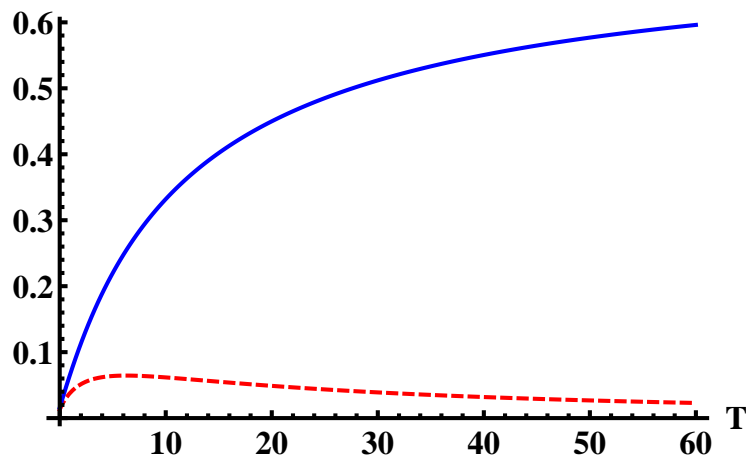


Figure 8.5: The mutual information  $I$  (solid blue line) and the Gaussian discord  $D$  (dashed red line) between the detectors as a function of field temperature, where  $r = 4$  and  $t = 2$ .

extractable entanglement vanishes with increasing temperature. It is known that discord tends to be more robust to decoherence than entanglement [133, 134, 135, 10, 7], but what we have found in this scenario is instead a complete reversal of behavior between the two measures.

This result can be looked at in one of two ways: either one takes this to mean that the Gaussian quantum discord is clearly not an appropriate measure of purely quantum correlations, or we count this as an excellent indication of how quantum computing may still be performed in noisy environments (as the case appears to be, even being enhanced in certain ways). Being optimistic, we will adhere to the latter. Recall that, as discussed in the introduction, it is known that discord can be used to locally activate distillable entanglement between the discordant system and an ancilla [33, 34, 73]. Our results therefore indicate that while thermal fluctuations are indeed detrimental to entanglement directly, it may be that they can actually greatly improve its rate of production in an indirect manner.

Before continuing to our discussion, we should briefly relate our scenario and results with that of [136]. The authors of that paper used a master equation approach and also discovered that the discord between detectors can increase with the temperature of a common environment. However, there is a key difference between their scenario and ours. That is, in [136] they considered their detectors to be *directly* coupled to each other in addition to being coupled to a common bath. This is unlike in our scenario, where each detector is only interacting locally with the field. In particular, their study can not be considered an example of harvesting. Interestingly, in their case they discovered that the

discord increased monotonically with temperature, asymptoting to a finite value. This is unlike our finding, as in Fig. 8.5, in which the discord eventually starts to decrease for high enough temperatures. This difference may exactly be due to the additional direct coupling considered in the other paper.

## 8.3 Explanations

In this section we wish to give some further physical and mathematical insight into the surprising results presented above. We do this by first giving a brief discussion of the spatial correlation function of the field and point out that its form is in fact completely consistent with the result of thermal amplification of extracted correlations. We also give some speculation on how our results may also be understood in terms of system-environment entanglement. We then go on to give a large discussion on how this behavior can be understood in terms of the translational invariance of the periodically-identified cavity field. Not only will this allow us to readily predict for what choices of parameters the thermal amplification will be strongest and weakest, it will also reveal an interesting new perspective on the procedure of correlation harvesting in general that we feel is worthy of consideration in its own right. We briefly point out that with this new perspective we can also immediately explain the result of entanglement degradation, as seen in Fig. (8.2), via the known entangling properties of passive Gaussian transformations.

### 8.3.1 Correlation function

It is commonly said that thermal states contain no correlations, or at least the amount of correlations present decreases with temperature. This is a rather vague statement, however, and depending on what exactly one means it can be demonstrably false. The statement that a thermal state contains *no* correlations is simply in reference to the different energy modes, which of course are in a product state with respect to each other (as they are also in the vacuum). This does not say anything about spatial correlations however, which are what we are interested in here. While it is certainly true that the entanglement between spatially separated regions decays with temperature [131, 132], this does not imply that the same is true for correlations in general.

Our detectors are placed at positions  $x_1$  and  $x_2$  in the cavity. These detectors become correlated due to the fact that the field fluctuations (both quantum and classical) at these two points are correlated. That is, the detectors are “measuring” the field at these points.



A standard way of determining the degree to which the measurement statistics of two quantum observables  $\hat{A}$  and  $\hat{B}$  on separate Hilbert spaces are correlated given some joint state is to compute the correlation function  $C(\hat{A}, \hat{B}) \equiv \langle \hat{A}\hat{B} \rangle - \langle \hat{A} \rangle \langle \hat{B} \rangle$ , where the expectation value is taken with respect to whatever state the joint system is in. To clarify, in this definition we are using the simplified notation  $\hat{A}\hat{B} = \hat{A} \otimes \hat{B}$ ,  $\hat{A} = \hat{A} \otimes \hat{I}$  and  $\hat{B} = \hat{I} \otimes \hat{B}$ .

If we wish to ask how much the field  $\hat{\phi}$  is correlated at points  $x_1$  and  $x_2$ , the simplest measure to compute is the correlation function:  $C(x_1, x_2) \equiv C(\hat{\phi}(x_1), \hat{\phi}(x_2)) = \langle \hat{\phi}(x_1)\hat{\phi}(x_2) \rangle - \langle \hat{\phi}(x_1) \rangle \langle \hat{\phi}(x_2) \rangle$ . Of course, in both the vacuum and any thermal state the first moment of the field will vanish (i.e. the Wigner function has zero mean). The correlation function thus takes the form of the equal-time Wightman function [39], which due to the translational invariance of the field will only depend on the distance  $r = |x_2 - x_1|$ :

$$C(r) \equiv C(x_1, x_2) = \langle \hat{\phi}(x_1)\hat{\phi}(x_2) \rangle. \quad (8.7)$$

Note that the condition  $C(r) = 0$  does *not* necessarily imply the lack of any correlations, however the condition  $C(r) > 0$  *does* imply the existence of correlations.

We now ask the question of how this quantity changes with field temperature. The answer is that it indeed grows with temperature in qualitative agreement with our results. For example it is known that in free space and in three spatial dimensions the equal-time Wightman function of a massless scalar field in a thermal state of temperature  $T$  is [137]

$$C_{\text{free}}(r) = \frac{T}{4\pi r} \coth(\pi T r). \quad (8.8)$$

This correlation function grows monotonically with  $T$ , and indeed linearly so for large  $T$ . Of course this is not the correct correlation function in our situation of a cavity field (periodically identified) in one spatial dimension. For us, the correct function is straightforwardly shown to be given by

$$C(r) = \frac{1}{L} \sum_{n>0} \frac{\nu_n}{\omega_n} \cos(\omega_n r), \quad (8.9)$$

where the sum is only over positive  $n$  and the values  $\nu_n$  are the symplectic eigenvalues of the thermal state as given by Eq. (8.3). The magnitude of this function also grows monotonically with temperature, and thus from this perspective it is not at all surprising that the correlations transferred to the detectors (corresponding to the correlated measurement statistics of the field) should grow with temperature. Nevertheless this does not give any real explanation as to why the discord experiences such a growth, as in the high temperature regime the correlation function has a purely classical limit. While we indeed see a

larger (and sustained) increase in mutual information, as expected, it is still surprising that we receive such a strong amplification of discord even up to quite large temperatures.

The function in Eq. (8.9) actually gives excellent predictions for how the harvested correlations that we compute directly behave with the distance between detectors. For example we note that for the cavity length of  $L = 100$  that was used in our results the magnitude of  $C(r)$  for high temperatures reaches a minimum (a zero in fact) at a distance of approximately  $r \approx 21$ . This minimum can be directly seen as a minimum in the extracted correlation when plotted as a function  $r$ ; see Appendix. C. For larger  $r$  beyond this the harvest *increases* until hitting a local maximum at  $L/2 = 50$  (as predicted by Eq. (8.9)). From here any further increase in distance actually corresponds to a decrease in distance, due to the periodicity of the cavity. We note that generally the phenomenon of thermal amplification appears to occur independent of the distance between the detectors, in the sense of a greatly increased discord harvest as compared to the vacuum state value.

### 8.3.2 Relation to system-environment entanglement

Here we wish to give a more physically insightful interpretation of our results by pointing out the possible connection between thermal amplification and the results presented in the papers [76, 68] and [9] (also given in Sect. 2.3), regarding the link between discord within a system and the entanglement between that system and its purifying environment.

In [76] and Sect. 2.3 it was demonstrated that the discord present in a general bipartite state is deeply related to the entanglement structure in the system's purification. In particular, the discord typically grows with the entanglement between the system and its purifying ancilla, and furthermore the presence of discord requires the presence of both bipartite and genuine tripartite entanglement in the purification. In [68] the authors considered a coupled, pure  $N$ -qubit system and then studied a 2-qubit subsystem from this ensemble. They observed that the discord between these two qubits is completely monotonic with the entanglement entropy between them and the other  $N - 2$  qubits; this is to be expected from the other two studies. The authors of [68] also discovered that there is an inverse relation between the 2-qubit entanglement (using the concurrence) and the 2-qubit discord, and furthermore [138] the former decreases while the latter increases upon increasing the total number of qubits  $N$  (i.e. enlarging the environment).

This last result sounds very similar to the findings presented here, and propose that both can be understood in terms of the system-environment entanglement. In the system of [68], we conjecture that the increase of  $N$  results in an increased system-environment entanglement which, despite the increased level of decohering noise, boosts the discord in

the system. Similarly in our situation, increasing the temperature of the field results in detectors that are more mixed and are thus more entangled with the environment <sup>1</sup>. This translates into an increased amount of discord between the detectors.

As a final word on this, we suggest that the evolution of discord in such systems can be understood as a competition between the decohering effect of the environment and the system-environment entanglement that such decoherence also tends to create. As we have seen, oftentimes the latter can win the day. The entanglement within the system, on the other hand, is not bolstered by the system-environment entanglement. Indeed it will generally be further impaired due to monogamy, and will therefore be far more easily destroyed.

### 8.3.3 Translational invariance

In this section we will attempt to give some further mathematical intuition towards the behavior discussed in Sect. 8.2 by exploiting the translational invariance of the field. In doing so we will uncover a new and interesting perspective on correlation harvesting that we feel is worthy of consideration in its own right. We will also be able to accurately predict for what choices of parameters the thermal amplification phenomenon is strongest, and for which it is weakest.

First let us note that although we use the translational invariance of the field as a convenient means of explanation, this does not imply that translational invariance is necessary for thermal amplification to occur. Indeed it is not, and we have also observed the same effect using a cavity field with mirror boundary conditions instead of periodic.

To begin our argument, we will make a simple observation. This is that the mutual information harvested by the detectors appears to be extremely monotonic with the *difference*  $|\nu_1 - \nu_2|$  of the symplectic eigenvalues of the detector-detector subsystem, given by the covariance matrix  $\sigma^{(d)}$  in Eq. (3.7). For example we can plot  $|\nu_1 - \nu_2|$  as a function of time of evolution and compare with the extracted mutual information. This is plotted in Fig. (8.6), where the field is initially in the vacuum state and all parameters are equivalent to those used in Fig. (8.4). We see that in comparison to the correlation measures plotted in Fig. (8.4-a), the qualitative behaviors are identical. For large temperatures the mutual

---

<sup>1</sup>In order to use the findings of [76, 9] in our argument we must consider an environment that is initially pure. The field is of course not pure when it is thermal. However, we can always consider the field plus its purifying ancilla, and the entanglement between the detectors and this larger environment is quantified simply by the two-detector entropy.

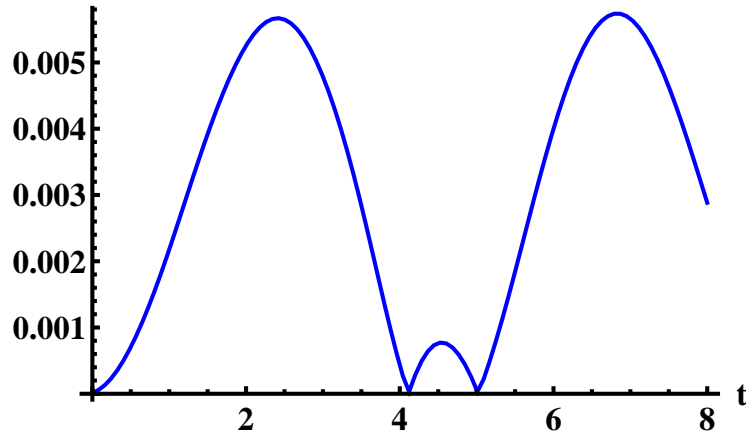


Figure 8.6: The difference  $|\nu_1 - \nu_2|$  of the symplectic eigenvalues of the detector-detector system as a function of time. The field was initially in its vacuum state and the detectors were placed a distance  $r = 4$  away from each other. These are the same parameters that were used to plot the mutual information and discord in Fig. (8.4-a), and we note that the qualitative behavior in that figure is exactly the same as we see here.

information continues to evolve monotonically with  $|\nu_1 - \nu_2|$ , however this becomes no longer true for discord.

Given this knowledge, we should wonder how  $|\nu_1 - \nu_2|$  changes with field temperature. Clearly if the field is initially in a high temperature state we should expect the response of the detectors to be more energetic and for them to become more mixed through their evolution. The symplectic eigenvalues of  $\sigma^{(d)}$  should therefore increase with larger temperature. This is indeed what occurs, as can be seen in Fig. (8.7) where we plot both  $\nu_1$  and  $\nu_2$  as a function of temperature  $T$ . However, we also observe that one increases faster than the other, meaning that their difference also grows with  $T$ . This is therefore consistent with the increase of mutual information  $I$  with  $T$ . Clearly, as can be seen in Fig. (8.5), the discord is no longer monotonic for high enough excitation.

The explanation of our results now requires two tasks: first, to explain why the mutual information and (for small temperatures) the discord are monotonic with  $|\nu_1 - \nu_2|$  and, second, to explain why this difference grows with  $T$ . We will attempt to perform both of these. We will focus on the latter of these to begin, and later give some insight into the former. Being tasked with explaining the behavior seen in Fig. (8.7), we will take this as an excuse to introduce an interesting new perspective on the evolution of our system that results from the translational invariance of the field. By this approach we are also

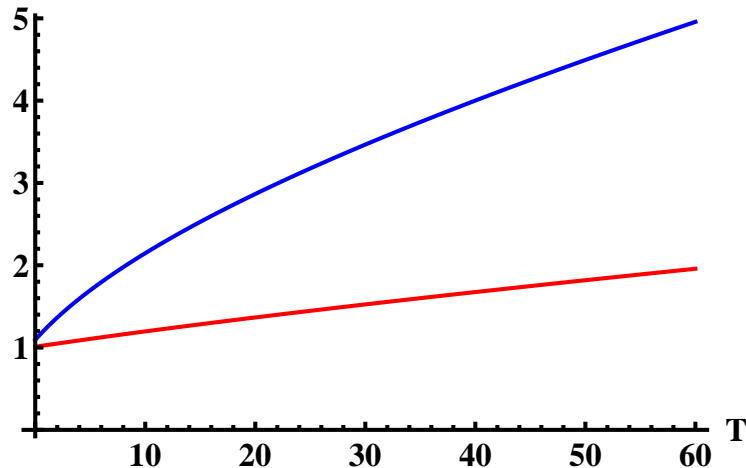


Figure 8.7: The two symplectic eigenvalues  $\nu_1$  and  $\nu_2$  of the detector-detector system as a function of initial field temperature  $T$ . The detectors were placed a distance  $r = 4$  away from each other and left to evolve for a time  $t = 2$ . We see that the difference  $|\nu_1 - \nu_2|$  grows with temperature.

very easily, and in a unique manner, able to explain the decay of entanglement seen in Fig. (8.2).

An immediate result of the translational invariance of the field is that both of the detectors will individually feel the exact same response. The detector-detector state is therefore invariant under exchange  $1 \leftrightarrow 2$  of the detectors. This implies both that the reduced states of each detector are equivalent  $\sigma_1 = \sigma_2$  (we will therefore refer to both as  $\sigma_1$  henceforth) and that the off-diagonal correlation matrix is symmetric:  $\gamma_{12} = \gamma_{12}^T$ . The covariance matrix of the detectors is therefore of the form

$$\sigma^{(d)} = \begin{pmatrix} \sigma_1 & \gamma_{12} \\ \gamma_{12} & \sigma_1 \end{pmatrix}. \quad (8.10)$$

This is an example of what is called a symmetric Gaussian state [45]. From this, it is easily seen that there is a simple symplectic transformation that transforms  $\sigma^{(d)}$  to a product state, void of any correlation. Of course this is true of any Gaussian state, but in general the correct transformation would depend on the details of the state and, in such a scenario as we have here, would depend on time  $t$  and on the chosen parameters. Here, the symmetric form of  $\sigma^{(d)}$  means that this is not the case, and there is a transformation that will *always* do the job irrespective of time or parameters. We will call this symplectic transformation

$\tilde{\mathbf{S}}$ , and it takes the form

$$\tilde{\mathbf{S}} = \tilde{\mathbf{S}}^T = \tilde{\mathbf{S}}^{-1} = \frac{1}{\sqrt{2}} \begin{pmatrix} -\mathbf{I}_2 & \mathbf{I}_2 \\ \mathbf{I}_2 & \mathbf{I}_2 \end{pmatrix}, \quad (8.11)$$

where  $\mathbf{I}_2$  is the  $2 \times 2$  identity matrix. When applied to the detector-detector state we indeed find that this transformation returns a product state:

$$\tilde{\mathbf{S}} \boldsymbol{\sigma}^{(d)} \tilde{\mathbf{S}}^T = \begin{pmatrix} \boldsymbol{\sigma}_- & \mathbf{0}_2 \\ \mathbf{0}_2 & \boldsymbol{\sigma}_+ \end{pmatrix}, \quad (8.12)$$

where the single-mode covariance matrices  $\boldsymbol{\sigma}_\pm$  are given by

$$\boldsymbol{\sigma}_\pm = \boldsymbol{\sigma}_1 \pm \boldsymbol{\gamma}_{12}. \quad (8.13)$$

We wish again to emphasize that as long as the detectors are initialized in the same states (their ground states in our case) then this single transformation will *always* bring our two-detector state to one devoid of correlations, independent of the time of interaction or the distance between them or any other parameters of our system.

Before continuing we wish to point out, as it will be useful later, that the transformation  $\tilde{\mathbf{S}}$  is passive, due to its orthogonality (recall the discussion of active and passive symplectic transformations given in Ch. 3). Specifically,  $\tilde{\mathbf{S}}$  is a 50 : 50 beam splitter [45, 139], an operation that is easily implemented in laboratory settings. The fact that the transformation takes this form will be useful in gaining insights towards the extractable entanglement, and we will discuss this shortly.

First, we wish to point out that while Eq. (8.12) is easily seen by the detector-exchange symmetry, this result can also be viewed in what is perhaps a more enlightening manner. Recall that the interaction Hamiltonian between the detectors and field, Eq. (5.40), is given in our current scenario by

$$\hat{H}_{\text{int}} = \sqrt{2}\lambda \left[ \hat{q}_{d1} \hat{\phi}(x_1) + \hat{q}_{d2} \hat{\phi}(x_2) \right], \quad (8.14)$$

where  $\hat{q}_{d1}$  and  $\hat{q}_{d2}$  are the position quadrature operators of the two detectors. This represents a local coupling between detector-1 and  $\hat{\phi}(x_1)$ , and between detector-2 and  $\hat{\phi}(x_2)$ . Of course because the observables  $\hat{\phi}(x_1)$  and  $\hat{\phi}(x_2)$  are correlated, as witnessed by the non-vanishing correlation function  $C(x_1, x_2) \neq 0$ , the two detectors are able to become correlated despite their individual interactions being local.

On the other hand, we can consider the system under the transformation  $\tilde{\mathbf{S}}$ , which when applied to the detector-detector phase space results in

$$\tilde{\mathbf{S}} \begin{pmatrix} \hat{q}_{d1} \\ \hat{p}_{d1} \\ \hat{q}_{d2} \\ \hat{p}_{d2} \end{pmatrix} = \begin{pmatrix} \hat{q}_- \\ \hat{p}_- \\ \hat{q}_+ \\ \hat{p}_+ \end{pmatrix}, \quad (8.15)$$

where the new set of quadrature operators are given by

$$\hat{q}_\pm = \frac{1}{\sqrt{2}}(\hat{q}_{d2} \pm \hat{q}_{d1}), \quad \hat{p}_\pm = \frac{1}{\sqrt{2}}(\hat{p}_{d2} \pm \hat{p}_{d1}). \quad (8.16)$$

We will refer to the corresponding modes as the (+)- and (-)-modes. It is with respect to these quadratures that the covariance matrices  $\boldsymbol{\sigma}_\pm$  are defined via Eq. (3.5). If we now express the interaction Hamiltonian in this new basis, we see immediately that it is

$$\hat{H}_{\text{int}} = \sqrt{2}\lambda \left[ \hat{q}_+ \hat{\phi}_+ + \hat{q}_- \hat{\phi}_- \right], \quad (8.17)$$

where

$$\hat{\phi}_\pm = \frac{1}{\sqrt{2}}(\hat{\phi}(x_1) \pm \hat{\phi}(x_2)). \quad (8.18)$$

Again, this represents a pair of local interaction between the (+)-mode with  $\hat{\phi}_+$ , and between the (-)-mode with  $\hat{\phi}_-$ . However, unlike between  $\hat{\phi}(x_1)$  and  $\hat{\phi}(x_2)$ , the measurement statistics of the observables  $\hat{\phi}_+$  and  $\hat{\phi}_-$  are completely uncorrelated in the vacuum and in thermal states. This can be seen as a direct consequence of translational invariance: for any pair of observables  $\hat{A}$  and  $\hat{B}$  that satisfy the  $1 \leftrightarrow 2$  exchange symmetry, it is trivially seen that  $C(\hat{A}_+, \hat{B}_-) = 0$ , where  $\hat{A}_+ = \hat{A}(x_1) + \hat{A}(x_2)$  and  $\hat{B}_- = \hat{B}(x_1) - \hat{B}(x_2)$ . This includes of course  $C(\hat{\phi}_+, \hat{\phi}_-) = 0$ . Thus the ( $\pm$ )-modes necessarily can never become correlated through the evolution, and are entirely dynamically decoupled, as we have seen. If they are initialized in a correlated state then the mutual information between them can never increase above its initial value (we have confirmed this by direct computation).

What we have found is that the process of correlation extraction (including entanglement) can be fully described by two dynamically decoupled interactions (each between a field and a *single* detector), followed by the beam splitter operation Eq. (8.11). We are thus able to gain a lot of insight by examining the form of these independent interactions along with the correlating capacity of the beam splitter operation. To proceed, let us first

examine the interactions that  $\hat{q}_+$  and  $\hat{q}_-$  experience. They are coupled to the operators  $\hat{\phi}_+$  and  $\hat{\phi}_-$ , respectively, which both take the standard form of a mode-decomposed field:

$$\hat{\phi}_{\pm} = \sum_n \frac{1}{\sqrt{4\pi|n|}} (v_n^{(\pm)} \hat{a}_n + v_n^{(\pm)*} \hat{a}_n^\dagger), \quad (8.19)$$

where  $\hat{a}_n$  and  $\hat{a}_n^\dagger$  are the same, standard ladder operators corresponding to plane-wave field modes (we are not performing a Bogoliubov transformation) and the “mode functions” are  $v_n^{(\pm)} = (\exp(ik_n x_2) \pm \exp(ik_n x_1))/\sqrt{2}$ , or equivalently:

$$v_n^{(+)} = \sqrt{2} \cos\left(\frac{k_n}{2}(x_2 - x_1)\right) e^{ik_n(x_2+x_1)/2}, \quad (8.20)$$

$$v_n^{(-)} = \sqrt{2}i \sin\left(\frac{k_n}{2}(x_2 - x_1)\right) e^{ik_n(x_2+x_1)/2}. \quad (8.21)$$

Thus, the interactions that the  $(\pm)$ -modes individually experience can be considered as a standard monopole-monopole coupling to a regular field, except that the effective coupling strengths are frequency- and position-dependent (via the cos and sin in the above equations). These interactions will then determine the evolution of the  $(\pm)$ -modes, and their states as a function of time will be represented by the covariance matrices  $\sigma_{\pm}$ .

This realization can in fact be used to understand the growth of  $|\nu_1 - \nu_2|$  seen in Fig. (8.7), and therefore indirectly the thermal amplification behavior. Furthermore, by examining  $v_n^{(\pm)}$  we are accurately able to predict for which parameter choices thermal amplification will be strongest, and for which it will be weakest. To see this, recall that the symplectic eigenvalues of a Gaussian state are symplectically invariant. It therefore follows that the symplectic eigenvalues  $\nu_+$  and  $\nu_-$  of the states  $\sigma_+$  and  $\sigma_-$  are identified with the original symplectic eigenvalues  $\nu_1$  and  $\nu_2$  of the detector-detector system. The differences are therefore also equivalent:  $|\nu_1 - \nu_2| = |\nu_+ - \nu_-|$ . Fortunately, the qualitative behavior of  $|\nu_+ - \nu_-|$  is easily predicted by the forms of  $v_n^{(\pm)}$  given above. Clearly, if the field state is thermal then we expect the mixedness of the  $(\pm)$ -modes, and thus both  $\nu_+$  and  $\nu_-$ , to increase with temperature  $T$ . However, we should also generally expect to find a difference between the two, and this is due to the difference in the magnitudes of  $\cos(k_n r/2)$  and  $\sin(k_n r/2)$  that appear in the effective coupling strengths. The mode that is coupled more strongly to the field will feel a stronger response, and will be affected more by an increase in temperature, than will the more weakly coupled mode.

For example let us consider the window in time  $t$  and distance  $r$  that we have examined in the above figures. This is well outside the regime at which a single-mode approximation



would be valid; we would need to go to much larger values of  $t$ . Therefore, roughly speaking, both of the  $(\pm)$ -modes couple equally to a wide range of modes, not taking account of the cos and sin factors. Taking these into account, however, the region of relatively small  $r$  that we have examined means that the magnitude of  $\sin(k_n r/2)$  is quite small for the many modes of small frequency  $k_n$  that are relevant in the evolution. For the same reason,  $\cos(k_n r/2)$  for these modes is quite close to unity. We thus find a significant difference in the values of  $\nu_+$  and  $\nu_-$ , with typically  $\nu_+ > \nu_-$  for the reasons just stated. If the field is hot, this difference in effective coupling is seen more clearly and thus the thermal amplification of correlations follows. Note that for small  $t$  and large  $r$  the contribution to the  $+$  and  $-$  should become roughly equivalent, and thus we expect the strength of thermal amplification to generally fall off with distance. If we allow ourselves to look at larger values of  $t$  it turns out that with this framework we are able to accurately predict for which values of  $r$  the thermal amplification is strongest, and for which it is weakest. So as not to get too off-track, we present this in Appendix. C.

Given that we now understand why the difference  $|\nu_1 - \nu_2| = |\nu_+ - \nu_-|$  grows with field temperature, we are left with the task of understanding better why the mutual information  $I$ , and to a lesser extent the Gaussian discord  $D$ , are monotonic with this difference. Fortunately we can use the framework just presented to gain some insight on the matter. The behavior of correlations present in  $\sigma^{(d)}$  of course stem from the correlating properties of the 50 : 50 beam splitter  $\tilde{\mathbf{S}}$ . For example we can use this fact, along with the well-known entangling properties of beam splitters, to easily explain the entanglement degradation with temperature; this is explained further in the following section. Aside from entanglement, however, there appears to be fairly little information in the literature on the beam splitter's ability to generate mutual information and discord in Gaussian states.

Notice that by inverting Eq. (8.13) we obtain

$$\sigma_1 = \sigma_2 = \frac{1}{2}(\sigma_+ + \sigma_-), \quad \gamma_{12} = \frac{1}{2}(\sigma_+ - \sigma_-). \quad (8.22)$$

Clearly if the states of the  $(\pm)$ -modes are the same,  $\sigma_+ = \sigma_-$ , then the difference in symplectic eigenvalues is zero and the detector-detector state is completely uncorrelated since  $\gamma_{12} = \mathbf{0}$ . That is,  $\tilde{\mathbf{S}}$  takes an uncorrelated pair of identical Gaussian states and outputs exactly the same thing. On the other hand, the larger the difference between  $\sigma_+$  and  $\sigma_-$ , the larger the correlation matrix  $\gamma_{12}$  will be. Of course an increase in this difference does not necessarily correspond to an increase in  $|\nu_+ - \nu_-|$ . However, in our particular scenario the forms that we obtain for  $\sigma_+$  and  $\sigma_-$  tend to be approximately thermal,  $\sigma_{\pm} \approx \text{diag}(\nu_{\pm}, \nu_{\pm})$ , at least for relatively small temperatures of the field. For exactly thermal states, one has exactly  $\gamma_{12} = \text{diag}(\nu_+ - \nu_-, \nu_+ - \nu_-)/2$ , and thus in this

case the magnitude of the correlation matrix does directly correspond with the magnitude  $|\nu_+ - \nu_-| = |\nu_1 - \nu_2|$ . This provides the qualitative explanation that we were searching for.

Of course the mutual information and discord do not depend purely on  $\gamma_{12}$ , and they will both decrease as the overall mixedness of the system is increased. In fact, if we continue with the above approximation of the states  $\sigma_{\pm}$  both being exactly thermal, one finds that both  $I$  and  $D$  are monotonically increasing with  $|\nu_+ - \nu_-|$ , but also monotonically decreasing with  $\nu_+ + \nu_-$ . The extraction of correlations therefore represents a competition between these two quantities. For the Gaussian discord it is seen that the sum  $\nu_+ + \nu_-$  plays a stronger role than in the mutual information. The discord is thus more sensitive to noise (as we have observed) but for small enough field temperatures  $T$  (yet still very large) this sensitivity is not enough to overcome the increase in  $|\nu_+ - \nu_-|$  achieved by increasing  $T$ .

We can display this in a more quantitative manner by plotting  $I$  as a function of the symplectic eigenvalues. Given Eq. (8.22), we see that the mutual information, Eq. (8.6) takes the form

$$I = 2f\left(\frac{1}{2}\sqrt{\det(\sigma_+ + \sigma_-)}\right) - f(\nu_+) - f(\nu_-), \quad (8.23)$$

where  $f$  is the function given by Eq. (3.25). In the case that  $\sigma_{\pm}$  are exactly thermal, and taking into account the identification of  $\{\nu_+, \nu_-\}$  with  $\{\nu_1, \nu_2\}$ , this simplifies to

$$I = 2f\left(\frac{1}{2}(\nu_1 + \nu_2)\right) - f(\nu_1) - f(\nu_2). \quad (8.24)$$

We plot this in Fig. 8.8. We see clearly in this figure the increase in  $I$  as the difference  $|\nu_+ - \nu_-|$  increases. The corresponding plot for Gaussian discord looks nearly identical to this, except that the functional decrease with  $\nu_1 + \nu_2$  is more dominant over the increase with  $|\nu_1 - \nu_2|$ .

### 8.3.4 Entanglement degradation

It is worth noting that with the framework presented above we can immediately explain the degradation of extracted entanglement with temperature, as seen in Fig. (8.2), via the known entangling properties of passive operations, which the 50 : 50 beam splitter represented by  $\tilde{\mathbf{S}}$  is an example of. This transformation happens to be its own inverse, and thus applying it to the product state  $\sigma_- \oplus \sigma_+$  returns back the detector-detector state,  $\sigma^{(d)}$ . It is known that for passive operations to create entanglement the original state

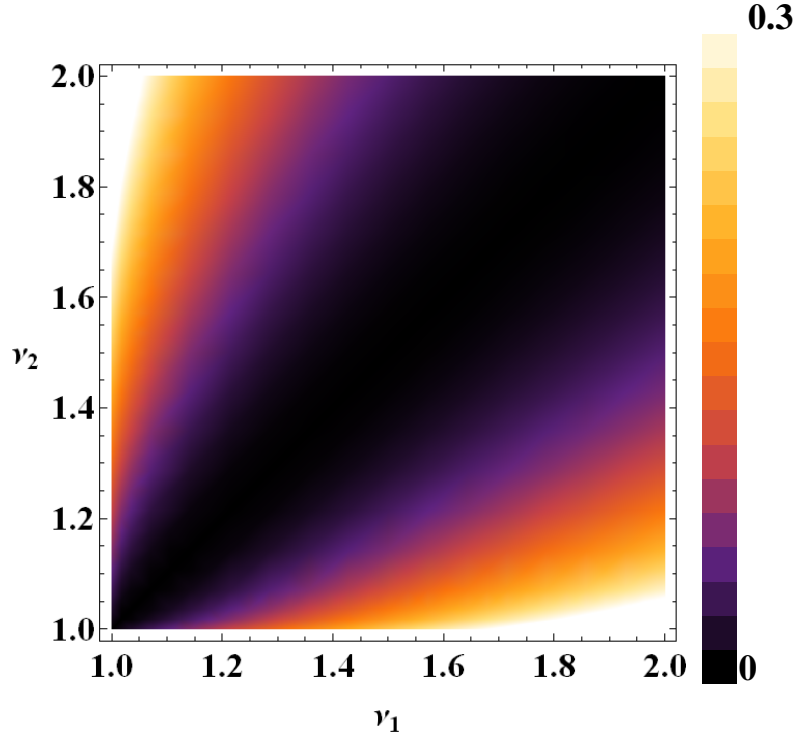


Figure 8.8: The mutual information, Eq. (8.24), as a function of  $\nu_1$  and  $\nu_2$ . We see clearly the increase with  $|\nu_1 - \nu_2|$ .

must be “nonclassical”, [139]. What this actually means generically and quantitatively is that an entangling passive operation exists iff the two smallest eigenvalues  $\lambda_1$  and  $\lambda_2$  (*not* the symplectic eigenvalues) of the original covariance matrix satisfy  $\lambda_1\lambda_2 < 1$  [140], and furthermore this product is used to provide a maximal amount of entanglement that can be achieved. Thus, if we can understand from the evolution of the ( $\pm$ )-modes how the eigenvalues of  $\sigma_- \oplus \sigma_+$  change with field temperature, then we are able to garner information on the entanglement that can be present in the state  $\sigma^{(d)}$ .

Due to  $\sigma_- \oplus \sigma_+$  being a product state, the eigenvalues of this matrix will just be the combination of the eigenvalues of the two individual ( $\pm$ )-modes. These are generically of the form  $\nu_-e^{r_-}$ ,  $\nu_-e^{-r_-}$ ,  $\nu_+e^{r_+}$ , and  $\nu_+e^{-r_+}$ . Here  $\nu_-$  and  $\nu_+$  are the symplectic eigenvalues presented above, and the values  $r_-$  and  $r_+$  are the single-mode squeezing parameters for each of the two modes [45]. Note that with large enough squeezing it becomes very easy to entangle via passive operations because the two smallest eigenvalues will be  $\nu_-e^{-r_-}$  and  $\nu_+e^{-r_+}$ , and they will become very small as  $r_+$  and  $r_-$  become large. In our scenario the

evolution does provide some amount of squeezing (it must, in order to get any entanglement at all). However, the symplectic eigenvalues  $\nu_{\pm}$  are what generically increase when the field temperature is increased (being directly related to the mixedness of the modes) and thus as this occurs the values of  $\nu_{\pm}$  will quickly overtake the squeezing such that the two smallest eigenvalues no longer satisfy  $\lambda_1\lambda_2 < 1$ . Once this inequality is broken, it is no longer possible to obtain any entanglement in  $\sigma^{(d)}$ .

It is interesting to note, however, that for the case of a product state (as we have) in which one of the modes is thermal (as we approximately have) then the *maximally* entangling passive operation is in fact a 50 : 50 beam splitter [140]. In a way then, the field is actually doing the best it possibly can to entangle the detectors. Unfortunately, despite this great effort, thermal fluctuations quickly win the day.

## 8.4 Discussion

We have used the non-perturbative, oscillator-detector formalism presented in Ch. 5 to exactly solve for the local harvesting of classical and quantum correlations (entanglement, Gaussian discord, and mutual information) from a periodic cavity field. We have furthermore explored the effect that thermal fluctuations in the field will have on the harvesting of these correlations. As expected, the harvested entanglement rapidly decays with the field temperature. Surprisingly, however, both the mutual information as well as the Gaussian discord (a measure of purely quantum correlations) can be greatly *increased* by heating up the cavity. Indeed, an improvement of multiple orders of magnitude is possible in this regard.

Although initially surprising, we go on to discuss that this result can be physically understood in several different ways. We have included an explanation of thermal amplification in terms of the field correlation function, as well as speculated on its possible relation to system-environment entanglement. Our primary explanation of the phenomenon relies on the translational invariance inherent in the periodic field. By this we are able to explain both the results of thermal degradation of entanglement as well as the thermal amplification of mutual information and discord purely in terms of the correlating capability of the 50 : 50 beam splitting operation. We can furthermore use this to accurately predict for what system parameters thermal amplification will be weakest, and for which it will be strongest, as seen in Appendix. C. We feel that, independent of its explanatory power that has been demonstrated here, the new perspective that we present on correlation extraction is interesting and worthy of consideration in its own right. This is because in general the evolution of a single detector with a field is much more easily understood intuitively than

is the collective behavior of two detectors. The ability to decompose our two-detector scenario into two dynamically decoupled, single-detector systems represents a tool for gaining intuition into harvesting and similar phenomena.

We note that the phenomenon of thermal amplification does not require translational invariance in order to occur. Indeed, we have also observed thermal amplification using a cavity field with Dirichlet boundary conditions, as would be the case in an actual optical cavity. In fact, we propose that thermal amplification may be a rather general phenomenon that can occur in a variety of quantum many body systems (for example other physical realizations of a collection of harmonic oscillators). The particular scenario that we have considered here may be just one instance of a much broader phenomenon.

The thermal amplification of discord appears to imply the possibility of locally generating what is an appreciable amount of quantum correlations. This is exciting both from the experimental perspective as well as, perhaps, practical discord-based quantum computation. For example, it is known that discord allows the local activation of entanglement with an ancilla system [33, 34, 73]. Interestingly then, even though thermal fluctuations are directly detrimental to entanglement, they may nevertheless be used as an indirect tool for its generation. This may moreover prove useful due to the fact that many of the significant technological hurdles facing quantum computation stem from the necessity to keep one’s system very cold. Our results suggest that in a specific scenario one may need not worry about thermal noise in their system, and indeed may even welcome it. Assuming that we are able to fully understand thermal amplification more generally (in all its possible physical realizations) and how to properly utilize the resources that it produces, this may very well give way to a type of “noise-assisted quantum computation”.

# Chapter 9

## Entanglement farming

Note: this chapter derives from the work [5], in collaboration with Eduardo Martín-Martínez, William Donnelly, and Achim Kempf.

We have discussed at length in this thesis the phenomenon of entanglement harvesting. This is of course interesting from a theoretical point of view, but one may also wonder about its practical application. Entanglement is understood as an important resource that provides the quantum advantage over classical computation that quantum information and computation has long promised. Studying the generation, transfer, and distribution of entanglement is therefore of extreme importance in this regard. The process of entanglement harvesting, as we have seen it, is unfortunately unlikely to be useful in practice. This is largely due to the fact that the amount of extracted entanglement is typically minute, resulting from the typically small coupling strengths between system and field.

Of course, while perhaps less theoretically interesting, one can also consider the case in which the detectors interact with the field long enough that they come into causal contact with one another (i.e. they are not entirely spacelike separated). In addition to becoming entangled by swapping spatial entanglement from the field, in this case they can also become entangled through the quantum communication mediated by real quanta in the field. The necessary energy for the existence of these quanta can come from two sources. Namely, the switching on of their interaction will make van der Waals-Casimir-Polder energy available [141, 142]. Also, and generally more dominantly, the process of switching on and off the interaction breaks the time-translation invariance of the Hamiltonian, which via Noether's theorem can provide energy to the system by parametric forcing. Unsurprisingly, one generally finds more entanglement generation between detectors in this regime (e.g. as seen in Fig. 8.1), but still not necessarily enough to make it practically useful. In

this chapter we will examine a scenario within this regime with which we find a method of continuously and (to a large degree) sustainably generating entanglement between pairs of detectors, which when taken as a total provides a very large amount.

As in previous chapters, we will consider two detectors initially in their unentangled ground states that interact for a brief time with a cavity field at fixed points in space. This can be taken to be a model of what happens to two atoms transversely traversing the cavity, in a matter similar to the experiments described in [143]. Here, however, we will consider a large number of pairs of detectors. Each pair interacts with the field for a given time and then exits the cavity, either having become entangled or not. A new, fresh pair of detectors is then made to do the same thing, where they interact with the *same* cavity field as the previous pair. Each pair has an effect on the field during their evolution cycle, and this will in turn affect how the field impacts the following pair. The periodic entering and exiting of the detectors will parametrically drive the cavity modes. In the long term (i.e., when continuing to send a large number of pairs of detectors through the cavity) will this excite and possibly heat up the cavity? Fresh detectors always arrive in their ground state, however. Does this lead to a cooling of the cavity? What is the impact of entanglement monogamy on continued entanglement extraction? In the long term, will the cavity modes be driven towards or away from a thermal state? Will the cavity modes be driven towards a stable or at least a metastable state? Finally, is the harvesting of entanglement by successive pairs of detectors pairs sustainable, i.e., do we have merely temporary harvesting of some total (perhaps small) amount of entanglement, or do we obtain a sustainable process from which we can gain large amounts of entanglement? We will answer these question in this chapter. In particular, we indeed find that we obtain an efficient and sustainable process by which to generate entanglement utilizing a single cavity field. We will refer to this process as *entanglement farming*.

We will continue to utilize the computational framework as in the previous chapters; namely that of Ch. 5. The work in this chapter actually represent an excellent example of the power of the oscillator-detector formalism. Not only are the calculations in this chapter near-trivial using this tool, but the scenario and the effects observed are very much non-perturbative in nature, and so could *not* be studied using the standard Unruh-DeWitt approach. Using our Gaussian approach we find that the dynamics of the detectors plus field system can be expressed as a linear dynamical system, allowing us to study the system's dynamics for arbitrarily long times, i.e., for a large number of detector pairs passing through the cavity.

Our results will show that keeping the interaction of the detectors in the cavity short enough to be spacelike separated is not efficient: it is not sustainable to extract entanglement over many cycles and the total amount that can be extracted is small. As one might

expect, allowing the interaction of the detectors in the cavity to be long enough to become non-spacelike (i.e., allowing the detectors to interact via the cavity field) makes the detectors' entanglement harvesting more efficient. What is surprising is the magnitude of the amount of entanglement that can be harvested by repeated detector insertions. Namely, we will first find that over repeated cycles of detector pair insertions, a cavity field that is initially in the vacuum state is driven towards a metastable, highly non-thermal state. Even a cavity field that is initially in a thermal state, from which no entanglement can be harvested, is driven towards that metastable state.

Second, we will find that this metastable state allows each new pair of detectors to become entangled. Therefore, by repeating this protocol, one would obtain a stream of significantly but not maximally entangled detectors, whose entanglement could then, for example, be distilled into maximally entangled EPR pairs. The metastable state is very long-lived under repeated entanglement harvesting by detector pairs, although this state eventually does turn into a non-entangling state. This happens when higher, off-resonant modes start to become significantly excited, and hence it is beyond the single-mode approximation. In practice, if the excitations of those higher modes slightly leak from the cavity, fully sustainable entanglement farming should be possible.

## 9.1 The model and evolution

The scenario and computational framework will be the same as that of the last few chapters, and we will therefore not repeat the information already contained above. The scenario is that of two oscillator detectors, each of frequency  $\Omega$ , each coupled to the field with strength  $\lambda$  (sharply switched) at locations  $x_1$  and  $x_2$ , in a cavity of length  $L$ . Unlike the previous chapters, we will consider a cavity field with Dirichlet boundary conditions, as would be found with an actual optical cavity. As before, we require only a finite number of field modes in our calculation, and we have made sure to include enough such that the results presented are not impacted by this cutoff. In this chapter we will also use a slight change of notation in that we take this number of field modes to be  $N - 2$ , such that the total number of oscillator degrees of freedom (field plus two detectors) is  $N$ . With all of this, the  $\mathbf{X}$  matrix used to specify the phase space interaction part of the Hamiltonian,

$$\mathbf{F}_{\text{int}}^{\text{sym}} = 2\lambda \begin{pmatrix} \mathbf{0}_4 & \mathbf{X}_D \\ \mathbf{X}_D^T & \mathbf{0}_{2(N-2)} \end{pmatrix}, \quad (9.1)$$



will be

$$\mathbf{X}_D \equiv \begin{pmatrix} \frac{\sin k_1 x_1}{\sqrt{\pi}} & 0 & \frac{\sin k_2 x_1}{\sqrt{2\pi}} & 0 & \dots & 0 & \frac{\sin k_{N-2} x_1}{\sqrt{(N-2)\pi}} \\ 0 & 0 & 0 & 0 & \dots & 0 & 0 \\ \frac{\sin k_1 x_2}{\sqrt{\pi}} & 0 & \frac{\sin k_2 x_2}{\sqrt{2\pi}} & 0 & \dots & 0 & \frac{\sin k_{N-2} x_2}{\sqrt{(N-2)\pi}} \\ 0 & 0 & 0 & 0 & \dots & 0 & 0 \end{pmatrix}. \quad (9.2)$$

Once the symplectic evolution matrix  $\mathbf{S}(t)$  has been obtained via Eq. (5.35), the process of cycling pairs of detectors in and out of the cavity is trivially performed. Note critically that  $\mathbf{S}(t)$  is independent of the initial state of the system. We thus need only compute the evolution once and can then use the same matrix for every cycle. The process is as follows. We begin with a cavity field in a state of our choosing,  $\sigma_f^{(0)}$  and a pair of detectors in a state of our choosing,  $\sigma_d^{(0)}$ . Assuming that the field and detectors are initially uncorrelated (this need not be assumed if one were interested in such a scenario) then the total system state is initially  $\sigma^{(0)} \equiv \sigma_d^{(0)} \oplus \sigma_f^{(0)}$ . We then inject the detectors into the cavity at time-zero; this sharply couples the detectors with the field by turning on the interaction Hamiltonian. The system is then left to evolve for a given time  $t_f$ . This evolution is governed by  $\mathbf{S}(t_f)$ , and so after this time the system is in a state of the form

$$\sigma^{(1)} \equiv \mathbf{S}(t_f)\sigma^{(0)}\mathbf{S}(t_f)^T \equiv \begin{pmatrix} \sigma_d^{(1)} & \gamma_{df}^{(1)} \\ \gamma_{df}^{(1)T} & \sigma_f^{(1)} \end{pmatrix}. \quad (9.3)$$

Here  $\sigma_d^{(1)}$  and  $\sigma_f^{(1)}$  are the reduced states of the detectors and field, respectively. The matrix  $\gamma_{df}^{(1)}$  encodes the correlations generated between the detectors and field during the evolution. The state of the detectors can now be examined and, for example, be tested for entanglement via Eq. (3.34).

After this first stage of evolution we immediately remove the detectors from the cavity. They can then be sent elsewhere to be utilized, and for the current protocol we ignore any correlations between the pair and the field. As soon as the first pair is removed we inject into the cavity a fresh new pair of detectors which have been prepared in the same way as the first pair (although this need not be the case). The state of the new detectors+field thus becomes  $\sigma_d^{(0)} \oplus \sigma_f^{(1)}$ . We then allow this system to evolve for time  $t_f$  (we could of course choose a different time if we wanted), after which we have the state  $\sigma^{(2)} = \mathbf{S}(t_f)[\sigma_d^{(0)} \oplus \sigma_f^{(1)}]\mathbf{S}(t_f)^T$ . As before, the detectors-block of this matrix can be examined and/or utilized. We then remove these detectors and immediately replace them

with a new pair, etc. After  $k$  iterations of this process the detectors-field system can be defined recursively as

$$\boldsymbol{\sigma}^{(k)} = \mathbf{S}(t_f)[\boldsymbol{\sigma}_d^{(0)} \oplus \boldsymbol{\sigma}_f^{(k-1)}]\mathbf{S}(t_f)^T. \quad (9.4)$$

Each cycle we lose the information about the detectors-field correlation, and we consider each produced pair of detectors to be their own entity and resource. If desired, it is straightforward to store this correlation information in the  $\gamma_{df}^{(k)}$ 's, to possibly utilize it in other protocols.

## 9.2 Results

Here we present our primary findings. First, in Sect. 9.2.1 we characterize the evolution of the field in terms of a Gaussian superoperator: a linear map on the space of covariance matrices of the cavity field. As a first step, we will initially ignore the contribution of highly off-resonant modes, i.e., we only include modes with frequencies within some resonant window centered on  $\Omega$ . Up to a very large number of cycles this produces a very good approximation for the evolution of the injected detectors. We find that over successive cycles, the cavity field rapidly converges toward a fixed point which is independent of the initial state of the field. Asymptotically approaching the fixed point, significant detector-detector entanglement is obtained every cycle. The cavity then effectively acts as a stable medium through which pairs of detectors can acquire entanglement.

However, when the highly off-resonant modes are also considered, we find that this fixed point becomes unstable after a very large number of cycles. Namely, after many iterations of the protocol, the off-resonant field modes diverge towards increasingly energetic and mixed states. Even though these modes are effectively very weakly coupled to the detectors because they are highly off-resonant, they eventually become sufficiently excited to have enough of a decohering effect that the generation of entanglement between the detectors is impeded. While the detectors will be interacting with the near resonant modes in the same way as they have previously, they will also now experience a highly energetic and highly populated photon gas. The detectors' interactions with this high-mode photon gas evidently introduces enough decoherence into their evolution that any entanglement garnered per cycle will be lost.

Interestingly, the timescale associated with this instability is long enough to allow an extremely large quantity of entanglement to be extracted. For example, depending on the chosen parameters this could easily be on the order of  $10^5$  total amount of logarithmic

negativity, when added up over all detector pairs (recall that the logarithmic negativity is additive on product states,  $E_N(\hat{\rho}_1 \otimes \hat{\rho}_2) = E_N(\hat{\rho}_1) + E_N(\hat{\rho}_2)$ ). Notice that the instability is an effect which is beyond the single-mode approximation that is commonly used in quantum optics, and it occurs independently of how long each cycle is. We will discuss this effect in more detail in Sect. 9.2.4.

Unless otherwise stated, all data presented in this section was obtained using the following parameters:  $\lambda = 0.01$ ,  $L = 8$ ,  $\Omega = \pi/8$  (resonant with the fundamental mode),  $x_1 = L/3$ , and  $x_2 = 2L/3$  (such that the distance between the detectors is  $r = 8/3$ ). There is nothing special about this choice and similar (correspondingly scaled) results would be obtained for different values of the parameters.

### 9.2.1 Fixed point analysis

A key question that we aim to answer in this chapter is how many times a cavity may be reused for entanglement extraction. The field evolution is expressed as a Gaussian superoperator, i.e. a linear map acting on the field covariance matrix. This allows us to treat the field evolution as a linear discrete dynamical system, and to characterize the evolution. In particular we will find regimes in which there is an evolution toward a long-lived metastable state from which entanglement can be extracted.

As described above, one interaction cycle consists of three steps: introducing two new detectors in their ground states, evolving for a fixed amount of time under a quadratic Hamiltonian, and tracing over the detector Hilbert space. Let  $\sigma_f^{(k)}$  denote the state of the field after  $k$  iterations of the cycle have already occurred, and let  $\mathbf{S}$  be the symplectic transformation describing the system evolution over a single cycle, as computed by Eq. (5.35). We can express this transformation in block form as

$$\mathbf{S} = \begin{bmatrix} \mathbf{A} & \mathbf{B} \\ \mathbf{C} & \mathbf{D} \end{bmatrix}, \quad (9.5)$$

where  $\mathbf{A}$  is a 4-dimensional matrix and  $\mathbf{D}$  is  $2(N - 2)$ -dimensional, corresponding to the detectors and field respectively. After an interaction cycle, it is trivially seen that the field will be left in the state

$$\sigma_f^{(k+1)} = \mathbf{D}\sigma_f^{(k)}\mathbf{D}^T + \mathbf{C}\mathbf{C}^T. \quad (9.6)$$

We call the map described by Eq. (9.6) the Gaussian superoperator.

We can cast this into a more familiar form if we view the matrix  $\sigma_f^{(k)}$  as a vector  $\mathbf{v}^{(k)}$  in the symmetric subspace of the tensor product  $\mathbb{R}^{2(N-2)} \otimes \mathbb{R}^{2(N-2)}$  where  $N - 2$  is the

number of field modes. Equation (9.6) then takes the form

$$\mathbf{v}^{(k+1)} = (\mathbf{D} \otimes \mathbf{D})\mathbf{v}^{(k)} + \mathbf{c} \quad (9.7)$$

where  $\mathbf{c}$  is the vector corresponding to the matrix  $\mathbf{C}\mathbf{C}^T$ .

Eq. (9.7) is an affine discrete dynamical system, and its dynamics is characterized by the eigenvalues of the matrix  $\mathbf{D} \otimes \mathbf{D}$ . These are completely determined by the eigenvalues of  $\mathbf{D}$ ,  $d_1, \dots, d_{2N}$ . Let us order these according to  $|d_1| \geq |d_2| \geq \dots$ . The eigenvalues of  $\mathbf{D} \otimes \mathbf{D}$  are just given by the products  $d_i d_j$ . Thus we can determine aspects of the dynamics of the dynamical system (9.7) from the eigenvalues of the matrix  $\mathbf{D}$ .

If the eigenvalues of  $\mathbf{D}$  (and therefore those of  $\mathbf{D} \otimes \mathbf{D}$ ) are all within the unit circle, then the field is driven toward a unique fixed point, given by

$$\mathbf{v}_{\text{fixed}} = (\mathbf{I} - \mathbf{D} \otimes \mathbf{D})^{-1}\mathbf{c}. \quad (9.8)$$

By converting this vector back into a matrix we then obtain the fixed point covariance matrix  $\boldsymbol{\sigma}_{\text{fixed}}$ .

The rate at which such a fixed point is approached is determined by the largest modulus eigenvalue  $d_1$  of  $\mathbf{D}$ . The eigenvector corresponding to eigenvalue  $d_1$  will converge exponentially to the fixed point in a number of cycles on the order of

$$n = -1/\log |d_1|. \quad (9.9)$$

A generic initial state will have a nonzero projection in this direction, and therefore its approach to the fixed point is determined by eigenvalue with the largest modulus.

In the case where  $\mathbf{I} - \mathbf{D} \otimes \mathbf{D}$  is not invertible, there is a subspace of fixed points. This occurs when there are modes that are completely uncoupled with the detectors, such as in the case where both detectors sit at nodes of the corresponding mode functions. There can also be approximate fixed points for modes that are weakly coupled to the detectors, as in the case of modes that are far from resonance. Since there are many off-resonant modes, our system has a large space of approximate fixed points.

If  $|d_1| > 1$  the system has no absolutely stable fixed point. The initial covariance matrix can be expanded in the eigenbasis of the superoperator, and generically the projection onto the eigenspace with eigenvalue  $d_1$  will be nonzero. If this is the case, the covariance matrix will grow exponentially in some direction in the space of symmetric matrices, and the time scale of this growth (in number of iterations) is

$$n = 1/\log |d_1|. \quad (9.10)$$

Although the growth of the covariance matrix depends on the initial state, this dependence is linear while the dependence on  $d_1$  is exponential in the number of iterations. Thus in practice we find that Eq. (9.10) yields a good indication of the timescale for instability.

This instability has a strong effect on the process of entanglement extraction. After interaction with the field, the covariance matrix of the detectors is linear in the initial state of the field. Even though the growing modes of the field interact only weakly with the detectors, the field is growing exponentially, and will eventually overcome the weakness of the coupling. The highly mixed state of the field therefore leads to a highly mixed state of the detectors. Beyond the number of iterations set by Eq. (9.10), we expect that the state of the detectors will become sufficiently mixed that no further entanglement can be extracted. However, if  $|d_1|$  is sufficiently close to 1, the number of iterations is large and much entanglement can be extracted before the instability interferes with entanglement extraction.

We will see that if a cutoff is introduced on the field modes so that only the few modes closest to resonance are included, the system approaches a stable fixed point. These modes are the most relevant to the entanglement extraction process, so this fixed point captures well the dynamics of the system up to a very large number of iterations.

The dynamics of the system is therefore roughly characterized by three phases. In the first phase, the field converges rapidly toward the approximate fixed point. In this phase the energetic cost and extracted entanglement depend strongly on the initial state of the cavity field (we will be exploring this physics in the sections below). In the second phase, the field has reached an approximate fixed point, and the modes most relevant for entanglement extraction have lost their memory of the initial state. The state of the field in this resonant window no longer changes between cycles, and it is only the highly off-resonant modes that are being very slightly modified every cycle (specifically, becoming more energetic and mixed). In the third phase, after many iterations, the off-resonant modes become highly excited enough that they begin to have a significant effect on the field's ability to entangle pairs of detectors. Once this happens the extracted entanglement per cycle correspondingly drops off, eventually reaching zero. The time scale for this instability is only weakly dependent on the initial state, and can be estimated from the dynamics alone.

## 9.2.2 Sustainable entanglement extraction

One might expect intuitively as we proceed through detector-field interaction cycles that the field's ability to impart entanglement to the detectors would decrease. This is because

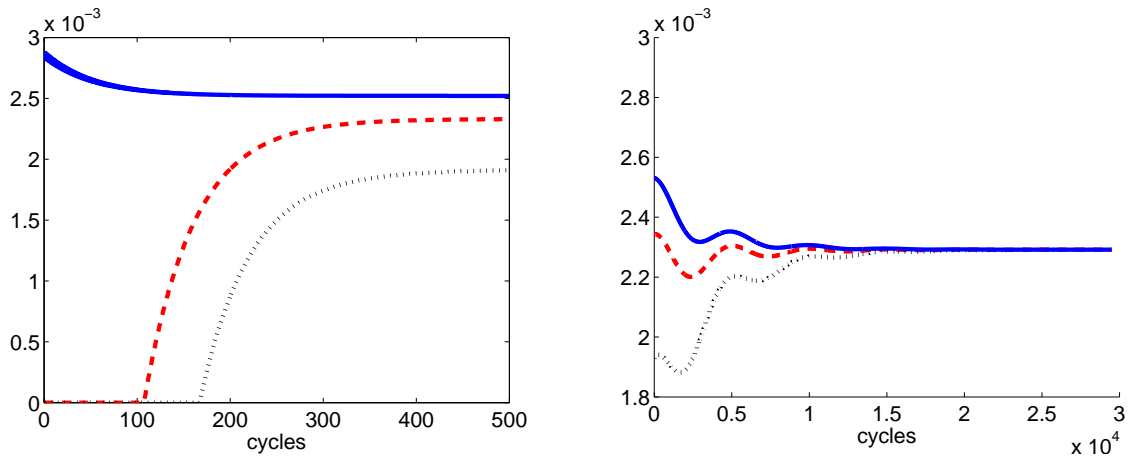


Figure 9.1: We plot the logarithmic negativity attained per cycle by detector pairs, as a function of cycle number. On the left this is plotted for a small number of cycles, and on the right for a large number. The three lines correspond to different initial states of the field. The solid (blue) line corresponds to the vacuum state, whereas the dashed (red) line corresponds to a thermal state of temperature  $T = 0.5$  and the dotted (black) line to a temperature of  $T = 1$ . The time of evolution per cycle was set to  $t_f = 20$ .

of noise generated by switching on and off the interaction during each cycle; since the cavity is of a finite volume these excitations reflect off of the walls of the cavity rather than propagating away. Furthermore, any correlations produced between the detectors and the field each cycle would be expected to induce additional noise in the field as we remove each pair. Both of these effects are expected to increase the mixedness of the state and therefore to extinguish the entanglement that can be acquired by putting two detectors into interaction with it. Thus, if a fixed point of the field exists one might expect it to be unable to impart entanglement to the detectors via additional interaction cycles.

However, we have found this intuition to be incorrect. Under a suitable mode truncation, the field does indeed approach a fixed point, and this fixed point does in fact entangle fresh detectors every cycle, even though the field itself is unchanged between the beginning and end of each such cycle. This can be confirmed by directly computing the fixed point via Eq. (9.8). We must question, however, attractiveness and stability of this state. We find that the fixed point is in fact very stable and attractive, and indeed independent of the initial state of the field. Remarkably, this means that even if the initial state of the field is such that entanglement cannot be extracted during a single cycle, the repetition of the process drives the field to a state for which it can. To quantify the amount of entanglement

extracted we use the logarithmic negativity, which is additive under tensor products.

Plotted in Fig. 9.1 is the logarithmic negativity imparted per cycle onto the detector pairs, as a function of cycle number. This is for the case that the time of evolution is larger than the light-crossing time between the detectors, specifically with  $t_f = 20$ . This was performed using the algorithm laid out in Sec. 9.1. We include two plots, one examining the short term behavior (i.e. small number of cycles) as well as that of the long term (large number of cycles, but not large enough to observe the decohering effect of the highly off-resonant modes). In each plot we display the results for several different initial states of the field, specifically the vacuum state and two thermal states. In the short term regime we observe that, as expected, thermal fluctuations in the field prohibit the extraction of entanglement. After several cycles, however, the field has been driven to a non-thermal state (see Sect. 9.2.3) such that extraction becomes possible. In the long term behavior we observe two important points. First, after many cycles the amount of entanglement obtained per cycle becomes constant and non-zero. At this point we have effectively reached the fixed point, and the state of the field is then observed to match the state obtained directly via Eq. (9.8). As claimed, the entanglement obtained every cycle is non-zero, even though the field is no longer changing. Second, it is clearly seen that the fixed point behavior is independent of what state the field was initially in. It can be confirmed that the field state in all three cases reaches the same fixed point. In Sect. 9.2.3 we will further discuss several important aspects of this evolution in regards to initial thermality of the field.

Summarizing this result: a cavity with an arbitrary state of the field can, in theory, be used as a source of entanglement for an extremely large number of detector pairs, independently of the initial state of the cavity. This knowledge can be useful in order to devise experimental implementations where the quantum field is used as a renewable entangling resource.

Of course, there is an energy cost to this process. This cost is easily computed by taking the difference of the expected energies of our system (detectors and field) at the end and beginning of each cycle, where the energy is computed via Eq. (3.9). This would then be the energy per cycle that must be input. For example one can compute the energy cost of the procedure once the fixed point has already been reached and find that it is of course finite and positive. Since the field is not changing, this is simply the internal energy gained by the pair of detectors over the course of a cycle. Physically, work must be done in order to inject the atoms into the cavity (the changing coupling strength as they enter the field will cause a repulsive force). When the atoms leave the cavity they exit with less kinetic energy than that with which they were input, the extra energy having gone into the internal degrees of freedom of the atoms.

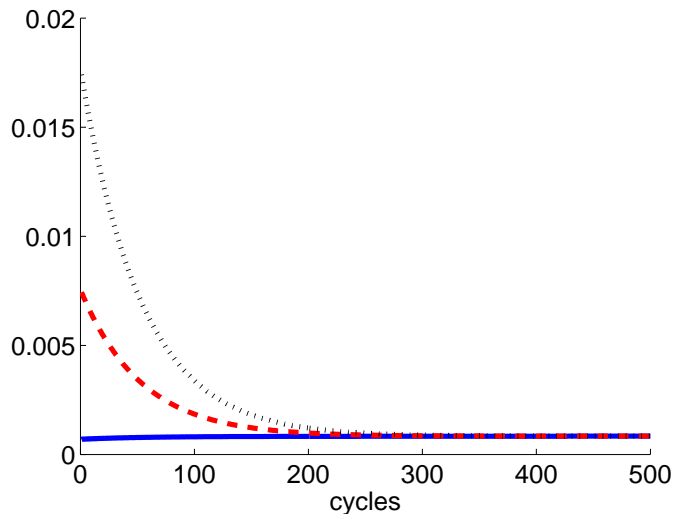


Figure 9.2: The energy input per cycle as a function of cycle number. The solid (blue) line corresponds to the case in which the field is initially in its vacuum state, whereas the dashed (red) line corresponds to a thermal state of temperature  $T = 0.5$  and the dotted (black) line to a temperature of  $T = 1$ . The time of evolution per cycle was set to  $t_f = 20$ .

As an interesting aside, we have computed the energy input per cycle in the short time regime described above. The results are displayed in Fig. 9.2. We see that, interestingly, thermality of the field greatly increases the energy required to drive the field to a non-thermal state that allows entanglement extraction.

### 9.2.3 Initial thermal field

In the previous subsection, as well as in this section, the number of cycles that we have considered is small enough that only the near-resonant modes of the field are relevant for the behavior of the detectors. The instability associated with off-resonant modes (which will be discussed further in the next subsection) occurs only after many more cycles have occurred. In this subsection we will be examining certain properties of the field during the first few cycles. In doing so we only include in this analysis the modes that are relevant for the detectors, such that we can easily identify the important aspects of the field's evolution over several cycles with the evolution of the detector-detector entanglement seen in the previous subsection.



When allowing long interaction times per cycle we have seen that we can harvest entanglement from a cavity field without modifying the state of the field, thus proving its sustainability. A question that arises, however, is how easy it would be to prepare the field in this specific fixed point. As we have seen in the right-hand plot of Fig. 9.1 this turns out to not be a problem. The fixed point is stable and attractive, and is reached independently of the initial state of the field. We also see in the left plot of this figure that, as expected, thermality in the initial field state interferes with our ability to extract entanglement from it or to acquire entanglement via effective interaction of the detectors through the field. With increasing temperature, the field quickly becomes incapable of providing any entanglement at all. If, however, we start cycling detectors through the field, a regime will be reached at which the state of the field has been modified enough that we can begin to obtain entanglement, before it continues on to eventually converge to the fixed point. We have also observed that this driving of the field towards an entanglement-enabling state requires significant amounts of energy as compared to the energy expense once the fixed point is reached. Here we study further this initial transition that is observed when the field is initialized in a thermal state.

During this transition period the field is being driven to a more pure state. This can easily be seen using the measure of purity Eq. (3.26). Plotted in Fig. 9.3 is the purity of the field under the same evolution. Thermality of the field obviously means that the state's purity is initially quite low, but we observe that over the course of several cycles the detectors are acting to purify the field during their time in the cavity. A initial interpretation of this phenomenon would be based on the observation that we are continually inserting cold oscillators (they are in their ground state) into a hot cavity. This would seem to indicate that the freshly injected oscillators are acting to cool down the field until the temperature is low enough to allow entanglement extraction.

However, we have found that that this interpretation is not entirely correct, or at least not complete. This is because during the period of decreasing mixedness the field is also becoming very non-thermal. This can be seen using the relative entropy as a measure of the distance from thermality [144]. We discuss the relative entropy between Gaussian states, and in particular when dealing with thermal states, in Appendix. D. With respect to this measure the closest thermal state to a given state  $\hat{\rho}$  is that which has the same energy  $E_\rho$  as  $\hat{\rho}$ . The relative entropy between  $\hat{\rho}$  and this closest thermal state is then the difference of their entropies:  $S_{\text{th}} - S(\hat{\rho})$ , where  $S_{\text{th}}$  is the entropy of the closest thermal state. We must be careful when using this however because for low energies (corresponding to low temperatures) the smallness of  $S_{\text{th}}$  may lead us to believe that  $\hat{\rho}$  is very nearly thermal, even if it is as far from thermality as can be achieved while staying on the energy shell  $E_\rho$ . To counter this we instead use a relative distance measure by dividing by  $S_{\text{th}}$ . Lastly, since

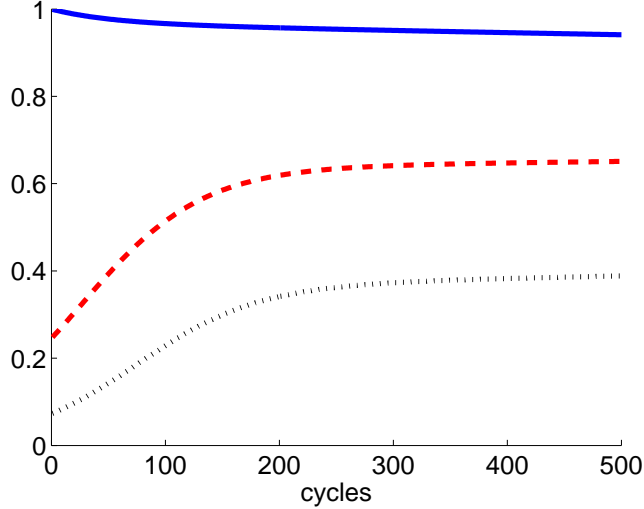


Figure 9.3: The field purity as a function of cycle number. The solid (blue) line corresponds to the case in which the field is initially in its vacuum state, whereas the dashed (red) line corresponds to a thermal state of temperature  $T = 0.5$  and the dotted (black) line to a temperature of  $T = 1$ . The time of evolution per cycle was set to  $t_f = 20$ .

we would like a “thermality estimator”, we will impose that it equates to unity in the case that  $\hat{\rho}$  is exactly thermal. With this, we define our thermality estimator  $D$  as

$$D(\hat{\rho}) \equiv 1 - \frac{S_{\text{th}} - S(\hat{\rho})}{S_{\text{th}}} = \frac{S(\hat{\rho})}{S_{\text{th}}}. \quad (9.11)$$

This measure is bounded from above by one, which is saturated when  $\hat{\rho}$  is exactly thermal, and is bounded from below by zero, which is achieved in the case that  $\hat{\rho}$  is pure.

We are now able to plot  $D(\hat{\rho})$ , applied to the field, as a function of the cycle number and observe that, as stated, the field becomes very non-thermal during the time that it is becoming less mixed. This is plotted in Fig. 9.4. Note that the odd initial value of  $D(\hat{\rho})$  observed when  $\hat{\rho}$  is the vacuum state is due to the fact that  $D(\hat{\rho})$  is ill-defined in the unique case of the vacuum state. In the plot the initial point actually represents the field after one cycle has been performed, in order to avoid this problem.

This shows that we are not trivially cooling down the field. Rather, the field is being driven far off the thermal manifold into a non-thermal, entanglement providing state. In fact, for the parameters being used here it is easy to check for the case of initial temperature  $T = 1$  that when considering the field state after 500 cycles (i.e. at the ends of the

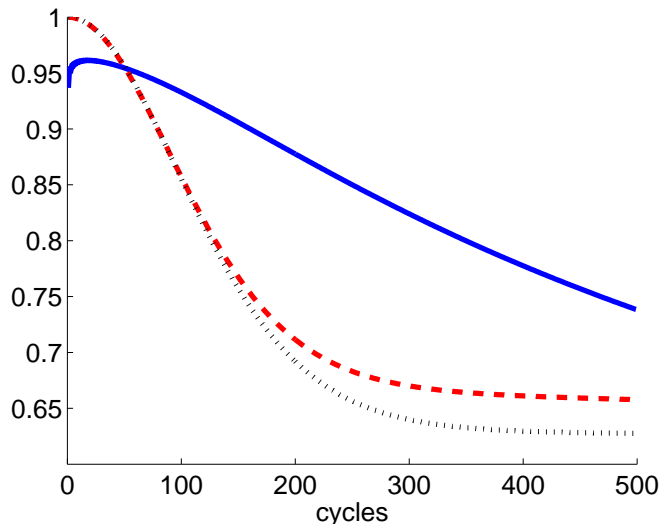


Figure 9.4: The thermality estimator  $D$  as a function of cycle number. The solid (blue) line corresponds to the case in which the field is initially in its vacuum state, whereas the dashed (red) line corresponds to a thermal state of temperature  $T = 0.5$  and the dotted (black) line to a temperature of  $T = 1$ . The time of evolution per cycle was set to  $t_f = 20$ .

figures) the closest thermal state (the one with the same energy as the field) does not provide any entanglement to the detectors. Even more surprising, if we instead consider the thermal state that has the same mixedness as the field, but is less energetic, this state *also* provides no entanglement. This is despite the fact that the actual state itself *does* provides entanglement, as seen in Fig. 9.1. Remarkably, the field appears to be non-thermally driven to a state that is very well designed for providing entanglement, and this is far from a simple cooling process.

As an aside, it is interesting to note that if we increase the time of evolution per cycle then the field is actually driven to an even less thermal state. This is contrary to the intuition that a longer interaction-time might mean that the field thermalizes with the detectors, and thus that it would remain or become relatively thermal as we cycle through detector pairs. This reinforces the idea that the process of cyclicly repeating the entanglement extraction protocol cannot be understood as a cooling process.

## 9.2.4 Onset of the instability

We discussed above that we can find a fixed point in the evolution provided that we truncate the mode expansion of the quantum field. This truncation accurately captures the relevant dynamics of the protocol even for a very large numbers of iterations. However, when all the higher, off-resonant modes are included we generically find that the cavity state eventually becomes unstable (although only after an extremely large number of cycles), and therefore that the mode truncation is not reliable past a given number of iterations of the protocol.

What occurs when highly off-resonant modes are included is as follows. In each individual cycle, the effect that the oscillators have on these off-resonant modes is minute, as it must be, and similarly the effect that these modes have on the detectors is insignificant (assuming the modes are not yet extremely energetic). Over many cycles however, the tiny effects appear to accumulate such that eventually the off-resonant modes become highly excited and mixed enough that they begin to have an observable effect on the detectors. At some point, the detectors become sufficiently entangled with the off-resonant modes that tracing over these modes when the detectors exit the cavity has a sufficiently decohering effect that the entanglement generated between the detectors in each cycle drops off to zero.

We demonstrate this effect in Fig. 9.5, where we plot the logarithmic negativity as a function of the number of cycles on a logarithmic scale. The field was initially in its vacuum state, and all parameters in this plot are the same as those in Fig. 9.1. Note that we can see the same plateau of about  $E_N \approx 2.3 \times 10^{-3}$  as observed in Fig. 9.1, but we also discover now that over the course of many more cycles the generated entanglement begins to slowly degrade as the off-resonant modes become more highly excited before eventually dropping off to zero. It should be noted that even though the total amount of extractable entanglement is limited when the highly off-resonant modes are included, the total amount of logarithmic negativity (added over all detector pairs) that could be obtained from the scenario in Fig. 9.5 is still on the order of  $10^4$ , which is enough distillable entanglement to produce a large number of Bell pairs via entanglement distillation. Note that the sharpness of the drop in this plot is due to a lack of resolution, since it was generated by evaluating the extracted entanglement at every  $2^n$ 'th cycle.

As we showed in Sect. 9.2.1, the stability of the system is governed by the maximal eigenvalue of the field superoperator. The maximum eigenvalues are expected to derive from the off-resonant modes, and thus by Eq. (9.10) we are able to estimate the number of cycles  $n$  needed for the off-resonant modes to make significant contributions to the detectors, and thus to interfere with entanglement generation. We have observed that indeed this method gives a good estimate of after how many cycles the entanglement begins

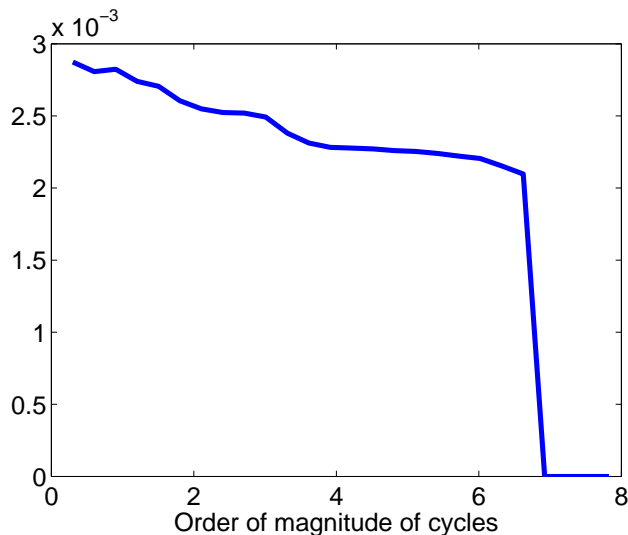


Figure 9.5: The logarithmic negativity obtained by the detectors as a function of  $\log_{10}(\text{number of cycles})$ . The field was initially in its vacuum state. We see that after a large number of cycles, approximately  $10^7$ , the entanglement decays to zero as a result of the increasingly excited off-resonant modes. Note that the sharpness of the drop is due to a lack of resolution, since this plot was generated by evaluating the extracted entanglement at every  $2^n$ 'th cycle.

to wane, and we can thus use this eigenvalue approach to easily explore the behavior of this critical number of cycles  $n$ .

For example, we plot in Fig. 9.6 the critical number of cycles (on a logarithmic scale) as a function of the coupling constant  $\lambda$ . Here the evolution time per cycle was set to  $t_f = 21$ . We see that increasing the coupling reduces the critical number of cycles. This makes sense physically as a larger coupling results in a larger impact per cycle on the off-resonant modes, meaning that they don't need as many cycles to become excited enough to the point of relevance. This behaviour can also be understood mathematically as a consequence of the weakness of the coupling between the detector and quantum field. To zeroth order in  $\lambda$ , the eigenvalues of the matrix  $\mathbf{D}$  are pure phases, so have unit absolute value. The first perturbative corrections to  $\mathbf{D}$  occur at second order in  $\lambda$ , so we expect the maximal eigenvalue to be approximately  $1 + O(\lambda^2)$ . Translating this into  $n$  via Eq. (9.10), it is consistent with the numerical results.

We also plot in Fig. 9.7 the critical number of cycles (on a logarithmic scale) as a function of the time per cycle  $t_f$ . We would like to stress this result because, when the

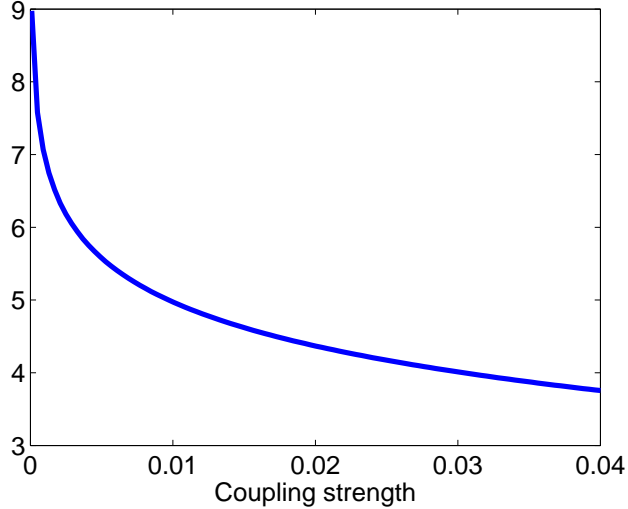


Figure 9.6: The order of magnitude of the number of cycles needed for the highly off-resonant modes to start having impact on the detector evolution, leading to entanglement extinction, as a function of coupling constant  $\lambda$ .

time evolution per cycle is large enough, it is commonplace in the field of cavity quantum optics to resort to the so-called single mode approximation [145]. This approximation consists of neglecting the dynamics coming from the coupling of the off-resonant modes with the particle detectors. It is easily seen that the effect of the off-resonant modes in the quantum state of a particle detector at leading order in perturbation theory becomes negligible for times much larger than the light-crossing time of the cavity (see for instance [98]).

Importantly for our scheme of cyclic entanglement extraction, the critical number of cycles as a function of the cycle duration is not monotonically increasing with  $t_f$  as might naively be expected from the single mode approximation. In this case it is important to remember that the single mode approximation is effective because one can neglect the contribution of the off-resonant modes *relative to the resonant modes*. However, it is not the case that the contribution of the off-resonant mode decays with the time per cycle; rather, it is the contribution of the resonant modes that is growing. The relevant coupling of the off-resonant modes is oscillatory in time rather than decaying, as is captured in Fig. 9.7. Thus, while we may be well within the domain of applicability of the single-mode approximation for describing a single iteration of our protocol, this approximation is not appropriate for describing the dynamics after a very large number of iterations.

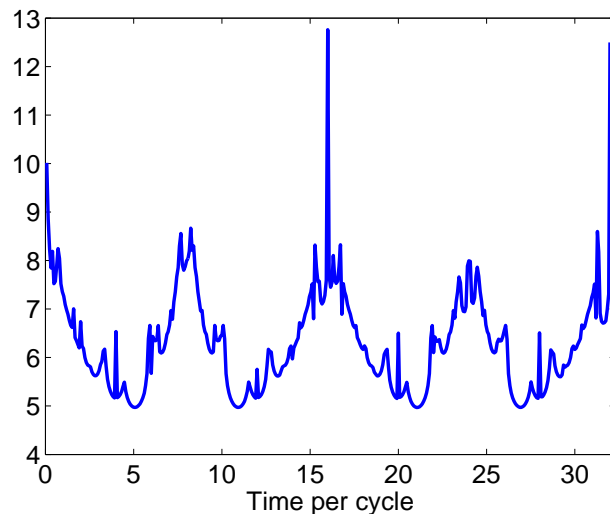


Figure 9.7: The order of magnitude of the number of cycles needed for the off-resonant modes to impact the detectors, as a function of the cycle time  $t_f$ . This magnitude is periodic with a period of 16, which is twice the cavity length.

Since the instability is an effect of the off-resonant modes, it is sensitive to the switching function of the detectors. Here we have assumed sudden switching, for which the strength of the interaction with a given mode decays quadratically with the mode's frequency. For smoother switching functions the decay may be of a higher power, exponential, or even Gaussian. If the switching is done in a smoother way one would therefore expect the time scale of the instability to increase. The role of the switching function is deserving of further study, but this is left as an area for future work.

We conclude this section with an intuitive way to understand how the off-resonant modes are destabilizing the fixed point: The system has a parameter that describes the coupling strength, namely the parameter that we use to switch the interactions on and off. This means that we are dealing with a system that is parametrically driven, with the possibility of parametric resonance. All the field modes are parametrically driven by the rhythm of switching on and off the interaction, i.e., by the entering and exiting of the detector pairs. The cycle length (and the form of the switching function) is important because it determines which frequencies the switching will parametrically excite. The Fourier transform of the switching function (and thus the cycle length and smoothness of the switching) determines which modes are by how much parametrically excited. We postulate that as the off-resonant modes become parametrically driven they are exponentially

fast excited, as is common for parametric resonance, up until at some point where their population is so large that non-perturbative effects destabilize the fixed point. For the destabilization to happen faster, some off-resonant modes' frequencies should therefore be represented strongly in the Fourier transform of the switching function. This may account for the nontrivial dependence of the destabilization time as a function of the cycle length, as shown in Fig. 9.7. This perspective will also be explored in later work.

### 9.2.5 Is a fixed point possible for short cycle times?

We discussed above that there is always a metastable fixed point provided that the duration of every cycle is large enough, meaning that up until a great many cycles have occurred only a small number of modes are relevant to the dynamics of the detectors. However, we have found that there are some regimes where the application of the cycle repetition protocol does not lead to a fixed point. In other words, when the duration of the cycle  $t_f$  is below some threshold the system does not reach a fixed point. While this minimum duration does depend on the particular parameters of our setting, the cycle time scales where there is not a fixed point are of the order of the light-crossing time between the two detectors (and therefore in the zone where spacelike entanglement harvesting occurs).

An interesting question to ask now is what happens with our ability to entangle the two detectors in the ground state by coupling them to the field in these regimes where a fixed point does not exist. In other words, can we harvest a considerable amount of entanglement from the field in the regime where the detectors remain spacelike separated with the technique presented here? We can answer that question by evaluating the amount of entanglement extracted per cycle when the cycle time is below the fixed point threshold. Note that in doing this, due to the smaller time of evolution, there are many more modes that are relevant to the dynamics of the detectors and therefore must be included in the numerical analysis of the problem. We plot in Fig. 9.8 the logarithmic negativity obtained per cycle using much shorter interaction cycles than that considered above (although still slightly greater than the light-crossing time). We see that in this regime we cannot reliably extract entanglement over many cycles, and in fact over the course of many cycles the field is driven towards a less-entangling state (as initial intuition would suggest) rather than the opposite behaviour observed above for the long cycle duration regime.

This provides a convenient opportunity to give some further discussion on whether or not a fixed-point field is possible in the  $t_f < r$  regime (spacelike separation), and whether or not such a fixed point endows entanglement onto the detectors. Numerically, and at least in the current scenario, the answer appears to be that a fixed point is not reached.



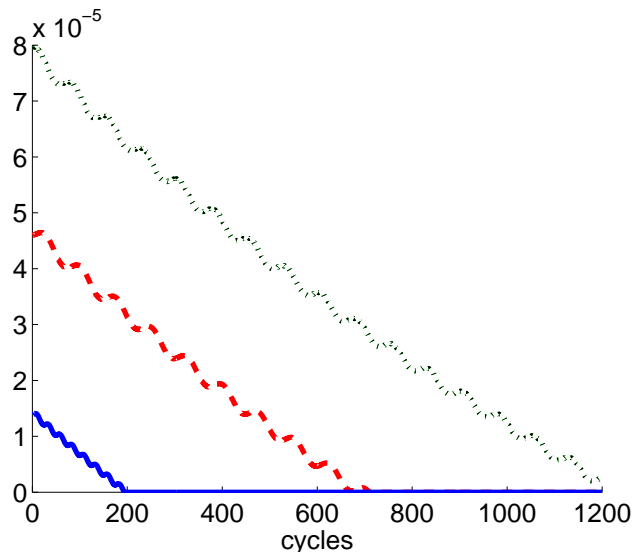


Figure 9.8: The logarithmic negativity obtained per cycle in some regimes where there is no fixed point. The field was initially in its vacuum state. The three lines correspond to three different interaction times per cycle,  $t_f$ . We represent this in terms of the light-crossing time between the detectors, which since the speed of light is set to unity is just the distance  $r = 8/3$  between them. The solid (blue), dashed (red), and dotted (black) lines correspond to  $t_f = 1.44r$ ,  $t_f = 1.48r$ , and  $t_f = 1.52r$ , respectively.

We will discuss that while there are some obvious arguments to make towards why this must necessarily be the case based on intuition coming from information theory, we will argue that such an argument is flawed in the case of quantum fields and there is actually no reason to think *a priori* that such a fixed point is necessarily impossible.

The naive argument for why it must be impossible goes as follows. Assume there exists a fixed point in the spacelike regime ( $t < r$ ) which provides entanglement to the detector pairs. The pair of detectors never come into causal contact, so that they only interact locally with the field. But entanglement cannot be increased under local operations. Therefore, the total entanglement of the detectors plus that of the spacelike separated regions of the field at their locations can not be increased, and thus if the detectors become entangled this entanglement should have previously resided in the field. Therefore, the appearance of entanglement in the detectors should impact the state of the field and make the existence of a fixed-point impossible.

Even if the detectors do not become entangled one can make a similar argument using

any correlations in general (for example as quantified by the mutual information). A detector-field interaction of the type considered, giving an evolution of the form in Eq. (5.35), will generically generate correlations between the detectors starting immediately at time  $t = 0$ . To see this, one can Taylor expand the exponential in Eq. (5.35) with respect to  $t$  and easily show that the off-diagonal block  $\gamma_{12}$  of the detector-detector covariance matrix generically grows as  $t^2$  for small  $t$ . However, correlations in general cannot be increased solely by local interactions, and thus if the detectors never come into causal contact the same argument as above still applies: the correlations must be extracted from the field state and therefore the field state must necessarily change. This is because, even if a fixed-point field does not provide entanglement to the detectors, it will in general provide other correlations. Thus, we come to the conclusion that a fixed-point is impossible to obtain in the  $t_f < r$  regime.

The problem with this argument is that it omits important aspects of our protocol. In particular, each detector can locally generate correlations between either itself and a field quanta or between multiple quanta, and the free evolution of the field can transport these correlations to different parts of the cavity. For  $t_f < r$  these correlated quanta of course cannot transport their newly produced correlation to both detectors over the course of a single cycle, but they can do so over multiple cycles. For example imagine that we have obtained a fixed point, such that the state of the field is the same at times  $t = 0$  and  $t = t_f$ , and an aspect of this state may be that it contains a travelling pair of correlated quanta that were produced during the previous cycle and will be absorbed by the detectors (one quanta for each) during the next cycle. That is, local field correlations generated in a previous cycle may then be transferred to the detectors at a later cycle. Another way to state this type of scenario is that the detectors indeed drain the field of correlations, but that their local interaction plus the free evolution of the field is then allowed to regenerate this loss.

Thus while we have described previous protocols as “harvesting” entanglement from a quantum field, here the protocol is analogous to farming entanglement: in addition to extracting entanglement from the quantum field, the interaction with the detectors is also “sowing” the seeds of entanglement to be extracted in subsequent cycles. However we know that harvesting entanglement at spacelike separation is a more difficult process. While we see no reason in principle that it cannot be done, we have not yet found detector settings that allow for entanglement farming in the spacelike regime.

## 9.3 Discussion

We have studied a protocol for harvesting and even sustainably farming quantum entanglement from a quantum field in a cavity. The protocol consists of placing temporarily two detectors, that are in their ground states, into an optical cavity. They interact with the cavity field for some cycle time,  $t_f$ . The now entangled detectors exit the cavity and a new pair of detectors in their ground state enters the cavity for a new cycle to begin.

The entanglement that the detectors acquire in each cycle has two distinct sources: On the one hand, the detectors can swap entanglement from the cavity field, a process that can take place even when the detectors remain spacelike separated while in the cavity. We have found this type of entanglement harvesting to be transient, however, i.e., we have not found a regime in which this entanglement extraction could be sustained over many cycles. It should be interesting in this context to study if there exists a fundamental limit to entanglement extraction in this case, perhaps similar to the fundamental limit to work extraction in a Carnot cycle.

On the other hand, the detectors can become entangled by interacting via the cavity field if the cycle time is long enough to allow the causal exchange of quanta between the detectors. To this end, we first studied the case where the highly off-resonant modes of the cavity can be neglected and where the cycle times are long enough to enable causal detector interactions via the cavity field. In this case, after some number of cycles the cavity field reaches a fixed point state that is highly non-thermal and independent of the field's initial state. Perhaps surprisingly, this fixed point state of the cavity allows for sustainable significant entanglement harvesting by the successive pairs of detectors. We determined the considerable amount of entanglement that can be harvested in this way, and computed the associated energy cost per cycle.

Due to the sustainability of the method, we call this entanglement farming rather than mere entanglement harvesting. We also found that the field reaches a fixed point regardless of the initial field state in the cavity. This is of interest with regards to possible experimental realizations because it means that this useful fixed point state will be reached independently of any noise or imperfections in the preparation of the initial state of the cavity. The cycling of detector pairs in and out of the cavity drives the field to a steady-state that can be used to entangle detectors, even if the initial state of the field did not yield any entanglement. For example, we have shown that it is possible to apply the protocol even to thermal states. Our methods have also allowed us to calculate the behaviour of the off-resonant modes for large cycle numbers. We found that there is a third stage of evolution after a very large number of iterations. In this final stage, off-resonant modes of the cavity become sufficiently excited as to make further entanglement

harvesting from the cavity impossible. In practice, if the excitations of these off-resonant modes are sufficiently leaking, the third stage need not occur, so that the entanglement farming is sustainable indefinitely. In regards to intuition, our results indicate that the protocol of repeatedly inserting pairs of cold detectors in the cavity does not constitute an efficient cooling process, because the result is not a thermal state. Instead, our results indicate that the detector insertion and removals may be better understood as a periodic parametric driving, a perspective that will be pursued further in forthcoming work.

Additionally, we can view our setup as an entangling quantum gate which has the advantage that it is stably produceable and controllable by iterating a process that yields a fixed point. This combined with 1-qubit universal gates over atoms using relativistic motion (as in the scheme proposed in [146]) would give a complete set of universal gates based on atomic motion in optical cavities that would allow for quantum computing via relativistic effects. The main disadvantage of a scheme based on the setting presented in this chapter would be that the two-qubit gates are also depurifying. It is expectable that variations in the interaction Hamiltonian could lead to a fixed point with a smaller depurifying effect over the atoms. I.e. We would like entanglement to be generated between the two atoms without increasing the entropy of the field so that it does not get entangled with the two atoms system but merely act as a carrier of their interaction. This path will be explored in future work.

Let us also discuss scenarios in which the setting presented here could be implemented experimentally. The most straightforward experimental implementation appears in the context of quantum optics. Namely, the theoretical scenario analyzed here could be implemented with optical cavities [145] being traversed by successive pairs of atoms along the transverse direction of the cavity. The transverse profile of the modes effectively couples and decouples the interaction in a way similar to that suggested in this chapter. Any such implementation requires of course a careful analysis of the cavity losses. But as discussed above, in a realistic experimental setup the higher frequency modes of the cavity have the lowest quality factor, and an enhanced leakage of higher frequency modes could be beneficial. This is because any such leakage would suppress the accumulation of field excitations in the off-resonant modes, which would in turn further stabilize the fixed point.

Additionally, experimental implementations in other systems such as trapped ions or superconducting circuits appear to be within reach. Indeed, the kind of interaction Hamiltonians that we consider in this work can be implemented straightforwardly and with a high degree of control in both superconducting circuits and trapped ion settings (see, e.g., [123]).

We conclude with the observation that reliable mass production of entanglement, or

entanglement farming, on the basis of a fixed point state should be possible also in many other experimental settings. Namely, instead of successively temporarily coupling pairs of particles to a cavity field, one may successively temporarily couple pairs or triplets, etc. of qudits to a suitable reservoir system. The qudits and the reservoir system could have any arbitrary physical realization, even outside quantum optics. In each cycle,  $N$  fresh qudits in their ground states are coupled to the reservoir system, then removed. The key requirement for the farming of  $N$ -partite entanglement by this method would be that the coupling between the qudits and the reservoir is such that the iterated coupling of fresh qudits drives the reservoir system to a fixed point state that is entangling the qudits. As we saw here, such a fixed point does exist in the case where the qudits and the reservoir system are composed of harmonic oscillators, and we also found that the fixed point is completely stable if the number of harmonic oscillators in the reservoir is small enough. It should be very interesting to find the sufficient and necessary conditions on qudit-reservoir systems for such a useful fixed point state of the reservoir to exist.

# Chapter 10

## Quantum seismology

Note: this chapter derives from the work [6], in collaboration with William Donnelly, Achim Kempf, Robert C. Mann, Eduardo Martín-Martínez, and Nicolas C. Menicucci.

This chapter is somewhat a continuation of the previous, in that we will modify the entanglement farming scenario in such a way that it becomes potentially useful for quantum metrological purposes, in addition to the generation of entanglement. As we have seen, entanglement farming involves successively sending pairs of ‘particle detectors’ (such as atoms, ions, molecules, etc.) transversely through an optical cavity, all initialized in their ground states. As each pair of atoms<sup>1</sup> traverses the cavity, the state of the cavity field is slightly modified. As pair after pair traverses the cavity, the field approaches a fixed-point state through a non-perturbative and non-thermal process. When the fixed point is reached, every pair of atoms emerges from the cavity in the same state, which is generically entangled. Due to the stability of the fixed-point state, this protocol provides a potentially useful method for producing a stream of reliably entangled pairs. Additionally, this protocol was proven to be robust to variation of the parameters and, most importantly, almost entirely independent of what the initial state of the field—in particular, not requiring it to be the vacuum state for the fixed point to be quickly reached.

Entanglement farming depends on the (meta-)stable fixed point of the cavity that is produced by successively passing pairs of atoms through the cavity. This fixed point can be calculated using non-perturbatively and is was found to be generally stable to small changes in the parameters of the setup (e.g., positions, time of flight, energy gap, cavity length, etc.). Here we will show that this robustness breaks down dramatically when the frequency at which atoms traverse the cavity is at resonance with a multiple of the cavity’s

---

<sup>1</sup>Henceforth, we use the term ‘atom’ for the generic system interacting with the cavity field.

fundamental frequency. Concretely, we can tune the parameters (including the waiting time between pairs of atoms) so that the steady state is highly sensitive to changes in these other parameters. This finding opens up opportunities to use this setup to detect small parameter changes with very high sensitivity, and we will be looking at one such application in this chapter. In particular, we choose this free parameter to be the cavity length—i.e., we study the sensitivity of entanglement farming to small deviations in the length of the cavity, which makes our setup sensitive to vibrations. A technical aspect of our approach relates to the fact that time-dependent boundary conditions introduce nontrivial effects on quantum fields, such as particle creation by moving mirrors (the dynamical Casimir effect [141]). We will restrict our analysis to settings in which these effects are negligible; that is, regimes in which the cavity vibration is slow compared to the speed of light. It will turn out that the sensitivity of our setup to the parameters of interest remains significant even in this adiabatic regime. The sensitivity furthermore remains even when the frequency of vibration is several orders of magnitude below the fundamental optical frequency of the cavity, making this potentially a very sensitive apparatus for detecting mechanical perturbations of optical cavities—a kind of *quantum seismograph*.

## 10.1 Setup

The setup of the quantum seismograph will be essentially the same as that of the entanglement farming scheme, discussed in Ch. 9. There will, however, be crucial differences. We continue to analyze the dynamics of two atoms of equal energy gap  $\Omega$ , initialized in their ground state and which only interact with the field for a finite amount of time  $T$ . After this time, the two original atoms are removed, and a fresh pair is set to interact with the field in the cavity, again for a time  $T$ . We repeat the whole process iteratively, eventually reaching a fixed point and recovering pairs of entangled atoms. As before, the physical implementation of such setting consists of beams of atoms traversing the cavity in a direction perpendicular to the quantization direction  $x$ , in a similar way as in [143].

Given the Dirichlet boundary conditions linking length and frequency scales, only time (or alternatively length) units are free to be chosen: We let the fundamental frequency of the cavity  $\omega = \pi/L$  carry the relevant units for the physical system in question. Hence, all the other quantities of the simulation should now be interpreted relative to this fundamental frequency. For instance, a cavity whose fundamental frequency is 10 GHz (microwave cavity) corresponds to a length of roughly  $L \approx 3$  cm. If the frequency is 500 THz then  $L$  would be roughly  $\approx 600$  nm.

There will be two differences between the protocol in this chapter and that of the last.

The first is rather unimportant, only providing slight quantitative differences to our results. This is that we will no longer use a sudden switching function. Rather, we will take the coupling to be time dependent, of the form  $\lambda(t) = \lambda\chi(t)$ , where the constant  $\lambda$  is still used to determine the overall strength of the interaction, and  $\chi(t)$  will be a function on the order of unity that contains the chosen time dependence. In particular, we will ramp up the strength of the interaction between the atoms and the cavity modes with the following smooth ( $C^\infty$ ), compactly supported switching function:

$$\chi(t) = \begin{cases} S[\pi t/\delta] & 0 \leq t < \delta, \\ 1 & t \in [\delta, T - \delta), \\ S[\pi(T - t)/\delta] & T - \delta \leq t \leq T, \\ 0 & \text{elsewhere,} \end{cases} \quad (10.1)$$

where  $S(x) = [1 - \tanh(\cot x)]/2$ . This function smoothly switches from 0 to the full coupling strength  $\lambda$  and back to 0, where  $\delta$  is the switching time-scale. In Fig. 10.1 we plot an example of this function that we will use in our scenario, with  $\delta = 0.2T$  and  $T = 20$ . We chose to use a smooth switching function in order to avoid any spurious switching excitations from degrading the potential of our seismograph. As we found, whether or not one uses a sharp function or that of Eq. (10.1) makes only quantitative differences that are not of great significance.

Note that, since we are using a time dependent coupling  $\lambda(t)$ , we are no longer able to use the solution in Eq. (5.35) to compute the evolution during each cycle. Rather, we must integrate the equation of motion Eq. (5.34). This is trivially done numerically and, as before, we only need to solve for the evolution  $\mathbf{S}(t)$  once and then apply the same transformation each cycle.

Unless otherwise stated, we will employ the following system parameters. The coupling constant is  $\lambda = 0.01$ . The boundaries of the cavity are located at  $x = 0$  and  $x = L_0$  and the two atoms are located at  $x_1 = L_0/3$  and  $x_2 = 2L_0/3$  (such that the distance between them is  $L_0/3$ ). We choose the frequency of the atoms to be resonant with the fundamental mode of the cavity:  $\Omega = \pi/L_0$ . The time of interaction for each cycle (i.e., how long each pair of atoms spend in the cavity) is  $T = 2.5L_0$ . Note that this is well beyond the light-crossing time  $L_0/3$  between the atoms, as required for the farming procedure to work. Lastly, we will take the parameter  $\delta$  contained in the switching function to be  $\delta = 0.2T$ . The choice that we have made here for  $L_0$  is entirely arbitrary. As will be discussed later, we can scale down the cavity length to that of an optical cavity or cavity QED setup and, by similarly scaling the other dimensionful quantities, we can obtain exactly the same results. Indeed,



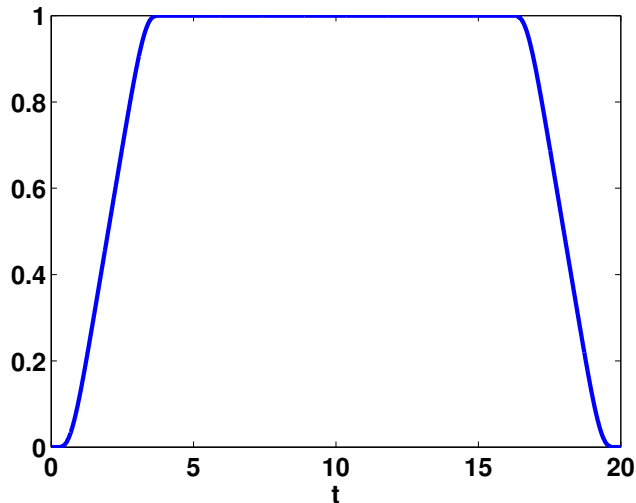


Figure 10.1: The function  $\chi(t)$  with  $T = 20$  with  $\delta = 0.2T$ .

we will discuss how the results we obtain here with the above parameters are equivalent to what can currently be achieved within cavity QED systems.

## 10.2 Sensitivity of the fixed point to time delays

The second change from the setup in Ch. 9, and the one that is critical to our quantum seismograph proposal, is to introduce a delay of some duration  $\Delta t$  between the exit of one pair of atoms and the entry of the next pair. During this delay, the field will undergo free evolution. A natural question arises: To what extent does the fixed-point state depend on  $\Delta t$ ? We find that the introduction of such a delay typically does not strongly affect the steady state. However, we show below that for delays in the vicinity of particular isolated critical values of  $\Delta t$ , the steady state can vary greatly with very small changes in this delay.

We plot in Fig. 10.2 the logarithmic negativity of the state of a pair of atoms once the fixed-point state is reached, as a function of the time between successive pairs of atoms traversing the cavity, in units of the light crossing time of the cavity,  $f = (T + \Delta t)/L_0$ . As Fig. 10.2 shows, there are remarkably sharp valleys at integer values of  $f$ . Note that we have assumed a lossless cavity. It is possible that a more detailed analysis, including losses, would reduce the sharpness of this effect. We leave this to future work.

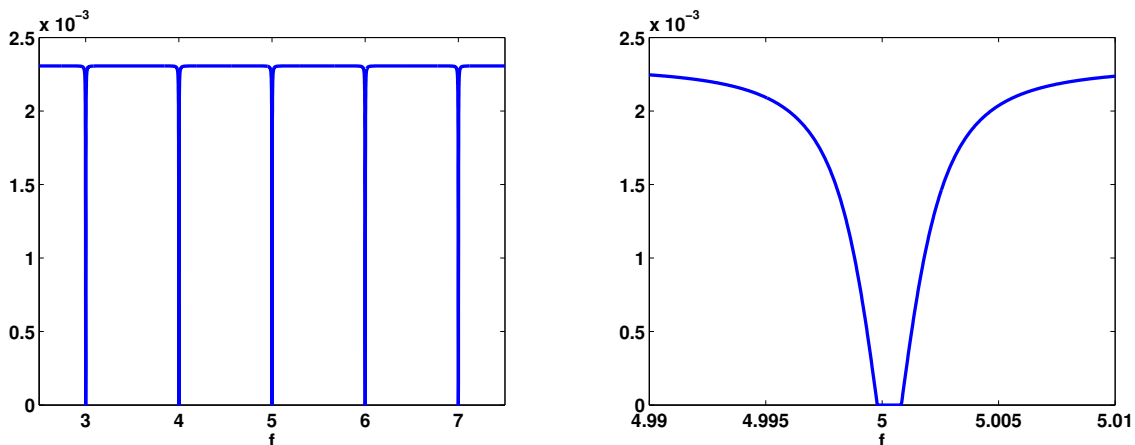


Figure 10.2: The steady-state logarithmic negativity as a function of  $f = (T + \Delta t)/L_0$ , where  $\Delta t$  is the varied parameter. The other parameters are  $\Omega = \pi/L_0$  (resonant with the fundamental mode),  $T = 2.5L_0$ , and with the switching parameter  $\delta = 0.2T$ . On the left we see that the steady state entanglement is nearly constant as the delay time is changed, except for very well-defined points in which it drops drastically. On the right we zoom in on one of the valleys, and we see that in fact the steady-state entanglement is zero within a small window.

The presence of these valleys suggests an interpretation as a resonance effect. By iterating our protocol, we introduce a periodic time-dependent perturbation to the Hamiltonian of strength  $\lambda$  whose frequency is at resonance with the modes of the cavity precisely when  $f$  is an integer. When  $f$  is close to an integer, this perturbation induces transitions between levels of the system, which in our setup corresponds to emission and absorption of field quanta by the atoms. The width of such a resonance in frequency space scales as  $\lambda^2$  with the coupling constant  $\lambda$ , which explains the sharpness of the valleys. Note that although our perturbation is not harmonic in time (its shape is given by the switching function in Fig. 10.1), our results suggests it is only the periodic nature of the perturbation that is important. Indeed, we have investigated how the valleys depend on the switching function, and we found almost identical valleys even for completely sharp switching. While this suggests that the simplifying assumption of sharp switching could be used instead of smooth (as in Ch. 9) without creating artifacts, we nevertheless continue to use the smooth function, Eq. (10.1), to ensure maximum confidence in our results.

The sharpness of these valleys—i.e., the extremely strong sensitivity of the fixed-point state—suggests applications to metrology. The idea is to prepare an entanglement farming

system with initial parameters such that the steady state is within one of these valleys, preferably at the steepest point of one of the valley's walls. Then, even a weak disturbance (for example, a tiny change in the length of the optical cavity) may displace the system out of this sharp valley and cause a significant change to our readout, yielding a strong signal. As we will show, this does occur. Importantly, not only do we receive a remarkably strong signal in the entanglement between atoms but also directly in more measurable quantities such as the quadrature correlation functions.

### 10.3 Cavities with time dependent length

Let us now suppose that the cavity is disturbed, say by a mechanical wave of some kind, so that the cavity's proper length becomes time-dependent. When a mechanical wave deforms the cavity we will make the assumption that the atoms keep their positions constant relative to the instantaneous cavity length, e.g.  $x_1 = L(t)/3$  and  $x_2 = 2L(t)/3$ . We acknowledge that engineering this condition might be challenging and that this might not be the most natural model for a practical implementation. Nevertheless, we choose it for this analysis because it yields a lower bound on the sensitivity and is therefore a conservative approach to estimating the strength of the signal. If the atoms were instead to move relative to the cavity (in the longitudinal direction), they would likely feel an even larger disturbance given the variation of their effective coupling strength due to the inhomogeneous spatial profile of the field modes. Keeping the relative positions constant, any change we see in the farming output must result solely from a change of field state rather than just a direct change in the coupling strength of the atoms to the field modes, which of course also induces a detectable change in the atoms' dynamics.

Intuitively, as long as the time-dependence of the cavity length is slow enough, the modes in that cavity should be approximately the same as those for a stationary cavity, except that each mode's frequency now varies in time. We call this assumption (specifically,  $|\dot{L}| \ll 1$ ) the *adiabatic approximation*, because it is equivalent to the usual adiabatic approximation  $\dot{\omega} \ll \omega^2$  in terms of the mode frequencies  $\omega \sim 1/L$ . We know that when the cavity walls' speed is comparable to that of light ( $\dot{L} \sim 1$ ), relativistic effects render this naive description inaccurate due to the dynamical Casimir effect [141]. Fortunately, there exists a wide range of wall motion parameters that (a) are consistent with the adiabatic approximation and (b) produce an observable disturbance of the entanglement farming process.

In other words, the system of uncoupled harmonic oscillators that are the field modes

becomes a system of uncoupled oscillators with time-dependent frequencies  $\omega_n(t)$  given by

$$\omega_n(t) = k_n(t) = \frac{n\pi}{L(t)} \quad (10.2)$$

which in turn means that the free-field Hamiltonian is

$$\hat{H} = \sum_n \omega_n(t) \hat{a}_n^\dagger \hat{a}_n + \mathcal{O}[\dot{L}(t)]. \quad (10.3)$$

In Appendix. E, we justify the form of this Hamiltonian and our use of the adiabatic approximation for a cavity comprised of one fixed mirror and another undergoing forced oscillations. As a possible extension of this work, Appendix. F provides preliminary calculations for a cavity deformed by the passage of a gravitational wave, producing a similar distortion. In the rest of this chapter we assume the adiabatic approximation.

## 10.4 Quantum seismograph

### 10.4.1 Two-stage evolution

The idea behind the quantum seismograph is to prepare an entanglement-farming setup in a steady-state configuration with initially fixed cavity length, such that small changes in the length of the cavity, due to temporary vibrations, produce a detectable change in the extracted entanglement and other measurable quantities.

Modelling the evolution of this system involves two stages. The first is to calculate the steady-state response of the system to a variety of (fixed) parameters, including cavity length  $L_0$ , interaction time  $T$ , and delay between interactions  $\Delta t$ , in order to determine which ones should be used as the unperturbed cavity parameters. These parameters are assumed to be constant during this first stage. The system is allowed to reach a steady state, which is assumed to be the unwavering behavior of the system before any vibrations have affected it.

For the second stage of the evolution, we imagine that the system is happily continuing in its steady state (as above) when suddenly the cavity experiences a vibration, resulting in a sinusoidal variation in cavity length,

$$L(t) = L_0 + A \sin(\gamma t) \quad (t > 0), \quad (10.4)$$

with amplitude  $A$  and angular frequency  $\gamma$ . To keep within the adiabatic approximation (see Sec. 10.3), we require

$$\gamma A \ll 1, \tag{10.5}$$

which ensures that the cavity walls’ motion is nonrelativistic ( $|\dot{L}| \ll 1$ ).<sup>2</sup> We do not calculate the steady state of the system during this (time-dependent) evolution, since we want to consider the case where the system does not have time to reach the steady state (if such a state exists). Instead, we numerically integrate the full dynamics with Eq. 5.34 for this stage of the evolution, using the time-dependent free-field Hamiltonian given in Eq. (10.3), along with interaction between field and atoms as done throughout the rest of this Part of the thesis, and delay  $\Delta t$  between cycles as described above. The initial state for the evolution is taken to be the steady-state solution resulting from the previous stage of the evolution. From our simulations, we extract information about observables associated with each pair of atoms after it exits the cavity.

## 10.4.2 Choice of unperturbed cavity parameters

In order to maximize the response we get from a change in  $L$ , we should optimize our choice of unperturbed cavity parameters. We do this by preparing the system initially such that its steady state corresponds to a point on a very steep part of one of the “valleys” seen in Fig. 10.2. The idea behind this choice is that small periodic changes in  $L$  should result in movement along this steep “wall” of the valley, producing a large change in the extracted entanglement with detectable time dependence. This intuition relies on the tacit assumption that the steady-state plot shown in Fig. 10.2 is still relevant in stage two of the evolution (i.e., full dynamics, including vibrations in  $L$ , Eq. (10.4)). We expect this intuition to be valid when a single period of the vibration lasts over many interaction cycles (including both the interaction time  $T$  and the time of free evolution  $\Delta t$ )—in other words, if we choose

$$\gamma(T + \Delta t) \ll 1. \tag{10.6}$$

We must stress, however, that this assumption is not required for numerical stability of the simulation or for validity of the results we calculate. This is because the steady-state calculations (which use fixed  $L_0$ ) are used only to determine the initial state of the cavity field. The simulation calculates the full evolution of the system starting from this state, as discussed in the previous subsection.

---

<sup>2</sup>Notice that this allows  $A$  to be large as long as  $\gamma$  is sufficiently small. In practice, however, if we want to detect weak vibrations, then we expect  $A \ll L_0$ , as well.

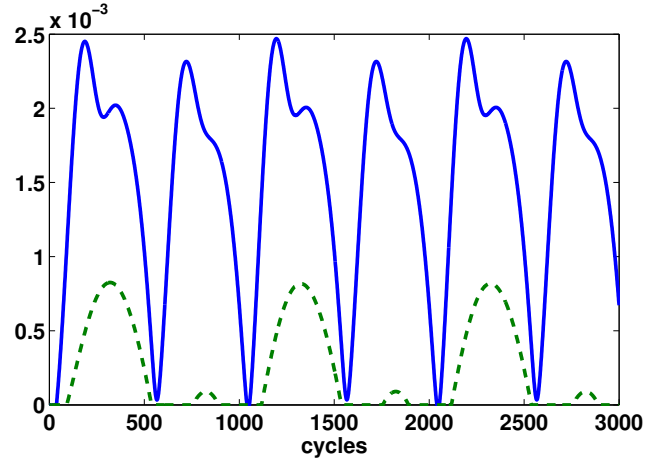


Figure 10.3: The logarithmic negativity received per cycle during the period of vibration. Here the vibrational period is set to 1000 times the cycle time (interaction plus rest period totaling a time of  $T + \delta t = 2T$ ) and we track three periods of the vibration. Before the vibration the steady-state entanglement was zero, and the entanglement shown in this plot is due solely to the vibration, despite the frequency being such that  $\gamma/\omega_1 = 4 \times 10^{-4}$ . The two lines correspond to different vibration magnitudes. The solid (blue) line is such that  $A = (1 \times 10^{-3})L_0$  and the dashed (green) line corresponds to  $A = (2 \times 10^{-4})L_0$ .

### 10.4.3 Detecting vibrations

We choose the time of interaction to be  $T = 2.5L_0$  and the rest time of the field to be the same  $\Delta t = T$ , which puts us into the valley at  $f = 5$  as seen in Fig. 10.2. We allow the system to reach its steady state. Then, as seen in the figure, we receive no entanglement from each pair of atoms that emerges from the cavity. Thus, if nothing disturbs the system a steady stream of unentangled pairs emerges from the cavity.

We now let a vibration occur that is weak in magnitude and of low frequency (as compared with the optical frequency of the cavity). As stated above, by setting  $f = 5$  we have prepared our system within a precariously thin “valley”. Does this indeed mean that the fixed point is extremely sensitive to even such a non-invasive disturbance? Consider an example where the frequencies of the atoms are  $\Omega = \pi/L_0$  (resonant with the first mode). Considering the logarithmic negativity per cycle of each successive pair of atoms, which is initially zero, we see in Fig. 10.3 that a very significant response is obtained due to the presence of a wave. In this example the frequency of the wave is  $\gamma = (4 \times 10^{-4})\omega_1$ , where  $\omega_1$  is the fundamental frequency of the cavity, and the amplitudes corresponding to the

two responses shown are  $A = (1 \times 10^{-3})L_0$  and  $A = (2 \times 10^{-4})L_0$ . While the value of the logarithmic negativity obtained is small, recall that to leading order the logarithmic negativity generated between two atoms interacting with a field goes as  $\lambda^2 = 10^{-4}$ . Here, we are finding that a very weak and low-frequency disturbance can cause the generated entanglement to jump from a zero value to even an order of magnitude *higher* than what is generally expected from the harvesting scenario. In this sense, we have found an extremely strong signal.

Whereas this variation in the per-pair entanglement could be amplified through entanglement distillation, it is not very convenient experimentally to rely on the amount of produced entanglement to encode the information about the perturbation. While it is interesting to see how the generated entanglement is affected by a mechanical vibration of the cavity, we should also consider the impact on other, more directly measurable, quantities. To this end we will consider the quadrature correlators as well. In particular, let us look at the observables  $2\langle\hat{q}_1\hat{q}_2\rangle$  and  $2\langle\hat{q}_1\hat{p}_2\rangle$ , where  $\hat{q}_1$  and  $\hat{p}_2$  are the internal position quadrature of atom 1 and momentum of atom 2, respectively. First, we will look at how the steady-state values of these quantities change with the delay time  $\Delta t$ , as we did with the logarithmic negativity in Fig. 10.2. These are displayed in Figs. 10.4 and 10.5. As expected, we find peaks at the same positions that were observed in the Fig. 10.2, except that the peaks are antisymmetric in the case of the  $2\langle\hat{q}_1\hat{p}_2\rangle$  correlator. To see why this is not surprising recall that, for our interaction, the Heisenberg equation for  $\hat{q}_2$  tells us that  $\hat{p}_2$  is just the time derivative of  $\hat{q}_2$ , so we have that

$$\langle\hat{q}_1\hat{p}_2\rangle = \left\langle\hat{q}_1\frac{d}{dt}\hat{q}_2\right\rangle = \frac{d}{dt}\langle\hat{q}_1\hat{q}_2\rangle - \left\langle\left(\frac{d}{dt}\hat{q}_1\right)\hat{q}_2\right\rangle. \quad (10.7)$$

Therefore

$$\langle\hat{q}_1\hat{p}_2 + \hat{p}_1\hat{q}_2\rangle = \frac{d}{dt}\langle\hat{q}_1\hat{q}_2\rangle. \quad (10.8)$$

Given that the detectors are identical and the setup is symmetric, the whole setting is invariant under the swap of the labels of the atoms,  $\langle\hat{q}_1\hat{p}_2\rangle = \langle\hat{q}_2\hat{p}_1\rangle$ , thus

$$2\langle\hat{q}_1\hat{p}_2\rangle = \frac{d}{dt}\langle\hat{q}_1\hat{q}_2\rangle, \quad (10.9)$$

which explains why Fig. 10.5 looks like the derivative of Fig. 10.4.

From these figures it appears that our seismograph would have more sensitivity if we measure  $2\langle\hat{q}_1\hat{q}_2\rangle$ , since the variation in this parameter from the inside to outside of the peaks is greater than for the  $2\langle\hat{q}_1\hat{p}_2\rangle$  measure. Indeed this is the case if the quadrature

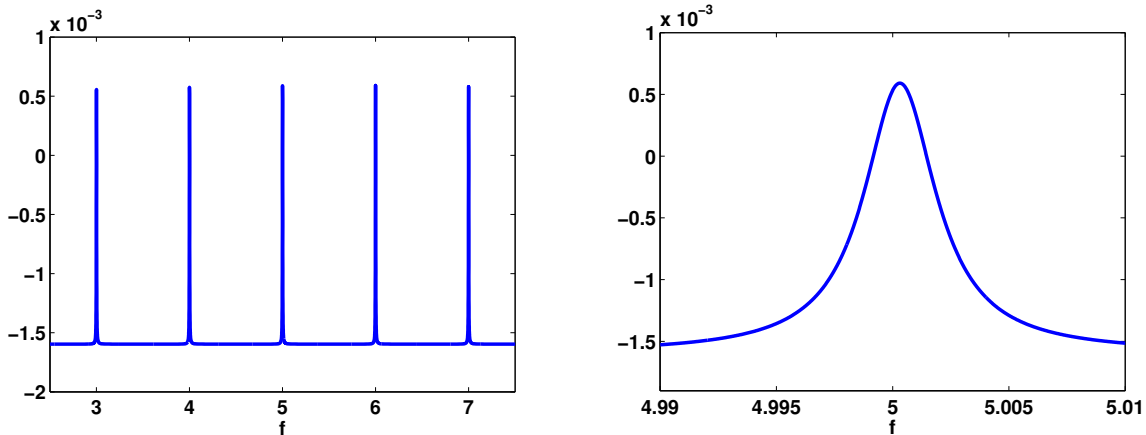


Figure 10.4: The steady-state value of  $2 \langle \hat{q}_1 \hat{q}_2 \rangle$  as a function of  $f = (T + \Delta t)/L_0$ , where  $\Delta t$  is the varied parameter. The other parameters are  $\Omega = \pi/L_0$  (resonant with the fundamental mode),  $T = 2.5L_0$ , and with the switching parameter  $\delta = 0.2T$

measurements are performed immediately after the atoms exit the cavity. We will take this opportunity, however, to discuss how the act of free evolution after exiting the cavity can allow us to choose which quadrature correlator to measure, without sacrificing sensitivity. This is because free evolution is simply a rotation of the  $\hat{q}$  and  $\hat{p}$  operators in phase space. In terms of the entanglement signal that we receive, this is of course unaffected by this evolution. The quadrature correlation functions, however, *do* change with time. The rotation in phase space means that the large signal we can get in  $2 \langle \hat{q}_1 \hat{q}_2 \rangle$  directly after exiting the cavity transitions into a large signal for the other correlators as the atoms freely evolve, only for the signal later to be concentrated again in  $2 \langle \hat{q}_1 \hat{q}_2 \rangle$ . Since it is reasonable to assume that in any laboratory setup a small period of free evolution will be needed upon exiting the cavity before a quadrature measurement can be performed, it makes sense to take this extra parameter into account. Indeed if one correlator is easier to measure than another, then by controlling the extra time of free evolution of the atoms we may optimize the signal that we obtain from our correlator of choice. Conversely, if the amount of extra time of evolution is fixed, we can optimize what correlator to measure in order to maximize the signal. In other words, if the free evolution time is fixed, we can optimize for the values of  $\alpha_{1,2}, \beta_{1,2}$  in  $\langle (\alpha_1 \hat{q}_1 + \beta_1 \hat{p}_1)(\alpha_2 \hat{q}_2 + \beta_2 \hat{p}_2) \rangle$  to pick a correlator whose sensitivity to perturbations of the cavity length is maximal.

To demonstrate this point, we will consider the signal that we obtain from  $2 \langle \hat{q}_1 \hat{p}_2 \rangle$ , where we allow exactly a delay time  $\Delta t = T$  of free evolution for the atoms before looking at their state. We will see that by allowing this time, the signal we can get from this



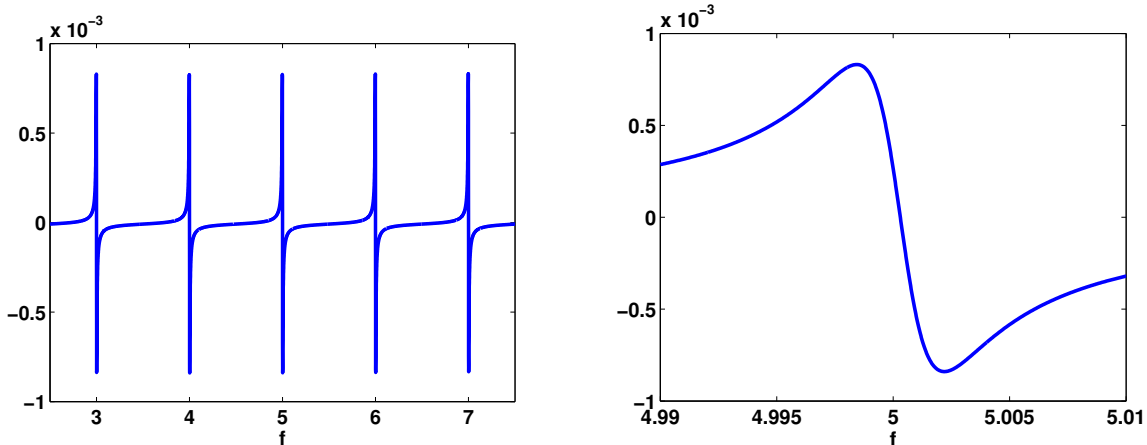


Figure 10.5: The steady-state value of  $2 \langle \hat{q}_1 \hat{p}_2 \rangle$  as a function of  $f = (T + \Delta t)/L_0$ , where  $\Delta t$  is the varied parameter. The other parameters are  $\Omega = \pi/L_0$  (resonant with the fundamental mode),  $T = 2.5L_0$ , and with the switching parameter  $\delta = 0.2T$

parameter is of the same strength as what would be expected from  $2 \langle \hat{q}_1 \hat{q}_2 \rangle$ , given Fig. 10.4. Let us consider the exact same scenario and parameters as those used in Fig. 10.3. The result is displayed in Fig. 10.6. Note that we achieve an order-of-magnitude variation from the steady-state value of  $2 \langle \hat{q}_1 \hat{p}_2 \rangle$  (approximately  $-0.25 \times 10^{-3}$ , as given by the initial value) due to the presence of the wave.

#### 10.4.4 Frequency response

An important question that must be answered is to what degree our proposed system is sensitive to a range of vibrational frequencies  $\gamma$ . To this end, we take a vibrational magnitude of  $A = (1 \times 10^{-3})L_0$  and consider the response due to a range of  $\gamma$  spanning over several orders of magnitude. For each frequency the wave will last for 10 periods, over however many atom-field interaction cycles are required for this time period. For each we will then take the maximum magnitude of  $2 \langle \hat{q}_1 \hat{p}_2 \rangle$  achieved over all cycles that occur during the wave. Figure 10.7 plots this quantity as a function of  $\log_{10} \gamma$  for two different sets of parameters, showing that our proposal can be tuned to be sensitive to a wide range of different frequencies.

We observe that for a given set of parameters we obtain a well-defined region of sensitivity, and furthermore by rescaling the parameters of our setup we can tune this to a region of our choosing. This rescaling involves modifying the initial length  $L_0$  of the cavity (thus

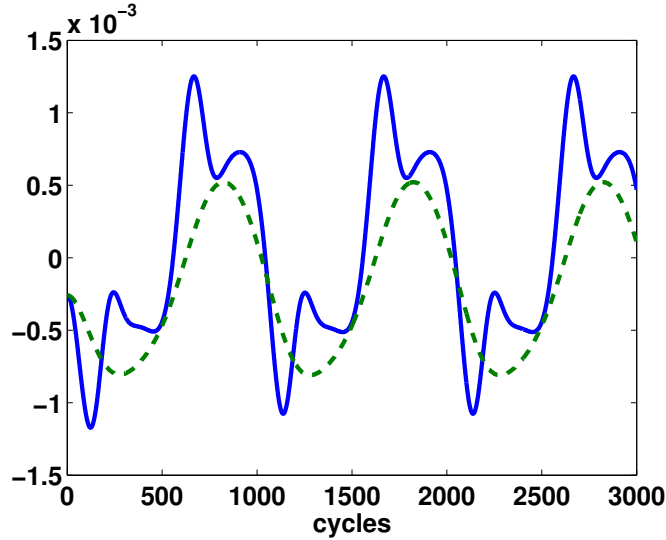


Figure 10.6: The correlation function  $2\langle\hat{q}_1\hat{p}_2\rangle$  per cycle during the period of vibration. The specific scenario and parameters are the same as in Fig. 10.3. The solid (blue) line corresponds to a vibrational amplitude of  $A = (1 \times 10^{-3})L_0$  and the dashed (green) line to  $A = (2 \times 10^{-4})L_0$ . Note that we achieve an order-of-magnitude increase in this quantity due to the presence of the wave, as compared to the steady state value (approximately  $-0.25 \times 10^{-3}$ , as given by the initial value in this plot).

changing the fundamental frequency) and also scaling the other dimensionful quantities accordingly, such that  $\lambda L_0$ ,  $\Omega L_0$ ,  $T/L_0$ ,  $\Delta t/T$ , and  $A/L_0$  remain the same. Such a scaling leaves invariant the dynamics of the system, and the exact same results are obtained from the calculation. This is, of course, assuming that the vibrational frequency has also been scaled accordingly. Thus, as we see an example of in Fig. 10.7, we can use this scaling to obtain sensitivity to different vibrational frequencies. If we have several such systems running concurrently, for example, then we would have achieved sensitivity over a large frequency range, as well as the capacity to distinguish and filter specific desired frequency regions.

#### 10.4.5 Experimental prospects

Here we briefly consider how the above results translate to what can actually be achieved using current superconducting circuit technology. As discussed above, the results that have been presented are invariant under a change of cavity length (fundamental frequency)

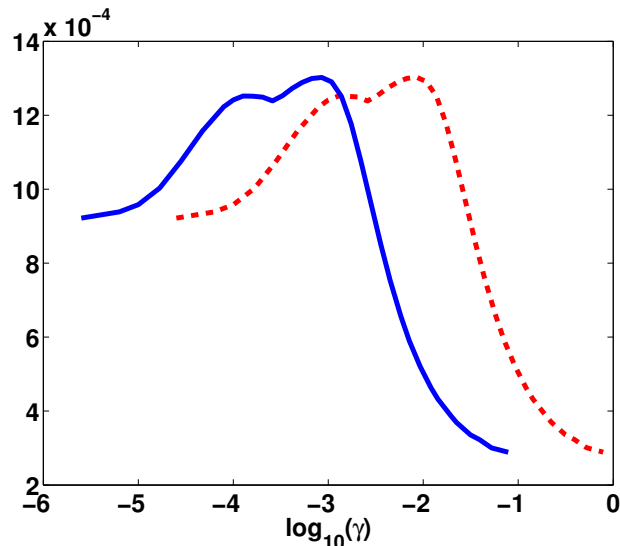


Figure 10.7: The maximum value of  $2\langle\hat{q}_1\hat{p}_2\rangle$  achieved over the course of 10 vibrational periods as a function of the log of the vibrational frequency  $\gamma$ . The parameters for the solid line (blue) are the same as for Fig. 10.6:  $L_0 = 8$ ,  $\Omega = \pi/L_0$ ,  $\lambda = 0.01$ , and  $T = 20$  with  $\Delta t = T$ . The dashed line (red) represents the case that all parameters have been scaled by an order of magnitude:  $L_0 = 0.8$ ,  $\Omega = \pi/L_0$ ,  $\lambda = 0.1$ , and  $T = 2$  with  $\Delta t = T$ . In both cases the amplitude of vibration is assumed to scale with the initial length, such that  $A = (1 \times 10^{-3})L_0$  always. We see that by scaling our system in such a way we can achieve sensitivity coverage over a range of vibrational frequencies.

as long as the other parameters are scaled accordingly. This means, in fact, that the magnitude of signal achieved above is exactly what can be achieved with current technology, since a coupling constant within the neighborhood of  $\lambda \sim 0.01\omega_1$  is achievable in the strong and ultra-strong coupling regimes [147]. With circuit QED systems one typically has a fundamental frequency of the order of the GHz's. On the other hand, given Figs. 10.6 and 10.7 we see that (somewhat surprisingly) the peak sensitivity of our proposal occurs at  $\gamma \sim 10^{-4}\omega_1$ . Thus within a cavity QED setup we can expect to be most sensitive to frequencies in the range  $\gamma \sim 10^5$  Hz. Remarkably, this is, for example, on the edge of the frequency range expected from gravitational radiation.

Given the current state of the art in superconductor technology one can in fact obtain significantly higher coupling constants than what we have considered above. Interestingly, however, we find that this does not significantly increase the seismograph sensitivity as compared with Fig. 10.6. This is because while the steady state entanglement indeed

increases (scaling as  $\lambda^2$ ), the valleys seen in Fig. 10.2 (which are fundamental to our proposed sensitivity) also become significantly wider and less sharp, meaning that a larger perturbation is required to displace the system out of the valley that it was prepared in. These two changes work against each other in such a way that they largely cancel out. Still, some improvement can be achieved with increased  $\lambda$ , approaching a signal magnitude near to  $2 \langle \hat{q}_1 \hat{p}_2 \rangle \approx 6 \times 10^{-3}$ .

This realization may actually be employed to further tune one’s apparatus based on experimental restrictions and the strength of vibration one is searching for, such that even typical optical couplings as small as  $\lambda = (10^{-6}\omega_1 - 10^{-5}\omega_1)$  may still be useful. By turning  $\lambda$  down, the valleys shown in Fig. 10.2 get sharper and thinner (increasing the sensitivity to very weak vibrations), while at the same time reducing the steady state (out of valley) height of the plot (decreasing the maximum response we can obtain). For stronger vibrations having a larger  $\lambda$  is preferable since the maximum response (achieved by exiting the valley) is increased. However for very weak vibrations it would actually be preferable to have a weaker coupling; a larger response would be observed in this case (assuming that  $\lambda$  is not so low as to make the maximum response unmeasurable).

## 10.5 Discussion

The quantum seismograph scheme consists of successively sending pairs of atoms in their ground state transversely through an optical cavity. As expected, this drives the cavity field to a metastable fixed point. Here we find that, surprisingly, the parameters of the farming protocol can be tailored so that the resulting metastable fixed point is highly sensitive to variations of external parameters, such as the cavity length. This in turn affects the correlations acquired by the pairs of atoms, which constitutes a detectable signal even for relatively small perturbations. We are proposing to exploit this sensitivity by utilizing the entanglement farming protocol for high precision measurements of small, length modulating vibrations: a quantum seismograph.

The proposed sensor has high sensitivity and a sharp spectral response, which should allow one to tune the seismograph to the detection of particular frequencies while screening out noise. The peak frequency in the spectral response of the seismograph can be tuned by adjusting the parameters of the setup.

This quantum seismograph proposal could be used to detect any kind of vibrational perturbation. In particular, if the cavity walls are coupled through some elastic force, the passage of a gravitational wave would induce vibrations on the positions of the walls [148],

opening the door to potentially using this construction as a novel approach to gravitational wave detection. Although our current work is still far from making a concrete proposal, we sketch how this scheme may be adapted to detect the passage of a gravitational wave in Appendix. F.

In addition to a seismograph, our sensor's settings can be easily adapted to carry out measurements of different parameters of the entanglement farming setup, such as the coupling strength, the atomic gap or the travel time of the pairs of atoms. In this sense, our proposal may have many further metrological applications outside of seismology. In addition, the extreme sensitivity that we have uncovered in the entanglement farming scenario is likely characteristic of any number of other quantum mechanical systems that are capable of displaying the resonant behavior we have used here. This approach may thus be far more general, and an extended study of the fundamental physics at play is warranted.

Finally, it should also be very interesting to study the quantum seismograph's behavior when the measured parameters behave quantum mechanically. This could potentially yield a new method for measuring mechanical quantum fluctuations, such as those of positions or distances. For example, the length of the cavity may be uncertain due predominantly to quantum fluctuations—e.g., if the cavity mirrors are harmonically bound, ultracold, and put into a state that is nearly pure. We leave such questions to future work.

## Part III

# Localized Projective Measurements

In this part of the thesis we will turn to another model of measurement that is very different from the particle-detector setup we have so far worked with. Here, we will take as inspiration the usual projective measurement postulate of quantum mechanics and consider projective measurements onto single field modes. As a model for measurement this represents a relativistic generalization of the Glauber model [149], in which we assume we may construct quadratic quadrature expectation values (i.e. covariance matrix elements) of a given field mode based on the results of projective measurements on that mode. The derivation and exposition of this formalism as it applies here are given in [150, 151]. Note that in this Part we will move away from cavity field physics and considering instead free space fields. We will also be making direct use of the Rindler quantization scheme as explained in Sect. 4.3.

Typically, as we have seen, the mode basis that one expands a field in is a global basis, meaning that those modes cover the whole space being considered (or, in the case of a cavity, the whole cavity). Given that the free Hamiltonian of the theory is a globally defined operator, typically it makes computational sense to define one's working basis as such. Operationally, however, in a world where a laboratory is confined to some localized region, it would really make more sense to consider a basis consisting of local modes (or at least semi-localized). Given this, we imagine a scenario in which an observer, perhaps undergoing non-inertial motion, carries a measurement device designed to filter out all but some localized mode function  $\psi$  and then perform projective Fock state measurements on this mode. Assuming we are working with a Gaussian field state, the reduced covariance matrix of this mode will provide all of the measurement statistics that such an observer is expected to obtain. In particular, we consider localized modes  $\psi(x, t)$  that are positive frequency, meaning that they share a vacuum state with the standard Minkowski plane-wave modes. This implies that an inertial observer in the vacuum state will, by definition, measure zero particles under this prescription. As explained in [150], while certainly an idealization as we consider it here, such a procedure can be experimentally implemented by use of a light lens fabricated to capture the specific mode of interest (which will be of the size of the lens). This lens will then focus the mode into a single-mode optical fiber, thus filtering out all other field modes, which transmits the light to a photon detector [152, 153].

Here we use such a model to study the effects of non-inertial motion. For example if an observer carrying such a measurement device is undergoing uniform acceleration then, assuming the integrity of the device isn't compromised by the acceleration, the local mode that is filtered will be that mode defined with respect to the Rindler coordinate system, as defined in Eq. (4.28). That is, while an inertial observer with coordinates  $(x, t)$  will projectively measure mode function  $\psi(x, t)$ , a uniformly accelerating observer will instead measure that mode given by  $\psi(\xi, \tau)$ . Given that the transformation from Minkowski to

Rindler modes is non-passive,  $\psi(\xi, \tau)$  will *not* be positive frequency with respect to the Minkowski mode basis, even though  $\psi(x, t)$  is so by definition. Such an observer will therefore measure particle content in the Minkowski vacuum, as should be expected from the Unruh effect.

We will perform two studies in this Part of the thesis, using this measurement model. In Ch. 11 we will consider the response of a uniformly accelerating observer. Unlike the typical case in which one assumes the field state is the Minkowski vacuum, we will instead take it to be a Minkowski thermal state (i.e. the field is thermal as seen by a given inertial observer). To the author's knowledge such a scenario has not been (properly) studied previously, as the calculational difficulties are very intensive. We find, however, that this setting can be analyzed using the technology of the local projective measurement formalism. We find that the response of such an observer has two contributions, one from acceleration and one from field thermality. Interestingly, these two contributions are distinguishable. Next, in Ch. 12, we will take on a historically seminal scenario of interest in the relativistic quantum information community: the degradation of quantum correlations due to acceleration. That is, if two observers share some entangled field state, how does the acceleration of one or both observers affect the amount of entanglement they may access from this state? Our work is different from the large collection of work on this setting in that, while the others have considered entangled states of global field modes, we use the more physically realistic case of local modes. With this change, we find that the degradation of both entanglement and quantum discord is in fact qualitatively worse than that claimed in the previous works.



# Chapter 11

## Accelerating in a thermal bath

Note: this chapter represents a work in progress, in collaboration with Andrzej Dragan.

Here we consider applying the technique introduced in [150, 151] to describe what a uniformly accelerating observer would detect if, rather than the scalar field being in the global (Minkowski) vacuum state, it is instead in a thermal state of some temperature  $T$ . As we saw in Sect. 4.5, if the field is in the vacuum state then a uniformly accelerating observer with acceleration  $a$  will think themselves in a thermal bath of temperature  $T_U = a/2\pi$ , and that they will be unable (at least according to their field-detection mechanism) to determine whether this thermality originates from the field or from their acceleration. This raises a question: is an observer of this type even in principle able to measure their acceleration? In addition to purely theoretical interest, such a question is of critical importance for any future experimental proposal aimed at detecting the Unruh effect. To be successful, such a proposal must be capable of distinguishing between a genuine Unruh response and standard thermal noise from the environment.

This leads to the primary question that we would like to answer in this chapter: is the response of a measurement device with acceleration temperature  $T_1 = a/2\pi$  in a thermal bath of temperature  $T_2$  the same as that of an equivalent device with acceleration temperature  $T_2$  in a thermal bath of temperature  $T_1$ , or different? Put informally, can we distinguish between quantum and thermal fluctuations? Unfortunately, the scenario of uniform acceleration within a Minkowski thermal state has been studied very little, due to the calculational difficulties involved. Those works that have examined the issue, [154, 155], focus on detector response rates or spectra. Here, we will use the projective measurement formalism to obtain the complete *state* of a localized, accelerated mode, this being necessary to make a complete statement about distinguishability or indistinguishability of

quantum and thermal fluctuations.

The answer to this question was attempted in [156], and their result was that the two are indistinguishable. However, in this work the actual field state that was considered was *not* a Minkowski thermal state but rather a thermal state with respect to the Unruh mode basis (recall the Unruh modes from Sect. 4.3). While it is true the Unruh basis shares a vacuum state with the Minkowski mode basis, this does not mean that a thermal state with respect to the Unruh basis (the physicality of which is extremely suspect since the Unruh modes are not of definite-energy) may at all be used as an approximation for a Minkowski thermal state (i.e. the thermal state defined with respect to the free Hamiltonian that actually describes the field theory). Indeed in such a setup it is not at all surprising that they find indistinguishability between the two responses, as this follows directly from the Gaussian mechanics of applying a two-mode squeezing operation (from the Unruh basis to the Rindler basis) on a thermal state.

Here, we will instead consider Minkowski thermal states. In this case we find, unlike the previously mentioned work, that indeed our measurement device *can* distinguish between the Unruh and thermal responses. Concretely, the localized, accelerated mode being measured is in a thermal state with symplectic eigenvalue equal to the product of two individual symplectic eigenvalues,  $\nu = \nu_U(a)\nu_{\text{th}}(T, a)$ , where  $\nu_U(a)$  represents the standard Unruh response and  $\nu_{\text{th}}(T, a)$  is due to the field thermality. We find that this second contribution depends non-trivially on the acceleration  $a$ , and indeed in such a way that brings into question the validity of Rindler quantization. The result will also, however, suggest at the possibility of using acceleration as a means of very low-temperature thermometry.

## 11.1 Calculations

We take our detector mechanism to be a projective measurement on some given (semi-localized) mode of the field. To make the measurement meaningful we demand that this mode be a purely positive-frequency linear combination of whatever mode-basis the observer uses to describe the field. If the observer is stationary, their detection mode would be a linear combination of positive-frequency Minkowski modes. If the observer is uniformly accelerating, however, his or her mode will consist of positive-frequency Rindler modes, which will generally have negative-frequency contribution in the Minkowski basis. It is this latter case that we will consider, and we will label the annihilation operator of the accelerating detector-mode by  $\hat{d}$ , and the corresponding spatial function by  $\psi$ . We take the observer to be confined to the right-hand Rindler wedge, as in Fig. 4.1, so this mode will consist of right-hand Rindler modes only. In terms of the Minkowski ladder operator

$\{\hat{a}_k, \hat{a}_k^\dagger\}$  (with corresponding mode functions  $u_k$ ) and the (right-hand) Rindler operators  $\{\hat{b}_\ell, \hat{b}_\ell^\dagger\}$  (with corresponding mode functions  $w_\ell$ ) we have in general

$$\hat{d} = \int dk [(\psi, u_k) \hat{a}_k + (\psi, u_k^*) \hat{a}_k^\dagger] = \int d\ell (\psi, w_\ell) \hat{b}_\ell, \quad (11.1)$$

where here  $(\cdot, \cdot)$  is the Klein-Gordon inner product as defined in Eq. (4.5).

In order to take the field state to be in a global (Minkowski) thermal state, it will be easiest to consider a pure state of two orthogonal fields (only one of which is the actual field that our detector projects onto) consisting of two-mode squeezed states between the modes of the two fields (i.e. the mode  $k$  of one field to be squeezed with the mode  $k$  of the other by some amount, for all  $k$ ), such that upon tracing out one of the fields we are left in a thermal state. The pure state of the two fields is thus given by  $\hat{S}_{12} |0\rangle |0\rangle$ , where  $\hat{S}_{12}$  is the appropriate squeezing operation. Specifically, in order to put each individual field into a thermal state of temperature  $T$  the two-mode squeezing parameter for mode  $k$  must be  $s_k = \tanh^{-1}(e^{-|k|/2T})$ . Given this, the squeezing operation is fully specified by its action on the annihilation operators of the fields. This is given by

$$\hat{S}_{12}^\dagger \hat{a}_k \hat{S}_{12} = \cosh(s_k) a_k + \sinh(s_k) \hat{a}_k^{(2)\dagger}, \quad (11.2)$$

where  $\hat{a}_k^{(2)}$  are the annihilation operators of the secondary field. The corresponding action on  $\hat{a}_k^\dagger$  follows immediately from this.

We can use this technology to very easily obtain expressions for the response of a detector that performs a projective measurement of mode  $\psi$ . We simply evaluate what the state of this specific mode is. Since the field that we consider is in a Gaussian state, we can fully characterize the state of mode  $\psi$  by its  $2 \times 2$  covariance matrix  $\sigma$ . Following the definition of Eq. (3.5), in terms of the mode ladder operators the entries of this matrix are

$$\sigma_{11} = \langle (\hat{d} + \hat{d}^\dagger)^2 \rangle, \quad (11.3)$$

$$\sigma_{22} = -\langle (\hat{d} - \hat{d}^\dagger)^2 \rangle, \quad (11.4)$$

$$\sigma_{12} = \sigma_{21} = -\frac{i}{2} \langle (\hat{d} + \hat{d}^\dagger)(\hat{d} - \hat{d}^\dagger) + (\hat{d} - \hat{d}^\dagger)(\hat{d} + \hat{d}^\dagger) \rangle, \quad (11.5)$$

where here the expectation value is taken with respect to the pure state  $\hat{S}_{12} |0\rangle |0\rangle$ . Because the mode  $\psi$  only has support over one of the fields these expectation values will be equivalent to those taken with respect to a thermal state of that specific field only.

From Eqs. (11.1,11.2) it is straightforward to evaluate these entries of the covariance matrix in terms of the overlaps between  $\psi$  and the Minkowski modes. This gives the result

$$\boldsymbol{\sigma} = \int dk \left( \cosh(s_k)^2 + \sinh(s_k)^2 \right) \begin{pmatrix} |(\psi, u_k)^* + (\psi, u_k^*)|^2 & 2 \operatorname{Im}((\psi, u_k)(\psi, u_k^*)) \\ 2 \operatorname{Im}((\psi, u_k)(\psi, u_k^*)) & |(\psi, u_k)^* - (\psi, u_k^*)|^2 \end{pmatrix}. \quad (11.6)$$

At times, we will use the notation  $\tilde{\alpha}_k \equiv (\psi, u_k)^*$  and  $\tilde{\beta}_k \equiv -(\psi, u_k^*)^*$ , in the usual sense of a Bogolyubov transformation from the Minkowski basis to the detector mode. We can put this covariance matrix into another form by taking  $\cosh(s_k)^2 = 1 + \sinh(s_k)^2$  and using

$$\int dk |(\psi, u_k)^* + (\psi, u_k^*)|^2 = \int dk |(\psi, u_k)^* - (\psi, u_k^*)|^2 = 1 + 2 \int dk |\tilde{\beta}_k|^2. \quad (11.7)$$

To obtain these we used the Wronskian condition  $\int dk (\tilde{\alpha}_k \tilde{\alpha}_k^* - \tilde{\beta}_k \tilde{\beta}_k^*) = 1$  and the fact that  $\int dk \tilde{\alpha}_k \tilde{\beta}_k = 0$  (this follows from defining  $\psi$  as positive frequency in the Rindler basis, which will be straightforward to see once we define the Rindler and Unruh modes). With this we see that the covariance matrix takes the form

$$\boldsymbol{\sigma} = (1 + 2 \int dk |\tilde{\beta}_k|^2) \begin{pmatrix} 1 & 0 \\ 0 & 1 \end{pmatrix} + 2 \int dk \sinh(s_k)^2 \begin{pmatrix} |(\psi, u_k)^* + (\psi, u_k^*)|^2 & 2 \operatorname{Im}((\psi, u_k)(\psi, u_k^*)) \\ 2 \operatorname{Im}((\psi, u_k)(\psi, u_k^*)) & |(\psi, u_k)^* - (\psi, u_k^*)|^2 \end{pmatrix}. \quad (11.8)$$

Now, let us consider expressing this state using overlaps of  $\psi$  with (right-hand) Rindler modes. Let  $\alpha_{\ell k}$  and  $\beta_{\ell k}$  be the Bogolyubov coefficients associated with the right Rindler wedge, such that  $u_k = \int dk (\alpha_{\ell k}^* w_\ell - \beta_{\ell k} w_\ell^* + \text{left wedge})$ . Since  $\psi$  is assumed to have support only on the right-hand wedge and to be purely positive frequency in the Rindler basis (i.e.  $(\psi, w_\ell^*) = 0$ ) we have

$$(\psi, u_k) = \int d\ell \alpha_{\ell k}^* (\psi, w_\ell), \quad (\psi, u_k^*) = - \int d\ell \beta_{\ell k}^* (\psi, w_\ell). \quad (11.9)$$

From here we see for example that

$$\begin{aligned} \int dk |\tilde{\beta}_k|^2 &= \int \int d\ell d\ell' (\psi, w_\ell) (\psi, w_{\ell'})^* \int dk \beta_{\ell k}^* \beta_{\ell' k} \\ &= \int d\ell \frac{|(\psi, w_\ell)|^2}{e^{2\pi|\ell|/a} - 1}, \end{aligned} \quad (11.10)$$

where in the second line we have used well-known properties of the Rindler modes [39]. This is exactly the standard particle content  $\langle n_U \rangle$  expected from the Unruh response, the

contribution from each Rindler mode being weighted by that mode's contribution to our detector mode  $\psi$ . We see from Eq. (11.8) that in the case of zero field temperature ( $s_k = 0$ ) the detector measures exactly the Unruh response that should be expected. I.e. the state of the detector mode is a thermal state (in the sense that  $\sigma \propto \mathbf{I}$ ) with symplectic eigenvalue  $\nu = 1 + 2 \langle n_U \rangle$  (recall Eq. (3.21)). This of course is previously well-known, and what we are interested in here is the case where the field state is thermal.

To continue, let's actually specify the form of the Rindler Bogolyubov coefficients  $\alpha_{\ell k}$  and  $\beta_{\ell k}$ . The process of deriving these is quite intensive, and we will not reproduce the derivation here. The calculation can be found in [85] which, upon using the identity  $|\Gamma(iy)| = \sqrt{\pi/y \sinh(\pi y)}$  and the freedom to use the Bogoliubov coefficients up to overall phases, we find that

$$\alpha_{\ell k} = \begin{cases} \sqrt{\frac{1}{2\pi a|k|}} \sqrt{\frac{1}{e^{2\pi|\ell|/a} - 1}} e^{\pi|\ell|/a} e^{-i\frac{|\ell|}{a} \ln(\frac{|k|}{a})} & \text{if } \ell \text{ and } k \text{ same sign} \\ 0 & \text{if otherwise} \end{cases} \quad (11.11)$$

and

$$\beta_{\ell k} = -\alpha_{\ell k} e^{-\pi|\ell|/a}, \quad (11.12)$$

where here  $a$  is the acceleration. For convenience we will actually consider using another function (which happens to be equivalent to an Unruh Bogolyubov coefficient, but that doesn't even need to come into play here) which we define as

$$A_{\ell k} \equiv \frac{1}{\cosh r_\ell} \alpha_{\ell k} = \begin{cases} \frac{1}{\sqrt{2\pi a|k|}} e^{-i\frac{|\ell|}{a} \ln(\frac{|k|}{a})} & \text{if } \ell \text{ and } k \text{ same sign} \\ 0 & \text{if otherwise} \end{cases} \quad (11.13)$$

where  $r_\ell \equiv \tanh^{-1}(e^{-\pi|\ell|/a})$ .

With this, let us continue on to try to calculate the elements of Eq. (11.6). Consider for example the factor  $|(\psi, u_k)^* + (\psi, u_k^*)|^2$  in  $\sigma_{11}$ . To make things simpler, we will define  $\psi$  to be such that its overlap with the Rindler modes  $(\psi, w_\ell)$  are all real-valued. With this we have

$$|(\psi, u_k)^* + (\psi, u_k^*)|^2 = \int \int d\ell d\ell' (\psi, w_\ell) (\psi, w_{\ell'}) (\alpha_{\ell k} - \beta_{\ell k}^*) (\alpha_{\ell' k}^* - \beta_{\ell' k}) \quad (11.14)$$

$$= \int \int d\ell d\ell' (\psi, w_\ell) (\psi, w_{\ell'}) \cosh(r_\ell) \cosh(r_{\ell'}) (A_{\ell k} + A_{\ell k}^* e^{-\pi|\ell|/a}) (A_{\ell' k}^* + A_{\ell' k} e^{-\pi|\ell'|/a}) \quad (11.15)$$

$$= \int \int d\ell d\ell' (\psi, w_\ell) (\psi, w_{\ell'}) [\cosh(r_\ell + r_{\ell'}) \text{Re}(A_{\ell k} A_{\ell' k}^*) + \sinh(r_\ell + r_{\ell'}) \text{Re}(A_{\ell k} A_{\ell' k})], \quad (11.16)$$

where in the last line we have done several things: we have used the fact that  $e^{-\pi|\ell|/a} \cosh(r_\ell) = \sinh(r_\ell)$ , that  $\cosh(x+y) = \cosh(x)\cosh(y) + \sinh(x)\sinh(y)$  and  $\sinh(x+y) = \cosh(x)\sinh(y) + \sinh(x)\cosh(y)$ , and then noted that the imaginary parts of the integrand vanish upon integration due to antisymmetry under  $\ell \leftrightarrow \ell'$  (as of course they must since we are computing a squared magnitude). It is similarly shown that

$$|(\psi, u_k)^* - (\psi, u_k^*)|^2 \quad (11.17)$$

$$= \int \int d\ell d\ell' (\psi, w_\ell)(\psi, w_{\ell'}) [\cosh(r_\ell + r_{\ell'}) \operatorname{Re}(A_{\ell k} A_{\ell' k}^*) - \sinh(r_\ell + r_{\ell'}) \operatorname{Re}(A_{\ell k} A_{\ell' k})], \quad (11.18)$$

and

$$2 \operatorname{Im}((\psi, u_k)(\psi, u_k^*)) = - \int \int d\ell d\ell' (\psi, w_\ell)(\psi, w_{\ell'}) \sinh(r_\ell + r_{\ell'}) \operatorname{Im}(A_{\ell k} A_{\ell' k}). \quad (11.19)$$

Then, to actually compute the elements of the covariance matrix in Eq. (11.6) we need to integrate these over  $k$  and with the appropriate factor  $(\cosh(s_k)^2 + \sinh(s_k)^2)$ , which we will label  $\nu_k$  since this is exactly the thermal symplectic eigenvalue of Minkowski mode  $k$ . Expressing this in terms of exponentials gives

$$\nu_k = \frac{e^{-|k|/T} + 1}{e^{-|k|/T} - 1}. \quad (11.20)$$

Then, the entries of the covariance matrix are given, for example, by

$$\sigma_{11} = \int dk \nu_k |(\psi, u_k)^* + (\psi, u_k^*)|^2 \quad (11.21)$$

$$= \operatorname{Re} \frac{1}{2\pi a} \int_0^\infty \frac{dk}{k} \nu_k \int \int d\ell d\ell' (\psi, w_\ell)(\psi, w_{\ell'}) \left[ \cosh(r_\ell + r_{\ell'}) e^{i\frac{-\ell+\ell'}{a} \ln(\frac{k}{a})} + \sinh(r_\ell + r_{\ell'}) e^{i\frac{-\ell-\ell'}{a} \ln(\frac{k}{a})} \right] \quad (11.22)$$

where the  $k$  integration is only over half the line because the Rindler modes are zero when  $k$  and  $\ell$  are different signs; since the only dependence is on  $|k|$  we can just take the integration over the positive half. We can do the change of variable to  $y = \frac{1}{a} \ln(\frac{k}{a})$  to get

$$\sigma_{11} = \operatorname{Re} \frac{1}{2\pi} \int_{-\infty}^\infty dy \nu(y) \int \int d\ell d\ell' (\psi, w_\ell)(\psi, w_{\ell'}) \left[ \cosh(r_\ell + r_{\ell'}) e^{i(-\ell+\ell')y} + \sinh(r_\ell + r_{\ell'}) e^{i(-\ell-\ell')y} \right], \quad (11.23)$$

where

$$\nu(y) = \frac{e^{\frac{\alpha}{T}e^{\alpha y}} + 1}{e^{\frac{\alpha}{T}e^{\alpha y}} - 1}. \quad (11.24)$$

We similarly have

$$\sigma_{22} = \text{Re} \frac{1}{2\pi} \int_{-\infty}^{\infty} dy \nu(y) \int \int d\ell d\ell' (\psi, w_\ell) (\psi, w_{\ell'}) \left[ \cosh(r_\ell + r_{\ell'}) e^{i(-\ell + \ell')y} - \sinh(r_\ell + r_{\ell'}) e^{i(-\ell - \ell')y} \right], \quad (11.25)$$

and

$$\sigma_{12} = \sigma_{21} = -\text{Im} \frac{1}{2\pi} \int_{-\infty}^{\infty} dy \nu(y) \int \int d\ell d\ell' (\psi, w_\ell) (\psi, w_{\ell'}) \sinh(r_\ell + r_{\ell'}) e^{i(-\ell - \ell')y}. \quad (11.26)$$

From here we will make some approximations. Let us define our detector mode to be a Gaussian of positive frequency, such that in  $k$ -space it is peaked at some defined frequency  $\Omega_d$ , with thickness  $\tilde{L}$  such that

$$(\psi, w_\ell) = \frac{1}{(\sqrt{\pi}\tilde{L})^{1/2}} \exp\left(-\frac{(\ell - \Omega_d)^2}{2\tilde{L}^2}\right). \quad (11.27)$$

Recalling that  $(\psi, w_\ell)$  are just the  $\alpha$  coefficients of an (approximately) purely positive frequency Bogoliubov transformation, the normalization constant is such that this overlap satisfies the Wronskian condition  $\int d\ell |(\psi, w_\ell)|^2 = 1$ . Now, in obtaining Eqs. (11.23, 11.25, 11.26) we have made no assumptions about what the overlap  $(\psi, w_\ell)$  is aside from that it be real. What we want, however, is a purely positive frequency mode (in the Rindler basis) such that  $(\psi, w_\ell) = 0$  for  $\ell < 0$ . Our choice, Eq. (11.27), while mathematically convenient, does not strictly satisfy this. We can, however, make it approximately so by dictating that the peak frequency is large compared to the width of the Gaussian:  $\Omega_d \gg \tilde{L}$ . Given this assumption we can significantly simplify our expressions for the elements of  $\boldsymbol{\sigma}$ . It is straightforward to demonstrate that  $\sigma_{12}$  and  $\sigma_{21}$ , as well as the second terms in  $\sigma_{11}$  and  $\sigma_{22}$  (i.e. those with  $\sinh(r_\ell + r_{\ell'})$ ), will vanish for purely positive frequency  $(\psi, w_\ell)$  upon integration. For our choice of mode, these terms can be shown to go as  $\sim \exp(-\Omega_d^2/\tilde{L}^2)$ . Thus we can drop these terms by assuming  $\Omega_d \gg \tilde{L}$ , giving us  $\sigma_{11} = \sigma_{22}$  (just retaining the first term in each) and  $\sigma_{12} = \sigma_{21} = 0$ . Namely, our projective detector mode is in a thermal state.

Considering the remaining factor in  $\sigma_{11} = \sigma_{22}$ , we see that we can factor the two  $\ell$  integrations (by expanding  $\cosh(r_\ell + r_{\ell'})$  into a product again) and then we get integrals of

the form

$$\int d\ell(\psi, w_\ell)e^{\pm i\ell y} \cosh(r_\ell), \quad \int d\ell(\psi, w_\ell)e^{\pm i\ell y} \sinh(r_\ell). \quad (11.28)$$

We will now take another approximation by assuming that the acceleration scale is small compared to the energy scale of our detector,  $\Omega_d \gg a$ . I.e. we assume a small Unruh response. Given this, the functions  $\cosh(r_\ell)$  and  $\sinh(r_\ell)$  vary so little over the integration of the Gaussian that it can be well approximated as a constant, evaluated at  $\ell = \Omega_d$ . The integrals then reduce to Fourier transforms of  $(\psi, w_\ell)$  which, given our choice in Eq. (11.27), evaluate to

$$\int d\ell(\psi, w_\ell)e^{\pm i\ell y} = (2\sqrt{\pi}\tilde{L})^{1/2} \exp\left(-\frac{\tilde{L}^2 y^2}{2} \pm i\Omega_d y\right). \quad (11.29)$$

Given these approximations, it is then easy to work out that

$$\sigma_{11} = \sigma_{22} \approx \frac{\tilde{L}}{\sqrt{\pi}} \left( \frac{e^{2\pi\Omega_d/a} + 1}{e^{2\pi\Omega_d/a} - 1} \right) \int_{-\infty}^{\infty} dy \nu(y) e^{-\tilde{L}^2 y^2}, \quad (11.30)$$

where, again,

$$\nu(y) = \frac{e^{\frac{a}{T}e^{\alpha y}} + 1}{e^{\frac{a}{T}e^{\alpha y}} - 1}. \quad (11.31)$$

Notice that if the field is in its vacuum state,  $T = 0$ , then  $\nu(y) = 1$  and we obtain exactly the Unruh response that we would expect. In the case of nonzero temperature what we find is that  $\sigma$  is a thermal state with a symplectic eigenvalue that is the product of two symplectic eigenvalues, one corresponding to the standard Unruh response and the other being a thermal contribution from the field that depends nontrivially on the acceleration of our observer. Importantly, we note that this state is *not* symmetric between exchange of the Unruh temperature  $T_U = a/2\pi$  and the temperature of the field,  $T$ . This disproves the claim made in [156]. Indeed, interestingly, while the Unruh response appears unaffected by the Minkowski field temperature, the response from the field thermality depends strongly on the acceleration of the observer.

This result is, however, troublesome from several different perspectives. First, we see that the response from the field thermality is *independent* of the peak detector frequency  $\Omega_d$  (it does, however, depend on the bandwidth  $\tilde{L}$ ). Mathematically this occurs because  $\Omega_d$  only comes in as a phase in Eq. (11.29). These phases cancel with each other when



performing the double integration over  $\ell$  and  $\ell'$  in the first (non-vanishing) terms of Eqs. (11.23,11.25). This only occurs given our approximation  $\Omega_d \gg a$  and, given this, the result is not overly surprising since a single Rindler frequency has non-vanishing contributions from *all* Minkowski frequencies, and this becomes more so the case as  $a$  becomes smaller. Within the parameter range valid for the approximations made this result should hold. Clearly there is a first order correction to these approximations that, presumable, would indeed depend on  $\Omega_d$ . Second, it appears that in place of the detector energy gap determining how strongly the field temperature is felt, it is instead the acceleration that determines this! That is, as  $a$  decreases the detector feels the field thermality *more strongly*. Very roughly, we have

$$\sigma \sim \left( \frac{e^{2\pi\Omega_d/a} + 1}{e^{2\pi\Omega_d/a} - 1} \right) \left( \frac{e^{a/T} + 1}{e^{a/T} - 1} \right) \mathbf{I}. \quad (11.32)$$

What is troubling about this behavior is that as  $a \rightarrow 0$  the response diverges. Clearly this is unphysical, as we know that at exactly  $a = 0$  the detector will simply observe the standard thermal fluctuations of the field. While it is possible that one or more of the assumptions we have made is obscuring a more correct result in the small  $a$  limit, ultimately this behavior comes from the variable transformation  $y = \frac{1}{a} \ln(\frac{k}{a})$  that was made right before Eq. (11.23), which was before any approximations were made. It is known that the Rindler transformation is ill-defined in the  $a \rightarrow 0$  limit, and this appears to be what we are seeing here. As already said, as  $a$  becomes smaller a single Rindler frequency becomes *more* spread out in Minkowski  $k$ -space, including in the ultra-low frequency regime. As  $a$  decreases, the mode  $\psi$  has a larger and larger overlap with lower and lower Minkowski frequencies, thus inducing a larger and larger thermal response from the finite field temperature. The divergence derives from the fact that the Minkowski zero-mode is infinitely excited from any finite temperature. Fortunately, as such, this problem is alleviated if we apply a Minkowski IR cutoff to the thermal field. Applying such a cutoff at  $k_{\min} = \Lambda$  corresponds to applying a lower limit of  $y_{\min} = \ln(\Lambda/a)/a$  to the integral in Eq. (11.30). Critically, we have  $y_{\min} \rightarrow \infty$  as  $a \rightarrow 0$ . As this limit is taken, therefore, the integration window falls well outside the Gaussian present in Eq. (11.30) and thus we have an exponential falloff that halts the divergence in this limit.

## 11.2 Discussion

In this chapter we have used a basic model of measurement in field theory, [150, 151], to examine what occurs when an observer uniformly accelerates not in the Minkowski vacuum

but rather in a Minkowski thermal state. Under a set of approximations we have arrived at the result that such an observer measures their detection mode to be in a thermal state of symplectic eigenvalue equal to Eq. (11.30), which is the product of two symplectic eigenvalues, one being the standard Unruh response and the other being an acceleration-dependent thermal contribution from the field temperature. We see, among other things, that these two contributions are distinguishable. That is, an observer is able to distinguish the case in which he or she is accelerating at rate  $a = 2\pi T_1$  through a Minkowski bath of temperature  $T_2$  from the case that they accelerate with  $a = 2\pi T_2$  through a bath of temperature  $T_1$ . This is in contrast to the claim made in [156].

Our result, however, has troubling behavior in the small  $a$  limit that does not appear to be the result of any approximation. Namely, in the small  $a$  regime the response resulting from the field temperature becomes *stronger* with decreasing acceleration. In the  $a \rightarrow 0$  limit the response diverges, which is clearly not physical. The Rindler transformation is known to be ill-defined in this limit, and we will therefore not concern ourselves with this limit specifically, especially since the problem would probably be alleviated if we were to apply an IR cutoff to the thermal field. Rather, let us take the result at face value and consider the implications of amplifying thermal fluctuations through the use of small acceleration.

This result has two consequences of potential experimental interest. First is in regards to actually detecting the Unruh effect in the laboratory, the primary problem with this being the enormous accelerations necessary to obtain a measurable thermal response. If, on the other hand, in the “low” acceleration regime there is a strong amplification induced of existing thermal fluctuations in one’s system then this may very well be more easily measured. While this is not the Unruh effect per say, a successful experiment of this kind would certainly lend credence to its existence in nature. Alternatively, one may instead consider using small accelerations as a means of ultra-cold temperature thermometry. If a small acceleration is able to amplify in a predictable way otherwise undetectable thermal fluctuations, then this would be a means of not only detecting them but of computing their associated ultra-cold temperature. Before attempting this leap, of course, we should better understand the nature of this effect and its limitations, which are clearly not depicted in our formulation here. We leave a better understanding of our results to future work.

## Chapter 12

# Quantum correlations in accelerated frames: local versus global modes

Note: this chapter derives from the work [7], in collaboration with Jason Doukas, Andrzej Dragan, and Robert B. Mann.

In this chapter we will use the local projective measurement formalism to study, from a different perspective, a seminal scenario of interest within the relativistic quantum information community. In this setting one considers the entanglement shared between two observers, Alice and Rob, in the case that Alice is inertial whereas Rob is uniformly accelerating. The Unruh radiation experienced by Rob is expected to degrade the entanglement between the two parties, and characterizing this degradation (as well as that of quantum discord) was for years a primary line of research within the community, e.g. [157, 158, 159, 160, 161, 162, 135, 10, 163] among, frankly, many others (see [7] for a more comprehensive list). Such a program is of interest, for example, in determining the capacity of non-inertial observers to perform quantum teleportation protocols. As expected, these works found that quantum correlations decay due to acceleration, limiting their use in non-inertial settings. In particular, the qualitative trend among these studies is that the entanglement shared between the observers reaches zero only in the infinite-acceleration limit, and the discord (known to generally be more robust to decohering noise) remains finite even in this limit.

It was eventually realized, however, that there were some serious problems with the standard way that researchers were going about examining this scenario [164]. Namely, the field state that was commonly considered was an entangled state of Unruh mode Fock states (recall the Unruh modes from Sect. 4.3). This has been referred to as the

single mode approximation (not to be confused with the single mode approximation in quantum optics). A fundamental problem with this setup is that, by the definition of the Unruh modes, by varying the acceleration of Rob one was not simply seeing the effect of acceleration on the accessible entanglement of a given state but was rather changing the state under consideration itself.

Another problem with the old approach in general, and the one we will be focusing on here, is that the field states previously under consideration were entangled between Fock states of global field modes, spread over all space. While mathematically convenient, this clearly represents an unphysical situation. A laboratory is a local setup, and the entanglement that we may experimentally probe and utilize will therefore be between localized modes. Attempts to move past this problem within the old framework have proven very challenging [165]. Here we will tackle the problem of using localized modes in this scenario from the perspective of local projective measurement, utilizing previous calculations obtained in [151]. We will take the field state to be the vacuum but for a two mode squeezed state between localized wavepackets, one of which is measured by inertial Alice and the other by accelerating Rob.

As with previous research in this subject, we find that both entanglement and discord are damaged by the acceleration of Rob. However, the transition from global to local modes appears to produce a qualitatively different decay pattern than those results obtained in the papers listed above. In particular, here we find that the entanglement shared decays to zero at *finite* acceleration, and that the discord decays to zero in the infinite-acceleration limit. That is, the degradation due to acceleration in any realistic setup will be qualitatively worse than previously thought.

## 12.1 Setting

First let us define the sort of field states that we will consider in this chapter. Consider two arbitrary field modes with annihilation operators  $\hat{a}$  and  $\hat{b}$ , with associated (possibly unlocalized) wave-packets  $\phi_A$  and  $\phi_B$ , respectively. We will assume that  $\phi_A$  and  $\phi_B$  are superpositions of positive frequency Minkowski plane waves only. These modes correspond to two inertial observers, Alice and Bob, whom we assume each have full access to their respective modes. Our intention is to view this state from the perspective of two observers: Alice who is inertial and has access to mode  $\phi_A$ , and Rob, who has uniform acceleration  $a$  and thus only has possibly partial access to Bob's mode  $\phi_B$ , due to the Rindler horizon experienced by Rob. This setup is illustrated Fig. 12.1.

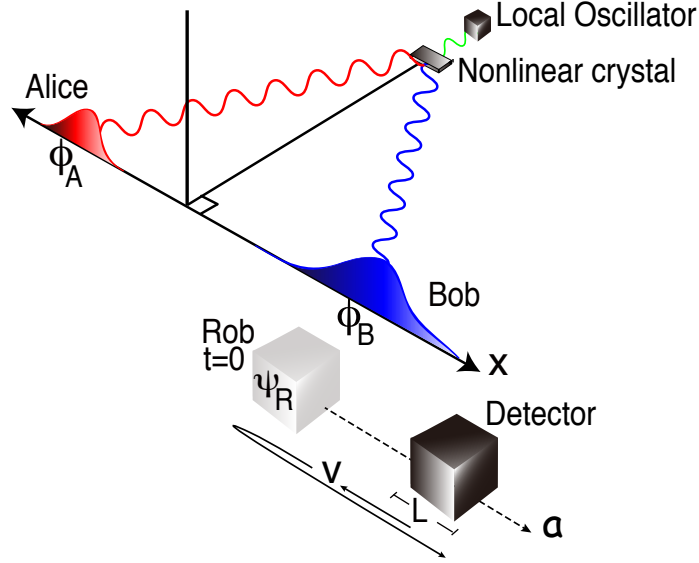


Figure 12.1: A schematic of the type of setup we consider. A two-mode squeezed state is produced from a non-linear crystal in two Gaussian modes  $\phi_A$  (Alice) and  $\phi_B$  (Bob). An observer Rob accelerating with constant proper acceleration  $a$  in the  $x$ -direction carries a detector that makes measurements of the field in a mode  $\psi_R$  at time  $t = 0$  when his velocity,  $v$ , is zero.

For the Bell-type entangled Fock state commonly used in previous analyses (see citations above) the considered state is given by  $(1 + \hat{a}^\dagger \otimes \hat{b}^\dagger)|0\rangle$ . However here we are primarily interested in the two-mode squeezed state of the form  $\exp\left[s(\hat{a}^\dagger \hat{b}^\dagger + \hat{a}\hat{b})\right]|0\rangle$ , with squeezing parameter  $s$ . We suppose Alice (Rob) is in the possession of an inertial (accelerating) detector that projectively measures the mode of the field  $\psi_A(x, t)$  ( $\psi_R(\xi, \tau)$ ), where  $(\xi, \tau)$  are the Rindler coordinates as defined by Eq. (4.28), such that Rob is located at  $\xi = 0$  and his proper time is  $\tau$ . In the same manner that we obtained Eq. (11.8) in the previous chapter, the joint covariance matrix of the state  $\exp\left[s(\hat{a}^\dagger \hat{b}^\dagger + \hat{a}\hat{b})\right]|0\rangle$  as observed by Alice

and Rob is straightforwardly computed to be [151]

$$\begin{aligned} \boldsymbol{\sigma} = & \mathbf{I} + 2 \langle n_U \rangle \begin{pmatrix} 0 & 0 & 0 & 0 \\ 0 & 0 & 0 & 0 \\ 0 & 0 & 1 & 0 \\ 0 & 0 & 0 & 1 \end{pmatrix} + 2 \sinh^2 s \begin{pmatrix} |\alpha|^2 & 0 & 0 & 0 \\ 0 & |\alpha|^2 & 0 & 0 \\ 0 & 0 & |\beta + \beta'^*|^2 & 2 \operatorname{Im}(\beta\beta') \\ 0 & 0 & 2 \operatorname{Im}(\beta\beta') & |\beta - \beta'^*|^2 \end{pmatrix} \\ & + \sinh 2s \begin{pmatrix} 0 & 0 & -\operatorname{Re}[\alpha(\beta + \beta'^*)] & -\operatorname{Im}[\alpha(\beta - \beta'^*)] \\ 0 & 0 & -\operatorname{Im}[\alpha(\beta + \beta'^*)] & \operatorname{Re}[\alpha(\beta - \beta'^*)] \\ -\operatorname{Re}[\alpha(\beta + \beta'^*)] & -\operatorname{Im}[\alpha(\beta + \beta'^*)] & 0 & 0 \\ -\operatorname{Im}[\alpha(\beta - \beta'^*)] & \operatorname{Re}[\alpha(\beta - \beta'^*)] & 0 & 0 \end{pmatrix}, \end{aligned} \quad (12.1)$$

where  $\alpha \equiv (\psi_A, \phi_A)$ ,  $\beta \equiv (\psi_R, \phi_B)$ ,  $\beta' \equiv (\psi_R, \phi_B^*)$ , these being mode overlaps with respect to the usual Klein-Gordon inner product, Eq. (4.5). Here  $\langle n_U \rangle$  is the average particle number Rob would measure if he were accelerating through the Minkowski vacuum,

$$\langle n_U \rangle = \int d\ell \frac{|(\psi_R, w_\ell)|^2}{e^{2\pi|\ell|/a} - 1}, \quad (12.2)$$

as in Eq. (11.10), where  $w_\ell$  are the (right-wedge) Rindler modes.

Here is where our approach diverges somewhat from that of the last chapter, and where we will rely on the lengthy calculations already performed in [151]. We assume that Alice's detector  $\psi_A$  perfectly detects the mode  $\phi_A$ , i.e.,  $\psi_A = \phi_A$ . We therefore have that  $\alpha = 1$ . Unlike in the last chapter, however, we will assume that for each acceleration Rob may choose a detector that maximizes the entanglement extracted from the considered state. In this formalism, the degradation of quantum correlations comes ultimately from two factors. The first, and obvious, is that Rob will experience decohering Unruh noise on his part of the state. The second is the fact that an accelerating Rob can not perfectly match his detector mode  $\psi_R$  to the mode  $\phi_B$ . This occurs because a portion of  $\phi_B$  will generally be beyond the Rindler horizon experienced by Rob. As Rob's acceleration increases he gets closer to this horizon, and thus the mode mismatch becomes worse and the decay of quantum correlations along with it. We assume that, given an acceleration  $a$ , Rob may optimally tune his detection mode to obtain the best measurement possible. It has been shown in [151] that Rob's optimal choice is given by

$$\psi_R = \frac{\int_{\Lambda}^{\infty} d\ell (w_\ell, \phi_B) w_\ell}{\sqrt{\int_{\Lambda}^{\infty} d\ell |(w_\ell, \phi_B)|^2}}, \quad (12.3)$$

where  $\Lambda$  is a cut-off frequency of the detector <sup>1</sup>.

Once we have chosen a mode  $\phi_B$ , found the corresponding optimal detection mode  $\psi_R$  for Rob, and computed the resulting quantities  $\beta$ ,  $\beta'$ , and  $\langle n_U \rangle$ , then we have the covariance matrix Eq. (12.1). Again, we assume that Alice is capable of perfectly tuning her detector to her part of the two-mode squeezed state,  $\alpha = 1$ . From here it is an easy matter to compute the logarithmic negativity and the Gaussian quantum discord, Eqs. (3.34) and (3.36) respectively, and observe how they behave as a function of Rob's acceleration. For example from the formula for the logarithmic negativity we know that the state will become separable when the smallest partially transposed symplectic eigenvalue,  $\tilde{\nu}_-$ , becomes unity. This occurs when  $\tilde{\Delta} = 1 + \det\sigma$ , where  $\tilde{\Delta} = \det\sigma_A + \det\sigma_R - 2\det\gamma$  and where  $\sigma_A$ ,  $\sigma_R$ , and  $\gamma$  are the upper left (Alice) block, lower right (Rob) block, and the upper right off-diagonal block of Eq. (12.1) respectively. For our covariance matrix, this is equivalent to the condition

$$|\beta|^2 = \langle \hat{n}_U \rangle \left( 1 - \frac{|\beta'|^2}{1 + \langle \hat{n}_U \rangle} \right). \quad (12.4)$$

Roughly, we see that entanglement vanishes as the Unruh noise  $\langle n_U \rangle$  becomes comparable to the overlap  $\beta$  between  $\phi_B$  and  $\psi_R$ , as makes intuitive sense.

We will now go on to consider two different scenarios: one in which the field state is put into a two-mode squeezed state using global Unruh modes, so as to compare our formalism with previous work, and one in which we take a two-mode squeezed state of local modes.

## 12.2 Global analysis

As we will see in the next section, by using local modes we obtain qualitatively different results from those obtained in previous literature using global Unruh modes [157, 158, 159, 160, 161, 162, 135, 10, 163]. In these papers the field state under consideration was taken to be  $(1 + \hat{a}^\dagger \otimes \hat{d}_\Omega^{(1)\dagger})|0\rangle$ , where  $\hat{d}_\Omega^{(1)}$  is an Unruh mode annihilation operator (recall Sect. 4.3) and here we label the modes by the dimensionless parameter  $\Omega = |\ell|/a$ . This parameter  $\Omega$

---

<sup>1</sup>We are compelled to introduce an IR cutoff because of divergences in the low Rindler frequency limit of the integrand. However, this cutoff is also required on physical grounds since no detector can resolve arbitrary low frequencies. Indeed, the wavelength of the IR cutoff is naturally related to the physical dimension  $L$  of the detector. One might also have expected a UV cutoff. However, for the Gaussian mode considered the integrand vanishes for large  $k$ , and therefore the integrals are independent of any (sufficiently) large UV cutoff.

is that which the previous literature varied over in order to see the effects of acceleration on quantum correlations. As is clear, however, such an approach does not correspond to seeing how observers of different acceleration see the same state, but rather corresponds to changing the field state itself!

Given this, before going on to a (correct) local mode analysis in Sect. 12.3, it is important to ensure that the differences we will see there are due to the fact that we use local modes in place of global ones, rather than being due to the different overall approach being taken (i.e. two-mode squeezed states rather than Fock states). To this end, let us first perform an analysis using our method where we consider the field state to be in an Unruh two-mode squeezed state of the form  $\exp\left[s(\hat{a}^\dagger \hat{d}_\Omega^{(1)\dagger} + \hat{a} \hat{d}_\Omega^{(1)})\right] |0\rangle$ . If, given this setting, we obtain the same qualitative results as those achieved in previous studies, then we can be assured that our differing results in the local analysis of Sect. 12.3 are in fact due to the local nature of its setup.

In the present case of the Unruh two-mode squeezed state, i.e. in which  $\phi_B$  is an Unruh mode of parameter  $\Omega$ , the analysis becomes very simple. It is easy to see that the optimal mode  $\psi_R$  that Rob can use, Eq. (12.3), is exactly the right-wedge Rindler mode  $\psi_R = w_\ell$  of frequency  $\ell = a\Omega$  (clearly, delocalized). From here, the parameters that go into our covariance matrix, Eq. (12.1), are computed to be

$$\beta = \cosh r_\Omega, \tag{12.5}$$

$$\langle n_U \rangle = \sinh^2 r_\Omega, \tag{12.6}$$

$$\beta' = 0, \tag{12.7}$$

where  $r_\Omega = \tanh^{-1}(e^{-\pi\Omega})$ .

Given all of this, in Fig. 12.2 we choose  $s = 1$  and plot the logarithmic negativity and the Gaussian quantum discord (both  $D(A, B)$  and  $D(B, A)$ , which recall are not necessarily equivalent) as a function of  $z \equiv e^{-2\pi\Omega} = \langle n_U \rangle / (\langle n_U \rangle + 1)$ , where the function  $z$  has been chosen to rescale the entire frequency domain down to the unit interval. As expected, we see a degradation of all quantities. In particular we see that the entanglement decays to zero, but only in the  $\Omega \rightarrow 0$  ( $z = 1$ ) limit. This qualitatively matches the results obtained in the previous literature. We also see that in this limit the discord  $D(B, A)$  asymptotes to a finite value. Similarly, this result matches the behavior previously observed using the Unruh-mode Fock states [135]. It is also possible to find an analytic expression for this residual discord as a function of the squeezing parameter:  $\lim_{\Omega \rightarrow 0} D(B, A) = 2 \log(\coth s) \sinh^2 s$ . Curiously, this function quickly asymptotes to a value of  $1/\ln 2$  for large squeezing values  $s$ . This means that even though the correlations could be arbitrarily large in the inertial



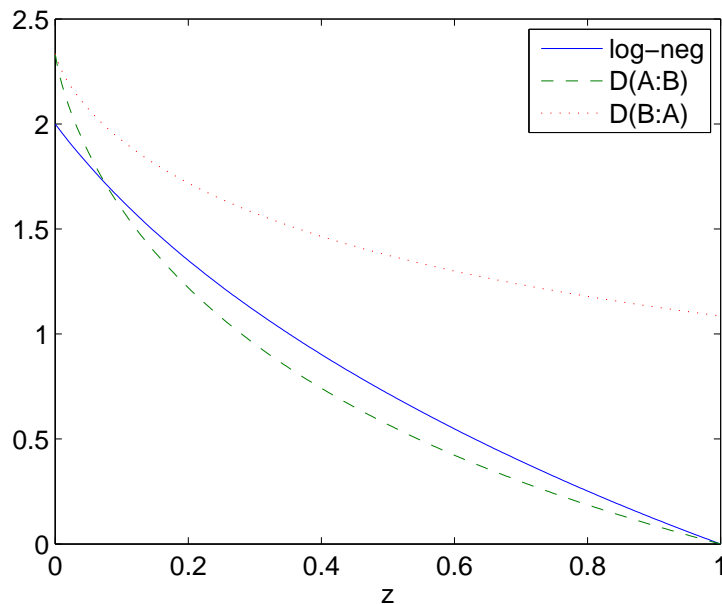


Figure 12.2: A plot of logarithmic negativity  $E_N$  (blue, solid), discord  $D(A, B)$  (green, dashed) and discord  $D(B, A)$  (red, dotted) as functions of  $z = e^{-2\pi\Omega}$ , where the state in consideration is a two-mode squeezed state using Unruh modes with squeezing parameter  $s = 1$ . We see that  $E_N$  and  $D(A, B)$  decay to zero as  $\Omega \rightarrow 0$  whereas  $D(B, A)$  asymptotes to a finite value.

frame (arbitrarily large squeezing), in the accelerating frame they will always be bounded by this amount. On the other hand, we observe that when the optimized measurement is over Rob's subsystem, the discord  $D(A, B)$  decays to zero in the  $\Omega \rightarrow 0$  limit. It is worth pointing out that this novel result is computationally intractable in the analogous Fock state scenario.

We have confirmed what we set out to confirm in this section: that by using Unruh modes within our formalism we obtain the same qualitative behavior as that seen in the previous literature. We are now able to continue on to a local-mode analysis and, presumably finding different results, be assured that these differences are due to the local versus global nature of the modes in question rather than the difference in taking a Fock state versus a squeezed state.

## 12.3 Local analysis

Here, we will take the mode  $\phi_B$  to be semi-localized to some length  $L$ . Specifically, we will let it be a Gaussian in frequency space with some positive peak frequency, meaning that in position space it takes the form

$$\begin{aligned}\phi_B(x, 0) &= \frac{1}{\sqrt{N}\sqrt{2\pi}} \exp\left[-\frac{x^2}{L^2} + i\frac{N}{L}x\right] \\ \partial_t\phi_B(x, 0) &= -i\frac{N}{L}\phi(x, 0),\end{aligned}\tag{12.8}$$

where  $L$  characterizes the width of the mode and  $N/L$  is the characteristic frequency of the mode. We assume that the accelerated observer, Rob, passes through the centre of this mode at  $t = 0$  and we choose the origin of the Rindler frame accordingly. Equivalently, we can keep the accelerated frame fixed and translate the mode  $\phi_B(x) \rightarrow \phi_B(x - 1/a)$ .

Unlike in the previous section, the computation of Rob's optimized mode  $\psi_R$  and of the parameters  $\beta$ ,  $\beta'$ , and  $\langle n_U \rangle$  is quite intensive and must be performed numerically. In the interest of brevity and relevance we will not delve into these details here, but the reader may find an expanded discussion of this procedure in [151]. Here, we will simply use the numerics developed in that paper to explore the questions of interest here.

Before continuing, it is worth noting that in [150, 151] an explicit detector model was used which was assumed to have finite extent  $L$  and perform measurements of the field at  $t = 0$ . The detector cut-off wavelength,  $1/\Lambda$ , was therefore naturally related to the size of the detector, since wavelengths larger than this would be difficult to resolve. It was further assumed that the whole detector was approximately accelerating at a constant proper acceleration throughout the whole of the device, which placed the constraint  $aL \ll 1$  on the magnitude of accelerations that could be explored for a given size of the mode. Here we go beyond this limit, and in particular investigate large accelerations. To do so we assume that the detector can focus Bob's mode,  $\phi_B$ , down to a size small enough so that it is measured in a small neighbourhood about the centre of the detector,  $\xi = 0$ . This position corresponds to the path followed by the hypothetical point-like accelerated observer Rob. Thus, while the focusing lens and other detector components are assumed to be rigid (and thus must accelerate at different rates), the measurement itself takes place in a region where the acceleration and proper-time have an approximately unique value.

As mentioned in Sect. 12.1, the degradation of quantum correlations in this formalism comes both from the standard Unruh noise experienced by Rob but also from the fact that an accelerating Rob is not able to perfectly tune his detector to measure the Gaussian  $\phi_B$ .

In the large acceleration limit, the center of  $\phi_B$  asymptotes to the position  $x = 0$  and the penetration of the mode through the horizon stabilizes to an approximately constant value (i.e. half of the mode is located outside Rob's horizon). This means that the parameter  $\beta$  asymptotes to a finite value for large accelerations. On the other hand the average Unruh particle content continues to grow with acceleration. In the infinite acceleration limit,  $\langle n_U \rangle$  will also diverge. The interplay of these two behaviors leads to an interesting conclusion not previously realized in global mode studies of the entanglement degradation in non-inertial frames: the entanglement extractable by Alice and Rob for large enough acceleration will always lead to an entanglement sudden death. To see this we recall that the state transitions from entangled to separable when the condition in Eq. (12.4) is satisfied. In the considered range of parameters  $|\beta'|^2$  is typically small and so the entanglement sudden death occurs, for all values of initial squeezing, when the average vacuum particle number is approximately as large as  $|\beta|^2$ .

Indeed, we plot in Fig. 12.3 the entanglement and discords as a function of acceleration up to  $aL = 70$ , in the case that the squeezing parameter is  $s = 1$ . The results of this calculation confirm that the entanglement in this state experiences sudden death at a finite acceleration. This is in contrast to the entanglement behavior seen when considering Unruh modes, as claimed in previous literature and shown in Fig. 12.2. Furthermore, in the large acceleration limit it is straightforward to demonstrate that, given the behavior of  $\beta$  and  $\langle n_U \rangle$  just discussed, both the discords  $D(A, B)$  and  $D(B, A)$  as computed by Eq. (3.36) will vanish in the  $aL \rightarrow \infty$  limit. This, similarly, is markedly different from the previously obtained result in [135].

This realization, that there is a qualitative difference between the localized and delocalized settings, is important because of the considerable amount of work in the literature that uses delocalized Unruh modes in order to study acceleration-induced entanglement degradation. The use of these modes was for computational ease and it has been argued that they should produce qualitatively the same behavior as would more realistic, localized setups. We have demonstrated here that this is in fact not the case. Indeed the origin of this difference is easily discernible within our formalism. As discussed, in the localized setting the entanglement experiences sudden death because the overlap parameter  $\beta$  asymptotes to a finite value whereas the noise  $\langle n_U \rangle$  continues to rise with acceleration. In the global scenario, on the other hand, the  $\beta$  parameter in Eq. (12.6) does not cease increasing as  $\Omega \rightarrow 0$  (equivalent to the infinite acceleration limit). Indeed we see that in this limit the relationship becomes  $\beta \approx \sqrt{\langle n_U \rangle}$ . Thus the off-block-diagonal terms (i.e. those that represent correlations) in the covariance matrix of Eq. (12.1) increase comparably with the diagonal terms, and some presence of quantum correlations can therefore exist even in this limit.

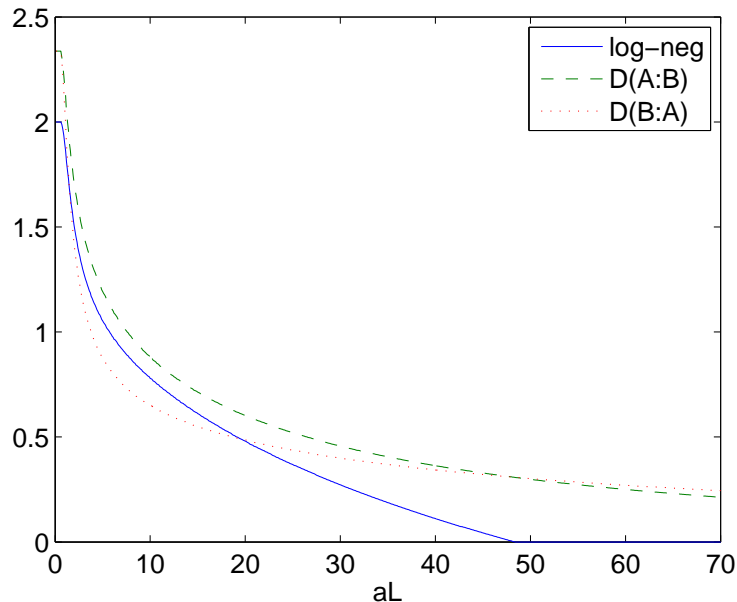


Figure 12.3: A plot of logarithmic negativity  $E_N$  (blue, solid), discord  $D(A, B)$  (green, dashed) and discord  $D(B, A)$  (red, dotted) as functions of acceleration, where the state being considered is the two-mode squeezed state, with squeezing parameter  $s = 1$ , and with Bob’s mode in the localized Gaussian,  $\phi_B(x - 1/a)$  with  $N = 6$  and cut-off value chosen to  $\Lambda L = \frac{1}{3}$ . We see that, unlike when Unruh modes are used, the entanglement experiences sudden death at a finite acceleration. The quantum discord remains even beyond this point of entanglement extinction. Both of the discords, however, decay to zero in the  $aL \rightarrow \infty$  limit.

## 12.4 Discussion

We have used the formalism developed and explored in [150, 151] to study the Unruh-degradation of quantum correlations in two-mode squeezed states, and in particular to understand the difference between the cases of localized Gaussian modes and the delocalized Unruh modes so often used in the literature, [157, 158, 159, 160, 161, 162, 135, 10, 163] among others. Although most past studies that used Unruh modes did so with Fock states, rather than squeezed states, we have shown that the degradation of quantum correlations are qualitatively equivalent between the two cases. In regards to this we have found that the non-vanishing quantum discord previously observed in the case of a zero frequency Unruh mode appears only to be true when the optimized measurement is over Alice’s

subsystem but not so when it is over Rob's.

Comparing the cases of localized and delocalized modes reveals qualitatively different results, indicating that many of the conclusions presented in previous literature may have to be reconsidered. In particular we have found in the localized modes that the entanglement reaches a point of sudden death at a finite acceleration, and that the quantum discord vanishes in the infinite acceleration limit (both  $D(A, B)$  and  $D(B, A)$ ). That is, the acceleration induced degradation of quantum correlations appears to be significantly *worse* than previously thought, when considering more physically realistic setups. This realization may be of central importance in the development of relativistic quantum information in and out of the laboratory. While we have previously discussed in this thesis ways in which relativistic effects may aid us in quantum informational tasks, the present scenario certainly appears to be one in which they harm us. Understanding the limitations imposed by acceleration-induced decoherence, and perhaps ways of overcoming these limitations, has and still is a topic of concern within this field. Further studies that use localized scenarios, but which utilize different formalisms from ours, will represent important next steps in scrutinizing the generality of our results.

## Part IV

What does it mean for half of an  
empty cavity to be full?

In the last Part of thesis (not including the conclusion) we will take a single chapter to discuss a very different, but arguably more powerful and general operational view of vacuum fluctuations and entanglement. We have seen much with regards to vacuum entanglement in this thesis. Ultimately, both it and the vacuum fluctuations with which it goes hand in hand are a result of the fact that the vacuum state is defined with respect to global operators. The elementary excitations of quantum field theory are countable, a crucial feature for making it able to deal with the physics of elementary particles. These are described by operators which carry information about the energy momentum that these excitations take or give to the field. The vacuum state of the field is then that from which no quanta can be removed. Excitations of this state then describe the states with one or more particles with well defined momenta. This positive energy Fock quantization provides simple global operators for the field as a whole. However, it is important to recognize that what we call a particle under this definition is an entirely delocalized excitation (i.e. of definite momentum). This clearly goes against our intuitive notion of what a particle is supposed to be, as a localized entity. Theoretically, the total number of particles carried by any specified configuration is easy to address, but it is clear that this construction lacks appropriate tools to inquire on the local properties of the field. A question as simple as “where is this particle?” is difficult to address if not by indirect means due to the lack of a local particle number operator. The problem is that this construction does not admit states that assign zero probabilities outside bounded regions of space. In short, powerful as it is, the standard Fock basis associated with stationary modes of the global Hamiltonian provide only a feeble scaffolding for digging into issues pertaining to the localization of quanta. Here we will use an alternative local Fock space representation [166] that enables us to address these questions.

The indefiniteness of local particle content means that the reduced state of a field localized to some given region will generally be mixed, and therefore excited! It follows, since globally the vacuum is a pure state, that this region must be entangled with other regions of space, as we well know. Relativistic quantum phenomena involving the observer-dependence of particle number, such as the Unruh and Hawking effects, are often attributed to this, as we saw in Sect. 4.3. Moreover, vacuum entanglement occurs also in enclosed systems, such as an optical cavity or a superconducting circuit. This introduces a conceptually challenging fact: at least formally, *half of an empty box is not empty*. This is a mathematical result which alone gives us little intuition towards actual physical consequences. Under what operational conditions does this phenomenon present itself; what physically sensible measurements (in general) can be made to give this mathematical fact experimental significance? In the following chapter we shall give a precise answer to this question.

# Chapter 13

## Slamming a mirror

Note: this chapter derives from the work [8], in collaboration with Marco del Rey, Hans Westman, Juan León, and Andrzej Dragan.

If an experimentalist has an empty (vacuum state) optical cavity in their laboratory then, as just discussed, in some sense the left-side of cavity contains photons (indeed, many), as does the right-side. What can the experimentalist do to detect these particle in, say, the left-hand side? The answer, as will be explained, is to very quickly introduce a physical boundary (in this case a mirror) between the two sides of the cavity, thus blocking off any influence from the right-hand side while the experimentalist measures the left-hand side. Of course, quickly introducing a boundary (i.e. quickly modifying the Hamiltonian) produces particles similar to what occurs in the dynamical Casimir effect (DCE) [115], which has recently been experimentally observed [112]. The key observation of this chapter is that these real excitations, created by slamming down the mirror, are mathematically equivalent to the local particles attributed to the subregions prior to the introduction of the mirror. This is what it operationally means for half of an empty box to be non-empty. In addition to giving a satisfying interpretation to the question of local particle content, this realization also suggests a simple experimental setup that can be used to reveal, measure, and perhaps even utilize vacuum entanglement.

In this chapter we consider both massive and massless scalar fields in a one-dimensional cavity with Dirichlet boundary conditions (i.e. mirrors on the ends). We perform several tasks. We begin by discussing the difficulties that appear when we intend to measure local vacuum excitations and the different scenarios that could allow us to circumvent them. We will be using the formalism of local quantization introduced in [166], which allows us to characterize the reduced state of a sub-region in the cavity and study its local properties



formally. We will utilize Gaussian quantum mechanics in order to easily compute and characterize the reduced states of sub-cavity regions and the correlations between them, explaining how this equivalently describes the physics of slamming mirror(s) into the cavity. We will discuss and analyse the spatial structure of entanglement between regions, similar to what has been done in [167] for lattice systems.

We will move on to consider what occurs if a mirror is very quickly introduced into the cavity, discussing the time-evolution of the system after this occurs and observe what one would expect: a burst of particles propagating away from it. These excitations, however, are mathematically one and the same with those previously attributed to vacuum entanglement in the local analysis (the only difference is that now they evolve according to a different Hamiltonian). Equivalently, the real excitations produced in the left and right-hand sides are quantum entangled. We later consider the case in which two mirrors are simultaneously introduced, some distance apart. In this case the particles produced in the left and right-hand sides (but ignoring the middle section) can similarly be entangled, despite no common mirror between them. This is possible because, as follows from the main point of our work, the entanglement is simply that which was already present in the vacuum prior to the introduction of the mirror. The energy introduced into the system, in the form of real quanta, provides the necessary resource with which the previously present vacuum entanglement manifests itself.

Lastly, we discuss the experimental feasibility of simulating this scenario to verify vacuum entanglement using current technologies. We note that introducing a mirror in fact represents a very efficient means of harvesting the vacuum entanglement, since afterwards you have two new cavities that contain *all* of the entanglement (up to a UV cut-off determined by how fast the mirror is introduced). This entanglement could then be a resource for quantum computational tasks. This method of harvesting could potentially be much more promising than the usual proposed method of locally interacting a pair of other quantum systems (e.g. artificial atoms) with the field [168, 44, 5], since this is severely limited by the interaction strength.

### **13.1 How does one measure the vacuum excitations in a subregion?**

To begin, we need to ask ourselves in a general sense what one must do in order to measure localized vacuum fluctuations. What operational procedures can be implemented to do this? Mathematically these fluctuations can arise when tracing out a spatial region

of a vacuum field. That is, because there is entanglement between spatial regions, the reduced state of such a region must necessarily be mixed (and therefore excited). This thus motivates the idea that at least one possible way of measuring these excitations is to isolate oneself to only the subregion of interest. But this means more than simply staying at a fixed location. As we will show later in more detail, a stationary detector interacting with a vacuum field only at a given point or region will still register zero particle detection if it is allowed to measure for a long enough time. Rather, isolating oneself to only a subregion means losing causal contact with the outside; information cannot be allowed to reach our observer from outside the region of interest. Uniform acceleration, for example, is one way of achieving this [21, 39]. Another way is for one to turn their detection device on for only a short time  $\Delta t$ ; doing this ensures that the detector is causally isolated from any part of space more than a distance  $c\Delta t$  away from it. Indeed switching one's detector on fast enough does cause spurious detection events [1, 169], however it is questionable if this can be fully attributed to vacuum excitations (i.e. to entanglement) inside a cavity since formally the probability of detection limits to zero only as  $\Delta t \rightarrow \infty$ , which is clearly larger than the cavity length.

Are there any other ways to isolate oneself from outside influence? Indeed, another option that gets the job done is simply to erect a physical boundary. In the cavity scenario this corresponds to placing a perfect mirror at the bipartition boundary. Certainly once such a mirror is installed then an observer in the left-side of the cavity will receive no information from the right-side. Would such an observer then be free to measure local vacuum excitations? How could it be that such a setup suddenly allows the observer to measure what they could not have beforehand? Furthermore, one should be concerned about the fact that quickly placing a mirror in the middle of the cavity is expected to create real particle excitations, similar to what occurs in the dynamical Casimir effect (DCE) [115, 112]. That is, by rapidly changing (in this case, introducing) a boundary condition we are rapidly modifying the Hamiltonian of the system. This will create real excitations in the field that will propagate away from the mirror upon being introduced, and an observer located on one side of this mirror will detect these excitations. Will these particles interfere with the observer's ability of detect the local vacuum excitations that are associated with entanglement between regions?

The answer, as we will elaborate, is that a detection of the mirror-created particles *is* exactly a detection of the local entanglement excitations.

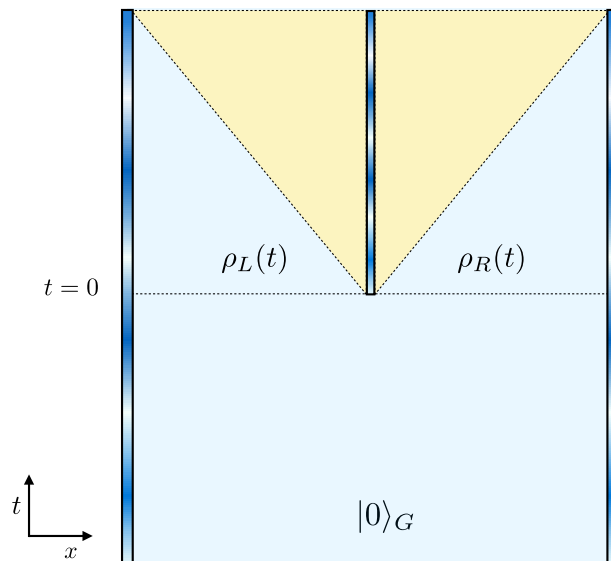


Figure 13.1: Sketch of the one dimensional cavity setting. We start ( $t < 0$ ) considering a cavity in its vacuum state  $|0\rangle_G$ . At some instant ( $t = 0$ ) we slam a mirror separating the cavity into two regions. As explained in the text, the normal modes in these separated subcavities correspond to the localized modes of the cavity without mirror, which we will show suffice to analyze states, correlations and particle production after slamming the mirror. The horizontal line corresponds to  $t = 0$ , the diagonal lines represent the light cone starting at the slamming event.

## 13.2 Formulation and setting

The first purpose of this section is to present a mathematical framework for the computation and analysis of global cavity states using a local formalism. We will start describing the quantum states in the cavity by introducing a bipartition of it into two subregions, precisely those in which the cavity will eventually be separated by the introduction of a slamming mirror at some instant of time. Later on, in the second part of this section, we will use this formalism to study the physical scenario where a mirror is abruptly introduced in the middle of the cavity.

We will find it convenient to do a change of notation from that used throughout the rest of this thesis. This is because, as we will see, a defined set of local modes will be the primary basis with respect to which we represent the cavity field, as opposed to the global modes of the cavity. Thus, throughout this chapter we will ascribe mode functions

$u_m(x, t)$  of frequencies  $\omega_m$  and corresponding annihilation operators  $\hat{a}_m$  to a set of *local modes* (the definition of which we will see below). On the other hand, we will use the notation  $U_n(x, t)$ ,  $\Omega_n$ , and  $\hat{A}_n$  to respectively denote the mode functions, frequencies, and annihilation operators of the global modes.

### 13.2.1 Local mathematical analysis: local vs. global modes

Here we will briefly introduce the field-theoretic formalism required for our analysis [39, 166].

The aim is to spell out what can be ascertained about the physics of a non-localized state spanning the whole cavity, as is the case of the quantum vacuum and generic cavity states, by using localizing mathematical tools. We do not yet introduce a mirror in the middle of the cavity. We will postpone this to the next subsection, once the present goal is achieved.

We will consider a scalar field  $\hat{\phi}(x, t)$  of mass  $\mu$  within a Dirichlet cavity of length  $R$ , such that  $x \in [0, R]$  and  $\hat{\phi}(0, t) = \hat{\phi}(R, t) = 0$ . The standard, stationary set of modes with respect to which we expand  $\hat{\phi}$  are what we will refer to here as the *global modes*  $U_n$ , as given by Eq. (4.54). In the notation of this chapter, these mode functions are

$$U_n(x, t) = \frac{1}{\sqrt{R\Omega_n}} \sin\left(\frac{\pi n x}{R}\right) e^{-i\Omega_n t} = \mathcal{U}_n(x) e^{-i\Omega_n t}, \quad (13.1)$$

where  $\Omega_n^2 = \frac{\pi^2 n^2}{R^2} + \mu^2$  is the frequency of mode  $n$ . As explained in Ch. 4, this choice is convenient because the corresponding Fock states are energy eigenstates of the free-field regularised Hamiltonian (which we will also call the *global Hamiltonian*)

$$\hat{H}_G = \sum_{n=1}^{\infty} \Omega_n \hat{A}_n^\dagger \hat{A}_n, \quad (13.2)$$

where here  $\{\hat{A}_n, \hat{A}_n^\dagger\}$  are the ladder operators corresponding to the global modes. As has often been the case throughout this thesis, we will be primarily interested in the vacuum state of the field, which here we specify as being the *global vacuum state*  $|0_G\rangle$ , defined to satisfy  $\hat{A}_n |0_G\rangle = 0$  for all  $n$ . This is the state of lowest energy with respect to  $\hat{H}_G$ , and is said to be the state of zero particles, because no A quanta can be removed from it, i.e. a cavity in this state is empty (although not from a local point of view as we discuss later).

While the field decomposition into the global modes is often the most convenient and physically relevant choice, we can also consider a decomposition into a mode basis better

suiting to study the local physics of a subregion inside the cavity. Say that we decompose our cavity into two regions, one that runs within  $x \in [0, r]$  (the left side) and the other within  $x \in [r, R]$  (the right side). The lengths of these two sides are thus  $r$  and  $\bar{r} \equiv R - r$ , and we can define a new set of modes  $\{u_m(x, t)\}$  and  $\{\bar{u}_m(x, t)\}$  for the left and right sides, respectively. The obvious way of doing this is to define these modes to have support at a certain time  $t = 0$  only over their corresponding subregions. As pointed out in [166], however, one must be careful that the new basis modes still satisfy the correct boundary conditions of the cavity (and in particular, not extra ones). This requirement immediately implies that, if say the set  $\{u_m\}$  are supported only in the left region at  $t = 0$ , then their support will necessarily exceed this region for later times ( $u_m$  satisfies the wave equation and we have not placed an extra boundary condition between the two regions). This does not turn out to be a hindrance in exploring local physics, however.

Since the global vacuum  $|0_G\rangle$  is a stationary state it does not matter at what time we examine its properties; we will choose time  $t = 0$ . The solution is then to simply define our local modes to be appropriately compactly supported at this instant. To this end, we will define our local modes  $u_m(x, t)$  to have initial conditions

$$\begin{aligned}
u_m(x, 0) &= \frac{\theta(r-x)}{\sqrt{r\omega_m}} \sin\left(\frac{\pi m x}{r}\right), \\
\dot{u}_m(x, 0) &= -i\omega_m u_m(x, 0), \\
\bar{u}_m(x, 0) &= \frac{\theta(x-r)}{\sqrt{\bar{r}\bar{\omega}_m}} \sin\left(\frac{\pi m(x-r)}{\bar{r}}\right), \\
\dot{\bar{u}}_m(x, 0) &= -i\bar{\omega}_m \bar{u}_m(x, 0),
\end{aligned} \tag{13.3}$$

where  $\omega_m^2 = \frac{\pi^2 m^2}{r^2} + \mu^2$  and  $\bar{\omega}_m^2 = \frac{\pi^2 m^2}{\bar{r}^2} + \mu^2$ . Given the above initial conditions, the local modes will evolve throughout the cavity according to the Klein-Gordon equation. These modes satisfy the proper boundary conditions and constitute a complete and orthonormal basis for the whole cavity [166], and thus form a proper expansion of the field. For our purposes in this section, however, we need only consider the instant  $t = 0$  at which they are localized to their respective sides of the cavity. Examining the global vacuum in this basis, at this instant, allows us to fully characterize the reduced state of the subregions and the quantum correlations between them. The decomposition in terms of local modes is depicted in Fig. 13.2.2.

Let us denote the local ladder operators associated with the above modes as  $\{\hat{a}_m, \hat{a}_m^\dagger\}$  for the left side, and  $\{\hat{\bar{a}}_m, \hat{\bar{a}}_m^\dagger\}$  for the right. The reduced state at time  $t = 0$  of, say, the left side of the cavity can then be represented with respect to the Fock basis corresponding to  $\{\hat{a}_m, \hat{a}_m^\dagger\}$ . As extensively discussed in [166], this provides a well-defined notion of the

reduced state within a localized region. Indeed it is equivalent, up to a change of basis, to any other well-formulated notion of spatial reduced state (for example by taking the continuum limit of a discretized lattice).

As per usual, solutions sets to the Klein-Gordon equation are related by a linear Bogoliubov transformation, meaning that our local modes are related to the global modes via some transformation of the form

$$\begin{aligned} u_m(x, t) &= \sum_{n=1}^{\infty} (\alpha_{mn} U_n(x, t) + \beta_{mn} U_n^*(x, t)), \\ \bar{u}_m(x, t) &= \sum_{n=1}^{\infty} (\bar{\alpha}_{mn} U_n(x, t) + \bar{\beta}_{mn} U_n^*(x, t)). \end{aligned} \quad (13.4)$$

Equivalently, in terms of the annihilation operators (from which the creation operators are trivially obtained) we have

$$\begin{aligned} \hat{a}_m &= \sum_{n=1}^{\infty} (\alpha_{mn}^* \hat{A}_n - \beta_{mn}^* \hat{A}_n^\dagger), \\ \hat{\bar{a}}_m &= \sum_{n=1}^{\infty} (\bar{\alpha}_{mn}^* \hat{A}_n - \bar{\beta}_{mn}^* \hat{A}_n^\dagger). \end{aligned} \quad (13.5)$$

The Bogoliubov coefficients, which are time-independent, are computed via the Klein-Gordon inner products between local and global modes. In our case, they evaluate to [\[166\]](#)

$$\alpha_{mn} = (U_n | u_m) = (\Omega_n + \omega_m) \mathcal{V}_{mn}, \quad (13.6)$$

$$\beta_{mn} = -(U_n^* | u_m) = (\Omega_n - \omega_m) \mathcal{V}_{mn}, \quad (13.7)$$

$$\bar{\alpha}_{mn} = (U_n | \bar{u}_m) = (\Omega_n + \omega_m) \bar{\mathcal{V}}_{mn}, \quad (13.8)$$

$$\bar{\beta}_{mn} = -(U_n^* | \bar{u}_m) = (\Omega_n - \omega_m) \bar{\mathcal{V}}_{mn}, \quad (13.9)$$

where

$$\mathcal{V}_{mn} = \int_0^R dx \mathcal{U}_n(x) u_m(x, 0) = \frac{\frac{m\pi}{r} (-1)^m}{\sqrt{Rr} \Omega_n \omega_m (\Omega_n^2 - \omega_m^2)} \sin \frac{n\pi r}{R}, \quad (13.10)$$

$$\bar{\mathcal{V}}_{mn} = \int_0^R dx \mathcal{U}_n(x) \bar{u}_m(x, 0) = \frac{-\frac{m\pi}{\bar{r}}}{\sqrt{R\bar{r}} \Omega_n \bar{\omega}_m (\Omega_n^2 - \bar{\omega}_m^2)} \sin \frac{n\pi r}{R}. \quad (13.11)$$

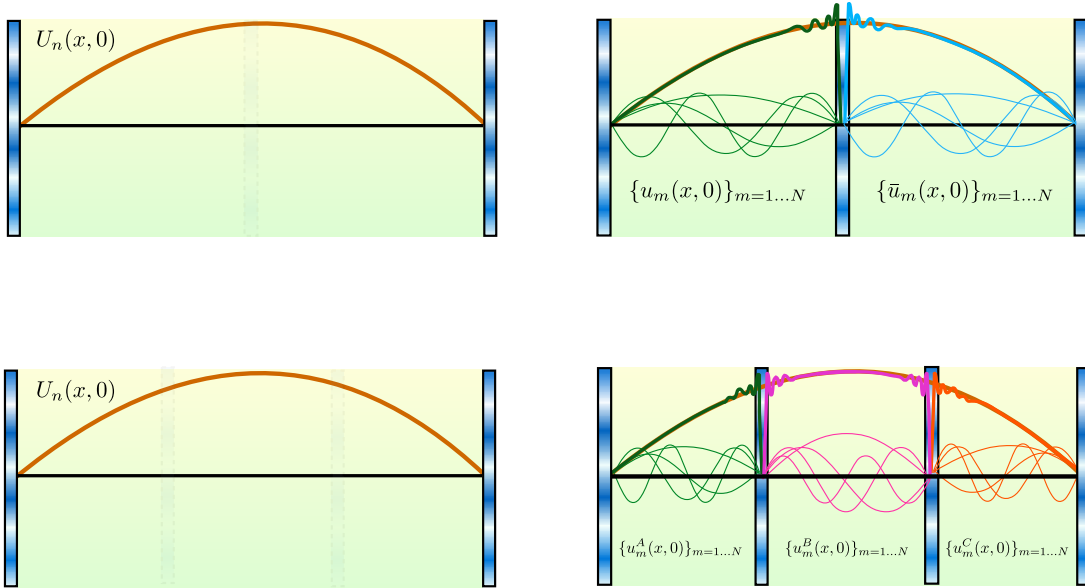


Figure 13.2: The cavity for the cases studied in this chapter. The figures on the left correspond to the full cavity without mirrors, the light dotted vertical bars indicating the border of the regions chosen to study localization into two (top) or three (bottom) spatial regions. The right figures show the decomposition in terms of local modes at  $t = 0$  for both settings.

The fact that the  $\beta$  coefficients are non-vanishing implies that the global vacuum  $|0_G\rangle$  is, in the local basis, an excited state in the sense that  $\hat{a}_m |0_G\rangle \neq 0$  and  $\hat{\bar{a}}_m |0_G\rangle \neq 0$ , i.e. local quanta can be removed from it, so in this picture the vacuum cannot be considered to be empty. Indeed, the reduced state of, say, the left side of the cavity, is a mixed state. These local excitations, and the local mixedness, are associated with the entanglement present between the two sides of the cavity.

Lastly, as with any Bogoliubov transformation, the above coefficients satisfy the necessary conditions [39]

$$\sum_k (\alpha_{mk} \alpha_{nk}^* - \beta_{mk} \beta_{nk}^*) = \delta_{mn}, \quad (13.12)$$

$$\sum_k (\alpha_{mk} \beta_{nk} - \beta_{mk} \alpha_{nk}) = 0, \quad (13.13)$$

and similarly for the barred coefficients.

### 13.2.2 Slamming down a mirror

If we compute the vacuum expectation value of the local number operators  $\hat{n}_m = \hat{a}_m^\dagger \hat{a}_m$  and  $\hat{\bar{n}}_m = \hat{\bar{a}}_m^\dagger \hat{\bar{a}}_m$  we find that these are non-zero for the global vacuum state  $|0_G\rangle$ , indicating the presence of a bath of ‘local particles’. While this observation is mathematically correct we must nevertheless ask ourselves if any operational significance can be attached to this theoretical notion of “local quanta”. Can we somehow detect the presence of such local quanta in the lab?

Taking as inspiration the discussion in Sect. 13.1, we claim that a generic (but perhaps not exhaustive) method of achieving this is to informationally block the local region of interest from the rest of the system. In a cavity-field system this can be achieved by introducing a mirror, separating the cavity into two new smaller ones. Indeed, as we will discuss, such an operation *does* allow the detection and characterization of local excitations. This is fundamentally due to the fact that we identify a “real” (i.e. measurable) particle to be an elementary excitation of a *stationary* field mode. By the act of introducing the mirror, what were nonstationary local modes of the full cavity translate into stationary modes of the new small cavity, thus facilitating the measurement of their excitations.

One may be concerned with the unique identification of “a real particle” with “an elementary excitation of a stationary mode”. In this work, however, we attempt to be operationally unambiguous and connect as closely as possible with the kinds of measurements that can actually be achieved in the laboratory, necessitating long measurement times as compared to the fundamental time-scale of the cavity. As a detection model we can consider a particle detector (as presented in Sect. 4.4 or in Ch. 5; the details are irrelevant) that remains at some specific location  $x_0$ . Let the initial state of the system is taken to be the  $|0_G\rangle \otimes |g\rangle$  where  $|g\rangle$  is the ground state of the detector. We will present two cases:

First, *without slamming a mirror*, we imagine adiabatically switching on the coupling between field and detector. The adiabatic theorem guarantees that if the system was originally in the ground state of the non-interacting theory, then the system at much later times will be found in the interacting ground state.<sup>1</sup> When we then adiabatically switch off the interaction the combined system will then be found in the non-interacting vacuum and thus will fail to detect the presence of local quanta. This then immediately shows that

---

<sup>1</sup>The adiabatic theorem requires a gap between the vacuum energy eigenvalue and other eigenvalues. This is guaranteed since we are dealing with a cavity with a naturally infrared cut-off defined by the size of the cavity  $R$ .



such a detector will not get excited. Such a procedure does not detect particles when the global system is in its ground state (thus allowing us to use the adiabatic theorem). It is for this reason that we relate the particle notion with the free stationary modes, which are the ones corresponding to the free eigenstates.

If, on the other hand, *we slam down a mirror* and then follow the same adiabatic detection procedure within one of the sub-cavities then we *will* detect the presence of particles. This is because the local modes, which are stationary after the mirror is introduced, are excited. Critical to the message of this chapter is that the measurement statistics that will be obtained from this procedure are equivalent to the local virtual particle statistics (i.e. those corresponding to one half of the box) obtained from the transformation presented in Sect. 13.2.1, which simply describes the local physics of the cavity and does not assume the introduction of a mirror.

Concretely, we consider what happens when we instantaneously introduce a mirror at  $x = r$  and  $t = 0$ , i.e. we impose the Dirichlet boundary condition  $\phi(r, t) = 0$  for  $t \geq 0$ . Clearly the instantaneous assumption is not physically realistic, however this turns out not to be a hindrance in elucidating the most realistic, finite-time case. This will be further discussed in Sect. 13.4.2. Given this scenario, it is clear that the set of local modes with initial conditions (13.3), which were non-stationary for  $t < 0$  prior to the introduction of the mirror, will have a different evolution than before,  $u'_m(x, t)$  and  $\bar{u}'_m(x, t)$ , which for  $t \geq 0$  will correspond to *stationary* modes, i.e.

$$u'_m(x, t) = \begin{cases} u_m(x, t) & \text{when } t \leq 0 \\ u_m(x, 0)e^{-i\omega_m t} & \text{when } t > 0 \end{cases} \quad (13.14)$$

$$\bar{u}'_m(x, t) = \begin{cases} \bar{u}_m(x, t) & \text{when } t \leq 0 \\ \bar{u}_m(x, 0)e^{-i\bar{\omega}_m t} & \text{when } t > 0 \end{cases} \quad (13.15)$$

Please note that after this section we will only need to consider the times  $t \geq 0$ , and thus will abuse notation by dropping the primes from the mode functions, meaning that for  $t > 0$  we will define  $u_m(x, t) = u_m(x, 0)e^{-i\omega_m t}$ .

Furthermore and analogously, the corresponding global modes  $U'_m(x, t)$  would only be stationary modes for  $t < 0$ ; for  $t \geq 0$  these modes would be non-stationary.

Equivalently, the sudden introduction of the mirror translates mathematically into a time-dependent Hamiltonian, i.e. we have

$$\hat{H} = \begin{cases} \sum_m \Omega_m \hat{A}_m^\dagger \hat{A}_m & t < 0 \\ \sum_m \omega_m \hat{a}_m^\dagger \hat{a}_m + \bar{\omega}_m \hat{\bar{a}}_m^\dagger \hat{\bar{a}}_m & t \geq 0 \end{cases} . \quad (13.16)$$

Physically, the time dependence of the Hamiltonian will cause particle creation similar to the Dynamical Casimir Effect [115, 112].

To determine exactly the amount of particle creation we need to calculate the Bogoliubov coefficients between the modes  $U'_m$  and  $u'_m$  and  $\bar{u}'_m$ . These are nothing but the Klein-Gordon inner products  $\alpha_{mn} = (u'_m|U'_n)$ ,  $\beta_{mn} = (u'_m|U'_n^*)$ ,  $\bar{\alpha}_{mn} = (\bar{u}'_m|U'_n)$ , and  $\bar{\beta}_{mn} = (\bar{u}'_m|U'_n^*)$ , which we can conveniently evaluate at time  $t = 0$ . Importantly, due to the specific choice of initial data at  $t = 0$  these Bogoliubov coefficients necessarily coincides with those of the previous section, i.e. Eq. (13.6). This means that the particle content generated by the mirror is exactly equivalent to the local particle content  $(a_m^\dagger a_m, \bar{a}_m^\dagger \bar{a}_m)$  before the mirror is introduced, i.e. the particle content that is associated with entanglement between the two sides of the cavity. Thus, although the sudden introduction of a mirror is usually understood as causing particle creation, it is at the same time an operation that does not change the *local* particle number of the state. The difference now being that these particle contents are associated with stationary modes, meaning that they can be measured using standard techniques of quantum optics.

Moreover, it is not just the particle content, but the state in general that does not change. That is, all particle statistics and correlations (including entanglement) are unchanged by the action of slamming the mirror. Slamming the mirror does of course change the time evolution of the system. For  $t < 0$  the system is time-independent, the global vacuum state being stationary with respect to the global Hamiltonian, whereas for  $t > 0$  the change of Hamiltonian will cause time evolution (e.g. particles propagating away from the mirror). The key observation, however, is that this difference in evolution is fully encompassed by the difference in spatial evolution of the mode functions themselves and not by any changes in particle content or correlations between them. The energy we are adding to the system, in the form of real particles, allows observation of the local-basis excitations that are mathematically attributed to their corresponding reduced regions. This action furthermore allows us to measure their cross-cavity correlations, including entanglement.

### 13.2.3 Three spatial regions

Before continuing we would also like to describe the case in which the cavity is split into three spatial regions, rather than only two. This will prove useful later when we discuss the operational implications of slamming down mirrors and the possible experimental verification of vacuum entanglement. Note that the extension to any number of regions follows analogously.

Let us proceed by considering a division of our cavity into three sections  $\Delta_A = [A_0, B_0]$ ,  $\Delta_B =$

$[B_0, C_0]$ , and  $\Delta_C = [C_0, R]$  with sizes  $A, B$  and  $C$  respectively. Let us define:

$$\Pi_Z(x) = \begin{cases} 1 & : x \in \Delta_Z \\ 0 & : x \notin \Delta_Z \end{cases},$$

and set

$$A_0 = 0, \quad B_0 = A, \quad C_0 = A + B, \quad R = A + B + C. \quad (13.17)$$

We can build the local modes for these three regions  $u_l^Z(x, t)$  by demanding that:

$$u_l^Z(x, 0) = \frac{\Pi_Z(x)}{\sqrt{Z\omega_l^Z}} \sin \frac{l\pi(x - Z_0)}{Z}, \quad (13.18)$$

$$\dot{u}_l^Z(x, 0) = -i\omega_l^Z u_l^Z(x, 0). \quad (13.19)$$

With:

$$\omega_l^Z = \sqrt{\left(\frac{m\pi}{Z}\right)^2 + \mu^2}, \quad Z = A, B, C.$$

The new Bogoliubov transformation, analogous to Eq. (13.4), is:

$$u_m^Z = \sum_n \alpha_{mn}^Z U_n + \beta_{mn}^Z U_n^*, \quad Z = A, B, C, \quad (13.20)$$

where

$$\alpha_{mn}^Z = (U_n | u_m^Z) = (\Omega_n + \omega_m^Z) \mathcal{V}_{mn}^Z, \quad (13.21)$$

$$\beta_{mn}^Z = -(U_n^* | u_m^Z) = (\Omega_n - \omega_m^Z) \mathcal{V}_{mn}^Z, \quad (13.22)$$

and

$$\mathcal{V}_{mn}^A = \int_0^A dx \mathcal{U}_n(x) u_m^A(x, 0) = \frac{\frac{m\pi}{A} (-1)^m}{\sqrt{RA\Omega_n \omega_m^A (\Omega_n^2 - \omega_m^{A^2})}} \sin \frac{n\pi A}{R}, \quad (13.23)$$

$$\mathcal{V}_{mn}^B = \int_A^{A+B} dx \mathcal{U}_n(x) u_m^B(x, 0) = \frac{\frac{m\pi}{B} \left[ (-1)^m \sin \left( \frac{n\pi(A+B)}{R} \right) - \sin \left( \frac{n\pi A}{R} \right) \right]}{\sqrt{RB\Omega_n \omega_m^B (\Omega_n^2 - \omega_m^{B^2})}}, \quad (13.24)$$

$$\mathcal{V}_{mn}^C = \int_{A+B}^R dx \mathcal{U}_n(x) u_m^C(x, 0) = \frac{-\frac{m\pi}{C}}{\sqrt{RC\Omega_n \omega_m^C (\Omega_n^2 - \omega_m^{C^2})}} \sin \frac{n\pi(A+B)}{R}. \quad (13.25)$$

Transforming to this mode basis allows us to describe the local physics of, and the correlations between, these three regions. Similar to the scenario discussed in Sect. 13.2.2, the mode basis described here can be used to describe the process of slamming down two mirrors simultaneously, thereby splitting the cavity into three regions. Exactly the same physics applies in this case, and we will thus not reiterate the material of Sect. 13.2.2.

## 13.3 Computing the state

In this section we will discuss how to obtain a local description of the global vacuum state<sup>2</sup>. This includes the evaluation of the reduced field state of a subregion of a cavity, and a description of the of vacuum entanglement between regions of the cavity. A key point to keep in mind, as discussed in the previous section, is that the Bogoliubov transformation (and thus the resulting state) is the same whether we consider this to be with or without the introduction of the mirror. As discussed further in Sect. 13.4.1, the covariance matrix that we compute (i.e. the state) equally well describes both cases.

### 13.3.1 The state of two regions

We will start by computing the form of the global vacuum upon transforming to the local-mode basis, in the case that we split the cavity into two regions. Let us define the canonically conjugate quadrature operators for the field modes, both global and local. Letting  $\{\hat{A}_n, \hat{A}_n^\dagger\}$  be the ladder operators for the global modes, we define the corresponding quadrature operators to be

$$\hat{Q}_n = \frac{1}{\sqrt{2}}(\hat{A}_n + \hat{A}_n^\dagger), \quad \hat{P}_n = \frac{i}{\sqrt{2}}(\hat{A}_n^\dagger - \hat{A}_n). \quad (13.26)$$

Similarly, for the ladder operators  $\{\hat{a}_m, \hat{a}_m^\dagger\}$  and  $\{\hat{\bar{a}}_m, \hat{\bar{a}}_m^\dagger\}$  of the local modes we have

$$\begin{aligned} \hat{q}_m &= \frac{1}{\sqrt{2}}(\hat{a}_m + \hat{a}_m^\dagger), & \hat{p}_m &= \frac{i}{\sqrt{2}}(\hat{a}_m^\dagger - \hat{a}_m), \\ \hat{\bar{q}}_m &= \frac{1}{\sqrt{2}}(\hat{\bar{a}}_m + \hat{\bar{a}}_m^\dagger), & \hat{\bar{p}}_m &= \frac{i}{\sqrt{2}}(\hat{\bar{a}}_m^\dagger - \hat{\bar{a}}_m). \end{aligned} \quad (13.27)$$

For notational convenience let us define the phase-space vectors  $\hat{\mathbf{X}} = (\hat{Q}_1, \hat{P}_1, \hat{Q}_2, \hat{P}_2, \dots)^T$ ,  $\hat{\mathbf{x}} = (\hat{q}_1, \hat{p}_1, \hat{q}_2, \hat{p}_2, \dots)^T$ , and  $\hat{\bar{\mathbf{x}}} = (\hat{\bar{q}}_1, \hat{\bar{p}}_1, \hat{\bar{q}}_2, \hat{\bar{p}}_2, \dots)^T$ .

In Sect. 4.8 we how to represent a Bogoliubov transformation symplectically. We now do this here. Within the representation we have presented it is straightforward to see that the Bogoliubov transformation from global to local modes, as given in Eq. (13.5), is given by the matrix transformations

$$\hat{\mathbf{x}} = \mathbf{S}\hat{\mathbf{X}}, \quad \hat{\bar{\mathbf{x}}} = \bar{\mathbf{S}}\hat{\mathbf{X}}, \quad (13.28)$$

---

<sup>2</sup>It must be pointed out that the mathematical toolbox presented here allow us to work with any Gaussian state, not just the global vacuum. We could, for example, start with with a global thermal state.

where the matrix  $\mathbf{S}$  takes the block form

$$\mathbf{S} = \begin{pmatrix} \mathbf{S}_{11} & \mathbf{S}_{12} & \cdots \\ \mathbf{S}_{21} & \mathbf{S}_{22} & \cdots \\ \vdots & \vdots & \ddots \end{pmatrix}, \quad (13.29)$$

with

$$\mathbf{S}_{mn} = \begin{pmatrix} \text{Re}(\alpha_{mn} - \beta_{mn}) & \text{Im}(\alpha_{mn} + \beta_{mn}) \\ -\text{Im}(\alpha_{mn} - \beta_{mn}) & \text{Re}(\alpha_{mn} + \beta_{mn}) \end{pmatrix}, \quad (13.30)$$

and similarly for  $\bar{\mathbf{S}}$  using the barred Bogoliubov coefficients. It is straightforward to show that such a transformation preserves the canonical commutation relations iff the Bogoliubov conditions Eq. (13.12,13.13) are satisfied.

Using the specific transformation for our scenario, Eq. (13.6), we find the  $2 \times 2$  blocks of matrices  $\mathbf{S}$  and  $\bar{\mathbf{S}}$  to be

$$\mathbf{S}_{mn} = 2\mathcal{V}_{mn} \begin{pmatrix} \omega_m & 0 \\ 0 & \Omega_n \end{pmatrix}, \quad \bar{\mathbf{S}}_{mn} = 2\bar{\mathcal{V}}_{mn} \begin{pmatrix} \bar{\omega}_m & 0 \\ 0 & \Omega_n \end{pmatrix} \quad (13.31)$$

We note that the off-diagonal entries of these blocks are zero, resulting from the fact that our Bogoliubov coefficients are purely real. This means that the transformation does not mix canonical position and momentum operators, rather the  $\hat{q}$  operators of the local basis are combinations of the global  $\hat{Q}$ 's only, and similarly for the momentum operators.

It is important to note and to keep in mind that individually the matrices  $\mathbf{S}$  and  $\bar{\mathbf{S}}$  are not symplectic. This is because individually they only map onto a subspace of the total Hilbert space of the field <sup>3</sup>. This is easily concluded from the fact that the reduced field states of the subregions of the cavity are mixed states, despite the global state being pure (the vacuum). A proper symplectic transformation in phase space can always be associated with a unitary operation acting in the Hilbert space, which will always bring a pure state to another pure state.

Rather, it is the combined transformation

$$\mathbf{S}_{\text{Bogo}} = \begin{pmatrix} \mathbf{S} \\ \bar{\mathbf{S}} \end{pmatrix} \quad (13.32)$$

---

<sup>3</sup>The definition of a symplectic matrix  $\mathbf{S}$  requires that it be square. However if a linear phase space transformation is not square it is still required to preserve the canonical commutation relations. That is, if we have an  $m \times n$  transformation matrix  $\mathbf{S}$  on phase space then it must still satisfy  $\mathbf{S}\Omega_n\mathbf{S}^T = \Omega_m$ , where  $\Omega_n$  is the  $n$ -mode symplectic form. If  $n > m$  then such a transformation corresponds to a symplectic transformation followed by a partial trace, which can of course bring a pure state to a mixed one.

that is formally symplectic (see the discussion in Sect. 13.5.2). This matrix transforms the global mode basis to the local mode basis, including both sides of the cavity:

$$\begin{pmatrix} \hat{\mathbf{x}} \\ \hat{\mathbf{p}} \end{pmatrix} = \mathbf{S}_{\text{Bogo}} \hat{\mathbf{X}}. \quad (13.33)$$

Given all of this, we are ready to transform the state itself. As we well know, the global vacuum  $|0_G\rangle$  is an example of a Gaussian state. It's covariance matrix, which we will label  $\boldsymbol{\sigma}_G$ , represented in the global-mode basis, is simply given by the identity:  $\boldsymbol{\sigma}_G = \mathbf{I}$ . To Bogoliubov transform this state to the local basis,  $\boldsymbol{\sigma}_{\text{loc}}$ , we apply the above symplectic transformation to  $\boldsymbol{\sigma}_G$ :

$$\begin{aligned} \boldsymbol{\sigma}_{\text{loc}} &= \mathbf{S}_{\text{Bogo}} \boldsymbol{\sigma}_G \mathbf{S}_{\text{Bogo}}^T \equiv \begin{pmatrix} \boldsymbol{\sigma} & \boldsymbol{\gamma} \\ \boldsymbol{\gamma}^T & \bar{\boldsymbol{\sigma}} \end{pmatrix} \\ &= \begin{pmatrix} \mathbf{S} \boldsymbol{\sigma}_G \mathbf{S}^T & \mathbf{S} \boldsymbol{\sigma}_G \bar{\mathbf{S}}^T \\ \bar{\mathbf{S}} \boldsymbol{\sigma}_G \mathbf{S}^T & \bar{\mathbf{S}} \boldsymbol{\sigma}_G \bar{\mathbf{S}}^T \end{pmatrix}. \end{aligned} \quad (13.34)$$

Here the covariance matrix  $\boldsymbol{\sigma} = \mathbf{S} \boldsymbol{\sigma}_G \mathbf{S}^T = \mathbf{S} \mathbf{S}^T$  represents the reduced field state for the left side of the cavity. Similarly,  $\bar{\boldsymbol{\sigma}} = \bar{\mathbf{S}} \bar{\mathbf{S}}^T$  fully characterizes the reduced state of the right side. The off-diagonal matrix  $\boldsymbol{\gamma} = \mathbf{S} \bar{\mathbf{S}}^T$ , on the other hand, contains the correlation structure between the two sides of the cavity.

These matrices are easily computed. We see that each can be split into  $2 \times 2$  blocks, for example the reduced state of the left side takes the form

$$\boldsymbol{\sigma} = \begin{pmatrix} \boldsymbol{\sigma}_{11} & \boldsymbol{\sigma}_{12} & \cdots \\ \boldsymbol{\sigma}_{21} & \boldsymbol{\sigma}_{22} & \cdots \\ \vdots & \vdots & \ddots \end{pmatrix}. \quad (13.35)$$

Here the  $2 \times 2$  block  $\boldsymbol{\sigma}_{mm}$  is the covariance matrix (i.e. it *is* the reduced state) of the  $m$ 'th local (left side) mode. The off-diagonal block  $\boldsymbol{\sigma}_{mn}$ , where  $m \neq n$ , contains the correlations between left local modes  $m$  and  $n$ . Using the fact that the  $\mathbf{S}_{mn}$  are symmetric we see that these blocks are given by  $\boldsymbol{\sigma}_{mn} = \sum_{\ell} \mathbf{S}_{m\ell} \mathbf{S}_{n\ell}$ . Similarly, the state  $\bar{\boldsymbol{\sigma}}$  and the correlation matrix  $\boldsymbol{\gamma}$  can be split into  $2 \times 2$  blocks that are given by  $\bar{\boldsymbol{\sigma}}_{mn} = \sum_{\ell} \bar{\mathbf{S}}_{m\ell} \bar{\mathbf{S}}_{n\ell}$  and

$\gamma_{mn} = \sum_{\ell} \mathbf{S}_{m\ell} \bar{\mathbf{S}}_{n\ell}$ , respectively. These are given by

$$\boldsymbol{\sigma}_{mn} = \sum_l 4\mathcal{V}_{ml}\mathcal{V}_{nl} \begin{pmatrix} \omega_m\omega_n & 0 \\ 0 & \Omega_l^2 \end{pmatrix}, \quad (13.36)$$

$$\bar{\boldsymbol{\sigma}}_{mn} = \sum_n 4\bar{\mathcal{V}}_{ml}\bar{\mathcal{V}}_{nl} \begin{pmatrix} \bar{\omega}_m\bar{\omega}_n & 0 \\ 0 & \Omega_l^2 \end{pmatrix}, \quad (13.37)$$

$$\boldsymbol{\gamma}_{mn} = \sum_l 4\mathcal{V}_{ml}\bar{\mathcal{V}}_{nl} \begin{pmatrix} \omega_m\bar{\omega}_n & 0 \\ 0 & \Omega_l^2 \end{pmatrix}. \quad (13.38)$$

Together, these blocks constitute a full characterization of the global vacuum in the local-mode basis, and in particular  $\boldsymbol{\sigma}$  fully characterizes the reduced state of the left side of the cavity. Although we have derived the full analytical expressions it should be noted that in the remainder of this chapter, when we present quantitative results, we have done so by computing the above matrix elements numerically, by performing the sums to convergence.

There are several observations that we can make from this result. The first is that the reduced states  $\boldsymbol{\sigma}$  and  $\bar{\boldsymbol{\sigma}}$  are clearly excited states, meaning in this language that they are not equal to the identity (the vacuum). Mathematically, this is what is meant by the statement “half of an empty box is non-empty”. Equivalently, this is a mathematical description of the particle creation due to instantaneously slamming down a mirror. Another observation is that the correlation structure of the global vacuum in this basis is extremely connected, meaning that every local mode is correlated (if perhaps not entangled) with every other local mode. That is, since the blocks  $\boldsymbol{\gamma}_{mn}$  are nonzero this means that every local mode of the left side is correlated with every local mode of the right, and vice versa. Similarly, every local mode is correlated with every other local mode of the same side, as demonstrated by the fact that the blocks  $\boldsymbol{\sigma}_{mn}$  and  $\bar{\boldsymbol{\sigma}}_{mn}$  are nonzero.

### 13.3.2 The state of three regions

We will now outline exactly the same procedure for the case of three regions in the cavity (equivalently, the case where two mirrors are simultaneously introduced). This will allow us to consider the entanglement between spatially-separated regions (i.e. the leftmost and rightmost regions). As we will see, this is crucial for demonstrating that the entanglement obtained by slamming mirrors is derived from the previously existing vacuum entanglement, rather than having been created by the slamming process.

The procedure follows from the Bogoliubov transformation described in Sect. 13.2.3. We will also describe how to obtain the reduced state of two out of the three regions (in fact

this is trivial in the language of covariance matrices). In the phase space representation we have equivalent matrix equations as those in Eq. (13.28,13.29,13.30), i. e.:

$$\hat{\mathbf{x}}^Z = \mathbf{S}^Z \hat{\mathbf{X}}, \quad Z = A, B, C \quad (13.39)$$

where  $\mathbf{S}^Z$  has the block form as given in Eq. (13.29):

$$\mathbf{S}_{mn}^Z = \begin{pmatrix} \text{Re}(\alpha_{mn}^Z - \beta_{mn}^Z) & \text{Im}(\alpha_{mn}^Z + \beta_{mn}^Z) \\ -\text{Im}(\alpha_{mn}^Z - \beta_{mn}^Z) & \text{Re}(\alpha_{mn}^Z + \beta_{mn}^Z) \end{pmatrix} \quad (13.40)$$

$$= 2\mathcal{V}_{mn}^Z \begin{pmatrix} \omega_m^Z & 0 \\ 0 & \Omega_n \end{pmatrix}. \quad (13.41)$$

The combined transformation, that which is formally symplectic, is given in analogy to Eq. (13.32):

$$\mathbf{S}_{\text{Bogo}} = \begin{pmatrix} \mathbf{S}^A \\ \mathbf{S}^B \\ \mathbf{S}^C \end{pmatrix}, \quad (13.42)$$

and transforms the global mode basis to the local mode basis of the three regions:

$$\begin{pmatrix} \hat{\mathbf{x}}^A \\ \hat{\mathbf{x}}^B \\ \hat{\mathbf{x}}^C \end{pmatrix} = \mathbf{S}_{\text{Bogo}} \hat{\mathbf{X}}. \quad (13.43)$$

Again, to Bogoliubov transform the global state  $\boldsymbol{\sigma}_G = \mathbf{I}$  to the local basis we apply this transformation to  $\boldsymbol{\sigma}_G$ :

$$\begin{aligned} \boldsymbol{\sigma}_{\text{loc}} &= \mathbf{S}_{\text{Bogo}} \boldsymbol{\sigma}_G \mathbf{S}_{\text{Bogo}}^T \equiv \begin{pmatrix} \boldsymbol{\sigma}_A & \gamma_{AB} & \gamma_{AC} \\ \gamma_{AB}^T & \boldsymbol{\sigma}_B & \gamma_{BC} \\ \gamma_{AC}^T & \gamma_{BC}^T & \boldsymbol{\sigma}_C \end{pmatrix} \\ &= \begin{pmatrix} \mathbf{S}^A \boldsymbol{\sigma}_G \mathbf{S}^{AT} & \mathbf{S}^A \boldsymbol{\sigma}_G \mathbf{S}^{BT} & \mathbf{S}^A \boldsymbol{\sigma}_G \mathbf{S}^{CT} \\ \mathbf{S}^B \boldsymbol{\sigma}_G \mathbf{S}^{AT} & \mathbf{S}^B \boldsymbol{\sigma}_G \mathbf{S}^{BT} & \mathbf{S}^B \boldsymbol{\sigma}_G \mathbf{S}^{CT} \\ \mathbf{S}^C \boldsymbol{\sigma}_G \mathbf{S}^{AT} & \mathbf{S}^C \boldsymbol{\sigma}_G \mathbf{S}^{BT} & \mathbf{S}^C \boldsymbol{\sigma}_G \mathbf{S}^{CT} \end{pmatrix}. \end{aligned} \quad (13.44)$$

The blocks again represent the reduced state of, and the correlations between, the three regions. For example  $\boldsymbol{\sigma}_A$  is the reduced state of the left-most region and  $\gamma_{AC}$  contains the correlations between the left-most and right-most regions. As before, each matrix can be



further split into 2x2 blocks given by  $\sigma_{mn}^Z = \sum_\ell \mathbf{S}_{m\ell}^Z \mathbf{S}_{n\ell}^Z$ ,  $\gamma_{mn}^{YZ} = \sum_\ell \mathbf{S}_{m\ell}^Y \mathbf{S}_{n\ell}^Z$ . These are given by

$$\sigma_{mn}^Z = \sum_l 4\mathcal{V}_{ml}^Z \mathcal{V}_{nl}^Z \begin{pmatrix} \omega_m^Z \omega_n^Z & 0 \\ 0 & \Omega_l^2 \end{pmatrix} \quad (13.45)$$

$$\gamma_{mn}^{YZ} = \sum_l 4\mathcal{V}_{ml}^Y \mathcal{V}_{nl}^Z \begin{pmatrix} \omega_m^Y \omega_n^Z & 0 \\ 0 & \Omega_l^2 \end{pmatrix}. \quad (13.46)$$

From here, one may easily study the reduced state of two of the three regions by simply taking the appropriate blocks of Eq. (13.44). For example the reduced state of system  $AC$  (the left-most and right-most regions) is obtained by tracing out  $B$ , which here simply results in the covariance matrix

$$\begin{aligned} \sigma_{AC} &= \begin{pmatrix} \sigma_A & \gamma_{AC} \\ \gamma_{AC}^T & \sigma_C \end{pmatrix} \\ &= \begin{pmatrix} \mathbf{S}^A \sigma_G \mathbf{S}^{A^T} & \mathbf{S}^A \sigma_G \mathbf{S}^{C^T} \\ \mathbf{S}^C \sigma_G \mathbf{S}^{A^T} & \mathbf{S}^C \sigma_G \mathbf{S}^{C^T} \end{pmatrix}. \end{aligned} \quad (13.47)$$

## 13.4 With vs. without a mirror

Before we proceed to analyse other local features like the entanglement between left and right regions of the cavity, we would like to make a stop to discuss a little bit more conceptually the differences between the analysis of the two possible scenarios, with and without introducing the mirror. Again, what does it mean for half of an empty box to be non-empty? We know that in some sense the reduced state of a subregion of the global vacuum is excited; certainly the state  $\sigma$  in Eq. (13.36) is an excited state (that is, excited with respect to the local-mode basis, which is the whole point). However, what does this mathematical fact have to do with reality? As discussed earlier, the answer, in fact, is that the real excitations produced by the mirror are mathematically equivalent to the virtual local excitations attributed to vacuum entanglement. Their measurement, therefore, constitutes an achievement of our goal.

### 13.4.1 Time evolution

Both of the scenarios, with and without a mirror, are equivalent at time  $t = 0$ . This implies that the Bogoliubov transformation will be exactly the same for both sets (primed and

unprimed modes as discussed in the previous sections) as the transformation coefficients are computed using the Klein-Gordon inner product, which contains only the mode functions and their first time-derivatives [39]). Thus, the field state of the left-cavity immediately following the introduction of the mirror will, in fact, be given exactly by the covariance matrix  $\sigma$  as given by Eqs. (13.35,13.36). The only difference now is that the mode-basis that  $\sigma$  is associated with is different, in the sense that it evolves differently for  $t > 0$ . Similarly the reduced state of the right-cavity will be given by  $\bar{\sigma}$  and the correlations between the two (separated) cavities will be contained in  $\gamma$ , the blocks of each being given by Eqs. (13.36). Importantly, this means that the entanglement structure contained in the state is exactly the same in both cases. That is, the real particles created in the left-side by slamming down a mirror are entangled with the created particles in the right-side, and this entanglement has exactly the same structure that the original vacuum entanglement present before the mirror was introduced. We will fully discuss this entanglement in Sect. 13.5.

But surely the state of the field has been changed due to the introduction of the mirror. Clearly in some sense it has. We have created real particles. We have added energy to the system by changing the Hamiltonian. The state of the new left-side cavity (for example) is certainly time-dependent. This is not surprising, as we would expect a burst of particles to be propagating away from the newly introduced mirror (shortly we will discuss this further). The reduced state of the left-side of the larger cavity (without a mirror), on the other hand, is by construction time-independent. The global vacuum  $|0_G\rangle$  is a stationary state with respect to the global Hamiltonian  $\hat{H}_G$ , and thus the reduced state will be time-independent as well. In this sense the two states are certainly different.

Nevertheless the state at  $t = 0$  is described by exactly the same covariance matrix. We will now elucidate the nature of time evolution in the case that a mirror has been slammed; indeed we will take advantage of a subtlety in the time evolution that is particularly apparent when working with covariance matrices. First consider, for example, working in the Schrödinger picture. In this case the field in the left-cavity is time-independent:  $\hat{\phi}(x, t) = \hat{\phi}(x, t = 0) = \sum_m (u_m(x, 0)\hat{a}_m + u_m^*(x, 0)\hat{a}_m^\dagger)$ , where  $u_m(x, 0) = \frac{1}{r\omega_m} \sin \frac{\pi m x}{r}$ . The state  $\hat{\rho}(t)$  is what evolves, and this gives a corresponding time evolution to the covariance matrix elements via  $\sigma_{mn}(t) = \text{Tr}(\hat{\rho}(t)(\hat{x}_m\hat{x}_n + \hat{x}_n\hat{x}_m))$ . As we have seen, this free evolution can be represented symplectically:  $\sigma(t) = \mathbf{S}_F(t)\sigma\mathbf{S}_F(t)^T$ , where the transformation consists of single-mode rotations:

$$\mathbf{S}_F(t) = \bigoplus_m \begin{pmatrix} \cos \omega_m t & \sin \omega_m t \\ -\sin \omega_m t & \cos \omega_m t \end{pmatrix}. \quad (13.48)$$

Alternatively we can work in the Heisenberg picture, in which the field is the time-

dependent operator

$$\begin{aligned}\hat{\phi}(x, t) &= \sum_m (u_m(x, 0)\hat{a}_m e^{-i\omega_m t} + u_m^*(x, 0)\hat{a}_m^\dagger e^{i\omega_m t}) \\ &= \sum_m (u_m(x, t)\hat{a}_m + u_m^*(x, t)\hat{a}_m^\dagger).\end{aligned}\tag{13.49}$$

A subtle issue, however, is that the Heisenberg evolution of the field can be viewed in two ways, as given by the two lines above. In the first line it is the operators themselves that evolve:  $\hat{a}_m(t) = \hat{a}_m e^{-i\omega_m t}$ . This corresponds to an evolution of the quadrature operators  $\hat{x}_m(t)$  that leads to a symplectic evolution  $\mathbf{S}_F(t)$  of the covariance matrix, equivalent to what was obtained in the Schrödinger picture. A key observation is that in both of these pictures it is the *time-independent mode-functions*  $u_m(x, 0)$  that the *time-dependent covariance matrix*  $\boldsymbol{\sigma}(t)$  is associated with. The other way of viewing the evolution, as indicated by the second line in Eq. (13.49), is to keep the ladder operators themselves time-independent (thus giving a time-independent  $\boldsymbol{\sigma}$ ) and to rather let the mode-functions  $u(x, t)$  contain the time evolution. In this case the covariance matrix does not change, but it is understood that the mode-functions with which it is associated *do* evolve.

This last picture is the one that we will adopt here, in all work below. In this way we do not need to actually consider any evolution in the covariance matrix directly; our state will always be described by the matrix  $\boldsymbol{\sigma}$ , the same one used to describe the spatial reduced state in the case without a mirror. The time-evolution induced by slamming a mirror is then trivial: it is simply given by the time-dependence already present in the  $t > 0$  mode functions defined within the left cavity as  $u_m(x, t) = u_m(x, 0)e^{-i\omega_m t}$  and within the right cavity as  $\bar{u}_m(x, t) = \bar{u}_m(x, 0)e^{-i\bar{\omega}_m t}$ .

### 13.4.2 Finite-time mirror

In the calculations of the next section we will continue to assume an instantaneous introduction of the mirror(s) in the cavity. Before devoting ourselves to this, however, we should briefly discuss how the physics changes if the introduction of the mirror takes place within a finite time window  $\Delta t$ , as of course will always be the case in any physical realization. Let us continue to assume that the introduction happens very fast as compared to the fundamental time scales of the reduced cavities:  $\Delta t \ll 1/\omega_1$  and  $\Delta t \ll 1/\bar{\omega}_1$ . In this case the low-energy local modes will still see the mirror appear very quickly (i.e. as compared to their free evolution time scale), and so their reduced states and correlations amongst themselves will be well approximated by the covariance matrices of Eq. (13.36). That is,

within a low energy sector (the limit of which is determined by how fast the mirror can be introduced) the results that we will present will hold to a good approximation. On the other hand for the very high-energy modes (that see the introduction of the mirror occur very slowly) we can make an adiabatic approximation to conclude that they will evolve to their local ground states. That is, if  $m$  is large enough such that  $\Delta t \gg 1/\omega_m$  then after the mirror is introduced the reduced state of this mode will approximately be  $|0\rangle_m$ , defined to satisfy  $\hat{a}_m |0\rangle_m = 0$ , and will have vanishing correlation with the rest of the system. Clearly there will be a smooth transition between these two regimes, which our work does not capture. Nevertheless by considering only a finite number of modes  $N$ , as we will numerically be doing, our description of this set will be accurate as long as  $\Delta t \ll 1/\omega_N$ .

Note also that, in terms of application, the amount of entanglement that one obtains between cavities after slamming a mirror (which we will discuss in the next section) depends on how fast one's mirror is slammed. The faster it can be achieved, the more entanglement will remain in the two cavities afterwards. This is because the high-energy modes contain entanglement, and thus the more of these modes whose states are not significantly altered by introducing the mirror, the more entanglement we will retained. For modes of too-high energy,  $\Delta t \gg 1/\omega_m$ , the act of slamming the mirror will destroy the correlations that they have with the opposite side of the cavity.

## 13.5 Entanglement

We will now enter the results section of this chapter. We will discuss various aspects of entanglement between the two sides of the cavity (equivalent in both the cases of with and without a cavity, as discussed above). As part of our exposition we will propose a spatial distribution of entanglement between the two sides of the cavity, and see how this naturally leads to the physical picture of bursts of (entangled) particles being produced by slamming down a mirror. We will begin by just discussing a single mirror, and later will move on to the two-mirror case. We will show that with two mirrors, slammed simultaneously some distance apart, there is still entanglement retained between separated regions (i.e. left-most and right-most). We will also discuss how the act of slamming down a mirror can be interpreted as an efficient method of vacuum entanglement harvesting.

Our result are computed numerically from the covariance matrices presented Sect. 13.3. To do so, however, we must restrict ourselves to finite matrices. This means taking only a finite number of local modes  $N$ , both on the left and right sides. That is, what we actually consider is the reduced state of the first  $N$  local modes on each side. This is actually not physically unrealistic since, as discussed in Sect. 13.4.2, our analysis will

only be valid for some low-energy regime anyway, depending on how fast the mirror is slammed. Numerically, unless otherwise stated we will take  $N = 200$ . Note, however, that the reduced state of these first  $N$  local modes is exact up to numerically negligible addends. That is, in performing the Bogoliubov transform we made sure to include enough global modes in the sum of Eq. (13.36), such that our results converge.

### 13.5.1 Mode-mode entanglement

With the state of the global vacuum represented in the local-mode basis, as given by Eq. (13.36), we can characterize the entanglement between the two sides of the cavity. We can, for example, consider the two-mode entanglement between each pair of local modes on the left and right side. The correlations between each pair (as given by the two-point correlators of the number operators) have already been computed in [166]. However, for each two-mode pair the fact that they are correlated does not imply that they are entangled because the two-mode state of this pair is mixed. Thus, to extend upon the results of [166] we compute the logarithmic negativity  $E_N$  [59] of each pair between the two sides.

To this end, we take the  $4 \times 4$ , two-mode covariance matrix (i.e. the reduced state) of mode  $m$  on the left and mode  $n$  on the right of the cavity. This is simply

$$\sigma_{\text{two mode}} = \begin{pmatrix} \sigma_{mm} & \gamma_{mn} \\ \gamma_{mn}^T & \bar{\sigma}_{nn} \end{pmatrix}. \quad (13.50)$$

From here, we can apply Eq. (3.34) to compute  $E_N$  between the two modes. The result is displayed in Fig. 13.3, where we consider field masses  $\mu = 0$  and  $\mu = 15/R$ . The cavity is split in two equal regions as  $r = 0.5R$ . We observe that, perhaps remarkably, nearly every mode is entangled with almost every other. Eventually as  $m$  and  $n$  become sufficiently different the two-mode entanglement tends to vanish (although they will always have nonzero correlation), but we can see that the decay is very slow. It should be noted that we can similarly compute the entanglement between different local modes from the same side, and in fact doing so produces a qualitatively equivalent plot. A particularly striking feature of the mode-mode entanglement is that the peak entanglement moves to higher mode numbers as the mass of the field is increased<sup>4</sup>. This figure clearly demonstrates that the two sides of the cavity are entangled. Even a single pair with nonzero entanglement

---

<sup>4</sup>This behavior is actually expected from the fact that the correlation length in a field goes as the Compton wavelength [170], meaning that correlations become more spatially confined with higher mass  $\mu$ . It follows that what correlations are present between the two sides should be more supported within the modes of smaller wavelength, i.e. those of higher frequency.

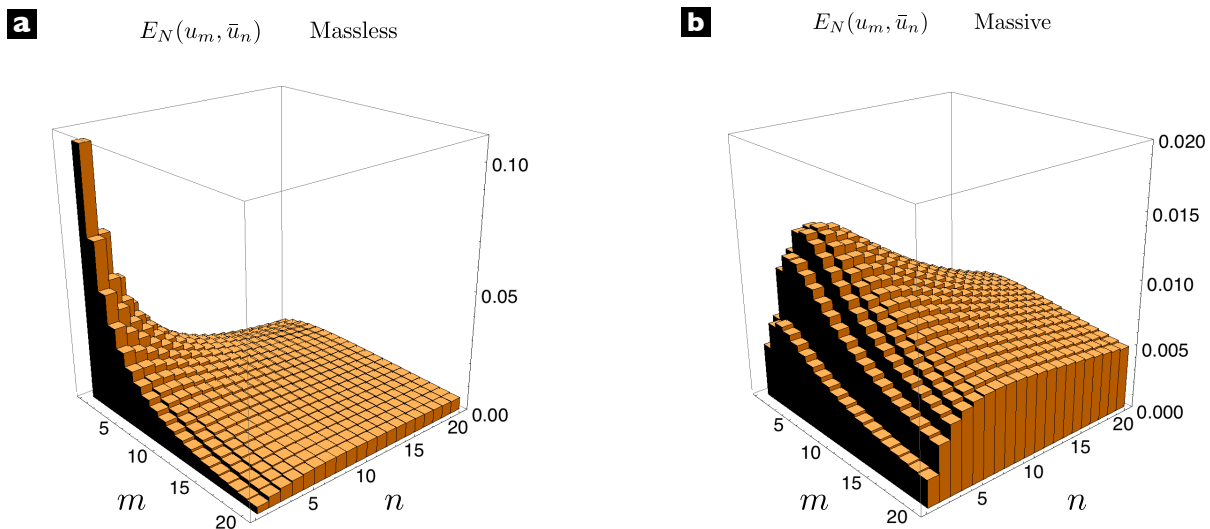


Figure 13.3: The logarithmic negativity  $E_N$  between local modes  $u_m$  and  $\bar{u}_n$  on the left and right sides of the cavity, respectively. The cavity is divided in two equal regions  $r = 0.5R$ . Left: a field mass of  $\mu = 0$ . Right: a field mass of  $\mu = 15/R$ .

demonstrates this. However even if every pair were separable this would *not* constitute a proof that the two sides as a whole are separable.

This leads to the question of the full, many-mode entanglement between the two sides. We can certainly compute this, given some set of  $N$  local modes on either side [45] (specifically we would compute the negativity, not the reduced entropy, as we explain in a moment). This of course gives a non-zero answer. However it is questionable how useful the numerical answer actually is because it will always depend on the number of local modes  $N$  considered. The entanglement increases with  $N$ , and we expect that it diverges in the  $N \rightarrow \infty$  limit (check footnote 5), given that the vacuum entanglement is typically known to be UV-divergent. We will thus not concern ourselves with this calculation explicitly. Nevertheless there is a related issue that should be discussed before moving on, which we will now focus on.

### 13.5.2 The mixedness problem

One would assume that in order to compute the entanglement one should simply compute the reduced entropy of one side of the cavity, since the global state is pure. Formally

this is true of course, but interestingly the reduced entropy will never be an entanglement measure if one only considers a finite number of local modes  $N$ , and in fact this can never be remedied by simply increasing  $N$ .

This occurs because, as we have just seen, there is quite a lot of correlation between local modes of different number. This means that the left-side state  $\sigma$  (with finite number of modes) will not just be entangled with the opposite side of the cavity but also with the higher-number modes on the same side. That is, the entropy  $S(\sigma)$  is *not* a measure of entanglement with the other side, but rather with the other side plus all of the higher modes that we have traced away. Put another way: if we compute the full state of both sides  $\sigma_{\text{loc}}$ , but with the understanding that this corresponds to the reduced state of the first  $N$  local modes on the left with the first  $N$  on the right (and their correlations), then this state will be mixed despite the fact that the global vacuum is pure. Equivalently, the transformation of Eq. (13.32) will never in practice be symplectic. What’s more (and rather interestingly) this problem does *not* get better as  $N$  is increased <sup>5</sup>.

Importantly, such an issue will never arise in any real scenario of a slamming mirror; a finite slamming time  $\Delta t$  fixes this mixedness problem. The introduction of a mirror is just represented by a time-dependent Hamiltonian, and so of course the evolution of the field under this action must be unitary. The system of the two new cavities combined, therefore, must be in a pure state. As discussed in Sect. 13.4.2, a finite  $\Delta t$  will mean that local modes of high enough frequency will not actually be in the state nor share the

---

<sup>5</sup>In fact, as we increase the number  $N$  of local modes considered (on both sides of the cavity) the global state we obtain becomes *more* mixed, with a higher entropy. We suspect that the entropy diverges in the  $N \rightarrow \infty$  limit, despite the fact that in a formal sense the result should be a pure state. After a moment of thought this is actually not overly surprising. Consider for a moment the very different system of a spatial volume in free Minkowski space with a field in the Minkowski vacuum. It is well known that the entropy of the reduced state inside the volume scales as its area, meaning that as this region is expanded it becomes more mixed. Thus, despite the field over all of space being in a pure state, one can never approach this by taking the limit of larger and larger regions (the entropy will diverge as the region expands to infinity). In this example the area-law can be physically understood by taking a spatial discretization of the field. A given spatial degree of freedom will largely only be entangled with its nearest neighbors, and thus the area law can be understood considering that the area is proportional to the number of nearest-neighbor connections that the entangling surface crosses. In our scenario we have seen that the global vacuum has a very densely connected entanglement structure in the local-mode basis. Every local mode is entangled with many others, including many others of higher frequency. Thus, by increasing the number of local modes  $N$  that we consider we are increasing the number of “entanglement connections” between low and high modes that are separated by the cutoff. Given this intuition it makes sense that the entropy of our global state should increase with increasing  $N$ ; it arises as a consequence of the system being highly connected. Even so, it is interesting (and perhaps disconcerting) that in the local-mode basis one can never approach purity by considering more and more modes. We suspect that this is deeply connected to the note made in [166] regarding the unitary inequivalence between the global and local mode bases.

correlations as predicted from the covariance matrices in Sect. 13.3, which were computed assuming instantaneous slamming. For a real situation, high-frequency local modes will be nearly in their ground states, and importantly have vanishing correlations with anything else, thus remedying the origin of the mixedness problem. The global state in the local basis will indeed be pure beyond a given energy scale, as it must be.

### 13.5.3 Symplectic diagonalization

Here we will describe the process of symplectically diagonalizing the local states  $\sigma$  and  $\bar{\sigma}$ . This is a method by which we can greatly simplify the entanglement structure between the two sides which, given the complexity seen in Fig. 13.3, will be a considerable advantage. We will see in later sections how this process also allows us to make conclusions about the spatial distribution of entanglement as well as see very clearly the propagating “burst” of particles that is produced by slamming down a mirror.

The specifics of local, symplectic diagonalization and the method for finding the correct transformations matrices are described in Sect. 3.3 and Appendix. A, respectively. We (numerically) find symplectic matrices  $\mathbf{S}_D$  and  $\bar{\mathbf{S}}_D$  that diagonalize  $\sigma$  and  $\bar{\sigma}$ , respectively:  $\mathbf{S}_D \sigma \mathbf{S}_D^T = \mathbf{D}$  and  $\bar{\mathbf{S}}_D \bar{\sigma} \bar{\mathbf{S}}_D^T = \bar{\mathbf{D}}$  where

$$\mathbf{D} = \bigoplus_m \begin{pmatrix} \nu_m & 0 \\ 0 & \nu_m \end{pmatrix}, \quad \bar{\mathbf{D}} = \bigoplus_m \begin{pmatrix} \bar{\nu}_m & 0 \\ 0 & \bar{\nu}_m \end{pmatrix}. \quad (13.51)$$

Here  $\nu_m$  and  $\bar{\nu}_m$  are the symplectic eigenvalues of  $\sigma$  and  $\bar{\sigma}$ , respectively. Let’s just consider the left side for a moment:  $\sigma \rightarrow \mathbf{D}$ . This is simply a change of mode-basis, and we can compute the mode functions associated with this new basis by reading off the Bogoliubov coefficients from  $\mathbf{S}_D$  via reversing Eqs. (13.29,13.30). Here we will label these coefficients  $\zeta_{\ell m}$  and  $\eta_{\ell m}$  (in place of the usual  $\alpha$  and  $\beta$  notation, respectively). These new mode functions, which we will label  $v_\ell(x, t)$ , are thus given by

$$\begin{aligned} v_\ell(x, t) &= \sum_m (\zeta_{\ell m} u_m(x, t) + \eta_{\ell m} u_m^*(x, t)) \\ &= \sum_m \frac{1}{\sqrt{r\omega_m}} \sin\left(\frac{\pi m x}{r}\right) (\zeta_{\ell m} e^{-i\omega_m t} + \eta_{\ell m} e^{i\omega_m t}). \end{aligned} \quad (13.52)$$

We can similarly define a new set of local modes  $\bar{v}_\ell(x)$  on the right side of the cavity.

We remind the reader that (as discussed in Sect. 13.4.1) we are working in the “Heisenberg picture”, but not such that the  $\hat{q}$  and  $\hat{p}$  operators evolve (i.e. our covariance matrix



is time-independent) but rather such that the mode functions with respect to which we represent the state themselves evolve. In this picture the diagonalizing transformations are of course time-independent (since the covariance matrix is time-independent). We could, however, arrive at the same set of  $v$ -modes working directly in the Schrödinger picture, in which the diagonalizing transformation would be time-dependent <sup>6</sup>.

This is a change of mode basis which results in all left-side modes  $v_\ell(x, t)$  being in a product state with respect to each other, and similarly with the right-side modes  $\bar{v}(x, t)$ . I.e. the transformation  $\mathbf{S}_D$  removes all correlations between modes on the left side. In this way we are isolating exactly the local spatial modes that contain the entanglement between  $\boldsymbol{\sigma}$  and the rest of the system. Furthermore, it turns out that in our system the first mode in this new basis, the one associated with symplectic eigenvalue  $\nu_1$  and spatial mode  $v_1(x, t)$ , is the mode that contains the large majority of the mixedness in  $\boldsymbol{\sigma}$ . That is, almost all of the symplectic eigenvalues have values very near to unity, meaning that the corresponding modes are very nearly pure. The first value,  $\nu_1$ , is by far the largest. For example with the parameters  $r = 0.5R$ ,  $\mu = 0$ , and  $N = 200$  (the number of local modes considered) the first several symplectic eigenvalues take the values  $\{\nu_\ell\} = (1.840, 1.051, 1.004, 1.000, \dots)$ . Note that as  $N$  is increased these values (and thus the entropy of  $\boldsymbol{\sigma}$ ) increase as well. All of this applies equally well to the right-side transformation  $\bar{\boldsymbol{\sigma}} \rightarrow \bar{\mathbf{D}}$  via  $\bar{\mathbf{S}}_D$ .

As elaborated on in Sect. 3.3, if the state  $\boldsymbol{\sigma}_{\text{loc}}$  of both sides were pure then applying the local transformation  $\mathbf{S}_D \oplus \bar{\mathbf{S}}_D$  to  $\boldsymbol{\sigma}_{\text{loc}}$  would also diagonalize the off-diagonal (correlation) block  $\boldsymbol{\gamma}$ . Were this the case then the local mode  $v_1(x, t)$  on the left side would be solely correlated with the corresponding mode  $\bar{v}_1(x, t)$  on the right side, and similarly for the higher  $v$ -modes. Unfortunately, as discussed above, when taking a finite  $N$  we necessarily find that  $\boldsymbol{\sigma}_{\text{loc}}$  is a mixed state. This means that a local symplectic diagonalization does not produce this one-to-one correspondence between the two sides. Despite this, however, we have found that in fact we very nearly do obtain this correspondence upon local diagonalization. This can be seen in Fig. 13.4 where we plot the logarithmic negativity between modes  $v_\ell(x, t)$  and  $\bar{v}_\ell(x, t)$  similarly to what is plotted in Fig. 13.3 for the  $u$ -modes. Here we have taken  $N = 200$  for both the left and right sides. We see that indeed, despite

---

<sup>6</sup>This can also be done in either of the pictures in which it is the covariance matrix that evolves,  $\boldsymbol{\sigma}(t) = \mathbf{S}_F(t)\boldsymbol{\sigma}\mathbf{S}_F(t)^T$ , and in which the spatial modes are time independent,  $u_m(x, 0)$ . In this case the diagonalizing transformation will be time-dependent:  $\mathbf{S}_D(t)$ . However the symplectic spectrum of  $\boldsymbol{\sigma}(t)$  will be time-independent, being symplectically invariant. Thus we have  $\mathbf{D} = \mathbf{S}_D\boldsymbol{\sigma}\mathbf{S}_D^T = \mathbf{S}_D(t)\boldsymbol{\sigma}(t)\mathbf{S}_D(t)^T = \mathbf{S}_D(t)\mathbf{S}_F(t)\boldsymbol{\sigma}\mathbf{S}_F(t)^T\mathbf{S}_D(t)^T$ , from which we can represent the time-dependent diagonalizing transformation as  $\mathbf{S}_D(t) = \mathbf{S}_D\mathbf{S}_F(-t)$ . We can use this to compute the corresponding time-dependent Bogoliubov coefficients  $\gamma_{\ell m}(t)$  and  $\eta_{\ell m}(t)$ . Using Eq. (13.48) and the relation between a symplectic transformation and its corresponding Bogoliubov coefficients, as given by Eqs. (13.29,13.30), it is straightforward to find that  $\gamma_{\ell m}(t) = \gamma_{\ell m}e^{-i\omega_m t}$  and  $\eta_{\ell m}(t) = \eta_{\ell m}e^{i\omega_m t}$ , in agreement with Eq. (13.52).

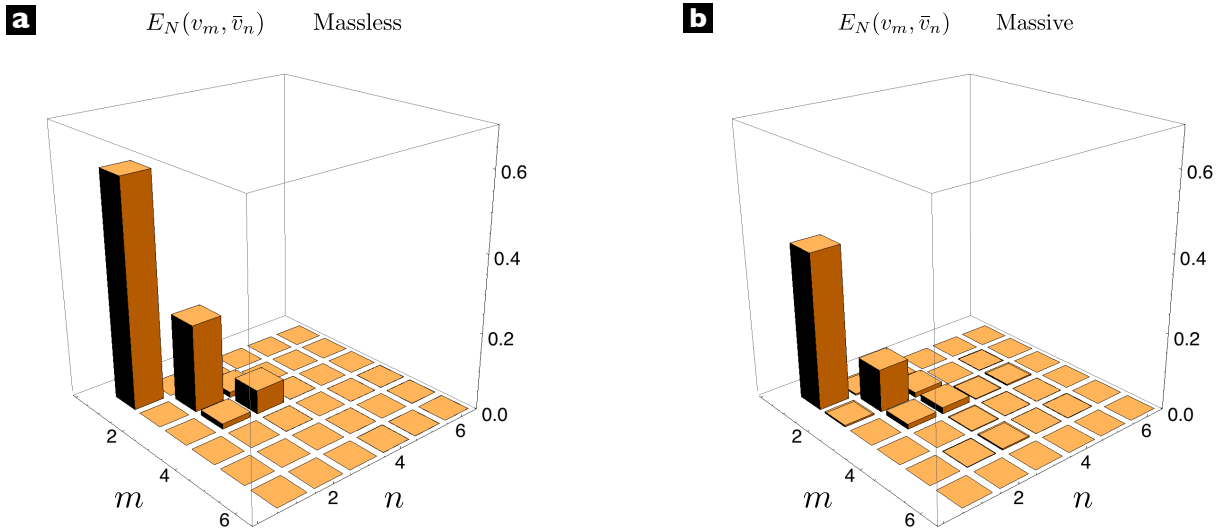


Figure 13.4: The logarithmic negativity  $E_N$  between local, diagonalizing modes  $v_m$  and  $\bar{v}_n$  on the left and right sides of the cavity, respectively. The cavity is split into two equal sides,  $r = 0.5R$ , and  $N = 200$  for both the left and right sides. Left: a field mass of  $\mu = 0$ . Right: a field mass of  $\mu = 15/R$ .

$\sigma_{\text{loc}}$  being mixed, the majority of the entanglement between the two sides is contained in  $v_1(x, t)$  and  $\bar{v}_1(x, t)$  (we could also plot the mutual information between modes, in order to get a better idea of the correlations in general, but the result looks nearly identical qualitatively).

### 13.5.4 Spatial structure of entanglement

One immediate application of finding the locally, symplectically diagonalizing basis is that we are able to discuss and make observations about the spatial structure of entanglement between the two sides of the cavity. For this section we will take  $t = 0$ , by which we are discussing the local physics of the cavity before the mirror has been introduced. That is, in this section we are simply asking about the local properties of a vacuum field, and not considering yet the time evolution caused by introducing a mirror.

We know that there is spatial vacuum entanglement; the two sides of the cavity are entangled. This fact alone, however, gives no information on how entanglement is spatially distributed. From what is known about vacuum entanglement we expect it to be spatially focused near the boundary between the two regions, since the correlation in a field decays

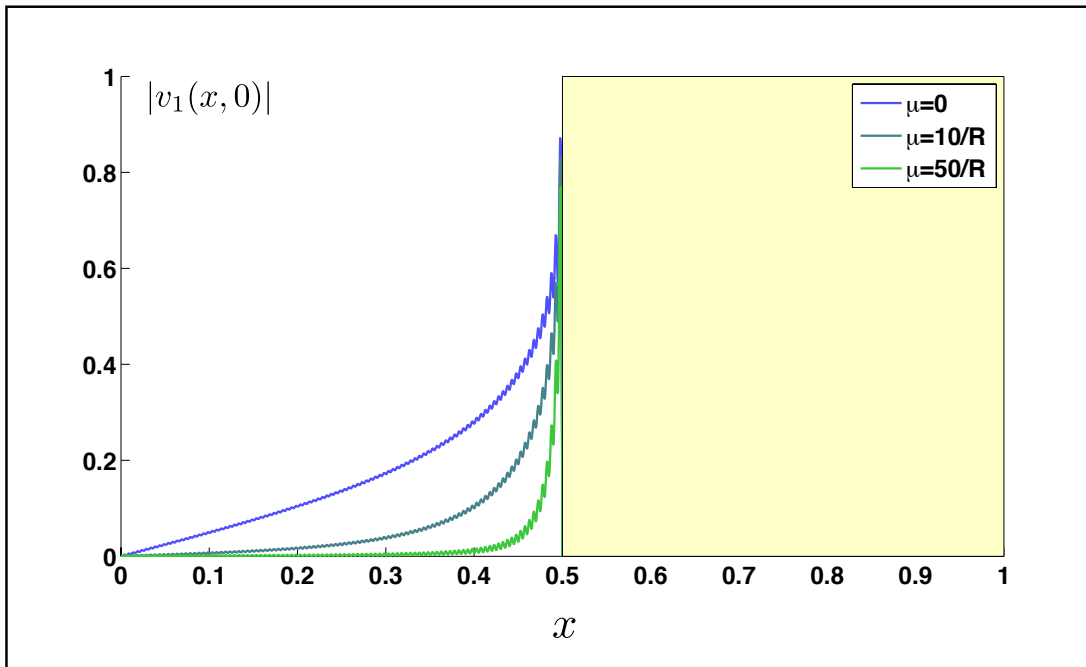


Figure 13.5: The function  $|v_1(x)|$  in the left-side of the cavity, representing the spatial distribution of entanglement with the opposite side. The parameters are given by  $r = 0.5R$ , and  $N = 200$ , with different field masses  $\mu$  considered: 0 (blue),  $10/R$  (light blue) and  $50/R$  (green). As can be seen: the larger the mass of the field, the closer the entanglement straddles the boundary between the two sides of the cavity, as expected.

with distance [93, 94, 95]. It is this that leads, for example, to the well-known area-law for the entanglement entropy. There is also evidence that the entanglement characteristic distance goes as the Compton wavelength of the field [170], thus we should also expect the entanglement spatial distribution to hug the boundary more closely as we increase the mass  $\mu$  of the field.

To obtain information on the spatial structure of entanglement we use a technique very similar to that in [167], which there was used within the context of lattice systems. Since the mode function  $v_1(x)$  contains the majority of the entanglement (right now working at  $t = 0$ ), what we propose is that the function  $|v_1(x)|$  gives information about the spatial structure of entanglement. The larger  $|v_1(x)|$  is at a given  $x$ , the more entanglement is localized at that point. Operationally this proposal makes sense; if one were to try to swap this entanglement into an Unruh-deWitt type detector model then it makes sense to

place the detector where  $|v_1(x)|$  is largest, since this directly translates into the coupling strength between this mode and the detector. Of course there is also entanglement in the higher  $v$ -modes, and these would form corrections to our  $|v_1|$  estimate. Seen another way, we can consider measuring the entanglement between regions by means of local projective measurements onto a pair of spatial modes [150, 7]. Since most of the entanglement is isolated between  $v_1(x)$  and  $\bar{v}_1(x)$ , it is these modes that we would want to measure in order to obtain the greatest amount of entanglement.

In Fig. 13.5 we plot the function  $|v_1(x)|$  at time  $t = 0$  using the parameters  $r = 0.5R$ ,  $N = 200$ , and for three mass values  $\mu$  of  $0$ ,  $10/R$ , and  $50/R$ . As can be seen, both of the conditions discussed above are satisfied. Namely, the distribution indeed straddles the boundary between the two sides of the cavity (in this case the boundary is to the right because we are looking at the left side). Furthermore, as the mass  $\mu$  of the field is increased we see that the distribution becomes more localized at the boundary, representing a decreasing correlation length.

Note that the small vibrations that can be seen in Fig. 13.5 are due solely to taking a finite number  $N$  of local modes. As  $N$  is increased these vibrations become smaller. However the overall shape of the function does not change upon increasing  $N$ ; a fact that further indicates that the function  $|v_1(x)|$ , as plotted, well represents the entanglement structure despite the mixedness problem.

All that we have done here is show the shape of the left-side mode function that contains most of the entanglement with the right side, and how much this can truly be considered a distribution of entanglement is questionable. A more thorough approach to discuss the entanglement spatial structure could be to consider the local reduced states for infinitesimally small regions and see how much these regions are entangled with the right side of the box.

### 13.5.5 Entangled bursts of particles

In the previous section we have looked at the form of  $|v_1(x, t = 0)|$  and claimed it to be a good representation of the spatial distribution of entanglement. A next obvious questions is: in the case that we slam down a mirror at  $t = 0$ , how does  $|v_1(x, t)|$  evolve for  $t > 0$  and what significance does this have? The time evolution is simply given by Eq. (13.52), i.e.  $v_1(x, t)$  evolves according to the Klein Gordon equation with initial conditions given by  $v_1(x, 0), \dot{v}_1(x, 0)$ , as shown in Fig. 13.5. As can be expected, the evolution is that of a wavepacket propagating away from the newly slammed mirror. For example in Fig. 13.6

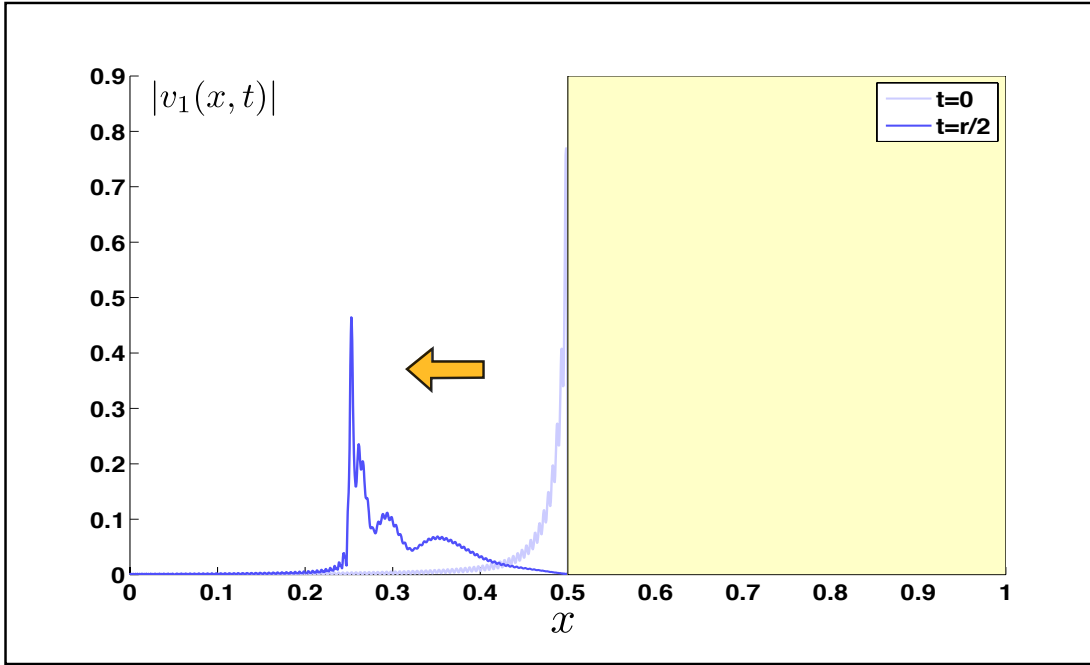


Figure 13.6: Evolution of the entanglement spatial distribution for the massive case  $\mu = 50/R$  after an elapsed time  $t = r/2$ . We can see a peak for the correlations at exactly the position of the particle-burst front as originated from the slamming. The cavity parameters are the same as in Fig. 13.5

we plot  $|v_1(x, t)|$  at time  $t = r/2$  for parameters  $r = 0.5R$ ,  $N = 200$ , and with a field mass of  $\mu = 50/R$ .

By construction, however, the state of this evolving mode and the correlations between it and the right-hand cavity are exactly the same as at  $t = 0$  (i.e. highly excited and highly entangled with right-hand mode  $\bar{v}_1$ ), when these correlations could be interpreted solely as vacuum entanglement. That is, the state of the propagating wavepacket seen in Fig. 13.6 is highly excited, and is highly entangled with the symmetrically evolving wavepacket in the right-hand cavity. That is, we see exactly the physics we expect, namely that slamming down a mirror produces bursts of particles that propagate away from it! Similarly in the right-hand cavity the function  $\bar{v}_1(x, t)$  represents a burst of particles propagating to the right. A detector placed within one of these cavities will then be able to measure these particles once they hit it <sup>7</sup>. Additionally we see that the bursts on the two sides

<sup>7</sup>One may be concerned that in Fig. 13.6 there appears to be an amount of acausal signaling. Of course,

are entangled, and that they are entangled exactly in the same manner that the vacuum was entangled prior to the introduction of the mirror! In fact, their entanglement directly results from (or rather, it simply *is*) the vacuum entanglement prior to the mirror being slammed.

This emphasizes and illustrates nicely our primary message: that the real excitations created by slamming down a mirror are identical to the “virtual” excitations attributed to the original vacuum entanglement. Furthermore, this perspective motivates an experimental approach to verifying, and perhaps even harvesting and using, vacuum entanglement. That is, if we were able to slam a mirror and measure the real particles, in such a way that we could confirm quantum correlation statistics on the two sides, then this would constitute a verification of vacuum entanglement. We discuss this further in Sect. 13.6.

We wish to point out that the correlations between the bursts on either side of the mirror have nothing to do with the symmetry introduced by the fact that we are slamming the mirror at the  $r = 0.5R$  point. Entanglement and similar correlations have to do with correlation between single-shot measurements performed locally on the two systems in question, and not on whether the two reduced states are the same or similar. The bursts of particles would continue to be entangled independent of where in the cavity the mirror is introduced.

The reader should also know that what we have presented is an approximate picture in regards to visualizing the burst of particles, as we are just using a single delocalized mode  $v_1(x, t)$ . It is a good approximate picture, given that this mode contains the majority of excitations. However, in order to gain the full structure of the burst one could instead monitor the change at different times of the expectation values of local number operators attached to small (perhaps infinitesimal) regions. As the burst reaches these small regions we expect these number expectation values to jump, and they will be different from the vacuum expectation values only inside the future light cone of the spacetime point at which we slam the mirror.

### 13.5.6 Two mirrors

We have just stated that the entanglement between the bursts of particles produced by the slammed mirror, in the left and right-hand sides, comes from the vacuum entanglement that was previously there to begin with. One may, however, be concerned that this is simply one

---

for a delocalized mode, it makes no sense to strictly talk about causality [1]. In any relevant calculation all modes would be considered and no acausal behavior would be seen.

perspective on the situation. One may argue that what really physically occurs is that the act of slamming the mirror locally creates entangled quanta which then propagate away, rather than this entanglement having been previously present.

To debunk this view we need simply consider a slightly different scenario: that of slamming *two* mirrors down simultaneously, some distance apart from each other. It is known (and we will confirm) that there is entanglement between regions of space even when they are separated. This means that when we slam two mirrors the resulting field states in the left-most and right-most cavities will be entangled, as would be measurable from the real particle statistics. In this case one cannot claim that this entanglement was simply created by the mirror, because now there is no common mirror connecting the two regions. In this case it is clear that the entanglement between the two cavities comes directly from the vacuum entanglement that was already present beforehand as no causal signal can connect them.

The mathematics of this scenario is exactly the same as before except that now we must consider splitting the cavity into three regions, as we have already discussed in Sect. 13.3.2. We choose some size for the three regions (here we will take regions  $A$  and  $C$  to be the same size, and separated by some distance  $B$ ). We can then take the reduced state of the left-most and right-most regions, as given by Eq. (13.47) and perform exactly the same entanglement analysis as we have done above. The result in short is that they are entangled. This validates our above argument since, by construction, this entanglement is present between real, stationary mode excitations after the mirrors have been introduced.

In particular, it is interesting to again perform the local, symplectic diagonalization such that we go to the local mode basis  $\{v_m^A, v_n^C\}$ . As discussed in Sect. 13.5.3, this procedure fails to produce a nice one-to-one entanglement structure when one's state is mixed. As we saw, the mixedness problem above only causes slight deviations from this structure. Now, however, the extra mixedness in the  $AC$  system caused by tracing out  $B$  *really* ruins this structure. We plot in Fig. 13.7 the mode-mode logarithmic negativity between the  $v^A$  and  $v^C$ -modes for the cases in which the distance  $B$  between the two regions is  $0.1R$  and  $0.2R$ , where we have taken  $N = 200$  for each region and we use a massless field  $\mu = 0$ . As we can see, the entanglement rapidly decays with the distance between the regions, as should be expected. We also note that in this case the *higher*  $v$ -modes become the dominant entanglement carriers, meaning that to actually measure such entanglement one should try to change the wavepacket form that one is measuring to conform with the shape of  $|v_2(x, t)|$  or  $|v_3(x, t)|$  or whichever mode carries the most entanglement. It is not overly surprising that  $v_1(x, t)$  becomes superseded for a large enough distance  $B$  once one realizes that  $v_1(x, t)$  largely contains the entanglement localized on the boundary between regions. Once there is no common boundary we therefore rapidly lose this entanglement

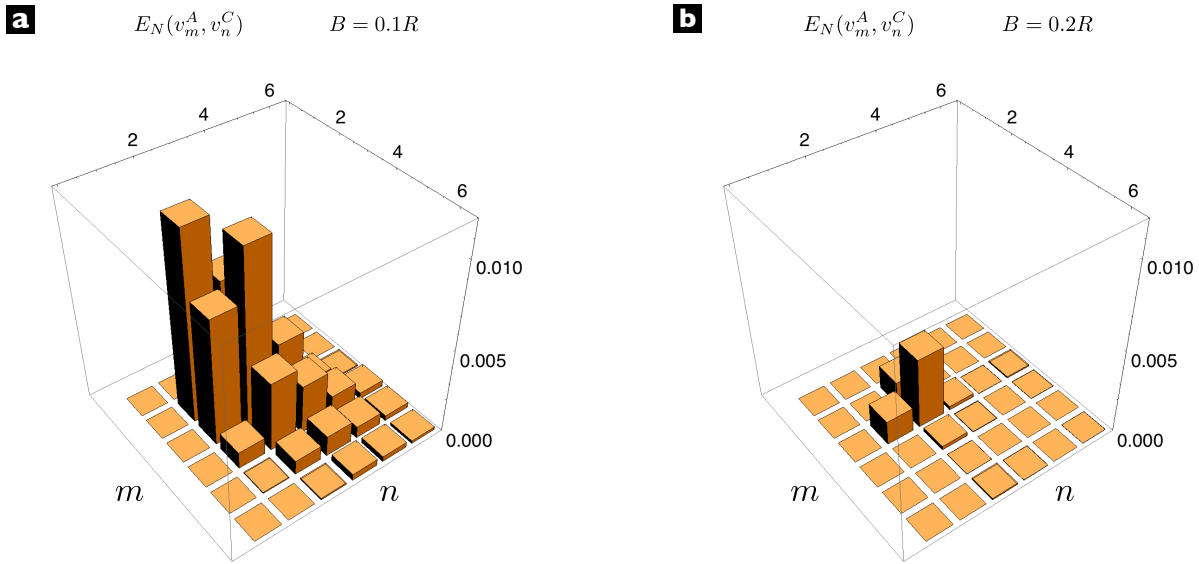


Figure 13.7: Two mirror case: logarithmic negativity  $E_N$  between local, diagonalizing modes  $v_m^A$  and  $v_n^C$  on the left and right-most sides of the cavity, respectively, in the case that the field is massless  $\mu = 0$ . The cavity is in this case split into three regions,  $\Delta_A = [0, 0.5R - B/2]$ ,  $\Delta_B = [0.5R - B/2, 0.5R + B/2]$ ,  $\Delta_C = [0.5R + B/2, R]$ . We have taken  $N = 200$ . Left: Size of the middle section  $B = 0.1R$ . Right: Size of the middle section  $B = 0.2R$ .

contribution.

## 13.6 Experimental motivations and prospects

We would like to devote this section to discuss possible experimental platforms with which to observe the phenomena described above. The primary motivation for such an experiment would be the verification of vacuum entanglement and, possibly in the future, an effective method of entanglement harvesting. We must point out that the description of our model so far has considered an idealized theoretical scenario and has not been adapted to any particular experiment. Moreover, a first analysis shows that such an experiment would be highly challenging and some of the requirements needed (mirror slamming times, high sensitivities...) may require considerable effort before becoming feasible.

First of all, let us focus on the essential elements of the theoretical scheme, which



should be imperatively implemented in any experiment of this sort. We require a quantum field in a cavity, which should be taken into its lowest energy state (the vacuum), and a boundary condition (here, a mirror) which will quickly appear somewhere inside the cavity and produce particles similar to the dynamical Casimir effect. For most platforms to be considered the field would be massless, as we will be dealing with electromagnetic fields. In addition, after these particles have been produced they must be detected and, if possible, their entanglement measured.

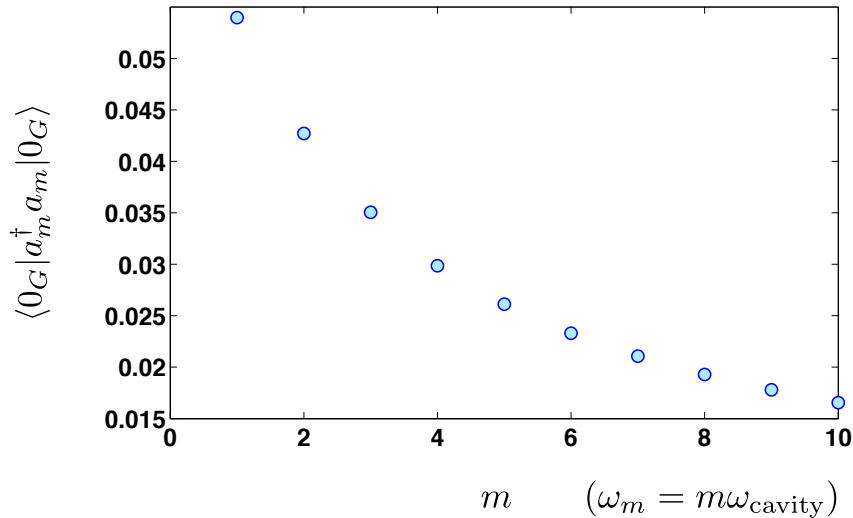


Figure 13.8: The number expectation value of local modes  $u_m$  for the case of a massless field  $\mu = 0$  and a cavity split in half  $r/R = 0.5$ .

Before anything else, we should check the amount of particles created. Based on previous results [166], Fig. 13.8 shows the average number of local particles created after slamming the mirror, dividing the cavity in two equal sides. We can see that the maximum amount of particle creation is achieved by the first local mode, but that even this is quite small (0.052). The expected value is independent of the cavity size or the speed of the mirror, which sets only the adiabatic UV-cutoff. Any detector that aims to extract those particles would therefore be highly sensitive (and the experiment would need to be run many times). The relative positioning of the mirror could be modified in order to improve those numbers, but that improvement is only slight and, from our point of view, not relevant enough to be discussed at this point.

The most natural set-up for such an experiment, given the theoretical set-up, would involve the use of an optical cavity [171]. In practice, however, this setup would be very

difficult to implement. In order to obtain reasonable particle production we require a slamming time that satisfies  $t_{\text{slam}} \ll 2L/c$ . For optical cavity setups this would require a slamming on the order of picoseconds. Certainly this is mechanically impossible with current technology if we are imagining physically inserting a mirror into an optical cavity. A more feasible approach would be to use a sheet of material that allows for rapid variation of reflectivity. Indeed a fractional variation of reflectivity has been achieved on the picosecond time scale [172]. Although not yet suitable for our purposes, such technology may in the future be sufficient to verify vacuum entanglement.

Another promising candidate would be Circuit Quantum Electrodynamics [110, 111]. Several experiments concerned with the peculiar properties of the quantum vacuum (similar to the one here discussed) have been carried on this platform, in particular the first observation of the Dynamical Casimir effect [112]. The kinds of techniques used in that experiment could be very useful in a future proposal. The build up of a mirror inside the cavity, is however, a very different matter, as it implies the “activation” of a boundary that previously was not there. In the case of circuit QED, meandering resonators of lengths  $\sim 20$  mm have been built [173, 174] but longer lengths could be achieved, say of 100 mm. For that size a mirror slamming time of 0.7 ns may be enough to show the effects that we want.

Along these lines, recent work in Circuit QED [175, 176] has shown that a superconducting qubit coupled to a waveguide can fully reflect single photons, while it being possible to modulate the coupling to the natural mode of the cavity in the ns timescale. That could be the first candidate for the slamming mirror. However for a mirror to reflect all photons the qubit would not be enough; rather the possibility of replacing the qubit with a frequency-tunable cavity which couples to the middle of the line could be studied. Very fast tuning of cavities has been proven before ( $\sim 3$  ns) and it is expected to be achievable in the subnanosecond regime [177].

Finally, another experimental platform worthy of consideration would be cold atoms in optical lattices. Although we would be dealing in that case with a discrete quantum field theory (e.g. Bose-Hubbard model), the possibilities for creating “mirror-like” conditions by raising and lowering potential barriers using holographic techniques in the subnanosecond-picosecond regime [178] might very well fit our needs.

## 13.7 Discussion

We have given an answer to the question of “what does it mean for half of an empty cavity to be full?” by considering a physical scenario in which this statement actually has

operational meaning. The procedure that we considered is that of very quickly introducing one or more mirrors into a cavity scalar field prepared in its vacuum state and observing the consequences. Unsurprisingly such an action induced particle creation in the field. The key observation, however, is that these real excitations are mathematically equivalent to the local vacuum excitations related to spatial entanglement in the field. As a result, the real particles that one obtains on either side of the newly introduced mirror are entangled with each other. Furthermore we have proven that this entanglement can not simply have been created by slamming down a mirror, and rather derives directly from the previously present vacuum entanglement. We proved this by also studying the case in which two mirrors, rather than one, are slammed down simultaneously and some distance apart. In this scenario the excitations in the left-most and right-most regions created from this cavity splitting are also entangled with each other, despite there being no common mirror and no possible communication between them. This entanglement is exactly the spatial vacuum entanglement that was already present, now manifest in the real (and measurable) quanta that we pump into the system by introducing a mirror.

As part of our exposition we utilized Gaussian quantum mechanics to easily derive the reduced states and correlations of the vacuum field in different subregions of the cavity. We have used this technology to discuss the entanglement structure between regions of the cavity and the time evolution that follows upon slamming down a mirror, including directly relating the entanglement between regions with the burst of particles created by the mirror. This work provides a solid operational interpretation for vacuum entanglement and the local excitations that derive from it; these “virtual” excitations are simply the real excitations that one gets when slamming down a mirror. In addition, this realization motivates a simple experimental proposal for the verification of vacuum entanglement in a cavity system. Indeed we discuss how the act of slamming down a mirror may represent a very effective method of harvesting the vacuum entanglement. We finished by briefly discussing some preliminary experimental prospects for the laboratory realization of this proposal.

In addition to working towards an experimental realization there are many shorer term, theoretical questions in regards to this scenario that can be the subject of future projects. Such projects could include properly taking into account a finite-time introduction of the mirror, computing the response of a detector due to the burst of the particles (and the subsequent entanglement harvesting), and extending the analysis into free space or higher dimensions. Furthermore, the notion of quickly introducing a mirror and the resulting excitations may in fact have strong connections to quantum black hole physics, such as holography [179] and firewalls [180]. An extended study of how our work relates to these areas may be the subject of future research.

# Chapter 14

## Conclusions

In this thesis we have examined, from several operational perspectives, the phenomena of quantum correlations and particle creation in relativistic quantum fields. Such effects lie at the interface between two historically disparate realms of physics: quantum field theory and quantum information. In the past decade there has been an explosion of interest in exploring the overlap between these two. The results have led, principally, to enlightening new perspectives on field theory itself as well as the connections between field theory and gravitation. This merging has also generated interest in elucidating the ways in which the nature of quantum fields may aid us in our quantum information and computational efforts.

We have devoted effort to both of these endeavors in this thesis. On the one hand, we examined questions regarding the nature of quantum correlations within scalar fields, their connection to particle creation phenomena such as the Unruh effect, and have made significant progress in deconstructing the interpretational hurdles associated with these aspects of nature. On the other hand, we have made novel proposals regarding the ways in which these phenomena may aid us or be useful as a resource in the quest to develop reliable and scalable quantum technologies. In both of these efforts we have used the general framework of operationalism. That is, we have approached problems by proposing and utilizing physical models aimed at emulating what may, at least in principle, be performed and observed within experimental setups. Rather than focusing on mathematical facts derivable from a given theory, we instead question what physical and observable consequences these facts imply. As we have seen, this allows us to entirely sidestep otherwise unsightly interpretational conundrums, and even provide solid and satisfying solutions to such issues. Working operationally, by its very nature, also facilitates a clean transition to questioning in what ways a theoretical prediction may be tested in the laboratory and, in many cases, making

promising proposals in this respect. In this thesis we have used three primary operational frameworks, each of which takes advantage of Gaussian quantum mechanics.

First, in Part. II we developed and made great use of a non-perturbative particle detector model, in which we took the detector to be a harmonic oscillator rather than a qubit. This model allows us to probe inherently non-perturbative features of relativistic quantum physics which cannot be studied using the canonical particle-detector approach. Examples of this include long-time effects such as thermalization and equilibration. After deriving the model itself, we used it in a variety of studies. We started by examining the Unruh effect within a cavity field, markedly different from the usual free-space scenario. Not only were we able to demonstrate that an accelerating detector *thermalizes* (a stronger result than the instantaneous transition rate) with temperature proportional to acceleration, but also that this result is largely independent of the boundary conditions placed on the cavity field. We went on to demonstrate the spacelike harvesting of genuine tripartite entanglement from the vacuum, as well as study the difference between entanglement harvesting and discord harvesting when the temperature of the field is increased. Surprisingly, we found that while entanglement rapidly decays with temperature (as expected) the discord can undergo remarkable *growth* from doing this. This seems to imply that either the quantum discord is simply an inappropriate measure of quantum correlation, or that in certain situations we may be able to actually use environmental noise (correlated noise) to aid us in quantum computational protocols. Next, we developed a scheme by which we may reliably and sustainably generate entanglement out of a cavity field, a protocol that we call entanglement farming. This consists of sending many pairs of detectors sequentially through a cavity, each time modifying slightly the state of field in the cavity. Eventually a fixed point state is reached, and is one that (somewhat remarkably) consistently produces detectors that emerge entangled. Finally, we modified the farming proposal by adding a time delay between sequential detector pairs. We discovered that this allows preparation of one's system in a manner very sensitive to perturbations on the system. We used this fact to propose a type of quantum seismograph, where minute vibrations of the cavity walls may produce significant changes to the system behavior. We pondered, very tentatively, what possible application such a system may have to gravitational wave astronomy.

Second, in Part. III we considered performing projective measurements onto localized field modes (as opposed to global modes, which would clearly not be physically feasible) by isolating the reduced Gaussian states of those modes. We performed two studies following this approach. In the first, we examined the response of an observer uniformly accelerating through a thermal bath, meaning that he or she will measure a response both from the Unruh radiation they experience as well as from the thermality already present in the field. In particular, we demonstrated that such an observer is capable of distinguishing between

these two contributions, and identify which is which, contrary to previous claims. In the next chapter, we considered the degradation of entanglement and quantum discord between two observers that occurs due to acceleration by one of those observers. This represents a seminal scenario of interest for relativistic quantum information, and our focus on local modes demonstrated that most previous works examining this setting make qualitatively incorrect claims.

Third, in Part. IV we returned to the question of what exactly it means for half of an empty box to be full. We discussed how the act of very quickly introducing a mirror within a vacuum cavity field (an operationally well-posed procedure) dynamically generates real particles out of the vacuum, unsurprisingly. The key interpretational insight, however, is that these real quanta are exactly those excitations that one mathematically associates with a reduced spatial region, with or without the mirror. The statement “half of an empty box is full” is therefore simply saying that placing a dynamical boundary condition produces excitations, which is not at all mysterious. Furthermore, the real particles on one side of the mirror are entangled with those on the other, this entanglement deriving from the previously present vacuum entanglement. We note that the use of Gaussian quantum mechanics was crucial for the computations performed in this work. In addition to providing a satisfying resolution to an otherwise troubling interpretational issue, this protocol also suggests an, in principle, straightforward experimental method of detecting vacuum entanglement for the first time.

We have made strides in this thesis towards both fundamental questions in relativistic quantum information, as well as questions of importance for its applicability to real-world quantum technologies. This represents, however, a very tiny fraction of what may be investigated and understood. While it is clear that, at least in principle, the nature of relativistic fields may prove useful for quantum computation and metrology, it is still far from clear whether or not in practice such procedures will ever be able to supersede more straightforward approaches in efficiency and impact. A push towards real-world implementation is therefore crucial for the continuation of such a program, so that the limits of applicability may actually be tested in the laboratory. An experimental fulfillment of the proposal made in Part. IV, for example, may well become possible within the next decade. Bringing the detection of vacuum entanglement to the point of experimental feasibility will be the first step in moving towards possible utilization. On the other side of the coin, there are yet many issues of fundamental concern that have been but barely explored. The nature of measurement in quantum field theory is still far from understood, as the standard measurement postulates applied in standard quantum mechanics break down when it comes to field theory [181]. As another example, standard concepts in quantum thermodynamics may become ill-defined when working relativistically. By applying ideas

from quantum information theory to the realm of quantum fields we have learned a great deal about the finer structure of that theory which describes the fundamental constituents of light and matter. Although we have not touched on gravitation in this thesis, it is also widely suspected that quantum information will play a crucial role in uncovering the quantum nature of gravity (or the gravitational nature of the quantum, if you prefer). It suffices to say that this journey has only just begun.

# APPENDICES



# Appendix A

## Symplectic diagonalization

Here we describe the method of symplectically diagonalizing a covariance matrix, i.e. putting into its Williamson normal form. We will, however, only consider the simplifying case in which there are no correlations between  $\hat{q}$  operators and  $\hat{p}$  operators, i.e.  $\langle q_i p_j \rangle = 0$ . States of this form are in fact the only ones that we will need to symplectically diagonalize in this thesis. Given this, let us work in a re-ordered phase space basis in which the  $q$ 's are packaged together and similarly for the  $p$ 's:  $\hat{\mathbf{x}} = (\hat{q}_1, \hat{q}_2, \dots, \hat{p}_1, \hat{p}_2, \dots)$ . Given our simplifying assumption, in this basis a covariance matrix takes the form

$$\boldsymbol{\sigma} = \begin{pmatrix} \boldsymbol{\sigma}^{(Q)} & \mathbf{0} \\ \mathbf{0} & \boldsymbol{\sigma}^{(P)} \end{pmatrix}, \quad (\text{A.1})$$

Note also that in the new basis ordering the symplectic form is given by

$$\boldsymbol{\Omega} = \begin{pmatrix} \mathbf{0} & \mathbf{I} \\ -\mathbf{I} & \mathbf{0} \end{pmatrix}, \quad (\text{A.2})$$

and that the Williamson normal (symplectically diagonalized) form of a covariance matrix is given by  $\mathbf{D} = \boldsymbol{\nu} \oplus \boldsymbol{\nu}$ , where  $\boldsymbol{\nu} = \text{diag}(\nu_1, \nu_2, \dots)$  contains the symplectic eigenvalues.

We would like to find the symplectic transformation  $\tilde{\mathbf{S}}$  that achieves this transformation. Specifically we will let  $\tilde{\mathbf{S}}^T (\boldsymbol{\nu} \oplus \boldsymbol{\nu}) \tilde{\mathbf{S}} = \boldsymbol{\sigma}$ . To this end, we will make an Ansatz and then prove that it is the correct choice. Let us define a matrix  $\mathbf{A} \equiv \sqrt{\boldsymbol{\sigma}^{(Q)}} \sqrt{\boldsymbol{\sigma}^{(P)}}$ . We claim that the symplectic eigenvalues  $\{\nu_i\}$  of  $\boldsymbol{\sigma}$  are given by the singular values of  $\mathbf{A}$ . That is, there are orthogonal matrices  $\mathbf{O}_1$  and  $\mathbf{O}_2$  such that

$$\mathbf{A} = \mathbf{O}_1^T \boldsymbol{\nu} \mathbf{O}_2. \quad (\text{A.3})$$

Let us take these and form another orthogonal matrix given by their direct sum  $\mathbf{O} \equiv \mathbf{O}_1 \oplus \mathbf{O}_2$ . We now claim that the symplectic matrix  $\tilde{\mathbf{S}}$  that diagonalizes  $\boldsymbol{\sigma}$  is given by

$$\tilde{\mathbf{S}} = (\boldsymbol{\nu} \oplus \boldsymbol{\nu})^{-1/2} \mathbf{O} \boldsymbol{\sigma}^{1/2}. \quad (\text{A.4})$$

Clearly from this definition it is true that  $\tilde{\mathbf{S}}^T (\boldsymbol{\nu} \oplus \boldsymbol{\nu}) \tilde{\mathbf{S}} = \boldsymbol{\sigma}$ , since  $\mathbf{O}$  is orthogonal. However, is it symplectic:  $\tilde{\mathbf{S}} \boldsymbol{\Omega} \tilde{\mathbf{S}}^T = \boldsymbol{\Omega}$ ? By expanding the left-hand side of this equation it is straightforward to see that the transformation will be symplectic iff  $\mathbf{O}_1 \mathbf{A} \mathbf{O}_2^T = \boldsymbol{\nu}$ , which is equivalent to Eq. (A.3).

Thus, finding the symplectic diagonalization is equivalent to finding the singular value decomposition of the matrix  $\mathbf{A}$ , which is easily done numerically. Note that to go from the matrix  $\boldsymbol{\sigma}$  to  $\boldsymbol{\nu} \oplus \boldsymbol{\nu}$  in the sense of  $\mathbf{S}_D \boldsymbol{\sigma} \mathbf{S}_D^T = \boldsymbol{\nu} \oplus \boldsymbol{\nu}$ , the correct transformation will be  $\mathbf{S}_D = (\tilde{\mathbf{S}}^T)^{-1} = (\boldsymbol{\nu} \oplus \boldsymbol{\nu})^{1/2} \mathbf{O} \boldsymbol{\sigma}^{-1/2}$ .

# Appendix B

## Hilbert space view of the detector symplectic evolution

This appendix presents an alternative method of computing the oscillator-detector evolution equation, presented in Sect. 5.2. While this alternative is much more laborious to derive and to use than the primary method used above, it nevertheless represents a mathematically interesting approach and one that we used to confirm several of the initial numerical calculations obtained using the main method.

Without invoking the full machinery of symplectic transformations, we can still take advantage of the quadratic nature of the interaction to derive the same results by numerically calculating the unitary time evolution operator directly in the interaction picture, an approach that is more standard within quantum field theory, but without relying on perturbation theory.

To start, let us consider the same situation as that described in Sect. 5.2, in which we have  $M$  oscillator detectors coupled to  $N$  field modes. In that section we constructed a phase-space vector consisting of the quadrature operators for each oscillator and mode, Eq. (5.25). Here we will find it more convenient to work directly with the creation and annihilation operators, rather than the quadratures. To this end, we will define the following two vectors of operators:

$$\begin{aligned}\hat{\mathbf{a}} &= (\hat{a}_{d_1}, \dots, \hat{a}_{d_M}, \hat{a}_1, \dots, \hat{a}_N)^T, \\ \hat{\mathbf{a}}^\dagger &= (\hat{a}_{d_1}^\dagger, \dots, \hat{a}_{d_M}^\dagger, \hat{a}_1^\dagger, \dots, \hat{a}_N^\dagger)^T.\end{aligned}\tag{B.1}$$

For a quadratic Hamiltonian, time evolution can be expressed in terms of displacements, squeezing, and rotation unitary operations [182]. In particular, the unitary evolution we

are looking to solve for can then be put into the form

$$\hat{U}(\tau) = e^{i\gamma(t)} \hat{S}(\mathbf{z}(t)) \hat{D}(\boldsymbol{\beta}(t)) \hat{R}(\boldsymbol{\phi}(t)), \quad (\text{B.2})$$

where  $\gamma$  is number valued and the squeezing, rotation and displacement operators are respectively defined as

$$\hat{S}(\mathbf{z}) = e^{\frac{1}{2} [(\hat{\mathbf{a}}^\dagger)^\text{T} \mathbf{z} \hat{\mathbf{a}}^\dagger - \hat{\mathbf{a}}^\text{T} \mathbf{z}^\text{H} \hat{\mathbf{a}}]}, \quad (\text{B.3})$$

$$\hat{R}(\boldsymbol{\phi}) = e^{i(\hat{\mathbf{a}}^\dagger)^\text{T} \boldsymbol{\phi} \hat{\mathbf{a}}}, \quad (\text{B.4})$$

$$\hat{D}(\boldsymbol{\beta}) = e^{\boldsymbol{\beta}^\text{T} \hat{\mathbf{a}}^\dagger - \boldsymbol{\beta}^\text{H} \hat{\mathbf{a}}}, \quad (\text{B.5})$$

where  $\mathbf{z}$  and  $\boldsymbol{\phi}$  are matrices, and  $\boldsymbol{\beta}$  is a column vector. The notation  $\mathbf{z}^\text{H}$  is used to represent the conjugate transpose of  $\mathbf{z}$ , the elements of which are number valued. Note that without loss of generality we can consider  $\mathbf{z}$  to be symmetric because it is only the symmetric part that contributes to  $\hat{S}(\mathbf{z})$ . Also note that  $\boldsymbol{\phi}$  must be a Hermitian matrix ( $\boldsymbol{\phi} = \boldsymbol{\phi}^\text{H}$ ) to ensure unitarity of  $\hat{R}(\boldsymbol{\phi})$ .

The exact form of these transformations can be obtained nonperturbatively by employing a technique introduced by Heffner and Louisell [183]. We will utilize the polar decomposition of  $\mathbf{z}$  into a product of a hermitian and a unitary matrix, which can always be achieved. This takes the form

$$\mathbf{z} = \mathbf{r} e^{i\boldsymbol{\theta}} = e^{i\boldsymbol{\theta}^\text{T}} \mathbf{r}^\text{T}, \quad (\text{B.6})$$

where  $\mathbf{r}$  and  $\boldsymbol{\theta}$  are hermitian matrices, and the second equality results from the assumed symmetry of  $\mathbf{z}$ . From here we wish to evaluate how such operators evolve the ladder operators of our system so that we can determine their corresponding symplectic transformations on the phase space and therefore the covariance matrix ascribed to, for example, a multimode squeezed state. Using the BCH's Hadamard lemma,  $e^A B e^{-A} = B + [A, B] + [A, [A, B]]/2! + \dots$ , it is straightforward to obtain

$$\hat{S}^\dagger(\mathbf{z}) \hat{\mathbf{a}} \hat{S}(\mathbf{z}) = \cosh(\mathbf{r}) \hat{\mathbf{a}} + \sinh(\mathbf{r}) e^{i\boldsymbol{\theta}} \hat{\mathbf{a}}^\dagger, \quad (\text{B.7})$$

$$\hat{R}^\dagger(\boldsymbol{\phi}) \hat{\mathbf{a}} \hat{R}(\boldsymbol{\phi}) = e^{i\boldsymbol{\phi}} \hat{\mathbf{a}}, \quad (\text{B.8})$$

$$\hat{D}^\dagger(\boldsymbol{\beta}) \hat{\mathbf{a}} \hat{D}(\boldsymbol{\beta}) = \hat{\mathbf{a}} + \boldsymbol{\beta}, \quad (\text{B.9})$$

and similarly

$$\hat{S}^\dagger(\mathbf{z}) \hat{\mathbf{a}}^\dagger \hat{S}(\mathbf{z}) = \cosh(\mathbf{r}^\text{T}) \hat{\mathbf{a}}^\dagger + \sinh(\mathbf{r}^\text{T}) e^{-i\boldsymbol{\theta}^\text{T}} \hat{\mathbf{a}}, \quad (\text{B.10})$$

$$\hat{R}^\dagger(\boldsymbol{\phi}) \hat{\mathbf{a}}^\dagger \hat{R}(\boldsymbol{\phi}) = e^{-i\boldsymbol{\phi}^\text{T}} \hat{\mathbf{a}}^\dagger, \quad (\text{B.11})$$

$$\hat{D}^\dagger(\boldsymbol{\beta}) \hat{\mathbf{a}}^\dagger \hat{D}(\boldsymbol{\beta}) = \hat{\mathbf{a}}^\dagger + \boldsymbol{\beta}^*, \quad (\text{B.12})$$

It is important to keep in mind that for our purposed we actually need not consider the displacement operator within this framework. This is because phase-space displacements are generated by linear terms in one's Hamiltonian, which for everything we have considered in this thesis are absent. From this point on we will therefore take the displacement operator to be unity, as we will have no such displacements in our work.

From a given generating Hamiltonian our goal is to solve for the resulting squeezing and rotation operators, in the sense that we solve for  $\mathbf{z}(t)$  and  $\boldsymbol{\phi}(t)$ . Once we have done this then finding the evolved covariance matrix of the detector+field system is straightforward. For this it will be easier, however, to work in a phase-space basis in which all of the  $\hat{q}$  operators are packaged together, and similarly for the  $\hat{p}$  operators. That is, we define the covariance matrix as in Eq. (3.5), but where we now define the phase-space vector to be ordered as  $\hat{\mathbf{x}} = (\hat{q}_{d_1}, \dots, \hat{q}_{d_M}, \hat{q}_1, \dots, \hat{q}_N, \hat{p}_{d_1}, \dots, \hat{p}_{d_M}, \hat{p}_1, \dots, \hat{p}_N)^T$ . In this basis, a generic covariance matrix splits into the block form

$$\boldsymbol{\sigma} = \begin{pmatrix} \boldsymbol{\sigma}_{qq} & \boldsymbol{\sigma}_{qp} \\ \boldsymbol{\sigma}_{qp}^T & \boldsymbol{\sigma}_{pp} \end{pmatrix}, \quad (\text{B.13})$$

where, for example,  $\boldsymbol{\sigma}_{qq}$  is the  $(M+N) \times (M+N)$  matrix containing all of the  $qq$  correlations. The form of these blocks is then straightforward to determine from the collection of identities Eqs. (B.7) and (B.10). For example if our detector+field state starts in the vacuum state then the evolved state is simply given by a multi-mode squeezed state  $\hat{S}(\mathbf{z})|0\rangle$ , since the vacuum is invariant under rotations. In this case, the blocks of the evolved covariance matrix take the form

$$\boldsymbol{\sigma}_{qq} = \frac{1}{2}(\cosh(2\mathbf{r}) + \sinh(2\mathbf{r})e^{i\boldsymbol{\theta}} + \cosh(2\mathbf{r}^T) + \sinh(2\mathbf{r}^T)e^{-i\boldsymbol{\theta}^T}), \quad (\text{B.14})$$

$$\boldsymbol{\sigma}_{pp} = \frac{1}{2}(\cosh(2\mathbf{r}) - \sinh(2\mathbf{r})e^{i\boldsymbol{\theta}} + \cosh(2\mathbf{r}^T) - \sinh(2\mathbf{r}^T)e^{-i\boldsymbol{\theta}^T}), \quad (\text{B.15})$$

$$\boldsymbol{\sigma}_{qp} = \frac{i}{2}(\cosh(2\mathbf{r}) - \sinh(2\mathbf{r})e^{i\boldsymbol{\theta}} - \cosh(2\mathbf{r}^T) + \sinh(2\mathbf{r}^T)e^{-i\boldsymbol{\theta}^T}). \quad (\text{B.16})$$

Once this is obtained then computing the covariance matrix for the detector(s) alone is trivial: one must simply isolate the rows and columns of  $\boldsymbol{\sigma}$  corresponding to the detector modes.

Before we can apply this, however, we still need to compute the squeezing and rotation matrices  $\mathbf{z}(t)$  and  $\boldsymbol{\phi}(t)$  resulting from the evolution generated by some Hamiltonian. In regards to our Hamiltonian of choice, let us define coefficient matrices  $\mathbf{w}(t)$  and  $\mathbf{g}(t)$ , in the same way that we did with  $\mathbf{F}(t)$  in Eq. (5.28), that represent a generic quadratic

Hamiltonian:

$$\hat{H}(t) = (\hat{\mathbf{a}}^\dagger)^\text{T} \mathbf{w}(t) \hat{\mathbf{a}} + (\hat{\mathbf{a}}^\dagger)^\text{T} \mathbf{g}(t) \hat{\mathbf{a}}^\dagger + \hat{\mathbf{a}}^\text{T} \mathbf{g}(t)^\text{H} \hat{\mathbf{a}}, \quad (\text{B.17})$$

where  $\mathbf{M}^\text{H} = \mathbf{M}^{*\text{T}} = \mathbf{M}^\text{T*}$  denotes the conjugate transpose of any matrix  $\mathbf{M}$ . We differentiate this from dagger notation so as not to cause confusion when mixing matrices and operators. Note also that, unlike the formalism presented Sect. 5.2, here we can work directly in the interaction picture. In the case of a detector-field interaction model, therefore, we may take  $\hat{H}(t)$  to be solely made up of the interaction Hamiltonian, represented in the interaction picture.

Given this Hamiltonian, how do we compute  $\mathbf{z}(t)$  and  $\phi(t)$ ? We will give the technical details below, but the answer is that (following the formalism presented in [183]) we must solve the following pair of coupled, matrix differential equations:

$$i\dot{\mathbf{C}}(t) = 4\mathbf{C}_s(t)\mathbf{g}^\text{H}(t)\mathbf{C}_s(t) + 2\mathbf{w}(t)\mathbf{C}_s(t) + \mathbf{g}(t), \quad (\text{B.18})$$

$$i\dot{\mathbf{D}}(t) = (4\mathbf{C}_s(t)\mathbf{g}^\text{H}(t) + \mathbf{w}(t))(\mathbf{D}(t) + \mathbf{I}), \quad (\text{B.19})$$

where  $\mathbf{w}(t)$  and  $\mathbf{g}(t)$  are the Hamiltonian coefficient matrices as defined in Eq. (B.17). We have defined  $\mathbf{C}_s \equiv (\mathbf{C} + \mathbf{C}^\text{T})/2$ , where the matrices  $\mathbf{C}_s$  and  $\mathbf{D}$  are identified with the squeezing and rotation by

$$\mathbf{C}_s = \frac{1}{2} \tanh(\mathbf{r}) e^{i\theta}, \quad (\text{B.20})$$

$$\mathbf{D} + \mathbf{I} = \text{sech}(\mathbf{r}) e^{i\phi}. \quad (\text{B.21})$$

where  $\mathbf{z} = \mathbf{r} e^{i\theta} = e^{i\theta^\text{T}} \mathbf{r}^\text{T}$ . By numerically solving Eqs. (B.18,B.19) with the initial conditions  $\mathbf{C}(0) = \mathbf{D}(0) = \mathbf{0}$  we can non-perturbatively solve the time evolution.

To see how this comes about, consider the unitary evolution operator  $\hat{U}(\hat{\mathbf{a}}^\dagger, \hat{\mathbf{a}}, t)$  that is generated by  $\hat{H}(t)$ . Let us denote its normal-ordered form  $\hat{U}^{(n)}(\hat{\mathbf{a}}^\dagger, \hat{\mathbf{a}}, t)$ , where for example,  $(\hat{a}_d \hat{a}_d^\dagger)^{(n)} = \hat{a}_d^\dagger \hat{a}_d + 1$ . As explained in [183], we can equally well represent this using a number-valued function corresponding to  $\hat{U}^{(n)}$  of the form  $\hat{U}^{(n)}(\hat{\mathbf{a}}^\dagger, \hat{\mathbf{a}}, t) \rightarrow \bar{U}^{(n)}(\boldsymbol{\alpha}^*, \boldsymbol{\alpha}, t)$ , where  $\boldsymbol{\alpha}$  and  $\boldsymbol{\alpha}^*$  are taken to be column vectors consisting of real, independent variables. That is, we put  $\hat{U}$  into normal form and replace  $\hat{\mathbf{a}}$  and  $\hat{\mathbf{a}}^\dagger$  by vectors of number-valued entries  $\boldsymbol{\alpha}$  and  $\boldsymbol{\alpha}^*$ . In this representation, Schrödinger's equation  $i\partial_t \hat{U}(t) = H(\hat{\mathbf{a}}^\dagger, \hat{\mathbf{a}}, t) \hat{U}(t)$  becomes

$$i \frac{\partial}{\partial t} \bar{U}^{(n)}(\boldsymbol{\alpha}^*, \boldsymbol{\alpha}, t) = \bar{H}^{(n)} \left( \boldsymbol{\alpha}^*, \boldsymbol{\alpha} + \frac{\partial}{\partial \boldsymbol{\alpha}^*}, t \right) \bar{U}^{(n)}(\boldsymbol{\alpha}^*, \boldsymbol{\alpha}, t), \quad (\text{B.22})$$

where  $\bar{H}^{(n)}(\boldsymbol{\alpha}^*, \boldsymbol{\alpha} + \partial/\partial\boldsymbol{\alpha}^*, t)$  is obtained by putting  $\hat{H}$  into normal-ordered form (which in our case it generally already is) and replacing  $\hat{\mathbf{a}}$  and  $\hat{\mathbf{a}}^\dagger$  by  $\boldsymbol{\alpha} + \partial/\partial\boldsymbol{\alpha}^*$  and  $\boldsymbol{\alpha}^*$  respectively. What we now have is a set of coupled, ordinary differential equations. An ansatz for the solution that we will use is  $\bar{U}^{(n)} = e^{G(\boldsymbol{\alpha}^*, \boldsymbol{\alpha}, t)}$ , turning the equation into one for  $G$ . Once the solution has been found, we can then obtain the normal ordered unitary by replacing back  $\boldsymbol{\alpha}$  and  $\boldsymbol{\alpha}^*$  by  $\hat{\mathbf{a}}$  and  $\hat{\mathbf{a}}^\dagger$  and applying the normal ordering operator  $\hat{U}^{(n)} = :e^{G(\hat{\mathbf{a}}^\dagger, \hat{\mathbf{a}}, t)}:$  where, for example,  $:\hat{a}_d\hat{a}_d^\dagger: = \hat{a}_d^\dagger\hat{a}_d$ .

Following the prescription of [183], we now want to find the evolution equation of the number-valued function  $\bar{U}^{(n)}$ . From Eq. (B.22), we have

$$i\frac{\partial\bar{U}^{(n)}}{\partial t} = \left[ (\boldsymbol{\alpha}^*)^\text{T}\mathbf{w} \left( \boldsymbol{\alpha} + \frac{\partial}{\partial\boldsymbol{\alpha}^*} \right) + (\boldsymbol{\alpha}^*)^\text{T}\mathbf{g}\boldsymbol{\alpha}^* + \left( \boldsymbol{\alpha}^\text{T} + \frac{\partial}{\partial(\boldsymbol{\alpha}^*)^\text{T}} \right) \mathbf{g}^\text{H} \left( \boldsymbol{\alpha} + \frac{\partial}{\partial\boldsymbol{\alpha}^*} \right) \right] \bar{U}^{(n)}, \quad (\text{B.23})$$

and making the ansatz  $\bar{U}^{(n)} = e^G$ , we have the equation for  $G$ :

$$i\frac{\partial G}{\partial t} = (\boldsymbol{\alpha}^*)^\text{T}\mathbf{w}\boldsymbol{\alpha} + (\boldsymbol{\alpha}^*)^\text{T}\mathbf{w}\frac{\partial G}{\partial(\boldsymbol{\alpha}^*)^\text{T}} + (\boldsymbol{\alpha}^*)^\text{T}\mathbf{g}\boldsymbol{\alpha}^* + \boldsymbol{\alpha}^\text{T}\mathbf{g}^\text{H}\boldsymbol{\alpha} + \boldsymbol{\alpha}^\text{T}\mathbf{g}^\text{H}\frac{\partial G}{\partial\boldsymbol{\alpha}^*} + \frac{\partial G}{\partial(\boldsymbol{\alpha}^*)^\text{T}}\mathbf{g}^\text{H}\boldsymbol{\alpha} + \frac{\partial G}{\partial(\boldsymbol{\alpha}^*)^\text{T}}\mathbf{g}^\text{H}\frac{\partial G}{\partial\boldsymbol{\alpha}^*} + \frac{\partial}{\partial(\boldsymbol{\alpha}^*)^\text{T}}\mathbf{g}^\text{H}\frac{\partial G}{\partial\boldsymbol{\alpha}^*}. \quad (\text{B.24})$$

Additionally, we can make the educated ansatz

$$G = (\boldsymbol{\alpha}^*)^\text{T}\mathbf{D}(t)\boldsymbol{\alpha} + (\boldsymbol{\alpha}^*)^\text{T}\mathbf{C}(t)\boldsymbol{\alpha}^* + \boldsymbol{\alpha}^\text{T}\mathbf{F}(t)\boldsymbol{\alpha} + A(t), \quad (\text{B.25})$$

where  $\mathbf{D}$ ,  $\mathbf{C}$  and  $\mathbf{F}$  are matrices. In general, we should also include terms linear in  $\boldsymbol{\alpha}$  and  $\boldsymbol{\alpha}^*$ , corresponding to phase space displacements, but in our case they will be absent due to the lack of linear terms in the relevant Hamiltonians and so we will not consider them. From here it is easy to show that

$$\frac{\partial G}{\partial\boldsymbol{\alpha}^*} = \mathbf{D}\boldsymbol{\alpha} + 2\mathbf{C}_s\boldsymbol{\alpha}^*, \quad (\text{B.26})$$

where  $\mathbf{C}_s = (\mathbf{C} + \mathbf{C}^\text{T})/2$  is the symmetric part of  $\mathbf{C}$ . The transposed version of this relation follows trivially. Lastly, it is easily shown that

$$\frac{\partial}{\partial(\boldsymbol{\alpha}^*)^\text{T}}\mathbf{g}^\text{H}\frac{\partial G}{\partial\boldsymbol{\alpha}^*} = 2\text{Tr}(\mathbf{g}^\text{H}\mathbf{C}_s). \quad (\text{B.27})$$

Given these relations it is now a simple matter of comparing coefficients between the right and left sides of Eq. (B.24). Doing so, we find the coupled set of differential equations

$$i\dot{A} = 2\text{Tr}(\mathbf{g}^H \mathbf{C}_s), \quad (\text{B.28})$$

$$i\dot{\mathbf{C}} = 4\mathbf{C}_s \mathbf{g}^H \mathbf{C}_s + 2\mathbf{w} \mathbf{C}_s + \mathbf{g}, \quad (\text{B.29})$$

$$i\dot{\mathbf{D}} = (4\mathbf{C}_s \mathbf{g}^H + \mathbf{w})(\mathbf{D} + \mathbf{I}), \quad (\text{B.30})$$

$$i\dot{\mathbf{F}} = (\mathbf{D}^T + \mathbf{I})\mathbf{g}^H(\mathbf{D} + \mathbf{I}), \quad (\text{B.31})$$

where  $\mathbf{I}$  is the identity matrix, and we have initial conditions  $A(0) = 0$  and  $\mathbf{C}(0) = \mathbf{D}(0) = \mathbf{F}(0) = \mathbf{0}$ .

Though these equations can already be numerically solved, some simplifications are possible. For example the matrix  $\mathbf{C}$  fully determines the squeezing matrix  $\mathbf{z} = \mathbf{r}e^{i\theta}$ , which, if our system is initially in the vacuum state, is all that we need (since the vacuum is invariant under rotations). For a more general initial state, one also needs to solve for  $\mathbf{D}$  in order to compute  $\phi$ . We will also see that there is no need to solve Eq. (B.31) for  $\mathbf{F}$  because it can be expressed purely in terms of  $\mathbf{C}$  and  $\mathbf{D}$  and is therefore a redundant variable. Lastly, the variable  $A$  will represent only an overall phase in the evolution, and therefore bears no importance.

Note that the form of these equations are entirely independent of the specific coupling matrices  $\mathbf{w}$  and  $\mathbf{g}$  that we choose. We are therefore free to choose an entirely different interaction Hamiltonian, and the evolution will still be represented by these equations. Once solutions have been found, we can return the (normal ordered) unitary to its operator form via  $\hat{U}^{(n)} = :e^{G(\hat{\mathbf{a}}^\dagger, \hat{\mathbf{a}})}:$ , which from Eq. (B.25) gives us

$$\hat{U}^{(n)}(t) = e^{A(t)} e^{(\hat{\mathbf{a}}^\dagger)^T \mathbf{C}(t) \hat{\mathbf{a}}^\dagger} :e^{(\hat{\mathbf{a}}^\dagger)^T \mathbf{D}(t) \hat{\mathbf{a}}}: e^{\hat{\mathbf{a}}^T \mathbf{F}(t) \hat{\mathbf{a}}}. \quad (\text{B.32})$$

Our problem is thus essentially solved; the last task required is to overcome the normal ordering and to put this unitary into a form that we are familiar with. We know that  $\hat{U}$  should be a product of rotation and squeezing operators, along with possible phases:

$$\hat{U} = e^{i\gamma} \hat{S}(\mathbf{z}) \hat{R}(\phi), \quad (\text{B.33})$$

where  $\hat{S}$  and  $\hat{R}$  are given by Eqs. (B.3,B.4). We know that the solutions (B.32) and (B.33) must be equivalent, and the task is now to find the relation between  $\gamma$ ,  $\mathbf{z}$ , and  $\phi$  and the results obtained for  $A$ ,  $\mathbf{C}$ ,  $\mathbf{D}$  and  $\mathbf{F}$ . Trivially we see that  $i\gamma = A$ , meaning that  $A$  represents an overall phase.



In order to find  $\mathbf{z} = \mathbf{r}e^{i\theta} = e^{i\theta^T} \mathbf{r}^T$  and  $\phi$  we recall the action that Eq. (B.33) will have on the ladder operator:

$$\hat{U}^\dagger \hat{\mathbf{a}} \hat{U} = \cosh(\mathbf{r}) e^{i\phi} \hat{\mathbf{a}} + \sinh(\mathbf{r}) e^{i\theta} e^{-i\phi^T} \hat{\mathbf{a}}^\dagger, \quad (\text{B.34})$$

$$\hat{U}^\dagger \hat{\mathbf{a}}^\dagger \hat{U} = \cosh(\mathbf{r}^T) e^{-i\phi^T} \hat{\mathbf{a}}^\dagger + \sinh(\mathbf{r}^T) e^{-i\theta^T} e^{i\phi} \hat{\mathbf{a}}. \quad (\text{B.35})$$

We now need to compute  $\hat{U}^\dagger \hat{\mathbf{a}} \hat{U}$  and  $\hat{U}^\dagger \hat{\mathbf{a}}^\dagger \hat{U}$  from the unitary in Eq. (B.32) in order to compare. To this end, we use the identities  $[\hat{\mathbf{a}}, \hat{U}] = \partial \hat{U} / \partial \hat{\mathbf{a}}^\dagger$  and  $[\hat{\mathbf{a}}^\dagger, \hat{U}] = -\partial \hat{U} / \partial \hat{\mathbf{a}}$ , or equivalently

$$\hat{U}^\dagger \hat{\mathbf{a}} \hat{U} = \hat{U}^\dagger \frac{\partial \hat{U}}{\partial \hat{\mathbf{a}}^\dagger} + \hat{\mathbf{a}}, \quad \hat{U}^\dagger \hat{\mathbf{a}}^\dagger \hat{U} = -\hat{U}^\dagger \frac{\partial \hat{U}}{\partial \hat{\mathbf{a}}} + \hat{\mathbf{a}}^\dagger \quad (\text{B.36})$$

To evaluate the right-hand sides, we use the straightforwardly shown identities:

$$\frac{\partial}{\partial \hat{\mathbf{a}}} :e^{(\hat{\mathbf{a}}^\dagger)^T \mathbf{D} \hat{\mathbf{a}}}: = \mathbf{D}^T \hat{\mathbf{a}}^\dagger :e^{(\hat{\mathbf{a}}^\dagger)^T \mathbf{D} \hat{\mathbf{a}}}:, \quad (\text{B.37})$$

$$\frac{\partial}{\partial \hat{\mathbf{a}}^\dagger} :e^{(\hat{\mathbf{a}}^\dagger)^T \mathbf{D} \hat{\mathbf{a}}}: = :e^{(\hat{\mathbf{a}}^\dagger)^T \mathbf{D} \hat{\mathbf{a}}}: \mathbf{D} \hat{\mathbf{a}}, \quad (\text{B.38})$$

$$(\mathbf{I} + \mathbf{D}^T) \hat{\mathbf{a}}^\dagger :e^{(\hat{\mathbf{a}}^\dagger)^T \mathbf{D} \hat{\mathbf{a}}}: = :e^{(\hat{\mathbf{a}}^\dagger)^T \mathbf{D} \hat{\mathbf{a}}}: \hat{\mathbf{a}}^\dagger, \quad (\text{B.39})$$

$$\hat{\mathbf{a}}^\dagger e^{\hat{\mathbf{a}}^T \mathbf{F} \hat{\mathbf{a}}} = e^{\hat{\mathbf{a}}^T \mathbf{F} \hat{\mathbf{a}}} (\hat{\mathbf{a}}^\dagger - 2\mathbf{F} \hat{\mathbf{a}}), \quad (\text{B.40})$$

along with the fact that  $\mathbf{F}$  is symmetric, as can be seen from Eq. (B.31). With these, Eq. (B.36) gives us

$$\hat{U}^\dagger \hat{\mathbf{a}} \hat{U} = [(\mathbf{D} + \mathbf{I}) - 4\mathbf{C}_s(\mathbf{D}^T + \mathbf{I})^{-1} \mathbf{F}] \hat{\mathbf{a}} + 2\mathbf{C}_s(\mathbf{D}^T + \mathbf{I})^{-1} \hat{\mathbf{a}}^\dagger, \quad (\text{B.41})$$

$$\hat{U}^\dagger \hat{\mathbf{a}}^\dagger \hat{U} = (\mathbf{D}^T + \mathbf{I})^{-1} (-2\mathbf{F} \hat{\mathbf{a}} + \hat{\mathbf{a}}^\dagger). \quad (\text{B.42})$$

Since these equations are just the adjoints of each other, we are able to compare the two and determine the additional relations

$$\mathbf{F} = -(\mathbf{D}^* + \mathbf{I})^{-1} \mathbf{C}_s^* (\mathbf{D} + \mathbf{I}), \quad (\text{B.43})$$

$$\mathbf{I} - 4\mathbf{C}_s \mathbf{C}_s^* = (\mathbf{D} + \mathbf{I})(\mathbf{D}^\dagger + \mathbf{I}). \quad (\text{B.44})$$

Given all of this, we find indeed that  $\hat{U}^\dagger \hat{\mathbf{a}} \hat{U}$  and  $\hat{U}^\dagger \hat{\mathbf{a}}^\dagger \hat{U}$  are of the form given in Eqs. (B.34, B.35), where we identify

$$\mathbf{C}_s = \frac{1}{2} \tanh(\mathbf{r}) e^{i\theta}, \quad (\text{B.45})$$

$$\mathbf{D} + \mathbf{I} = \text{sech}(\mathbf{r}) e^{i\phi}. \quad (\text{B.46})$$

Thus, once we have integrated Eqs. (B.29,B.30) for  $\mathbf{C}$  and  $\mathbf{D}$  we can use this result to solve for the corresponding squeezing and rotation matrices  $\mathbf{r}$ ,  $\boldsymbol{\theta}$ , and  $\boldsymbol{\phi}$ , from which we can obtain the covariance matrix in which all properties of the final state are encoded.

This concludes the derivation of this method. As can be seen, it is significantly more involved than that given in Sect. 5.2. Nevertheless, it provided an important check on several of the initial results derived from the primary method and itself represents an interesting piece of physics and mathematics.

# Appendix C

## Predicting the specifics of thermal amplification

Here we wish to briefly point out how the specific behavior of thermal amplification, as discussed in Ch. 8, can be accurately predicted using the explanations given in Sects. 8.3.1 and 8.3.3. That is, we can predict how strongly or weakly we expect to observe the thermal amplification of discord and mutual information for varying parameters. Displayed in Fig. C.1 is the extracted mutual information as a function of  $t$  and  $r$  in the case that the field temperature was initiated to be  $T = 2$ ; all other parameters are as they were in Sect. 8.2. Note that a similar plot of the Gaussian discord looks qualitatively almost identical, but with a somewhat reduced magnitude.

Notice that there is a clear transition at the light cone  $t = r$ . In the spacelike region,  $t < r$ , we see that there is a minimum at roughly  $r \approx 21$ . This value of  $r$  coincides with a local minimum (a zero, in fact) of the magnitude of the correlation function  $C(r)$  discussed in Sect. 8.3.1. Inside the light cone, however, when  $t > r$ , we see that this no longer plays a strong role. This is simply because for  $t > r$  the detectors have come into causal contact, and thus the generation of correlations can also follow from the direct exchange of quanta rather than the harvesting of correlations from the field. Interestingly, the behavior of  $I$  and  $D$  in the  $t < r$  region is qualitatively very similar to the behavior found in the vacuum, but for  $t > r$  the behavior is very different (in the case of the vacuum, there is no significant change in behavior across the light cone aside from a visible amplification near  $t = r$  due the exchange of real quanta).

In the region of causal contact,  $t > r$ , the behavior of  $I$  and  $D$  is very different from the spacelike region, and it is here that we observe the intensity of thermal amplification

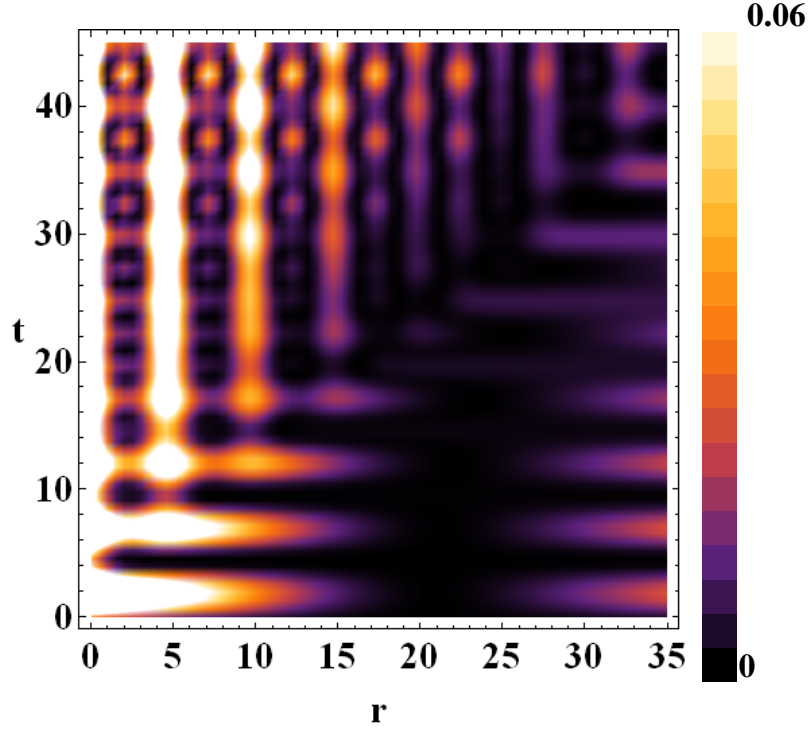


Figure C.1: The mutual information between detectors as a function of  $t$  and  $r$ , where the field was initiated in a thermal state of temperature  $T = 2$ .

following directly from the couplings of the  $(\pm)$ -modes to the field, Eqs. (8.20, 8.21). In this region we are starting to see resonant effects. This means that we expect to see the strongest contribution to the evolution of the detectors coming from the field modes near the resonance frequency  $|k_n| = \Omega = 40\pi/L$ , with  $L = 100$ . For example we notice the bands of strong amplification at distances of  $r = 0, 5, 10 \dots$ . From what we have learned in Sect. 8.3.3, these should correspond to large differences in the values of the symplectic eigenvalues  $\nu_+$  and  $\nu_-$ . Recalling that the  $(\pm)$ -modes are coupled to different field modes with strengths that go as  $\cos(k_n r/2)$  and  $\sin(k_n r/2)$ , we note that  $r = 0, 5, 10 \dots$  are exactly the values that satisfy  $\Omega r/2 = m\pi$  for integer values of  $m$ , meaning that the coupling of the  $(\pm)$ -modes to the resonant frequency are  $|\cos(\Omega r/2)| = 1$  and  $|\sin(\Omega r/2)| = 0$ . This maximum difference then leads to a large difference in the symplectic eigenvalues, and thus to a local maximum in the thermal amplification.

We also notice in Fig. C.1 that there are local maxima at values of  $r = 2.5, 7.5, 12.5 \dots$ ; these of course are the values that satisfy  $\Omega r/2 = m\pi/2$  and thus give  $|\cos(\Omega r/2)| = 0$  and

$|\sin(\Omega r/2)| = 1$ . This again translates into a maximum in the difference  $|\nu_+ - \nu_-|$  and thus in thermal amplification. However, why are these maxima much weaker than the others discussed above? This follows from the same reasoning that was discussed in the main text: given the timescale we are observing, we are still far from the single-mode approximation being accurate. There are thus significant contributions coming from the field modes  $k_n$  of small frequency, and for relatively small  $r$  this translates into  $\sin(k_n r/2)$  being very small for most of these modes and  $\cos(k_n r/2)$  being close to unity. Thus in this regime the value of  $\nu_-$  is not able to become appreciably larger than  $\nu_+$  even when the couplings to the resonant mode suggest that it would. As  $r$  increases (still within the  $t > r$  regime), we see that that this no longer becomes the case and the two classes of maxima become equivalent. Similarly, as  $t$  increases, the response deriving from the resonant mode becomes more dominant, and the  $r = 2.5, 7.5, 12.5 \dots$  maxima thus become more substantial, as we see in Fig. C.1. For large  $t$ , when the single-mode approximation becomes accurate, the maxima at  $r = 2.5, 7.5, 12.5 \dots$  should be comparable to those at  $r = 0, 5, 10 \dots$ .

# Appendix D

## Relative entropy between Gaussian states

We find it useful in Ch. 9 to consider the relative entropy between two Gaussian states. As the derivation of this is not common in the literature we will include a full derivation here.

The relative entropy of two density matrices  $\hat{\rho}_A$  and  $\hat{\rho}_B$  is defined as

$$S(\hat{\rho}_A||\hat{\rho}_B) = \text{Tr} \hat{\rho}_A(\log \hat{\rho}_A - \log \hat{\rho}_B). \quad (\text{D.1})$$

The relative entropy provides a measure of distinguishability of quantum states [144].

An important property of the relative entropy is *monotonicity*. Under any trace-preserving completely positive map  $\Phi$  we have

$$S(\Phi(\hat{\rho}_A)||\Phi(\hat{\rho}_B)) \leq S(\hat{\rho}_A||\hat{\rho}_B). \quad (\text{D.2})$$

In particular, if we choose  $\hat{\rho}_B$  to be a fixed point of the evolution ( $\Phi(\hat{\rho}_B) = \hat{\rho}_B$ ) then we have

$$S(\Phi(\hat{\rho}_A)||\hat{\rho}_B) \leq S(\hat{\rho}_A||\hat{\rho}_B) \quad (\text{D.3})$$

so that we have a measure of the distance between  $\hat{\rho}_A$  and the equilibrium state that is monotonic along the evolution. It therefore provides a measure of the degree to which the system has equilibrated.

Let us consider the case where  $\hat{\rho}_A$  and  $\hat{\rho}_B$  are Gaussian states of  $N$  modes, with covariance matrices  $\sigma^A$  and  $\sigma^B$  respectively:

$$\sigma_{ij}^A = \langle x_i x_j + x_j x_i \rangle_{\rho_A}, \quad \sigma_{ij}^B = \langle x_i x_j + x_j x_i \rangle_{\rho_B}. \quad (\text{D.4})$$

To compute the relative entropy, we express it as

$$S(\hat{\rho}_A||\hat{\rho}_B) = -S(\hat{\rho}_A) - \langle \log \hat{\rho}_B \rangle_{\rho_A}. \quad (\text{D.5})$$

The entropy term is easily computed from the symplectic eigenvalues of  $\sigma^A$ , as given by Eq. (3.24). Since  $\hat{\rho}_B$  is a Gaussian state,  $\log \hat{\rho}_B$  is a quadratic operator, and its expectation value is easily expressed in terms of the covariance matrix.

To find  $\log \hat{\rho}_B$ , we first symplectically diagonalize  $\sigma^B$ . That is, we put it into its Williamson normal form. This is done by some symplectic transformation  $\mathbf{S}$ , the entries of which are  $S_{ij}$ . We transform to a new quadrature basis  $\tilde{x}_i = \sum_j S_{ij} \hat{x}_j$  such that

$$\langle \tilde{x}_i \tilde{x}_j + \tilde{x}_j \tilde{x}_i \rangle_{\rho_B} = \sum_{kl} S_{ik} S_{jl} \sigma_{kl}^B = D_{ij} \quad (\text{D.6})$$

where  $\mathbf{D} = \text{diag}(\nu_1, \nu_1, \nu_2, \nu_2, \dots)$ , with symplectic eigenvalues  $\nu_1, \dots, \nu_N$ . As can be garnered from Sect. 3.2 (or as explained in [45]), the density matrix  $\hat{\rho}_B$  in this basis takes the form

$$\hat{\rho}_B = \bigotimes_{k=1}^N \frac{2}{\nu_k + 1} \sum_{n \geq 0} \left( \frac{\nu_k - 1}{\nu_k + 1} \right)^n |n\rangle_k \langle n|. \quad (\text{D.7})$$

Here  $|n\rangle_k$  are the eigenstates of the number operator

$$\tilde{N}_k = \frac{1}{2} (\tilde{x}_{2k}^2 + \tilde{x}_{2k+1}^2) - \frac{1}{2}. \quad (\text{D.8})$$

Taking the logarithm of Eq. (D.7), we find that

$$\log \hat{\rho}_B = \sum_{k=1}^N \left( \log \frac{2}{\nu_k + 1} + \log \frac{\nu_k - 1}{\nu_k + 1} \tilde{N}_k \right) \quad (\text{D.9})$$

$$= c + \sum_{i,j=1}^{2N} \tilde{H}_{ij} \tilde{x}_i \tilde{x}_j \quad (\text{D.10})$$

where  $\tilde{H}_{ij}$  are the entries of a matrix  $\tilde{\mathbf{H}}$ , and

$$c = \sum_k \frac{1}{2} \log \frac{4}{\nu_k^2 - 1}, \quad (\text{D.11})$$

$$\tilde{\mathbf{H}} = \text{diag}(H_1, H_1, H_2, H_2, \dots), \quad (\text{D.12})$$

$$H_k = \frac{1}{2} \log \frac{\nu_k - 1}{\nu_k + 1}. \quad (\text{D.13})$$

Changing from the  $\tilde{x}$  basis back to the  $\hat{x}$  basis,  $\log \hat{\rho}_B$  then takes the form

$$\log \hat{\rho}_B = c + \sum_{i,j=1}^{2N} H_{ij} x_i x_j, \quad H_{kl} = S_{ik} S_{jl} \tilde{H}_{ij}. \quad (\text{D.14})$$

The relative entropy is therefore given by

$$S(\hat{\rho}_A || \hat{\rho}_B) = -S(\hat{\rho}_A) - c - \frac{1}{2} \sum_{i,j=1}^{2N} \sigma_{ij}^A H_{ij}, \quad (\text{D.15})$$

with  $c$  and  $H$  given by Eqs. (D.11) and (D.14). The quantity  $S(\hat{\rho}_A)$  can be found by Eq. (3.24) in terms of the symplectic eigenvalues of the matrix  $\sigma^A$ .

When the state  $\hat{\rho}_B$  is a Gibbs thermal state

$$\hat{\rho}_B = Z^{-1} e^{-\beta \hat{H}}, \quad (\text{D.16})$$

of inverse temperature  $\beta$  with respect to some given Hamiltonian  $\hat{H}$ , the relative entropy reduces to the free energy difference

$$S(\hat{\rho}_A || \hat{\rho}_B) = \beta(F(\hat{\rho}_A) - F(\hat{\rho}_B)) \quad (\text{D.17})$$

where the free energy is defined as

$$F(\hat{\rho}_A) = \langle \hat{H} \rangle_{\rho_A} - \beta^{-1} S(\hat{\rho}_A). \quad (\text{D.18})$$

In Ch. 9 we will be interested in knowing, for a given Gaussian state  $\hat{\rho}_A$ , what thermal state  $\hat{\rho}_B$  is closest to  $\hat{\rho}_A$ . For this task we will use the relative entropy as our distance measure. To find the thermal state that minimizes the relative entropy (D.17), we simply extremize with respect to the inverse temperature  $\beta$ :

$$\frac{d}{d\beta} S(\hat{\rho}_A || \hat{\rho}_B) = \langle \hat{H} \rangle_{\rho_A} - \langle \hat{H} \rangle_{\rho_B} = 0. \quad (\text{D.19})$$

Thus the thermal state  $\hat{\rho}_B$  closest to the given state is that which has the same energy. Recall that the energy of a Gaussian state is easily computed via Eq. (3.9). When the temperature of the state  $\hat{\rho}_B$  is chosen in this way, the relative entropy is straightforwardly shown to be simply the entropy difference

$$S(\hat{\rho}_A || \hat{\rho}_B) = S(\hat{\rho}_B) - S(\hat{\rho}_A). \quad (\text{D.20})$$



The fact that the relative entropy is non-negative reflects the fact that the thermal state is the unique state of maximal entropy among states of a given energy.

Thus we establish an “effective temperature”  $\beta^{-1}$  of our state, obtained by solving for  $\beta$  as a function of the energy <sup>1</sup>, and a measure of distance to the manifold of thermal states.

---

<sup>1</sup>While we cannot find  $\beta$  analytically, it can be easily found numerically because the energy is monotonically increasing with temperature.

# Appendix E

## Adiabaticity for a moving cavity mirror

Here we will discuss the adiabatic approximation used in Ch. 10 in regards to a slowly vibrating cavity. We will do this by discussing the dynamics in general, and then observing how the adiabatic regime arises. Let us first consider the case of a cavity with one moving wall. It is clear that the adiabatic approximation does not hold in general; shaking the cavity walls produces field excitations [39]. To rigorously see this we must solve the equations of motion subject to time-dependent boundary conditions, and derive an appropriate Hamiltonian that takes such conditions into account. We introduce a mode expansion that satisfies Dirichlet boundary conditions (that the field is zero at the moving boundary  $\phi(L(t), t) = 0$ ):

$$\phi(x, t) = \sum_n \sqrt{\frac{2}{n\pi}} \varphi_n(t) \sin[k_n(t)x]. \quad (\text{E.1})$$

We can now quantize the field system by expressing the Klein-Gordon action in the variables  $\varphi_n(t)$  and deriving the Hamiltonian. Alternatively, we could derive the form of the dynamics by inserting this ansatz into the Klein-Gordon equation and obtaining the form of the expansion coefficients. Either way the result is that the field Hamiltonian can be written in terms of the usual stationary solutions plus corrections that are proportional to

the time derivative of the boundary condition:

$$\begin{aligned}
H = & \sum_n \frac{\omega_n(t)}{2} (\pi_n^2(t) + \varphi_n^2(t)) - \dot{L}(t) \sum_{m,n} \alpha_{nm} \omega_n(t) \pi_n(t) \varphi_m(t) \\
& + \frac{1}{2} \dot{L}^2(t) \sum_{nm} \left( \sum_k \alpha_{nk} \alpha_{mk} \omega_k(t) \right) \varphi_n(t) \varphi_m(t) + \frac{\dot{L}^2(t)}{L(t)} \sum_{m,n} \beta_{nm} \varphi_n(t) \varphi_m(t)
\end{aligned} \tag{E.2}$$

where the canonical conjugate momentum to  $\varphi_n$  is

$$\pi_n(t) = \frac{\dot{\varphi}_n(t)}{\omega_n(t)} + \sum_m \alpha_{nm} \varphi_m(t) \dot{L}(t) \tag{E.3}$$

The constants  $\alpha_{nm}$  and  $\beta_{nm}$  are defined by the coefficients of the Fourier sine series of the coefficients of the action after including all relevant time dependent terms. In particular, we have:

$$\alpha_{mn} = \begin{cases} -\frac{2(-1)^{m+n}\sqrt{mn}}{\pi(m^2-n^2)} & \text{if } m \neq n \\ \frac{1}{2\pi n} & \text{if } m = n \end{cases} \tag{E.4}$$

$$\beta_{mn} = \begin{cases} \frac{2(-1)^{m+n}\sqrt{mn}(m^2+n^2)}{\pi(m^2-n^2)^2} & \text{if } m \neq n \\ \frac{n\pi}{6} + \frac{1}{4\pi n} & \text{if } m = n \end{cases} \tag{E.5}$$

Now notice that the first term in Eq. E.2 is the usual Hamiltonian for the free Klein-Gordon field, but with time-dependent mode frequencies. That is exactly what we would get by making the assumption that the field admits the same mode expansion as in the stationary case. However, there are other time dependent terms present that allow for particle creation. Those terms are responsible for mechanisms such as the dynamical Casimir effect.

The remaining terms come with additional factors of  $\dot{L}$ , and hence will be small as long as the motion is sufficiently slow. In particular, the second term is parametrically smaller by a factor  $\dot{L}$ , and hence will be small if the speed of the wall is small compared to the speed of light. The third and fourth terms are parametrically smaller still by a factor  $\dot{L}$ , and hence will be even smaller. Hence the adiabatic approximation obtains whenever the motion of the cavity walls is nonrelativistic.

Under the assumption that the cavity walls' motion is non-relativistic, we will have no particle creation. Hence, we can approximate the field dynamics in the cavity by the time dependent mode expansion described by the first term above, thus treating the field under

the wall oscillations just like a free field in which we make the frequencies and wave numbers time dependent through  $L(t)$ . We call this the ‘adiabatic approximation’, which will be fulfilled in most realistic cases of cavity wall vibration (seismic waves, sound, motion, etc.).

# Appendix F

## Adiabaticity for gravitational waves

In regards to our approach to quantum seismology presented in Ch. 10, we now present some preliminary calculations for the case where changes in cavity length are due to a passing gravitational wave. We show that the dynamics in this case are similar to those of the physical model presented in Appendix E (which was used in our calculations) while acknowledging that further work would be required to refine this into a practical proposal for gravitational wave detection.

It has recently been claimed that relativistic effects in a Bose-Einstein condensate can be used for detection of gravitational waves [184]. Here we do not make any claims about the achievable sensitivity of our proposal in Ch. 10 to gravitational waves or the ability to distinguish between gravitational radiation and conventional vibrations; we merely point out the possibility that the technique could apply to the case of a gravitational wave. We leave more detailed questions of sensitivity and isolation from external noise as a possible avenue for future work.

We assume transverse-traceless gauge in which the metric is of the form

$$ds^2 = -dt^2 + (\delta_{ij} + h_{ij}(t))dx^i dx^j \quad (\text{F.1})$$

where  $h$  is a symmetric matrix with entries  $|h_{ij}| \ll 1$ ; the particular form of  $h_{ij}(t)$  will depend on the wave profile, and the polarization of the wave. Now suppose that the cavity is oriented along the  $x$  axis. The induced metric on the  $t - x$  plane will be

$$ds^2 = -dt^2 + (1 + h(t))dx^2 \quad (\text{F.2})$$

where  $h(t) = h_{xx}(t)$ . The gravitational wave causes the masses to transversely oscillate and to accelerate toward each other due to the gravitational attraction of the wave between

the test masses. Note, however, that any transverse motion of the masses does not affect the cavity length to first order in  $h(t)$ .

Suppose the walls of the cavity are coupled by a spring. We will assume that the spring couples the two walls instantaneously. Although this is not compatible with causality, it should be a reasonable approximation as long as the time scale for forces to propagate from one end of the cavity to another is shorter than the typical time scale of the gravitational wave signal. This condition is determined by the frequency of the gravitational wave  $\omega_{gw}$ , the speed of sound in the spring  $v_s$  and the cavity length  $L$ , and will hold as long as  $\omega_{gw} \ll v_s/L$ .

For simplicity, let us describe the walls of the cavity as a pair of masses  $m$  (whose separation vector is along the  $x$ -axis) coupled by an oscillator of quality factor  $Q$  and spring constant  $k$  (see [148]). We will take the coordinate difference to be  $x_1 - x_0 = L_0 + \delta x(t)$ , where  $L_0$  is the rest length of each cavity (the initial proper separation of the pair of test masses) and  $\delta x$  is assumed to be small. The potential of the spring is

$$V = \frac{1}{2}k[(1 + \frac{1}{2}h(t))(x_1 - x_0) - L_0]^2. \quad (\text{F.3})$$

The equation of motion can be expanded to linear order in  $h(t)$  and  $\delta x(t)$ , yielding

$$m\delta\ddot{x}(t) = -\frac{\omega}{Q}\delta\dot{x} - k\delta x(t) - \frac{1}{2}h(t)kL_0. \quad (\text{F.4})$$

We see that the gravitational wave results in a time-dependent external force applied to the spring. This results in a time-dependent proper length separations of

$$L(t) = L_0 (1 + \frac{1}{2}h(t)) + \delta x(t) \quad (\text{F.5})$$

and so by solving the equation of motion for  $\delta x(t)$  we find the proper length  $L(t)$  as a function of time.

Just as in the case of the moving mirror, we can solve the Klein-Gordon field theory in a mode expansion with moving boundary conditions, the only difference is the time-dependent metric (F.1). The resulting time-dependent Hamiltonian takes precisely the same form as Eq. (E.2), but with  $\omega_n(t) = n\pi/L(t)$  with  $L$  the time-dependent proper length of the cavity (F.5), and additional factors of  $(1 + \frac{1}{2}h(t))$  multiplying the matrices  $\alpha_{mn}$  and  $\beta_{mn}$  defined in Appendix. E.

The cavity here is described is a linear detector and so cannot distinguish gravitational radiation from tidal forces and other sources of noise. This could be overcome by considering two (or even three) cavities at right angles and looking for coincident signals. Even with

such a system, it will be a major challenge to see if our approach could be engineered to achieve levels of a sensitivity equivalent to or exceeding those of present-day gravitational wave detectors.

# References

- [1] Eric G. Brown, Eduardo Martin-Martinez, Nicolas C. Menicucci, and Robert B. Mann. Detectors for probing relativistic quantum physics beyond perturbation theory. *Phys. Rev. D*, 87:084062, 2013.
- [2] Wilson. G. Brenna, Eric G. Brown, Robert B. Mann, and Eduardo Martin-Martinez. Universality and thermalization in the unruh effect. *Phys. Rev. D*, 88:064031, 2013.
- [3] Krzysztof Lorek, Daniel Pecak, Eric G. Brown, and Andrzej Dragan. Extraction of genuine tripartite entanglement from the vacuum. *Phys. Rev. A.*, 90:032316, 2014.
- [4] E. G. Brown. Thermal amplification of field-correlation harvesting. *Phys. Rev. A*, 88:062336, 2013.
- [5] Eduardo Martín-Martínez, Eric G. Brown, William Donnelly, and Achim Kempf. Sustainable entanglement production from a quantum field. *Phys. Rev. A*, 88:052310, Nov 2013.
- [6] Eric G. Brown, William Donnelly, Achim Kempf, Robert B. Mann, Eduardo Martín-Martínez, and Nicolas C. Menicucci. Quantum seismology. *New J. Phys.*, 16:105020, 2014.
- [7] Jason Doukas, Eric G. Brown, Andrzej Dragan, and Robert B. Mann. Entanglement and discord: Accelerated observations of local and global modes. *Phys. Rev. A*, 87:012306, 2013.
- [8] Eric G. Brown, Marco del Rey, Hans Westman, Juan Leon, and Andrzej Dragan. What does it mean for half of an empty cavity to be full? *Phys. Rev. D.*, 2015:016005, 91.
- [9] Eric G. Brown, Eric J. Webster, Eduardo Martin-Martinez, and Achim Kempf. Purified discord and multipartite entanglement. *Annals of Physics.*, 337:153, 2013.



- [10] Eric G. Brown, Kyle Cormier, Eduardo Martin-Martinez, and Robert B. Mann. Vanishing geometric discord in noninertial frames. *Phys. Rev. A*, 86:032108, 2012.
- [11] Nicolai Friis, Marcus Huber, Ivette Fuentes, and David Edward Bruschi. Quantum gates and multipartite entanglement resonances realized by nonuniform cavity motion. *Phys. Rev. D.*, 86:105003, 2012.
- [12] J. D. Bekenstein. Black holes and entropy. *Phys. Rev. D.*, 7:2333, 1973.
- [13] S. Ryu and T. Takayanagi. Holographic derivation of entanglement entropy from ads/cft. *Phys. Rev. Lett.*, 96:181602, 2006.
- [14] Michael E. Peskin and Daniel V. Schroeder. *An introduction to quantum field theory*. Westview Press, 1995.
- [15] Steven Weinberg. *The quantum theory of fields*. Cambridge University Press, 2005.
- [16] ATLAS collaboration. Evidence for the spin-0 nature of the higgs boson using atlas data. *Phys. Lett. B.*, 726:120, 2013.
- [17] CMS collaboration. *Journal of High Energy Physics.*, 2013:1, 2013.
- [18] James M. Knight. Strict localization in quantum field theory. *J. Math. Phys.*, 2:459, 1961.
- [19] G. C. Hegerfeldt. Instantaneous spreading and einstein causality in quantum theory. *Annalen Phys.*, 7:716, 1998.
- [20] E. Karpov, G. Ordonez, T. Petrosky, I. Prigogine, and G. Pronko. Causality, delocalization, and positivity of energy. *Phys. Rev. A.*, 62:012103, 2000.
- [21] W. G. Unruh. Notes on black-hole evaporation. *Phys. Rev. D*, 14(4):870–892, Aug 1976.
- [22] Ryszard Horodecki, Pawel Horodecki, Michal Horodecki, and Karol Horodecki. Quantum entanglement. *Rev. Mod. Phys*, 81:865, 2009.
- [23] Michael A. Nielsen and Isaac L. Chuang. *Quantum Computation and Quantum Information*. Cambridge University Press, 2010.
- [24] Nicolas Gisin, Gregoire Ribordy, Wolfgang Tittel, and Hugo Zbinden. Quantum cryptography. *Rev. Mod. Phys.*, 74:145, 2002.

- [25] E. Schrodinger. *Proc. Camb. Phil. Soc.*, 32:446, 1936.
- [26] H. M. Wiseman, S. J. Jones, and A. C. Doherty. Steering, entanglement, nonlocality, and the einstein-podolsky-rosen paradox. *Phys. Rev. Lett.*, 98:140402, 2007.
- [27] P. Skrzypczyk, M. Navascues, and D. Cavalcanti. Quantifying einstein-podolsky-rosen steering. *Phys. Rev. Lett.*, 112:180404, 2014.
- [28] Nicolas Brunner, Daniel Cavalcanti, Stefano Pironio, Valerio Scarani, and Stephanie Wehne. Bell nonlocality. *Rev. Mod. Phys.*, 86:419, 2014.
- [29] Harold Ollivier and Wojciech H. Zurek. Quantum discord: a measure of quantum correlations. *Phys. Rev. Lett.*, 88:017901, 2001.
- [30] Kavan Modi, Aharon Brodutch, Hugo Cable, Tomasz Paterek, and Vlatko Vedral. The classical-quantum boundary for correlations: Discord and related measures. *Rev. Mod. Phys.*, 84:1655, 2012.
- [31] Animesh Datta, Anil Shaji, and Carlton M. Caves. Quantum discord and the power of one qubit. *Phys. Rev. Lett.*, 100:050502, 2008.
- [32] Borivoje Dakic, Vlatko Vedral, and Caslav Brukner. Necessary and sufficient condition for nonzero quantum discord. *Phys. Rev. Lett.*, 105:190502, 2010.
- [33] Marco Piani, Sevag Gharibian, Gerardo Adesso, John Calsamiglia, Pawel Horodecki, and Andreas Winter. All nonclassical correlations can be activated into distillable entanglement. *Phys. Rev. Lett.*, 106:220403, 2011.
- [34] Alexander Streltsov, Hermann Kampermann, and Dagmar Bruss. Linking quantum discord to entanglement in a measurement. *Phys. Rev. Lett.*, 106:160401, 2011.
- [35] Samuel L. Braunstein and Carlton M. Caves. Statistical distance and the geometry of quantum states. *Phys. Rev. Lett.*, 72:3439, 1994.
- [36] H. J. Kimble, Yuri Levin, Andrey B. Matsko, Kip S. Thorne, and Sergey P. Vyatchanin. Conversion of conventional gravitational-wave interferometers into quantum nondemolition interferometers by modifying their input and/or output optics. *Phys. Rev. D.*, 65:022002, 2001.
- [37] Mehdi Ahmadi, David Edward Bruschi, Carlos Sabin, Gerardo Adesso, and Ivette Fuentes. Relativistic quantum metrology: Exploiting relativity to improve quantum measurement technologies. *Scientific Reports.*, 4:4996, 2014.

- [38] Robert M. Wald. *Quantum field theory in curved spacetime and black hole thermodynamics*. The University of Chicago Press, 1994.
- [39] N. D. Birrel and P. C. W. Davies. *Quantum Fields in Curved Space*. Cambridge University Press, 1984.
- [40] B. L. Hu, Shih-Yuin Lin, and Jorma Louko. Relativistic quantum information in detectorsfield interactions. *Class. Quantum Grav.*, 29:224005, 2012.
- [41] Benni Reznik, Alex Retzker, and Jonathan Silman. Violating bell’s inequalities in vacuum. *Phys. Rev. A*, 71:042104, 2005.
- [42] Daniel Braun. Entanglement from thermal blackbody radiation. *Phys. Rev. A*, 72:062324, 2005.
- [43] Juan Leon and Carlos Sabin. Generation of atom-atom correlations inside and outside the mutual light cone. *Phys. Rev. A*, 79:012304, 2009.
- [44] Greg VerSteege and Nicolas C. Menicucci. Entangling power of an exanding universe. *Phys. Rev. D*, 79:044027, 2009.
- [45] Gerardo Adesso and Fabrizio Illuminati. Entanglement in continuous-variable systems: recent advances and current perspectives. *J. Phys. A: Math. Theor*, 40:7821, 2007.
- [46] J. F. Clauser, M. A. Horne, A. Shimony, and R. A. Holt. Proposed experiment to test local hidden-variable theories. *Phys. Rev. Lett*, 23:880, 1970.
- [47] B. S. Cirelson. Quantum generalzations of bell’s inequalities. *Lett. Math. Phys*, 4:93, 1980.
- [48] John S. Bell. On the einstein-podolsky-rosen paradox. *Physics*, 1:195, 1964.
- [49] A. Einstein, B. Podolsky, and N. Rosen. Can quantum-mechanical description of physical reality be considered complete? *Phys. Rev*, 47:777, 1935.
- [50] Artur K. Ekert. Quantum cryptography based on bells theorem. *Phys. Rev. Lett*, 67:661, 1991.
- [51] D. S. Naik, C. G. Peterson, A. G. White, A. J. Berglund, and P. G. Kwiat. Entangled state quantum cryptography: Eavesdropping on the ekert protocol. *Phys. Rev. Lett*, 84:4733, 2000.

- [52] W. Tittel, J. Brendel, H. Zbinden, and N. Gisin. Quantum cryptography using entangled photons in energy-time bell states. *Phys. Rev. Lett*, 84:4737, 2000.
- [53] C. Bennett and S. J. Wiesner. Communication via one- and two-particle operators on einstein-podolsky-rosen states. *Phys. Rev. Lett*, 69:2881, 1992.
- [54] Charles H. Bennett, Gilles Brassard, Claude Crpeau, Richard Jozsa, Asher Peres, , and William K. Wootters. Teleporting an unknown quantum state via dual classical and einstein-podolsky-rosen channels. *Phys. Rev. Lett*, 70:1895, 1993.
- [55] Asher Peres. Separability criterion for density matrices. *Phys. Rev. Lett*, 77:1413, 1996.
- [56] Michal Horodecki, Pawel Horodecki, and Ryszard Horodecki. Separability of mixed states: necessary and sufficient conditions. *Phys. Lett. A*, 223:1, 1996.
- [57] Michal Horodecki, Pawel Horodecki, and Ryszard Horodecki. Mixed-state entanglement and distillation: Is there a bound entanglement in nature? *Phys. Rev. Lett*, 80:5239, 1998.
- [58] G Vidal and R F. Werner. Computable measure of entanglement. *Phys. Rev. A*, 65:032314, 2002.
- [59] M. B. Plenio. Logarithmic negativity: A full entanglement monotone that is not convex. *Phys. Rev. Lett*, 95:090503, 2005.
- [60] Charles H. Bennett, David P. DiVincenzo, John A. Smolin, and William K. Wootters. Mixed-state entanglement and quantum error correction. *Phys. Rev. A*, 54:3824, 1996.
- [61] William K. Wootters. Entanglement of formation of an arbitrary state of two qubits. *Phys. Rev. Lett*, 80:2245, 1998.
- [62] Charles H. Bennett, Herbert J. Bernstein, Sandu Popescu, and Benjamin Schumacher. Concentrating partial entanglement by local operations. *Phys. Rev. A*, 53:2046, 1996.
- [63] D. M. Greenberger, M. A. Horne, and A. Zeilinger. Going beyond bells theorem in bells theorem, quantum theory, and conceptions of the universe. (*Kluwer Academic, Dordrecht*), 1989.

- [64] W. Dr, G. Vidal, and J. I. Cirac. Three qubits can be entangled in two inequivalent ways. *Phys. Rev. A*, 62:062314, 2000.
- [65] Ryszard Horodecki. Informationally coherent quantum systems. *Phys. Lett. A.*, 187:145, 1994.
- [66] Davide Girolami, Tommaso Tufarelli, and Gerardo Adesso. Characterizing nonclassical correlations via local quantum uncertainty. *Phys. Rev. Lett.*, 110:240402, 2013.
- [67] Alexander Streltsov and Wojciech H. Zurek. Quantum discord cannot be shared. *Phys. Rev. Lett.*, 111:040401, 2013.
- [68] Vaibhav Madhok, Vibhu Gupta, Angele M. Hamel, and Shohini Ghose. Signatures of chaos in the dynamics of quantum discord. *arXiv:1307.1405 [quant-ph]*, 2013.
- [69] T. K. Chuan, J. Maillard, K. Modi, T. Paterek, M. Paternostro, and M. Piani. Quantum discord bound the amount of distributed entanglement. *Phys. Rev. Lett.*, 109:070501, 2012.
- [70] Vaibhav Madhok and Animesh Datta. Quantum discord as a resource in quantum communication. *Int. J. Mod. Phys. B*, 27:1245041, 2013.
- [71] Marcelo de Almeida, Mile Gu, Alessandro Fedrizzi, Matthew A. Broome, Timothy C. Ralph, and Andrew G. White. Entanglement-free certification of entangling gates. *arXiv:1301.7110 [quant-ph]*, 2013.
- [72] Mile Gu, Helen M. Chrzanowski, Syed M. Assad, Thomas Symul, Kavan Modi, Timothy C. Ralph, Vlatko Vedral, and Ping Koy Lam. Observing the operational significance of discord consumption. *Nat. Phys.*, 8:671, 2013.
- [73] Gerardo Adesso, Vincenzo D'Ambrosio, Eleonora Nagali, Marco Piani, and Fabio Sciarrino. Experimental entanglement activation from discord in a programmable quantum measurement. *arXiv:1308.1680 [quant-ph]*, 2013.
- [74] Davide Girolami and Gerardo Adesso. Quantum discord for general two-qubit states: Analytical progress. *Phys. Rev. A*, 83:052108, 2011.
- [75] Gerardo Adesso and Animesh Datta. Quantum versus classical correlations in gaussian states. *Phys. Rev. Lett.*, 105:030501, 2010.

- [76] Felipe F. Fanchini, Marcio F. Cornelio, Marcos C. de Oliveira, and Amir O. Caldeira. Conservation law for distributed entanglement of formation and quantum discord. *Phys. Rev. A*, 84:012313, 2011.
- [77] B. L. Schumaker. Quantum mechanical pure states with gaussian wave functions. *Physics Reports*, 135:317, 1986.
- [78] D. F. Walls and Gerard J. Milburn. *Quantum Optics*. Springer, 2008, 1994.
- [79] R Simon. Peres-horodecki separability criterion for continuous variable systems. *Phys. Rev. Lett*, 84:2726, 2000.
- [80] Lu-Ming Duan, G. Giedke, J. I. Cirac, and P. Zoller. Inseparability criterion for continuous variable systems. *Phys. Rev. Lett*, 84:2722, 2000.
- [81] R. F. Werner and M. M. Wolf. Bound entanglement of gaussian states. *Phys. Rev. Lett*, 86:3658, 2001.
- [82] Paolo Giorda, Michele Allegra, and Matteo G. A. Paris. Quantum discord for gaussian states with non-gaussian measurements. *Phys. Rev. A*, 86:052328, 2012.
- [83] Saleh Rahimi-Keshari, Carlton M. Caves, and Timothy C. Ralph. Measurement-based method for verifying quantum discord. *Phys. Rev. A*, 87:012119, 2013.
- [84] W. Rindler. Kruskal space and the uniformly accelerated frame. *Am. J. Phys.*, 34:1174, 1966.
- [85] Lus C. B. Crispino, Atsushi Higuchi, and George E. A. Matsas. The unruh effect and its applications. *2008*, 80:787, Rev. Mod. Phys.
- [86] Alessandro Fabbri and Jose Navarro-Salas. *Modeling black hole evaporation*. Imperial College Press and World Scientific Publishing Co., 2005.
- [87] R. Kubo. Statistical-mechanical theory of irreversible processes. i. general theory and simple applications to magnetic and conduction problems. *Journal of the Physical Society of Japan*, 12:570, 1957.
- [88] Paul C. Martin and Julian Schwinger. Theory of many-particle systems. i. *Phys. Rev.*, 115:1342, 1959.
- [89] Rudolf Haag, M. Winnink, and N. M. Hugenholtz. On the equilibrium states in quantum statistical mechanics. *Comm. Math. Phys.*, 5:215, 1967.

- [90] S J. Summers and R Werner. *Commun. Math. Phys.*, 110:247, 1987.
- [91] Mark Srednicki. Entropy and area. *Phys. Rev. Lett.*, 71:666, 1993.
- [92] Sergey N. Solodukhin. Entanglement entropy in black holes. *Living. Rev. Relativity.*, 14:8, 2011.
- [93] H. Casini and M. Huerta. Entanglement entropy in free quantum field theory. *J. Phys. A: Math. Theor.*, 42:504007, 2009.
- [94] M. Cramer, J. Eisert, M. B. Plenio, and J. Dreissig. Entanglement-area law for general bosonic harmonic lattice systems. *Phys. Rev. A*, 73:012309, 2006.
- [95] L. Amico, R. Fazio, A. Osterloh, and V. Vedral. Entanglement in many-body systems. *Rev. Mod. Phys.*, 80:517, 2008.
- [96] M. Cramer J. Eisert and M. B. Plenio. Area laws for the entanglement entropy. *Rev. Mod. Phys.*, 82:277, 2010.
- [97] A. Retzker, J. I. Cirac, and B. Reznik. Detection of vacuum entanglement in a linear ion trap. *Phys. Rev. Lett.*, 94:050504, 2005.
- [98] Robert H. Jonsson, Eduardo Martín-Martínez, and Achim Kempf. Quantum signaling in cavity qed. *Phys. Rev. A.*, 89:022330, 2014.
- [99] Robert H. Jonsson, Eduardo Martín-Martínez, and Achim Kempf. Information transmission without energy exchange. *arXiv:1405.3988 [quant-ph]*, 2014.
- [100] B. DeWitt. *General Relativity; an Einstein Centenary Survey*. Cambridge University Press, 1980.
- [101] Eduardo Martín-Martínez, Miguel Montero, and Marco del Rey. Wavepacket detection with the unruh-dewitt model. *Phys. Rev. D.*, 87:064038, 2013.
- [102] W. G. Unruh and W. H. Zurek. Reduction of a wave packet in quantum brownian motion. *Phys. Rev. D*, 40:1071, 1989.
- [103] B. L. Hu and A. Matacz. Quantum brownian motion in a bath of parametric oscillators: A model for system-field interactions. *Phys. Rev. D*, 49:6612, 1994.
- [104] Serge Massar and Philippe Spindel. Einstein-podolsky-rosen correlations between two uniformly accelerated oscillators. *Phys. Rev. D.*, 74:085031, 2006.

- [105] Shih-Yuin Lin and B. L. Hu. Backreaction and the unruh effect: New insights from exact solutions of uniformly accelerated detectors. *Phys. Rev. D.*, 76:064008, 2007.
- [106] Jason Doukas, Shih-Yuin Lin, B. L. Hu, and Robert B. Mann. Unruh effect under non-equilibrium conditions: Oscillatory motion of an unruh-dewitt detector. *JHEP*, 11:119, 2013.
- [107] Andrzej Dragan and Ivette Fuentes. Probing the spacetime structure of vacuum entanglement. *arXiv:1105.1192 [quant-ph]*, 2011.
- [108] David E. Bruschi, Antony R. Lee, and Ivette Fuentes. Time evolution techniques for detectors in relativistic quantum information. *J. Phys. A: Math. Theor.*, 46:165303, 2013.
- [109] Nicolas C. Menicucci, S. Jay Olson, and Gerard J. Milburn. Simulating quantum effects of cosmological expansion using a static ion trap. *New J. Phys.*, 12:095019, 2010.
- [110] Alexandre Blais, Ren-Shou Huang, Andreas Wallraff, S M Girvin, and R J Schoelkopf. Cavity quantum electrodynamics for superconducting electrical circuits: An architecture for quantum computation. *Phys. Rev. A*, 69:062320, 2004.
- [111] J Q You and Franco Nori. Atomic physics and quantum optics using superconducting circuits. *Nature*, 474:589, 2011.
- [112] C. M. Wilson, G. Johansson, A. Pourkabirian, M. Simoen, J. R. Johansson, T. Duty, F. Nori, and P. Delsing. Observation of the dynamical casimir effect in a superconducting circuit. *Nature*, 479(7373):376–379, 11 2011.
- [113] Carlos Sabin, Borja Peropadre, Marco del Rey, and Eduardo Martin-Martinez. Extracting past-future vacuum correlations using circuit qed. *Phys. Rev. Lett.*, 109:033602, 2012.
- [114] Eduardo Martin-Martinez and Jorma Louko. Particle detectors and the zero mode of a quantum field. *Phys. Rev. D.*, 90:024015, 2014.
- [115] G. Moore. *J. Math. Phys.*, 11:2679, 1970.
- [116] S. W. Hawking. *Nature*, 248:30, 1974.
- [117] N. Narozhny, A. Fedotov, B. Karnakov, V. Mur, and V. Belinskii. *Phys. Rev. D.*, 65:025004, 2001.



- [118] Carlo Rovelli and Matteo Smerlak. Unruh effect without trans-horizon entanglement. *Phys. Rev. D*, 85:124055, Jun 2012.
- [119] L. Hodgkinson and J. Louko. Static, stationary, and inertial unruh-dewitt detectors on the btz black hole. *Phys. Rev. D*, 86:064031, 2012.
- [120] A. M. Fedotov, N. B. Narozhny, V. D. Mur, and V. A. Belinski. An example of a uniformly accelerated particle detector with non-unruh response. *Phys. Lett. A.*, 305:211, 2002.
- [121] N. B. Narozhny, A. M. Fedotov, B. M. Karanakov, V. D. Mur, and V. A. Belinskii. Reply to comment on boundary conditions in the unruh problem”. *Phys. Rev. D.*, 70:048702, 2004.
- [122] Detlev Buchholz and Christoph Solveen. Unruh effect and the concept of temperature. *Class. Quantum Grav.*, 30:085011, 2013.
- [123] Marco del Rey, Diego Porras, and Eduardo Martn-Martnez. Simulating accelerated atoms coupled to a quantum field. *Phys. Rev. A.*, 85:022511, 2012.
- [124] Alejandro Satz. Then again, how often does the unruh-dewitt detector click if we switch it carefully? *Class. Quantum Grav.*, 24:1719, 2007.
- [125] Jonathan Silman and Benni Reznik. Many-region vacuum entanglement: Distilling a wstate. *Phys. Rev. A.*, 71:054301, 2005.
- [126] Gerardo Adesso, Alessio Serafini, and Fabrizio Illuminati. Quantification and scaling of multipartite entanglement in continuous variable systems. *Phys. Rev. Lett.*, 93:220504, 2004.
- [127] Alessio Serafini, Gerardo Adesso, and Fabrizio Illuminati. Unitarily localizable entanglement of gaussian states. *Phys. Rev. A.*, 71:032349, 2005.
- [128] L Henderson and V Vedral. *J. Phys. A: Math. Theor*, 34:6899, 2001.
- [129] Massimo Borrelli, Carlos Sabin, Gerardo Adesso, Francesco Plastina, and Sabrina Maniscalco. Dynamics of atom-atom correlations in the fermi problem. *New Journal of Physics*, 14:103010, 2012.
- [130] Alexander Streltsov, Hermann Kampermann, and Dagmar Bruss. Behavior of quantum correlations under local noise. *Phys. Rev. Lett.*, 107:170502, 2011.

- [131] Janet Anders and Andreas Winter. Entanglement and separability of quantum harmonic oscillator systems at finite temperature. *Quantum Information and Computation*, 8:0245, 2008.
- [132] Alessandro Ferraro, Daniel Cavalcanti, Artur Garcia-Saez, and Antonio Acin. Thermal bound entanglement in macroscopic systems and area law. *Phys. Rev. Lett.*, 100:080502, 2008.
- [133] T. Werlang, S. Souza, F. F. Fanchini, and C. J. VillasBoas. Robustness of quantum discord to sudden death. *Phys. Rev. A*, 80:024103, 2009.
- [134] Bo Wang, Zhen-Yu Xu, Ze-Qian Chen, and Mang Feng. Non-markovian effect on the quantum discord. *Phys. Rev. A*, 81:014101, 2010.
- [135] Animesh Datta. Quantum discord between relatively accelerated observers. *Phys. Rev. A*, 80:052304, 2009.
- [136] Jose N. Freitas and Juan P. Paz. Dynamics of gaussian discord between two oscillators interacting with a common environment. *Phys. Rev. A.*, 85:032118, 2012.
- [137] H. Arthur Weldon. Thermal green functions in coordinate space for massless particles of any spin. *Phys. Rev. D.*, 62:056010, 2000.
- [138] Private communication.
- [139] M. S. Kim, W. Son, V. Buzek, and P. L. Knight. Entanglement by a beam splitter: Nonclassicality as a prerequisite for entanglement. *Phys. Rev. A.*, 65:032323, 2002.
- [140] Michael M. Wolf, Jens Eisert, and Martin B. Plenio. Entangling power of passive optical elements. *Phys. Rev. Lett.*, 90:047904, 2003.
- [141] H. B. G. Casimir and D. Polder. The influence of retardation on the london-van der waals forces. *Phys. Rev.*, 73:360, 1948.
- [142] Mathieu Cliche and Achim Kempf. Relativistic quantum channel of communication through field quanta. *Phys. Rev. A.*, 81:012330, 2010.
- [143] J M Raimond, M Brune, and Serge Haroche. Manipulating Quantum Entanglement with Atoms and Photons in a Cavity. *Rev. Mod. Phys.*, 73:565, 2001.
- [144] V. Vedral. The role of relative entropy in quantum information theory. *Rev. Mod. Phys.*, 74:197, 2002.

- [145] M. O. Scully and M. S. Zubairy. *Quantum optics*. Cambridge University Press, 1997.
- [146] Eduardo Martín-Martínez, David Aasen, and Achim Kempf. Processing quantum information with relativistic motion of atoms. *Phys. Rev. Lett.*, 110:160501, 2013.
- [147] A. Wallraff, D. I. Schuster, A. Blais, L. Frunzio, R.-S. Huang, J. Majer, S. Kumar, S.M. Girvin, and R.J. Schoelkopf. Strong coupling of a single photon to a superconducting qubit using circuit quantum electrodynamics. *Nature*, 431:162, 2004.
- [148] J. Weber. Gravitational-wave-detector events. *Phys. Rev. Lett.*, 20:1307, 1968.
- [149] R. J. Glauber. The quantum theory of optical coherence. *Phys. Rev.*, 130:2529, 1963.
- [150] Andrzej Dragan, Jason Doukas, Eduardo Martín-Martínez, and David E. Bruschi. Localised projective measurement of a relativistic quantum field in non-inertial frames. *Class. Quantum Grav.*, 30:235006, 2013.
- [151] Andrzej Dragan, Jason Doukas, and Eduardo Martin-Martinez. Localized detection of quantum entanglement through the event horizon. *Phys. Rev. A.*, 87:052326, 2013.
- [152] Andrzej Dragan. Efficient fiber coupling of down-conversion photon pairs. *Phys. Rev. A.*, 70:053814, 2004.
- [153] Konrad Banaszek, Andrzej Dragan, Wojciech Wasilewski, and Czeslaw Radzewicz. Experimental demonstration of entanglement-enhanced classical communication over a quantum channel with correlated noise. *Phys. Rev. Lett.*, 92:257901, 2004.
- [154] T. Padmanabhan and T. P. Singh. Response of accelerated detectors in coherent states and the semiclassical limit. *Phys. Rev. D.*, 38:2457, 1988.
- [155] Sandro S. Costa and George E. A. Matsas. Background thermal contributions in testing the unruh effect. *Phys. Rev. D.*, 52:3466, 1995.
- [156] Sanved Kolekar and T. Padmanabhan. Indistinguishability of thermal and quantum fluctuations. *arXiv:1308.6289 [gr-qc]*, 2013.
- [157] Paul M. Alsing and G. J. Milburn. Teleportation with a uniformly accelerated partner. *Phys. Rev. Lett.*, 91:180404, 2003.
- [158] Y. Shi. Entanglement in relativistic quantum field theory. *Phys. Rev. D.*, 70:105001, 2004.

- [159] Ivette Fuentes-Schuller and Robert B. Mann. Alice falls into a black hole: Entanglement in noninertial frames. *Phys. Rev. Lett.*, 95:120404, 2005.
- [160] P. M. Alsing, I. Fuentes-Schuller, R. B. Mann, and T. E. Tessier. Entanglement of dirac fields in noninertial frames. *Phys. Rev. A.*, 74:032326, 2006.
- [161] Gerardo Adesso, Ivette Fuentes-Schuller, and Marie Ericsson. Continuous-variable entanglement sharing in noninertial frames. *Phys. Rev. A.*, 76:062112, 2007.
- [162] K. Bradler. Eavesdropping of quantum communication from a noninertial frame. *Phys. Rev. A.*, 75:022311, 2007.
- [163] Alexander Smith and Robert B. Mann. Persistence of tripartite nonlocality for non-inertial observers. *Phys. Rev. A.*, 86:012306, 2012.
- [164] David E. Bruschi, Jorma Louko, Eduardo Martin-Martinez, Andrzej Dragan, and Ivette Fuentes. Unruh effect in quantum information beyond the single-mode approximation. *Phys. Rev. A.*, 82:042332, 2010.
- [165] Miguel Montero, Marco del Rey, and Eduardo Martin-Martinez. Nonmonotonic entanglement of physical electromagnetic field states in noninertial frames. *Phys. Rev. A.*, 86:012304, 2012.
- [166] Matias Rodriguez-Vazquez, Marco del Rey, Hans Westman, and Juan Leon. Local quanta, unitary inequivalence, and vacuum entanglement. *Annals of Physics*, 351:112, 2014.
- [167] A. Botero and B. Reznik. Spatial structures and localization of vacuum entanglement in the linear harmonic chain. *Phys. Rev. A*, 70:052329, 2004.
- [168] Benni Reznik, Alex Retzker, and Jonathan Silman. Violating bell’s inequalities in vacuum. *Phys. Rev. A*, 71:042104, Apr 2005.
- [169] Marco del Rey, Carlos Sabin, and Juan Leon. Short-time quantum detection: Probing quantum fluctuations. *Phys. Rev. A*, 85:045802, Apr 2012.
- [170] M. Zych, F. Costa, J. Kofler, and C. Brukner. Entanglement between smeared field operators in the klein-gordon vacuum. *Phys. Rev. D*, 81:125019, 2010.
- [171] Paul R. Berman, with contributions from, G. Barton, H.J. Carmichael, J.J. Childs, G. Gabrielse, J. Tan, S. Haroche, J.M. Raimond, E.A. Hinds, H.J. Kimble,

- P. Meystre, M. Wilkens, T.W. Mossberg, M. Lewenstein, and G. Raithel et al. *Cavity Quantum Electrodynamics (Advances in Atomic, Molecular and Optical Physics)*. Academic Press, 1993.
- [172] Sara R. Hastings, Michiel J. A. de Dood, Hyochul Kim, William Marshall, Hagai S. Eisenberg, and Dirk Bouwmeester. Ultrafast optical response of a high-reflectivity gaas/alas bragg mirror. *Applied Physics Letters*, 86:031109, 2005.
- [173] A. Wallraff, D. I. Schuster, A. Blais, L. Frunzio, R. S. Huang, J. Majer, S. Kumar, S. M. Girvin, and R. J. Schoelkopf. Strong coupling of a single photon to a superconducting qubit using circuit quantum electrodynamics. *Nature*, 431(7005):162–167, 09 2004.
- [174] Arjan F. van Loo, Arkady Fedorov, Kevin Lalumire, Barry C. Sanders, Alexandre Blais, and Andreas Wallraff. Photon-mediated interactions between distant artificial atoms. *Science*, 342(6165):1494–1496, 2013.
- [175] Io-Chun Hoi, C. M. Wilson, Göran Johansson, Tauno Palomaki, Borja Peropadre, and Per Delsing. Demonstration of a single-photon router in the microwave regime. *Phys. Rev. Lett.*, 107:073601, Aug 2011.
- [176] Io-Chun Hoi, Tauno Palomaki, Joel Lindkvist, Göran Johansson, Per Delsing, and C. M. Wilson. Generation of nonclassical microwave states using an artificial atom in 1d open space. *Phys. Rev. Lett.*, 108:263601, Jun 2012.
- [177] Per Delsing. *in a private communication*.
- [178] Philip Zupancic. *Dynamic Holography and Beamshaping using Digital Micromirror Devices*. LMU Munich, Grainer Lab Harvard, 2013.
- [179] Steven G. Avery and Borun D. Chowdhury. No holography for eternal ads black holes. *arXiv:1312.3346 [hep-th]*, 2013.
- [180] Samuel L. Braunstein, Stefano Pirandola, and Karol Zyczkowski. Better late than never: Information retrieval from black holes. *Phys. Rev. Lett*, 110:101301, 2013.
- [181] Dionigi M. T. Benincasa, Leron Borsten, Michel Buck, and Fay Dowker. Quantum information processing and relativistic quantum fields. *Class. Quantum Grav.*, 31:075007, 2014.
- [182] X. Ma and W. Rhodes. *Phys. Rev. A.*, 41:4625, 1990.

- [183] H. Heffner and W. H. Louisell. *J. Math. Phys.*, 6:474, 1965.
- [184] Carlos Sabin, David Edward Bruschi, Mehdi Ahmadi, and Ivette Fuentes. Phonon creation by gravitational waves. *New J. Phys.*, 16:085003, 2014.